

**Intelligent Systems, Control and Automation:
Science and Engineering**

Kenzo Nonami
Ranjit Kumar Barai
Addie Irawan
Mohd Razali Daud

Hydraulically Actuated Hexapod Robots

Design, Implementation and Control

Intelligent Systems, Control and Automation: Science and Engineering

For further volumes:
<http://www.springer.com/series/6259>

Kenzo Nonami • Ranjit Kumar Barai
Addie Irawan • Mohd Razali Daud

Hydraulically Actuated Hexapod Robots

Design, Implementation and Control



Springer

Kenzo Nonami
Department of Mechanical Engineering
Division of Artificial Systems Science
Graduate School of Engineering
Chiba University
Chiba, Japan

Addie Irawan
Faculty of Electrical and Electronics
Engineering
Robotics and Unmanned Systems
(RUS) group
Universiti Malaysia Pahang
Pahang, Malaysia

Ranjit Kumar Barai
Department of Electrical Engineering
Jadavpur University
Kolkata, India

Mohd Razali Daud
Faculty of Electrical and Electronics
Engineering
Robotics and Unmanned Systems
(RUS) group
Universiti Malaysia Pahang
Pahang, Malaysia

ISSN 2213-8986

ISBN 978-4-431-54348-0

DOI 10.1007/978-4-431-54349-7

Springer Tokyo Heidelberg New York Dordrecht London

ISSN 2213-8994 (electronic)

ISBN 978-4-431-54349-7 (eBook)

Library of Congress Control Number: 2013949168

© Springer Japan 2014

This work is subject to copyright. All rights are reserved by the Publisher, whether the whole or part of the material is concerned, specifically the rights of translation, reprinting, reuse of illustrations, recitation, broadcasting, reproduction on microfilms or in any other physical way, and transmission or information storage and retrieval, electronic adaptation, computer software, or by similar or dissimilar methodology now known or hereafter developed. Exempted from this legal reservation are brief excerpts in connection with reviews or scholarly analysis or material supplied specifically for the purpose of being entered and executed on a computer system, for exclusive use by the purchaser of the work. Duplication of this publication or parts thereof is permitted only under the provisions of the Copyright Law of the Publisher's location, in its current version, and permission for use must always be obtained from Springer. Permissions for use may be obtained through RightsLink at the Copyright Clearance Center. Violations are liable to prosecution under the respective Copyright Law.

The use of general descriptive names, registered names, trademarks, service marks, etc. in this publication does not imply, even in the absence of a specific statement, that such names are exempt from the relevant protective laws and regulations and therefore free for general use.

While the advice and information in this book are believed to be true and accurate at the date of publication, neither the authors nor the editors nor the publisher can accept any legal responsibility for any errors or omissions that may be made. The publisher makes no warranty, express or implied, with respect to the material contained herein.

Printed on acid-free paper

Springer is part of Springer Science+Business Media (www.springer.com)

Preface

Robotics technology covers very wide area. Fully autonomous robots in particular are associated with three functions, namely, manipulation, locomotion, and communication. Locomotion robots may be classified by the environment in which they travel: (1) Land or home robots are most commonly wheeled, unmanned ground vehicles (UGVs) but also include legged robots with two or more legs, like humanoids or resembling animals or insects. (2) Aerial robots are usually referred to as unmanned aerial vehicles (UAVs). (3) Underwater robots are usually called autonomous underwater vehicles (AUVs). Wheeled and tracked UGVs, UAVs, and AUVs are already in use for real applications. The exceptions are legged robots. Unfortunately, legged robots based on the use of animal-like and human-like legs are still in the research phase even though many research outcomes have been achieved. The main reason for their remaining in the research stage may be that the locomotion speed and the energy efficiency of legged robots are still very low compared with those of wheeled robots. However, wheeled vehicles are unable to move on rough, off-road or unmodified natural terrain and need paved surfaces in order to operate smoothly.

According to the United States Army, approximately half of the Earth's land surface is inaccessible to either wheeled or tracked vehicles. Legged animals and humans are capable of legged locomotion and as a result they can access any part of the Earth's land surface without great difficulty. These legged creatures can walk on rough or irregular terrain by establishing foot contact with the ground at selected points according to the terrain conditions and by varying their leg configurations in order to adapt themselves to irregularities in terrain. Thus, legs are inherently adequate systems for locomotion on rough and irregular terrain. This fact was a motivation for the development of artificial legged systems.

Among the various types of legged robots, hexapod walking robots offer a good static stability margin and locomotion speed, and at the same time they are fault-tolerant. Therefore, hexapod walking robots have emerged as a popular robotic system for various critical and hazardous field applications. The origin of our research motivation was to build a human-like de-mining robot using hexapod robots. We need a fast, safe, and robust technique for de-mining operations, and

walking robots can be considered an effective and efficient means for that purpose. Hydraulically actuated hexapod walking robots can be used for the detection and removal of landmines while providing safety and security for the operating personnel. Hydraulically actuated hexapod robots are mechanically robust, have a high level of static stability margin, and are suitable for operation in rough terrain. Therefore, their deployment for de-mining tasks is advantageous from the point of view of their safe locomotion capability in a mine field and their capability to carry large payloads of the tools required for de-mining missions. Nonami group at the Robotics and Control System Laboratory (Nonami Laboratory), Chiba University, Japan, has developed and successfully tested the hydraulically actuated hexapod robots COMET-III and COMET-IV for achieving robot-assisted de-mining. This book describes the essential design, implementation, and control of hydraulically actuated hexapod robots.

Chapter 1 covers various theoretical and practical aspects of legged locomotion and also introduces many popular and successfully implemented legged robots around the world. Chapter 2 presents a condensed perspective of the historical evolution of walking robots. Chapter 3 describes the group's attempt to fundamentally review the basic specifications of a robot, such as the mechanism, gait, drive system, and control system, and to approach the optimization-based design of COMET-IV—the hexapod dangerous-operations robot. Chapter 4 deals with kinematics and path planning of COMET-IV. In particular, the developed kinematics and dynamics are exploited to be used for end-effector force on foot detection and overall COMET-IV stability for force-attitude control purposes. In COMET-IV research, the total force on the foot is calculated for center-of-mass (CoM) identification as an input for robot attitude during walking sessions. Chapter 5 starts with a general description of position-control-based locomotion control of walking robots. Then the various nonlinearities of the hydraulic actuation system are briefly described. Finally, two sliding-mode-based locomotion control techniques and the robust adaptive fuzzy-control-based locomotion control technique of COMET-III in the position-control-based framework are presented with real-time experimental results. In Chap. 6, it is shown that, with the capability of active suspension (legs), the strong role of legged/walking robot design makes it possible to pass through any uneven terrain as long as the obstacles are lower than the robot's maximum or minimum overall body height, if compare to the wheel type robot. Therefore, force or impedance control is needed to make a dynamic response on each leg in order to identify the different level of the terrain or any sudden changes in the terrain. Moreover, this control is crucial in hidden areas that could not be identified by a vision system via pre-scanning and localization. Chapter 7 proposes several algorithms such as impedance control implementation for the hexapod robot COMET-IV. Also, in the case of heavy-weight and large-scale-structured robots, inclinometers from attitude angles must be designed to control the long-term attitudes of the body without any vibration caused by changes in support of the legs. This shaking is considered a natural scenario since the robot is using a hydraulic system and an automotive engine. Chapter 8 deals with cases of extreme environments, where it is difficult to achieve full autonomy. Therefore, a

teleoperation-based system has been designed on the COMET-IV for extreme environments. The teleoperation assistant system is designed to understand the ambient environment and the movement conditions of the robot. These include legged robot changes that affect the height of the body and the robot's attitude. In this chapter, we applied an omni-directional vision sensor and 3D robot animation. The online 3D virtual reality technique is proposed for achieving synchronous control between virtual 3D animation and the physical COMET-IV in a real environment. Chapter 9 proposes several methods for crossing an obstacle and descending and ascending a cliff based on LRF 3D point cloud data. Experimental results show that the proposed methods are useful for performing assigned tasks. Chapter 10 describes challenges and new frontiers.

Hydraulically actuated hexapod robots form a very useful class of walking robots in the context of service robotics, field robotics, search and rescue, and high-risk operations. They can also be utilized as a test bed for designing and validating various gaits and walking behaviors. Many potential applications may be possible with the advent of various technologies associated with the design and manufacturing of such robots.

I would like to express my sincere gratitude to Dr. Y. Ooroku, Mr. H. Sugai, Mr. M. Oku, Mr. H. Yang, Mr. G. Piao, Mr. K. Adachi, Mr. Y. Harada, Mr. K. Futagami, Mr. G. Lin, Mr. D. H. Tran, Mr. Y. Akutsu, Mr. R. Li, Mr. S. Imamura, Mr. A. Haneda, Mr. R. Namiki, Mr. Y. Tsuchida, Mr. Y. Tondok, and Mr. K. Zhao, who contributed so much to the work on COMET-IV. This book would not have been possible without their devoted efforts. I am also very grateful to many of my laboratory students who contributed to COMET-I, COMET-II, and COMET-III projects. Finally, we would like to thank Ms. Y. Sumino and Ms. T. Sato at Springer for their support and encouragement in undertaking this publication.

Chiba, Japan
Kolkata, India
Pahang, Malaysia
Pahang, Malaysia

Kenzo Nonami
Ranjit Kumar Barai
Addie Irawan
Mohd Razali Daud

Contents

1	Introduction	1
1.1	Introduction	1
1.2	Walking “Machines” or Walking “Robots”?	4
1.3	“Biologically Inspired” Designs and Development of Walking Robots	5
1.4	Classification of Walking Robots	6
1.5	Hexapod Walking Robots: A Popular Walking Machine for Field Robotics Applications	8
1.6	Walking Robot Terminology	15
1.7	Challenges of Navigation and Locomotion Control of Hexapod Walking Robot for the Field Robotics Applications	16
	References	17
2	Historical and Modern Perspective of Walking Robots	19
2.1	Introduction	19
2.2	Historical Perspective of Walking Robots	21
2.2.1	Emergence of Artificial Legged Locomotion from Ancient Civilizations: Imagination, Ideas, and Implementations	21
2.2.2	Evolution of Modern Walking Robots	27
2.3	Modern and Future Perspective of Walking Robot Research	37
	References	39
3	Design and Optimization of Hydraulically Actuated Hexapod Robot COMET-IV	41
3.1	System Construction	42
3.1.1	Conceptual Design	42
3.1.2	Overall Mechanical System Design	46

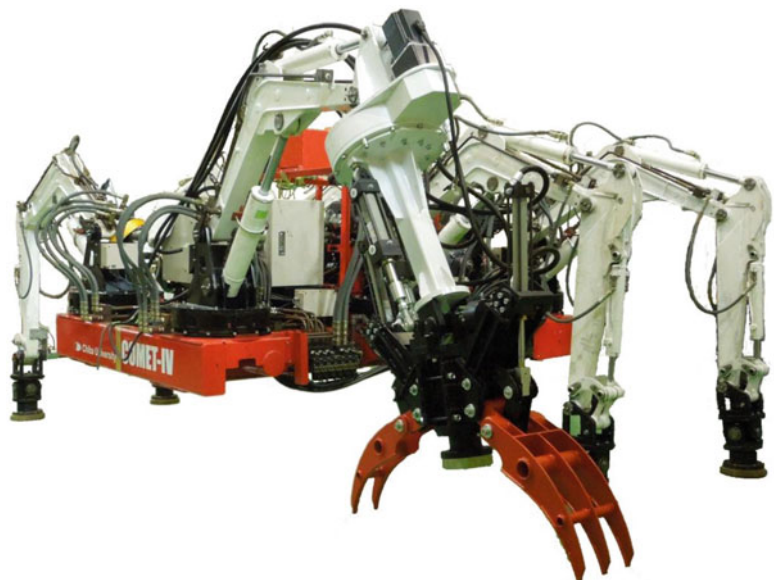
3.2	Building a Single-Leg Model	53
3.2.1	Leg Mechanism	53
3.2.2	Observations from the Evaluation Experiments	55
3.3	Kinematic Analysis	55
3.3.1	Forward Kinematics, Inverse Kinematics	55
3.3.2	The Jacobian	56
3.3.3	Manipulability	61
3.4	Analysis of the Foot Mechanism	64
3.4.1	Definition of the Required Cylinder Force and Torque	64
3.4.2	Jacobian Analysis	65
3.4.3	Analysis Results	65
3.4.4	Definition of the Necessary Workspace	69
3.4.5	Defining the Necessary Flow Rate and Walking Speed	70
3.5	Optimization of the Leg Mechanism	71
3.5.1	Optimization Process	71
3.5.2	Optimization Results	74
3.6	Exterior View of the Completed COMET-IV	78
	References	83
4	Kinematics, Navigation, and Path Planning of Hexapod Robot	85
4.1	COMET-IV Kinematics (Inverse/Direct) and Force Sensing	85
4.2	COMET-IV Center of Mass/Gravity	89
4.3	Navigation and Path Planning Issues in Field Robotics Applications	91
4.4	Movement Control Methods	93
4.5	Terrain Adaptive Foot Trajectory Using Force Threshold-Based Method	97
	References	103
5	Position-Based Robust Locomotion Control of Hexapod Robot	105
5.1	Introduction	105
5.1.1	Locomotion Control Techniques	106
5.1.2	Centralized Control	107
5.1.3	Distributed Control	108
5.2	Challenges of Position-Based Locomotion Control of Hydraulically Actuated Hexapod Robot	110
5.3	Independent Joint Control-Based Locomotion Control of Hydraulically Actuated Hexapod Robot	111
5.4	Robust Control Techniques for Locomotion Control of Hydraulically Actuated Hexapod Robot	112
5.4.1	Technical Description of COMET-III and Its Model Identification	113

5.4.2	Model Reference Sliding Mode Control	117
5.4.3	Preview Sliding Mode Control	122
5.4.4	Robust Adaptive Fuzzy Logic Control-Based Intelligent Control for Locomotion Control of Hydraulically Actuated Hexapod Robot	128
References		138
6	Force-Based Locomotion Control of Hexapod Robot	141
6.1	Position-Based Force Control for Hydraulically Driven Hexapod Robot Walking on Rough Terrain	141
6.1.1	Case Study: Hydraulically Driven Hexapod Robot Walking on Rough Terrain Issue	141
6.1.2	Compliant Control Using Pull-Back Method and Logical Attitude-Level Terrain Changes Switching for ETT Module	145
6.1.3	Experiment and Verifications	152
6.2	Impedance Control for Hydraulically Driven Hexapod Robot	156
6.2.1	Case Study: Hydraulically Driven Hexapod Robot Walking on Soft Terrain Issue	157
6.2.2	Impedance Control Schemes for Hexapod Robot	159
6.2.3	Experiment and Verification	162
References		166
7	Impedance Control and Its Adaptive for Hexapod Robot	169
7.1	Optimization of Impedance Control Using Virtual Forces from the Body's Moment of Inertia	169
7.1.1	Experiment and Verification	173
7.2	Optimization of Impedance Control by Self-Tuning Stiffness Using Logical Body's Attitude Control	179
7.2.1	Experiment and Verification	181
7.3	Impedance Forces Input Optimization Using Fuzzy Logic Control	185
7.3.1	Experiment and Verification	189
References		196
8	Teleoperated Locomotion Control of Hexapod Robot	199
8.1	Movement Control Methods	200
8.2	COMET-IV System Configuration	201
8.3	OmniDirectional Gait Control Procedure	203
8.4	Teleoperation Assistant System	205
8.5	Ambient Environmental Image View of Robot	208
8.6	Robot Animation Using 3D Geometric Models and Sensor Data	212
8.7	Experiment	214

8.8	COMET-IV 3D Simulator Modeling	216
8.8.1	Walking Trajectory Modeling	217
8.8.2	Environment Modeling	221
8.8.3	Control System Modeling	223
8.8.4	3D Geometric Modeling	226
8.9	Modeling Verification	229
8.10	Summary	233
	References	233
9	Fully Autonomous Locomotion Control of Hexapod Robot with LRF	237
9.1	Advantages of Hexapod Robot and Typical Quadruped Robot	237
9.2	Environment Modeling	239
9.2.1	Laser Range Finder	240
9.2.2	Grid-Based Environment Modeling	241
9.2.3	Path Planning	243
9.3	Locomotion Strategies in Stochastic Environment	244
9.3.1	Crossing Over and Ascending an Obstacle or a Step	244
9.3.2	Descending a Cliff	246
9.4	Experimental Results	248
9.4.1	Crossing Over an Obstacle: Results and Discussion	248
9.4.2	Crossing Over an Obstacle Longer than 0.6 m: Results and Discussion	251
9.4.3	Ascending and Descending a Cliff: Results and Discussion	253
9.5	Summary	256
	References	260
10	Challenges and New Frontiers of Hydraulically Actuated Hexapod Robots	263
10.1	Introduction	263
10.2	Mine Detection and Removal	265
10.3	Rescue and Disaster Management Applications	266
10.4	High-Risk Operations	266
10.5	Construction Application	267
10.6	Cargo Application	267
10.7	Underwater Operation	267
10.8	Forest-Cutting Machine	268
10.9	A Test Bed for Study and Research of Biological Walking	268
10.10	Other Possible Applications of Hydraulically Actuated Hexapod Robot	268
	References	269
Index		271



Fully autonomous walking robot COMET-IV: Walking mode



Fully autonomous walking robot COMET-IV: Working mode

Chapter 1

Introduction

Abstract Legs have evolved as a means of propulsion of the body of animals and insects through millions of years of evolution that enabled them for terrain adaptive locomotion on any part of the earth's land surface. Inspired from the observed advantages in locomotion of legged creatures in the biological world, scientists and engineers are applying the principles of biomechanics and bio-intelligence for the design of legged robots. Modern legged robotics research although biologically inspired, it is not yet possible to replicate completely the biological systems for design and implement a walking robot. This is due to the fact that the biological actuation, sensing, and reasoning principles and mechanisms are completely different from the current engineering principles and mechanisms of the actuation, sensing, and computer systems. Among various types of legged robots, hexapod walking robots offer good amount of static stability margin and locomotion speed, and at the same time they are fault tolerant. Therefore, hexapod walking robots have emerged as a popular robotic system for various critical and hazardous field applications. This chapter covers various theoretical and practical aspects of legged locomotion and also introduces many popular and successfully implemented legged robots around the world.

1.1 Introduction

The invention of wheels was a turning point in the history of civilization. Our ancestors developed wheeled vehicles several thousands of years ago, and even today our modern transport system depends on wheel as a means for propulsion of the vehicles. The mechanical prime movers have replaced the animals for the generation of the tractive efforts consequent to the industrial revolution, and later the electric motors replaced mechanical prime movers. Even today, the modern transportation, consisting of mainly automotive and railway system, on the Earth's

surface is still based on wheeled locomotion. The main drawback of the wheeled vehicles is that they are unable to move on rough, off-road, or unmodified natural terrain and need paved surface to operate smoothly. However, the synergistic combination of wheeled system and paved path or land surface leads to a very energy-efficient, high-speed, and long-distance transportation system [1]. Consequently, the mankind continuously destroyed the natural environment from the dawn of ancient civilizations for making paved surfaces for the sake of convenience of wheeled locomotion of carts and vehicles for the transportation of goods and also for communications.

According to the U.S. Army, approximately half of the Earth's land surface is inaccessible to either wheeled or tracked vehicles [1, 2]. Legged animals and human are capable of legged locomotion and as a result they can access any part of the Earth's land surface without much difficulty. These legged creatures can walk on rough or irregular terrain by establishing the foot contacts on the ground at selected points according to the terrain conditions and varying their leg configurations in order to adapt themselves to the terrain irregularities. Thus, legs are inherently adequate systems for locomotion on rough and irregular terrain [3]. In fact, this was a motivation for the mankind to develop artificial legged locomotion system. There are certain advantages of adopting legged locomotion in mobile robots [1, 3–8]:

1. Like legged animals, legged vehicles manifest a superior mobility in natural terrain compared to the wheeled mobile robots. Because, these vehicles use discrete footholds for each foot satisfying (a) the need of the terrain condition, (b) possible gait and stability, and (c) the feet remaining within the workspace boundary of the legs, whereas the wheeled mobile robots require continuous support on the ground surface for stable locomotion, which may not be possible in rough terrain. Therefore, properly built legged robots will be able to move over most of the earth's terrain.
2. Legs of the walking machines create discrete footprints during locomotion and, thus, legged locomotion causes smaller damage to the natural terrain compared to the wheeled vehicles. Wheeled vehicles require paved surface for locomotion and much damage is caused to the natural terrain during the construction of such paved surface.
3. As the legs have multiple degrees of freedom in the leg joints, transportation in legged vehicle is comfortable due to the isolation of the legged vehicle body from the terrain irregularities. A steady body attitude and height can be maintained for the payload and the sensors after adapting leg configuration with the ground irregularities and selected foothold positions by joint angle control of the legs during rough terrain locomotion.
4. Legged locomotion offers greater mobility than wheeled locomotion on soft and slippery ground.

5. Legged vehicles can cross ditches, climb stairs, and negotiate obstacles. It can also stride over obstacles without touching them.
6. Legged vehicles may change their gait pattern maintaining proper stability conditions depending upon the requirement of locomotion speed or rough terrain locomotion. For example, during moderate locomotion speed on level ground, the legged machines adopt statically stable periodic gait (continuous or discontinuous) like wave gaits. Whereas during ditch crossing, ascending or descending steps, or moving cluttered and rough terrain, the legged machines adopt statically stable aperiodic gaits like free gaits or follow-the-leader gaits. When the walking machines are required to move at a faster speed, they may adopt dynamically stable gaits like trot, canter, or gallop.
7. Legged machines have inherent omnidirectionality and it can travel in all directions without changing its body direction. Therefore, free from nonholonomic constraints.
8. Legged vehicles have an inherent failure tolerance during statically stable locomotion. If one or more joints are damaged, the legged robots may be able to continue to move with less efficacy and speed depending upon the number of healthy joints available to fit into any possible gait. For example, in hexapod walking robots there are few redundant joints. Therefore, hexapod walking robots may continue to operate with quadruped walking robot gaits in case few joints are damaged. In contrast, failure of one of the wheels of a wheeled mobile robot leads to the loss of mobility (and sometimes the loss of stability in motion too) since all wheels of wheeled vehicles should be in direct contact with the ground during the locomotion.

If a walking machine possesses all these useful features of locomotion, they can assist or fully replace humans in various sorts of dangerous works, such as maintenance of chemical and nuclear plants, rescue operation at the site of disasters, cargo transportation in mountainous areas, and humanitarian land mine removal [7]. Therefore, attempts have been made over the past hundred years to design and construct various legged machines combining the innovative engineering with the scientific observations of the agility and efficiency of legged animals [9]. However, it took several years to make a successful walking machine mainly due to the limited understanding of walking gaits and complexity of leg coordination control [10]. A historical account of the development of walking robots in the condensed form would be presented in Chap. 2.

This monograph intends to present a comprehensive guideline and methodology for the step-by-step design and development of the mechatronic structure as well as various control techniques of a hydraulically actuated hexapod robot for field applications.

1.2 Walking “Machines” or Walking “Robots”?

The word *robot* originated from the Czech word *robořa*, meaning work [11]. Until now, hundreds of definitions for industrial robots or manipulators have appeared in the literature. Robotic Institute of America (RIA) has given a very precise definition of industrial robot or manipulator as [11, 12]:

A robot is a *reprogrammable multi-functional* manipulator designed to move materials, parts, tools, or specialized devices, through variable programmed motions for the performance of a variety of tasks.

In ISO 8373, the International Organization for Standardization defines a robot as “an automatically controlled, reprogrammable, multipurpose manipulator with three or more axes.”

A very comprehensive definition of robots, covering a wide range and class of robots, has been given in [13] as:

A robot is a versatile mechanical device – for example, a manipulator arm, a multi-joint multi-fingered hand, a wheeled or legged vehicle, a free-flying platform, or a combination of these – equipped with actuators and sensors under the control of a computing system. It operates in the workspace within the real world. This workspace is populated by physical objects and is subject to the laws of nature. The robot performs tasks by executing motions in the workspace.

As per these definitions, a robot must possess [14, 15] (1) a versatile and multifunctional mechanical structure and mechanism; (2) automatic motion control system comprising of actuator, sensor, computing element, and control law or algorithm; (3) reprogrammable to change the control law as and when required; and (4) intelligence to interact with the environment, human, or other robot, for autonomous operation. Walking machines employ controlled and ordered movement of multiple legs for propulsion of the whole body. These coordinated ordered movements of the multiple legs, some of them are in swing and others for supporting the body, is a very complicated task and are invariably achieved through computer control. Moreover, when the walking or legged vehicles are employed for autonomous operation or interaction with the environment and human, they are equipped with appropriate computer algorithms. These algorithms, meant for computer control of sequenced motion of legs, interaction with the environment with the help of sensors or actuators, or autonomous operation, are always reprogrammable. These legged vehicles can be employed for a variety of tasks in home and office, companion and edutainment, field application, and search and rescue, by properly designing their mechatronic subsystems and control algorithms. Therefore, legged vehicles or walking machines are very much qualified to be termed as “walking robots.” In the light of the above discussion and retaining the spirit of classical definition of robot, we can define a walking robot as:

A mobile vehicle or machine that utilizes one or more leg mechanisms as a means for propulsion and having reprogrammability features for modifying the motion control algorithm and also for imparting intelligence to it so that it can perform multiple functions and execute variety of useful tasks, within the workspace as set by its mechatronic design, can be regarded as a walking robot.

1.3 “Biologically Inspired” Designs and Development of Walking Robots

Technology of industrial robot is quite mature, and the yearly production of large number of industrial robots around the world shows that robot manipulators have become an indispensable means of factory automation. These robots have fixed platform and cannot be used to perform some other jobs outside its fixed workspace when they are lying idle due to lack of mobility of its base. Therefore, a robot should not be fixed to the ground [16] and must have the capability of locomotion in order to act as a multifunctional machine and to perform a variety of tasks by virtue of its mechatronics and reprogrammability.

Even in the present state of the human civilization, the wheels remained the common means of propulsion and support for artificial terrestrial locomotion. This is mainly because wheeled vehicles can achieve high speed of locomotion at high energy efficiency and simplicity in design and control of wheeled vehicles. However, human and walking animals adopted legs as the means of propulsion during their locomotion due to the absence of continuously rotating joints in biological systems in nature mainly due to the physiological problems associated with the nutrient supply [1, 6]. Although the wheel-based locomotion is superior to the legged locomotion in terms of energy efficiency and higher operating speed, the maneuverability of wheeled vehicles is restricted in rough and cluttered environment. The all-terrain or off-road wheeled vehicles can only operate at a very slow speed (few miles per hour) and also necessitate large amount of power [1, 3] during rough terrain locomotion. Even large mammals can manifest larger speed and less power consumption compared to the wheeled vehicle during rough terrain locomotion. This fact is quite inspiring for the development and deployment of walking robots for fast and energy-efficient locomotion in rough terrain.

The design effort for a successful walking robot could be initiated either adopting classical engineering approach using (after refinement) the classical methods of multibody dynamics, principles of classical robotics (like *dexterity* and *manipulability*), and feedback control for the mechanical design and locomotion control of the robot [11, 17], or adopting as much from the biological paragons for locomotion for feasible mechanical designs and control architectures [18]. Studies of animal and insect behavior and locomotion have revealed several interesting facts about their morphological and neurological systems that have been optimized through millions of years of natural evolution in order to suit and adapt to their habitat [18–20]. The most significant of them are accumulation of a good amount of knowledge of geometrical structure and mechanical properties of legs and muscles, working principles of their sense organs and vision, functioning of their brain to generate various control actions, and generating deliberative and reflexive behaviors, cognitive functions, and intelligence [19, 21]. During the last three decades, there has been a growing interest for developing legged robots by amalgamating innovative engineering with scientific observations on legged animals that ultimately resulted in a number of artificial walking systems [6, 17]. In fact, careful observation of the biological world inspired

the robotics professionals in modeling robots based on the principles derived from walking animals, crabs, cockroaches, and ant and bee societies [19].

This *biological inspiration* may involve different degrees of inspiration: from vague resemblance to strict emulation [21]. At the one extreme, we could use the ideas from the observation of the biological world but not to copy them vividly. For example, the following observations [19, 21] from the biological world are quite interesting and may inspire robotics professionals:

- Animals use legs rather than wheels.
- Insects use six legs to generate stable locomotion.
- Legged animals employ bouncing principle during their movements and their legs bounce like pogo sticks, working like spring-mass systems that compress, store, and return energy, or six-legged animals run by using two legs on one side and one leg on the other to form a tripod that acts like one of our legs, while the opposing leg tripod swings forward.
- Arthropods with more than six legs use groups of legs from the front, mid, and rear sections to form the tripod.

At the other extreme, one could literally try to emulate, in every detail, a particular species of insect or animal to develop a walking robot. However, at present a true emulation of the biological system is not possible because the current level of maturity of mechatronics technology is far from the biological counterpart [4, 20]. For instance, muscle as actuation system in biological domain is superior to the present actuator and driver technology for leg construction and is much more effective for gait generation, lighter, more adaptive, fault tolerant, self-repairing, and with lower power consumption. Control systems inherent in biological world can adapt perfectly to environmental changes and requirements and are self-learning, highly adaptive, and self-repairing. The biological systems use completely different types of sensors than we use in the engineering applications, are much accurate, most of the time embedded inside the muscles and form a network, fault tolerant, and smart. Therefore, the biologically inspired design and development of walking machines may be started with the ideas from the interesting observations of the biological world and technology available for sensors, actuators, and control, remaining within the limits set by various practical constraints. It then improves upon the mechatronic design by application of high-performance optimization techniques and development of advanced control methods for the designed robotic system.

1.4 Classification of Walking Robots

During high-speed locomotion, any moving body may not fall on the ground even in the absence of proper support over the ground, provided it can maintain dynamic stability (viz., for any bounded change in command input, the system response is also bounded and does not fall out of step). This is called dynamically stable locomotion.

However, the same body when supposed to locomote over the ground at low speed, the locomotion is no longer a dynamically stable locomotion. Then the moving body needs proper support on the ground to maintain static stability in order to prevent fall on the ground. This is called statically stable locomotion.

Walking robots can be broadly categorized into two groups based on the stability in motion [9]: (1) passively or statically stable walking robots and (2) dynamically stable walking robots. The statically stable walking robots control their locomotion such that the legs in the support (*stance phase*) are placed on the foothold positions, followed by their *retraction*, and the legs in the swing(*transfer phase*) are lifted and moved for placing them in new foothold positions(*protraction*), should satisfy a constraint such that the vertical projection of the center of gravity of the walking machine is always contained within the succession of *support patterns* (*support polygons*) determined by the feet in contact with the ground. The locomotion speeds of statically stable machines are quite slow and they can stop their movement at any time in the locomotion cycle without losing the balance or stability of the robot body. Biped robot with large feet and in slow motion, quadruped robots in tripod gait (i.e., one leg in the air and three legs for support), and six-legged and eight-legged walking robots manifest static stability.

In dynamically stable walking robots, there is no such constraint as the static stability. Dynamically stable walking vehicles utilize dynamic forces and feedback to maintain control and are stable in a limit cycle that repeats once in each stride [9]. In such systems, velocity, kinetic energy, and potential energy of the walking robot play a crucial role [5]. Exchange of energy in various forms is important in dynamic locomotion of walking machines. Kinematic calculation, based on the geometry of the mechanisms alone, cannot precisely predict the motion of the dynamically stable system. Energy stored in different parts of the walking robot should also be considered in addition to the geometry of the mechanism for prediction of the motion of a dynamically stable system. Monopod hopping robot, biped or humanoid robot, and quadruped robots at high speed employ dynamic stability during their locomotion. Involvement of dynamics to stabilize the motion of the legged robotic systems renders them to be capable of balancing themselves actively. A legged robotic system that can balance it actively can tolerate the departure from static equilibrium. However, as the dynamically stable systems are more difficult to design and analyze than static systems, the early development of legged robots focused on statically stable machines.

Another very common classification of walking robots is based on the number of legs. Walking robots that have been developed so far are single legged (as the hopping machines developed at MIT) or multi-legged (like biped). Multi-legged walking robots are of biped (two-legged), quadruped (four-legged), hexapod (six-legged), or eight-legged types. Walking robots with one or two legs can only perform dynamically stable locomotion; therefore, they are preferred only for high-speed operations. Walking robots with more than two legs can perform statically stable locomotion and they are preferred for critical missions and low-speed operations.

Increasing the number of legs in a walking machine is advantageous to perform stable locomotion. For a machine with more legs, with vehicle speed and maximum foot return speed remaining unchanged, more legs support the machine at any instant, resulting in higher stability margin [6]. When a walking machine has more than four legs, it may be possible to recover its locomotion, though at reduced speed, from accidental situations when some legs are disabled. Moreover, maximum load each leg need to support will decrease with the increase in the number of legs; consequently, the leg design will become lighter. However, the arrangement and mounting of the legs and the associated linkages for driving their joints will become very complex due to the limited space available at the robot body. Control law for the coordination and control of the large number of leg joints will also become quite complex, and consequently the computational burden on the computer system will also increase to a great extent due to the execution of the control software in real time with the increase in number of legs. Most of the early machines were hexapods because six legs allow walking with a stable alternating tripod gait in which, at any instant, the machine can be supported by three legs (the middle leg of one side along with front and rear of the other). Statically stable walking requires that the machine should have a minimum of four legs so that three legs can maintain stability and the remaining one can be used for exchanging support. Since the isolation of the robot body from terrain irregularities requires at least three degrees of freedom in each leg, 12 independently controllable degrees of freedom are the minimum requirement for any statically stable terrain adaptive walker. For six- and eight-legged systems, these are 18 and 24, respectively. Therefore, choice of the number of legs is very critical while designing a walking robot intended for a particular application. Figures 1.1, 1.2, 1.3, 1.4, 1.5, 1.6, 1.7, 1.8, 1.9, and 1.10 depict few popular legged robots. Their working principles have been referred quite often in the literature [22–30].

1.5 Hexapod Walking Robots: A Popular Walking Machine for Field Robotics Applications

With the advent of civilization, the usefulness of the application of robot in hazardous and hostile environments outside the shop floor of the factory has been felt. For example, monitoring, repair, and maintenance inside nuclear reactor, mining of coal and minerals, oil exploration, subsea cable laying, cutting and mobilization of trees in dense forest, exploration on mars and moon, and land mine detection and removal. Therefore, a new area, popularly known as “field robotics,” has emerged which is characterized by the applications of robotics in the unstructured world to perform useful tasks. Thus, field robots should operate in remote, complex, or dangerous terrains like outdoors, underwater, underground, or even on other planets instead of shop floor of factories or other controlled settings. Therefore, autonomy in operation as well as in locomotion is advocated for field robots for performing the intended tasks in the hazardous and dangerous

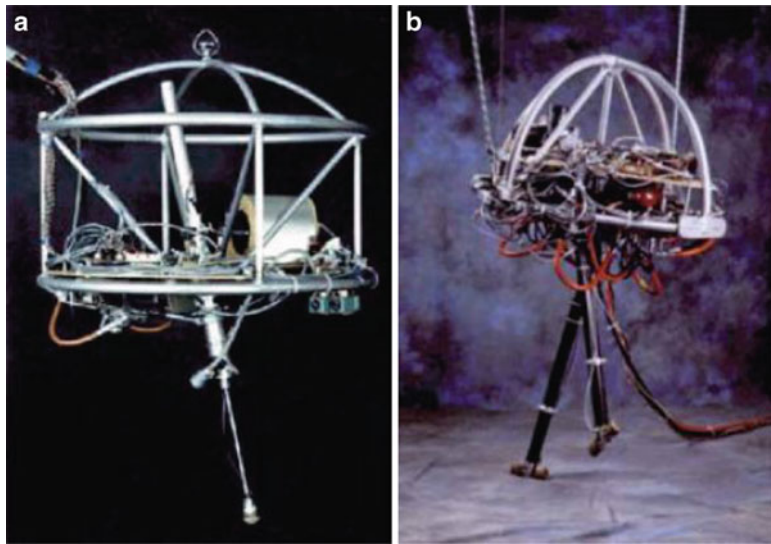


Fig. 1.1 Raibert's hopping robots [33]. (a) 3D one-legged Hopper [33], (b) 3D biped [33]

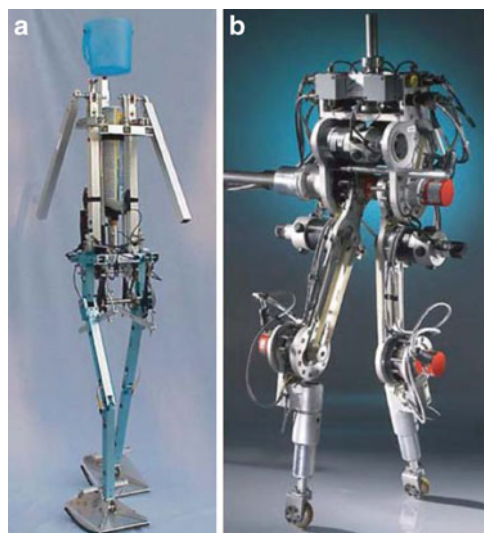


Fig. 1.2 Underactuated biped robots. (a) Denise [33], (b) Rabbit [33]

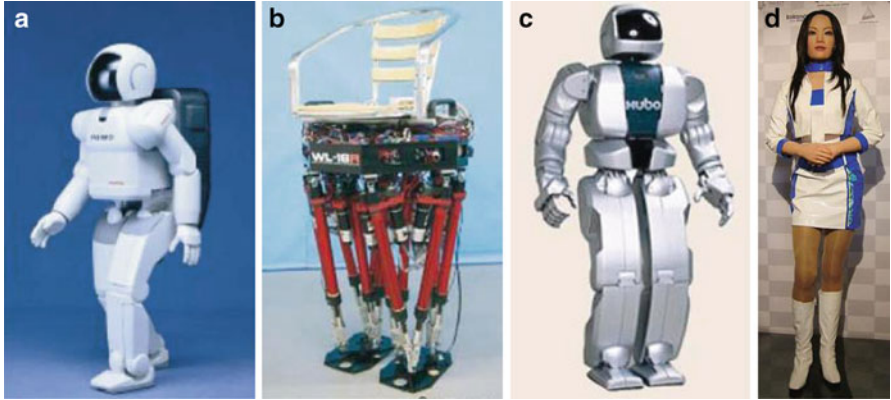


Fig. 1.3 Biped robots employing ZMP-based locomotion control. (a) ASIMO [33], (b) WL-16R [33], (c) HUBO [33], (d) Robot Girl

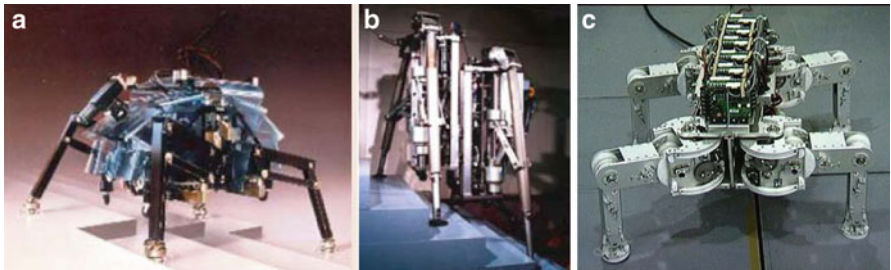


Fig. 1.4 Quadruped walking robot TITAN. (a) TITAN-III [33], (b) TITAN-IV [33], (c) TITAN-VIII [33]

domain of applications. Legged robots with enough static stability margins and sufficient degrees of freedoms are the best choice as field robots due to their inherent and robust capability for rough terrain adaptive locomotion. The present field robots are four-legged, six-legged, or eight-legged walking robots.

The field robot may need to carry large payloads consisting of the manipulators, end-effectors, various tools, various sensors, and sometimes carriages to pick up or place some kind of loads. As most of the natural terrain is rough in nature, the walking control for rough terrain locomotion of the legged robot becomes a challenging issue. In hazardous environment like mine field, the positioning control of the robot footsteps at the proper and permissible foothold positions is absolutely essential. Any wrong step of the robot during its walking may result into fatal consequences for the robot itself and others. Therefore, the walking robots should have the capability to adapt themselves in these situations when they are applied in field applications.

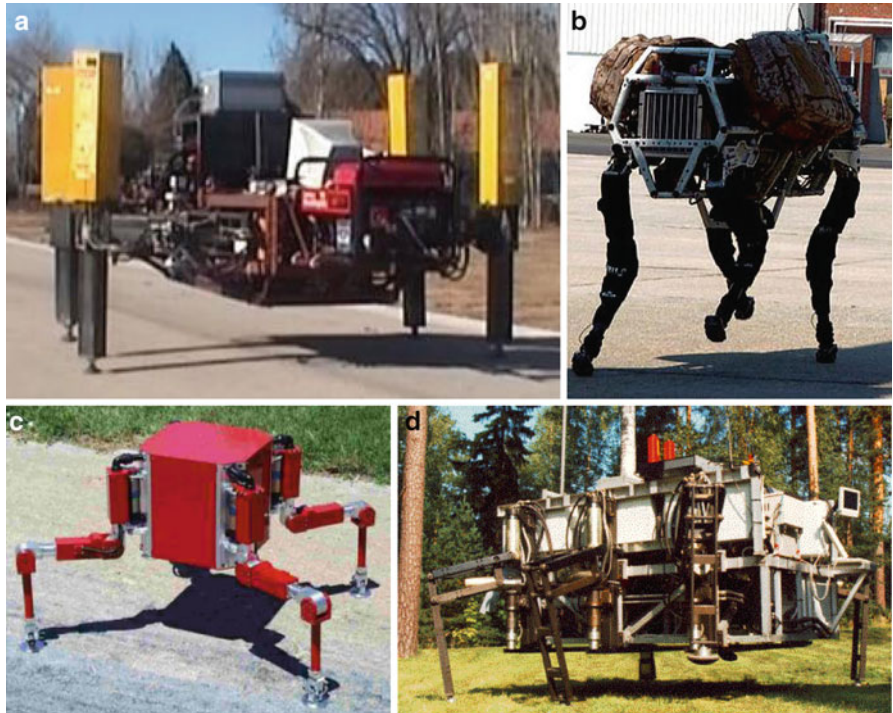


Fig. 1.5 Quadruped field robots. (a) ROBOCLIMBER [34], (b) Big Dog [33], (c) SILO4 [35], (d) MECHANT [36]

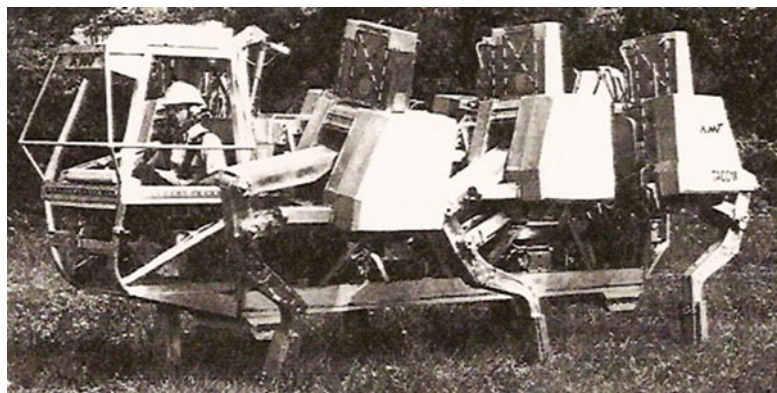


Fig. 1.6 Adaptive suspension vehicle [33]



Fig. 1.7 COMET (*Chiba university Operating Mine detection Electronics Tools*) robots.
(a) COMET-I, **(b)** COMET-II, **(c)** COMET-III, **(d)** COMET-IV



Fig. 1.8 Plustech, the forest-cutting machine employing legged locomotion [10]



Fig. 1.9 DANTE-II, an eight-legged robot for volcano exploration [33]

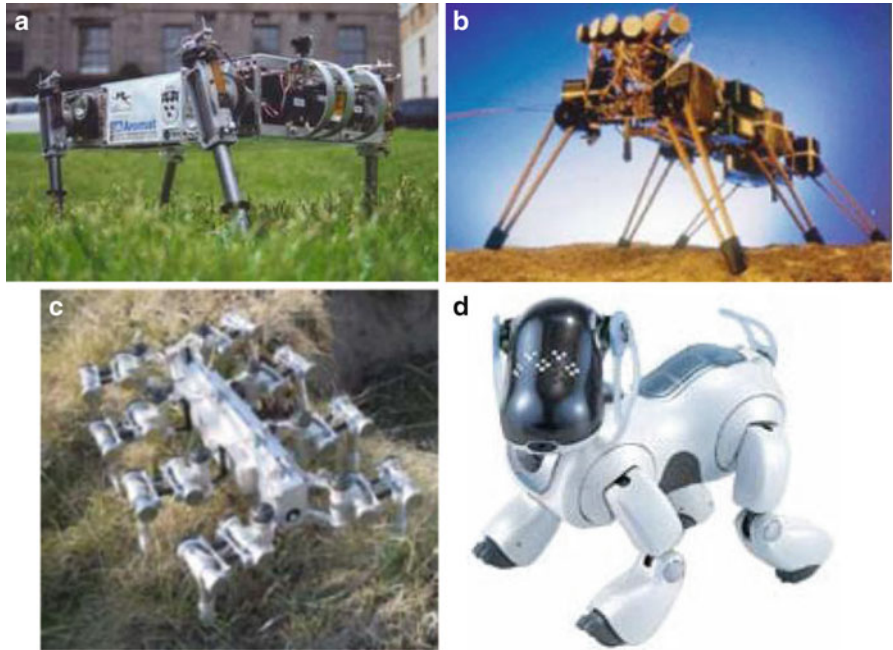


Fig. 1.10 Biologically inspired multi-legged robots. (a) SCOUT-II [37], (b) Genghis [33], (c) SCORPION [33], (d) AIBO [22]

It is quite clear that if the number of legs in a walking robot is large, the robot can use large number of footholds during locomotion making its locomotion very stable from the point of view of static stability and also results a stable body attitude of the walking robot. If the number of footholds increases, the robot can carry a larger payload with various gaits, thereby increasing the payload capacity of the robot. However, increasing the number of legs not only causes the increased power consumption but also makes the control system very complex. The field robots are expected to run in the remote field for a long time without recharging their battery or refueling the engine. Therefore, high rate of power consumption is always discouraged for field robotics applications. As a result, eight-legged robot has not become very popular for the field robotics applications. On the other hand, four-legged robots require less power and easier control systems, but they have very limited static stability margins. As they can lift only one leg during their locomotion and remaining three legs must support the body, they cannot locomote in very rough terrain and cannot choose any arbitrary foothold.

Six-legged or hexapod locomotion is a trade-off between the four-legged and eight-legged locomotion [31]. Six-legged robot can walk on the plain ground using regular gaits like wave gaits and also on the very rough terrain by free gait or follow-the-leader gait. They can cross any large obstacle, ascend on slope and descend from slope, and cross ditches very efficiently. Their power consumption is moderate and can carry quite large amount of payload. The use of six legs enables the robot to use three-, four- or five-leg support; therefore, it can select any arbitrary foothold while maintaining static stability and stable attitude. Six-legged creatures found in nature can carry a very large payload. For example, cockroach can move a weight of even 800 times its own weight [10]. These facts suggest that six-legged walking robot can be an ideal robot for field robotic application.

During the robot footstep planning for locomotion over rough terrain or hazardous terrain, the body velocity is varied depending upon the availability of the number of feasible footsteps. When the number of available feasible footsteps is limited, the robot body velocity is reduced by slowing down the propulsions of the robot legs. In that situation the robot must be able to properly support its body with the legs that are in the support phase so that the other legs (in the swing phase) can be placed in the next planned footsteps locations in the forward direction. This task can be carried out by the walking robot in a proper manner if the robot possesses a good amount of static stability margin. Hexapod walking robots can manifest various types of regular and irregular gaits during its locomotion. It can be shown [2] that in hexapod robot, the static stability margins for various gaits are quite high and most suitable for rough terrain locomotion. Moreover, different types of gaits of hexapod robot are advantageous for rough terrain locomotion because the robot can switch over from one gait pattern to another as per the nature and type of the terrain which may also save considerable amount of energy.

As the hexapod robots have six legs, they can carry large payloads. They can carry maximum payload during five-legged locomotion (*pentapod* configuration of *wave gait*) and minimum payload in three-legged locomotion (*tripod* configuration of *wave gait*). Moreover, placing the payload may change the center of gravity of

the whole robot body. The walking robot may face difficulty for maintaining the required static stability margin due to the frequent change in center of gravity. Hexapod walking robot can tackle this situation by properly changing the gait pattern during locomotion. Thus, application of hexapod walking robot for field robotics applications might be a prudent proposition.

1.6 Walking Robot Terminology

In this section we will describe the various definitions and terminologies often used in the study of multi-legged statically stable walking robots. For detailed descriptions and mathematical treatments, the readers may refer to [1, 2, 6, 32, 33].

1. *Transfer or swing phase*: The transfer phase (or swing) of a leg is the period in which the leg is in the air.
2. *Support or stance phase*: The support phase(or stance) of a leg is the period in which the leg is on the ground.
3. *Cycle time*: The cycle time is the time for a complete cycle of locomotion.
4. *Support pattern*: The support pattern of a legged system is a two-dimensional point set in a horizontal plane consisting of the convex hull of the vertical projection of all foot points in support phase.
5. *Gait*: A gait of any legged system is the corporate motion of the legs, coordinated with the motion of the body in order to move it from one place to another in such a manner that stability is always maintained. The condition for static stability of the system is that the vertical projection of its center of gravity falls inside the support pattern.
6. *Stability*: Stability of any walking machine state can be quantified by the parameter longitudinal stability margin, which is the shortest longitudinal distance from the vertical projection of the center of gravity to the boundaries of the support pattern in the horizontal plane (Fig. 1.11).
7. *Leg stroke*: Leg stroke (R) is the distance through which the foot is translated relative to the body during the support phase (Fig. 1.12).
8. *Duty factor*: The duty factor is defined as the fraction of the cycle time each foot is on the ground or is in the support phase(assumed to be the same for all feet).
9. *Leg phase*: The leg phase of a leg is the fraction of cycle time by which the contact of that leg on the ground lags behind the contact of the front leg of left side.
10. *Stride length*: The stride length is the distance the center of gravity translates during one complete locomotion cycle.
11. *Protraction*: Protraction is the forward movement of a leg relative to the body and ground.
12. *Retraction*: Retraction is the backward movement of a leg relative to the body with no movement of the leg relative to the ground.

Fig. 1.11 Longitudinal stability margin (d_1 : forward stability margin and d_2 : backward stability margin)

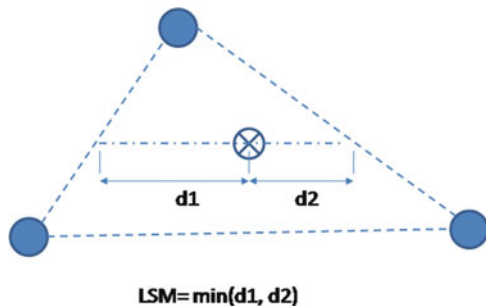
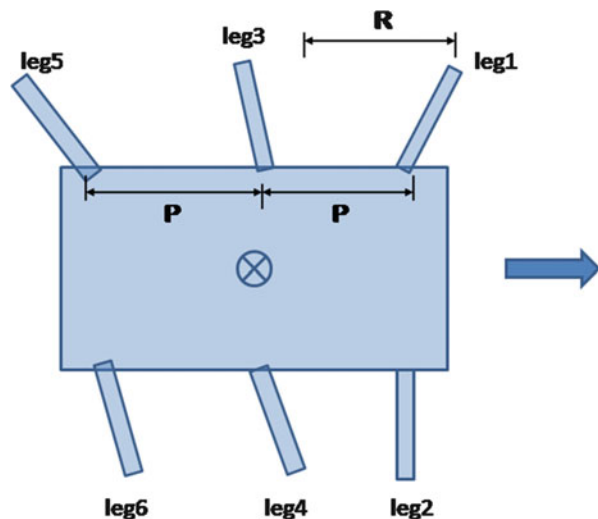


Fig. 1.12 Leg stroke in a typical walking robot



1.7 Challenges of Navigation and Locomotion Control of Hexapod Walking Robot for the Field Robotics Applications

Navigation of mobile robot involves self-localization of the robot and path planning for the safe locomotion by avoiding the obstacles, ditches, steep slopes, forbidden zones, etc. In case of walking robots, the navigation also involves obstacles negotiation when the robot can cross or climb on it or pass under it by proper maneuver of the body and legs. The path at first is planned in terms of the motion trajectory of the center of gravity of the robot body. But in field robotics applications, as the available feasible foothold positions ultimately determines the path for locomotion of the walking robot, the path of the body motion is to be transformed into foothold positions by kinematic transformations. Then the foothold positions are utilized to determine the foot trajectories depending upon the

type of the gait(s) the robot will follow. Foot trajectory must be planned keeping in view the optimum velocity profile of the foot at the swing phase so that the impact is minimum when it touches the ground. Foot trajectories are then utilized to calculate the leg joint angle trajectories employing the inverse kinematics of the leg mechanism. Impedance or force control may also be applied for achieving better locomotion performance compared to the position-based locomotion control. In hexapod walking robot, the navigation task is very much computation intensive because of the involvement of multiple gaits during path-planning stage for achieving terrain adaptive locomotion. Therefore, dedicated high-end computer systems are necessary when large number of sensor data is involved and various tools of Artificial Intelligence are employed.

Quite often the field robot may be required to perform the tasks in autonomous mode when the mission is not so critical and is repetitive in nature. Obviously, in autonomous operation the robot should have some amount of intelligence. The intelligent navigation and control algorithms will be necessary for autonomous navigation and task execution. Autonomous navigation task of hexapod robot may be quite complicated due to availability of multiple gaits and depending upon the amount of intelligence imparted on it. However, the execution of tasks in field robotics in autonomous mode does not require any special attention for hexapod robot.

References

1. McGhee RB (1985) Vehicular legged locomotion. In: Sirdis GN (ed) Advances in automation and robotics. Jai Press, Inc., Greenwich
2. Song SM, Waldron KJ (1989) The machine that walk: the adaptive suspension vehicle. MIT, Cambridge
3. Machado JAT, Silva M (2012) An overview of legged robots. <http://citeseerx.ist.psu.edu/viewdoc/summary?doi=10.1.1.106.8192>. Accessed 4 June 2012
4. Pfeiffer F, Josef S, Robmann T, Muchen TU (1998) Legged walking machines. In: Khatib O, Anibal TA (eds) Autonomous robotic systems. Springer, Germany
5. Raibert MH (1986) Legged robots. Commun ACM 29(6):499–514
6. Kar DC (2003) Design of statically stable walking robot: a review. J Robot Syst 20 (11):671–686
7. Arikawa K, Hirose S (2007) Mechanical design of walking machines. Phil Trans R Soc A 365(1850):171–183
8. Garcia E, Jimenez MA, Santos PGD, Armada M (2007) The evolution of robotics research. IEEE Robot Autom Mag 14(1):90–103
9. Boone G, Hodgins J (2000) Walking and running machines. In: MIT encyclopedia of the cognitive sciences. <http://rmf.net/~pennywiss/MITECS/Entry/boone.html>
10. Carbone G, Ceccarelli M (2005) Legged robotic systems. In: Kordic V, Lazinica A, Merdan M (eds) Cutting edge robotics. ARS International/pro literatur, Vienna/Mammendorf
11. Fu KS, Gonzalez RC, Lee CSG (1987) Robotics: control, sensing, vision, and intelligence. The McGraw Hill Companies, Inc., New York
12. Hirzinger G, Fischer M, Brunner B, Koeppe R, Otter M, Grebenstein M, Schäfer I (1999) Advances in robotics: the DLR experience. Int J Robot Res 18(11):1064–1087
13. Latombe JC (1991) Robot motion planning. Kluwer Academic Publishers, Massachusetts

14. Groover MP, Weiss M, Nagel RN, Odrey NG (1986) Industrial robotics – technology, programming, and applications. McGraw-Hill Book Company, Singapore
15. Trevelyan J (1999) Redefining robotics for the new millennium. *Int J Robot Res* 18(12): 1211–1223
16. Kobayashi HP, Inagaki K (1991) Basic design of a hexapod walking robot. *Fifth Int Conf Adv Robot* 2:1526–1529
17. Pfeiffer F, Eltze J WHJ (1995) Six-legged technical walking considering biological principles. *Robot Auton Syst* 14(2–3):223–232
18. Dillmann R, Albiez J, Gabmann B, Kerscher T, Zollner M (2007) Biologically inspired walking machines: design, control and perception. *Phil Trans R Soc A* 365:133–151
19. Voth D (2002) Nature's guide to robot design. *IEEE Intell Syst Mag* 17:4–6
20. Quinn RD, Ritzmann RE (1998) Construction of a hexapod robot with cockroach kinematics benefits both robotics and biology. *Connect Sci* 10(3–4):239–254
21. Beer R, Quinn RD, Ciel HJ, Ritzmann RE (1997) Biologically inspired approaches in robotics: what we can learn from insects. *Commun ACM* 40(3):30–38
22. Roennau A, Kerscher T, Dillmann (2010) Design and kinematics of a biologically-inspired leg for a six-legged walking machine. In: Proceedings of the 3rd IEEE RAS and EMBS international conference on biomedical robotics and biomechatronics, Tokyo, pp 626–631
23. Hasslacher B, Tilden MW (1995) Living machines. *Robot Auton Syst* 15(1–2):143–169
24. Weidemann HJ, Pfeiffer F, Eltze J (1994) The six-legged TUM walking robot. *Proc IEEE/RSJ/ GI Int Conf Intell Robots Syst* 2:1026–1033
25. Nonami K, Huang Q, Komizo D, Fukao Y, Asai Y, Shiraishi Y, Fujimoto M, Ikeda Y (2003) Development and control of mine detection robot COMET-II and COMET-III. *JSME Int J Ser C* 46(3):881–890
26. Zielinska T, Goh T, Chong CK (1999) Design of autonomous hexapod. In: Proceedings of the 1st IEEE workshop on robot motion and control, Kiekz, pp 65–69
27. Zielinska T (2000) Efficiency analysis in the design of walking machines. *J Theor Appl Mech* 3(38):693–708
28. Nonami K, Ikeda Y (2004) Walking control of COMET-III using discrete time preview sliding mode control. In: Proceedings of the IEEE/RSJ international conference on intelligent robots and systems, Sendai, pp 3219–3225
29. Barai RK, Nonami K (2007) Locomotion control of a hydraulically actuated hexapod robot by robust adaptive fuzzy control and dead zone compensation. *Robotica* 25(3):269–281
30. Braunl T (2008) Embedded robotics. Springer, Germany
31. Bailey P (1994) The merits of hexapods for robotic applications. *Proc IEE Colloquium Next Steps Ind Robot* 8:1–6
32. Kar DC, Issac KK, Jayarajan (2003) Gaits and energetic in terrestrial legged locomotion. *Mech Mach Theory* 38(4):355–366
33. Kajita S, Espiau B (2008) Legged robots. In: Siciliano B, Khatib O (eds) Springer handbook of robotics. Springer, Germany
34. Nabulsi S, Montes H, Armada M (2005) ROBOCLIMBER: Control system architecture. In: Armada M, Santos PG (eds) Climbing and walking robots. Springer, Berlin, pp 943–952
35. Santos PG, Garcia E, Estremera J (2006) Quadrupedal locomotion: an introduction to the control of four-legged robots. Springer, London
36. Hartikainen K, Halme A, Lehtinen H, Koskinen K (1992) MECANT I: a six legged walking machine for research purposes in outdoor environment. In: Series B, Technical Reports, 6. Helsinki University of Technology, Automation Technology Laboratory, Helsinki
37. Kimura H, Tsuchiya K, Ishiguro A, Witte H (2006) Adaptive motion of animals and machines. Springer, Tokyo

Chapter 2

Historical and Modern Perspective of Walking Robots

Abstract Study of historical evolution and modern point of view on a complex subject like robotics invokes motivations and professionalisms among the researchers. Research on walking machines started at the time of Leonardo da Vinci and that ultimately culminated into the development of the modern walking robots through the transformations and refinements of the ideas and design methodology over the centuries. Obviously, the allied technology of mechatronics, particularly for sensing, actuation, and control, available at various points of time in the past influenced the design and implementation of walking robot quite heavily. The urge for mimicking the walking creatures in the past and the various efforts to apply the knowledge gathered from the observations of the biological world in the design and control of walking robots has added a new dimension as well as posed many new challenges in the walking robot research. However, the various challenges faced during the design and implementation of walking robots in the past and lessons learned from them to overcome those challenges enriched the technology of walking robot and drove it toward maturity. Therefore, the knowledge of the historical evolution of walking robotics research and its modern point of view will definitely inspire a robotics researcher for undertaking new challenges for the design and development of walking robots and will also guide him to take correct design decision. This chapter presents the historical evolution of walking robots and its perspective in a condensed manner.

2.1 Introduction

The locomotion over a hard or soft solid surface by means of one or more limbs or legs can be defined as walking [1]. Walking in various forms observed among the insects and legged animals has always fascinated the mankind since the ancient time [2]. The hopping motion of kangaroo, dynamically stable locomotion of human, trotting and galloping motion of horse, statically as well as dynamically stable locomotion of quadruped animals, hexapod locomotion of cockroach and crabs,

and multi-legged locomotion (with more than six legs) of centipedes and millipedes motivated him to understand the underlying science of legged locomotion. They observed that legs are the most feasible solution for locomotion in the natural terrains consisting of obstacles like large rocks, loose soil, deep ravines, and steep slopes, because legged animals can avoid small obstacles by making discrete contacts and passing up undesirable footholds, can climb over obstacles and step across ditches, and can also get through terrain discontinuities of body scale while maintaining the body leveled and stable. Although wheels and wheeled vehicles were established technology since ancient time of human civilization, since then people were also curious to learn the technology of legged locomotion for conquering the rough terrain with walking machines. However, it took many centuries to develop at least a walking mechanism due to lack of the knowledge of mechanics and mechanism of legs and coordination and control associated with legged locomotion.

There is a long history associated with the evolution of walking machines [3–6]. From the ancient time, mankind was curious about development of artifacts that resembles to the animals and human. Mechanically powered walking machines and mechanisms in the disguise of animals and humanlike appearance can be traced back during the era of Greek civilization. Conceptual design and sketches of artificial systems and mechanisms capable of humanlike locomotion appeared in Europe during the time of renaissance. The artifacts that were materialized from their conceptual design mainly depended on complex mechanical systems comprising of many linkages, gears, cams, shafts, etc. for the control and coordination of the legs during the locomotion. This trend continued even after a decade of the Second World War. The walking robot technology was revolutionized with the application of computer and electronic circuits for the control and coordination of legs and generation of gaits for terrain adaptive locomotion. More and more advanced walking robots were later developed with the advancement of various branches of science and technology. With the present state of the art, the day is not very far when a fully autonomous and intelligent robot will become a part of the family to serve and give company to the human after complying with the social norms [37].

From the ancient era till the present time, the continuous efforts devoted by mankind for mimicking the walking creatures for the design and control of walking robots have added a new dimension as well as posed many new challenges in the walking robot research. However, lessons learned from the various challenges faced during the design and implementation of walking robots in the past while applying the knowledge gathered from the observations of the biological world and the techniques invented to mitigate those challenges enriched the technology of walking robot and drove it toward maturity. Therefore, the knowledge of the historical evolution of walking robotics research and its modern perspective will guide a robotics researcher in the proper direction during the design and development of walking robots as well as inspire and motivate him to undertake new challenges with professionalism.

2.2 Historical Perspective of Walking Robots

Like many other branches of engineering, the legged robotics research also emerged from imagination and innovative ideas and then refinements through prototyping and experimentations. In this section, we will give a concise historical account of the thoughts and ideas as well as the development of engineering of legged robot at various times in a chronological order. At first we will describe the emergence of artificial legged locomotion from imagination and ideas during the ancient times. Then we will give a chronological portrayal of the evolution of the technology of walking robots till the present time.

2.2.1 *Emergence of Artificial Legged Locomotion from Ancient Civilizations: Imagination, Ideas, and Implementations*

The interest to understand the technicalities of legged locomotion observed in nature and the efforts to replicate them to mobilize the artifacts by leg mechanisms have been mentioned in the mythology and ancient scripts from the ancient Greek, Indian, Egyptian, and Chinese civilization [2]. Although no technical details of the design and development of these ancient walking devices and the associated mechanisms are available, the imagination and ideas propounded by them are quite interesting and stimulating. These ideas, although not always emerged from the principles of physical science but from the common sense and the applied knowledge of craftsmanship, were pioneering in the history of the development of walking machines and sowed the seed of legged robotics research.

Homer (VIII c. BC) mentioned about one of the Greek gods in his great epic Iliad who built humanlike and many other different types of walking devices. Descriptions of mechanical elephants have been found in ancient Indian scripts [2]. A mechanical wooden dog dated around XX c. BC has been discovered from the Egyptian pyramids. Mimicking human and animal motions for creating artificial moving figures started in the society of ancient civilized nations around the Mediterranean region for decoration of the water organs and water clocks. Ctesibius (c. 270 BC), a genius and Greek engineer, was the precursor of creating this type of devices and applied his knowledge on pneumatics and hydraulics to produce the organ and water clocks with moving figures [3, 7]. His inventions of various types of moving figures, mimicking human and animal motions, were later complied by his student Philo of Byzantium (c. 200 BC) in his book “Mechanical Collection.” Hero (c. 85 AD), a genius from Alexandria, was influenced by the practical works of Ctesibius and wrote the first well-documented technical account on realizable robots: “On Automatic Theaters,” “On Pneumatics,” and “On Mechanics” [3]. He put forward the theaters with moving inanimate figures and was the precursor of entertainment robotics. The Greeks named these machines as “automatos” meaning

“machine that imitates the figure and movements of an animate being,” and it is believed that the current word automation has been originated from this word [8].

A wooden walking machine known as *Mu Niu Lu Ma* was built in the III c. AD in Sichuan province of China, under the supervision of a Chinese officer Zhu Ge-Liang during the preparation for the war against Wei kingdom. In Chinese, *MU* means wooden, *MA* means horse, *NIU* means cow, therefore, after free translation *Mu Niu Lu Ma* means “a device powerful as horse and fast as cow.” The *Mu Niu Lu Ma* walking machine, when pushed, transferred its legs in a sequence similar to that of a cow or a slowly moving horse. *Mu Nu Liu Ma* was used as a wheelbarrow for transportation of food supplies needed by the army. The machine was able to cover a distance of 10 km in a day in the rough terrain while carrying a load of 200–250 kg. However, no design details of *Mu Nu Liu Ma* are available [2]. This story of *Mu Nu Liu Ma* fascinated many researchers in China and Taiwan to reconstruct it in later times. The prototype reconstructed by Wan Jian from Xinjiang Institute of Technology (XX c) was the most famous one. His prototype was a very complex one consisting of ten links in each leg mechanisms resembling by view the horse or cow. The size and proportions of the mechanical components was chosen such that the leg-end trajectories were similar to the trajectories observed during walk of animals.

In the early ninth century the Khalif of Baghdad (786–833) took an initiative to retrieve the Greek texts that had been preserved by monasteries and scholars during the decline and fall of western civilization. He deputed three men, the Banu Musa, for this great mission. They compiled a great book *Kitab al-Hiyal* (The Book of Ingenious Devices) describing over hundred devices based on the works they collected while incorporating some additions of their own. The next significant work on automation was performed in the XII century AD by Badi’al-Zaman Isma’il ibn al-Razzaz al-Jazari. He compiled the text “The Science of Ingenious Mechanisms” consisting of various existing designs and some of his own inventions. He constructed a figure which upon manual emptying of a water basin automatically filled it again with water [8]. He also developed many other mechanical figures that were actuated by the force of gravity transferred by levers or hydraulics to move the limbs of figures.

The Arabs preserved, disseminated, researched, and applied the knowledge base of the Greek on the design and development of robotic mechanism during the age of decline and stagnation in the western civilization. This knowledge base later helped the scholars and genius like Leonardo da Vinci for the design and development of various mechanisms and robotic systems during the Renaissance of Europe [9]. It is interesting to note that the Arabs were interested to design and develop the mechanisms not only for creating dramatic illusion like Greeks but also for manipulating the environment for human comfort. Therefore, the greatest contribution of the Arabs was the idea of practical application of the earliest robotic science; this was the key element that was missing in Greek robotic science [8].

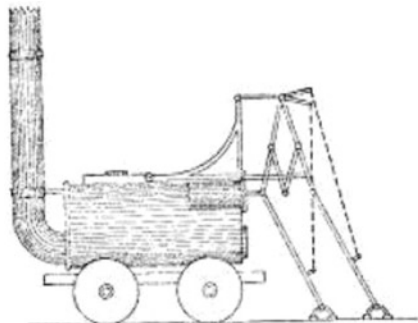
Leonardo da Vinci (1452–1519) was one of the great talents throughout the ages who performed much research and development works on robotics in a systematic manner with scientific outlook. The Renaissance revived the interest in the ancient

Greek art and science and at the same time also promoted the aspiration to verify, reconstruct, and improve upon the ancient achievements. Inspired by the spirit of Renaissance as well as Hero's works through the translated Arab texts, Leonardo actively engaged himself in verifying Greek reconstructions. A strong craftsmanship background acquired in his childhood apprenticeship in drawing, painting, sculpture, and architecture at Andrea del Verrocchio's workshop, as well as self-taught engineering and anatomy knowledge, provided Leonardo with the skills necessary to start where the ancient Greeks had ended [3]. His knowledge in anatomy and skill in drafting, metal working, tool making, armor design, and sculpture enabled him to build robotic mechanisms and machines. He used spring mechanisms as actuators in his ingenious machines [2]. Between 1495 and 1497 he designed and possibly built the first articulated anthropomorphic robot in the history of western civilization [3, 8, 10]. This armored knight, externally appeared as a typical German-Italian suit of armor of the late fifteenth century, was designed to sit up, wave its arms, and move its head via a flexible neck while opening and closing its anatomically perfect jaw. It was made of wood with parts of leather and brass or bronze and was cable operated.

In the XVI and XVII c., as the precision mechanics capabilities improved, dolls dancing and/or playing diverse musical instruments were designed by many watchmakers [2]. As we move through the ages toward the more recent time, examples of toys or machines with manipulation or locomotion abilities become more abundant. An excellent example of mechanical dolls was the mechanisms built in the XVIII c. by Swiss watchmakers Pierre Jaquet-Droz, Jean Frederic Leschat, Henri Jaquet-Droz, and Henri Millardet. Those dolls were programmable by exchange of pegs pushing cams. The dolls were capable of drawing and writing. As they were programmed, what was written or drawn could be changed. Very complex gears, cams, and levers inside their bodies were powered by spring mechanisms. Droz brothers miniaturized the mechanical components. In their dolls they often applied mechanism transferring the motion by chains and teeth wheels. Until now this mechanism in large size was used in milling machines, steam engines, and wall clocks.

In the eighteenth century, skilled craftsmen from the clock and watchmaking industry of Switzerland were hired, and the base technology of precision mechanical devices available in Switzerland was also adopted to build mechanical puppets in Europe [3]. These were basically entertainment devices and were programmable through stacked cams for achieving sophisticated movements. A mechanical duck was built by Jacques de Vaucanson and displayed throughout Europe in 1738. It was driven by multiple cams with one wing containing over 400 parts and was capable of eating, drinking, quacking, splashing its water, and even defecating. Excellent mechanical dolls were created by Swiss watchmakers Pierre Jaquet-Droz (1721–1790), Jean Frederic Leschat, Henri Jaquet-Droz, and Henri Millardet [2, 8]. Those dolls could write and draw figures and were programmable by exchange of pegs pushing cams. Very complex gears, cams, chains and teeth wheels, and levers inside their bodies were powered by spring mechanisms.

Fig. 2.1 Sketch of one of the first steam engine vehicles with legs [2]



From the XVII till the XIX century, legs were used as prerequisite for propulsion. An excellent example of a vehicle supported by wheels, but powered by legs, is the so-called Blueprint vehicle in XVIIIc. [2]. In the early steam engine vehicles, it was difficult to initiate and stop the motion of the vehicle due to low friction between the wheels and rails. Therefore, legs were added to stop and push the steam engine vehicles running over the rails [2, 3] (Fig. 2.1).

In 1850, the Russian mathematician Chebyshev presented a model for a locomotion system. It used a kinematic linkage to move the body along a straight horizontal path while the feet moved up and down to exchange support during stepping [3, 11]. People at that time viewed the task of building walking machines as the task of designing linkages that would generate suitable stepping motions when driven by a source of power [11].

Eadweard Muybridge was the pioneer in the study of animal locomotion on a scientific setting. He studied the different gaits of horses from the still photographs of trotting horses [3, 11, 12]. The results of this work were published on the Scientific American journal in 1878. After this initial study, Muybridge also studied and documented the gaits of 40 other mammals, including the gaits of human. His research and photographic data are still quite valuable resource for the modern robotics research and survived as a landmark in locomotion research.

L. A. Rygg in 1893 proposed the first quadruped machine, named “The Mechanical Horse” [3, 13] (Fig. 2.2). *The Mechanical Horse* was patented on 14 February 1893. In the design the stirrups were used as pedals so that the rider could power the mechanisms. The movement from the pedals was transmitted to the legs through gears that would result the stepping motions. However, there is no evidence to prove that he actually built this machine.

The Steam Man, a biped machine, was proposed by Georges Moore in 1893. Perhaps it is the earliest successful biped [3] (Fig. 2.3). It was powered by a 0.5 hp gas-fired boiler and reached a speed of 14 km/h. Stability was aided by a swing arm that guided him in circles. Traction was aided by heel spurs, smoke flowed from his head and steam from the nose, and a pressure gauge was conveniently mounted in his neck [8].

Fig. 2.2 Sketch of one of the first quadruped machines: *The mechanical horse* [3, 13]

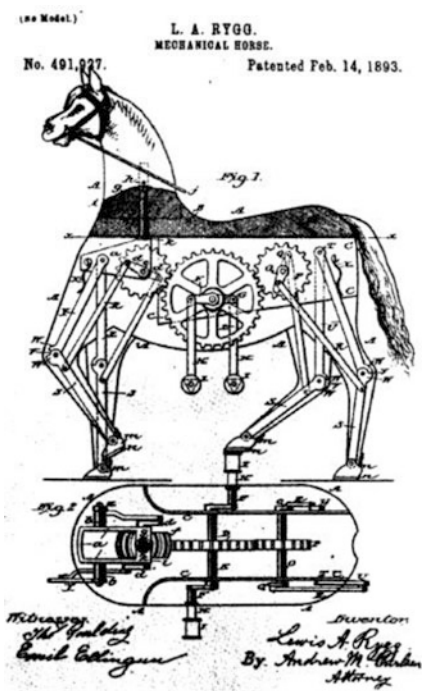
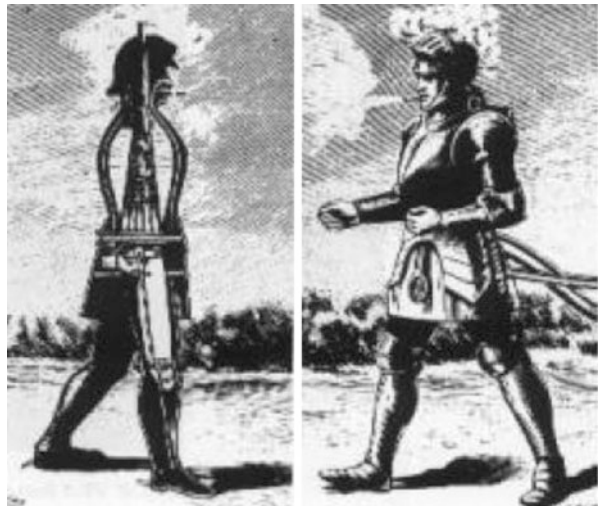


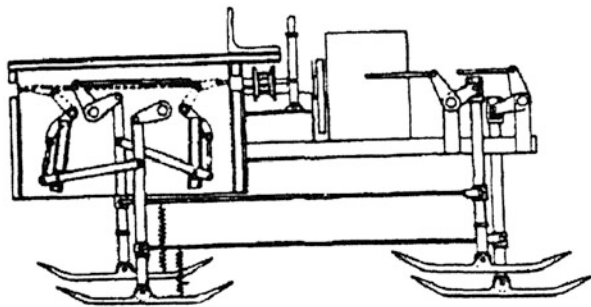
Fig. 2.3 The first biped machine: *Steam man* [3]



In 1913 the Bechtolsheim Baron patented a quadruped machine, shown in Fig. 2.4. There is no concrete evidence whether this machine was actually built [3, 13].

Although it is not quite apparent that which of the previously mentioned devices should be considered the first robot, the origin of the term “robot” is well known.

Fig. 2.4 Bechtolsheim baron's quadruped machine [3]



Karel Čapek, a Czechoslovakian playwright, introduced the term “robot” from the Czech word “robota” meaning slave work, in a play called R.U.R. (Rossum’s Universal Robots) in 1921 [14]. R.U.R. was a play about humanlike servants that were artificially created out of biological tissues to serve humans in factories and in the army. Čapek called these artificial workers as “robots” [3, 7].

Later on in 1940, the idea of what is a robot and what are its capabilities was influenced by science fiction, mainly due to Isaac Asimov [3]. Isaac Asimov produced a series of short stories about robots for Super Science Stories magazine. Over the next 10 years he produced more stories about robots that were eventually recompiled into the volume “I, Robot” in 1950. Asimov is generally credited with the popularization of the term “Robotics” which was first mentioned in his story “Runaround” in 1942. But probably Isaac Asimov’s most important contribution to the history of the robot is the foundation of his Three Laws of Robotics [7, 14]:

Law 1: A robot may not injure a human being, or, through inaction, allow a human being to come to harm.

Law 2: A robot must obey the orders given to it by human beings except where such orders would conflict with the First Law.

Law 3: A robot must protect its own existence as long as such protection does not conflict with the First or Second Law.

Asimov later adds a “zeroth law” to the list:

Zeroth law: A robot may not injure humanity, or, through inaction, allow humanity to come to harm.

From the foregoing discussion it is clear that various novel ideas related to artificial walking mechanisms emerged from the ancient times till the nineteenth century. Although the development of mechanisms dominated in most of the cases, other aspects of walking machines like actuation, sensing, and control got very little attention from the developers due to the technological bottleneck prevailing at the contemporary period. Nevertheless these inventions were great inspirations for the next generation robotics engineers for the design and development of more advanced and more sophisticated autonomous walking machines to perform the intended tasks. XX c. was marked by an extensive development of diverse walking machines, and the history of walking machines after the Second World War is very rich and will be described in the next section.

2.2.2 Evolution of Modern Walking Robots

Like many other branch of science and engineering, walking robotics research also gathered a new momentum after the Second World War due to the new inventions in mechanisms, material science, electronics, control system, and computers. This laid the foundation of modern walking robotics research for the systematic design and development of walking machines for their intended applications in rough terrain. A number of research groups started to study and develop walking machines in a systematic manner from the mid-1950s. It took another decade to successfully design and build modern walking machines [13, 15].

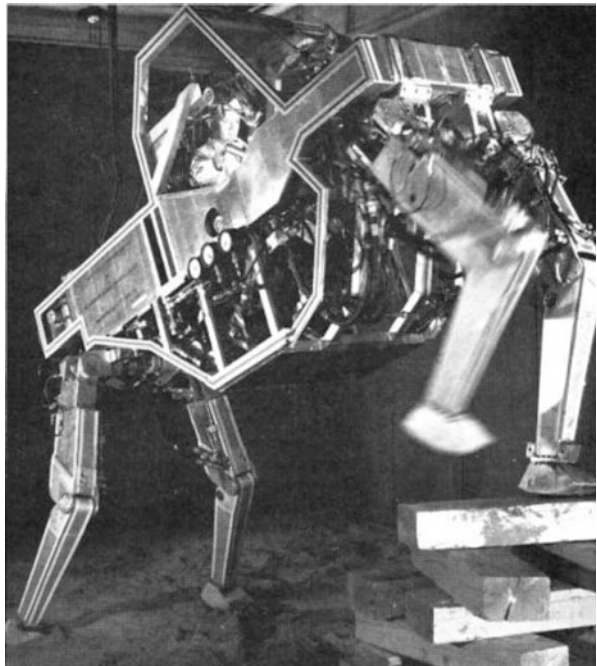
In 1960, an extensive research of linkage mechanisms for legged locomotion was performed by Shigley [3, 12]. He proposed several leg mechanisms based on four-bar linkages, cam linkages, pantograph mechanisms, etc. for walking machines. He also built a vehicle with four rectangular frames where each frame was nearly as long as the body and served as a leg. The legs were controlled by a set of double-rocker linkages and they had to move in pairs, and the stroke was quite short to ensure static stability. Although it worked, but it required noncircular gears for uniform velocity of foot motion and was found as impractical [3, 12, 13].

In the early 1960s, Space General Corporation developed one six-legged externally powered and another eight-legged with self-contained power source walking machines for their application as lunar rover with legged locomotion [3, 13]. The leg motions of both machines were coordinated by cams and transmitted by linkages. However, their terrain adaptability was poor due to lack of the necessary degrees of freedom.

Ralph Mosher of General Electric's General Engineering Laboratory started developing a four-legged walking truck, also known as the "General Electric quadruped" (Fig. 2.5), in the mid-1960s and finished the project in 1968 [3, 16]. This vehicle has three degrees of freedom (DOF) per leg—one in the knee and two in the hip. Each DOF was actuated through a crank by a linear hydraulic cylinder [13]. This vehicle, with 3.3 m height, 3 m long and 1,400 kg weight, was propelled by a 68 kW internal combustion engine. The machine control was dependent on a well-trained operator in order to function properly. The operator controlled the four legs through four joysticks and pedals that were hydraulically connected to the robot legs, with force reflection [3]. Controlling 12 DOF by human as a "supervisory controller" in the control loop was quite demanding. For this reason few people were able to operate it, and they also used to get tired after some time. However, this invention is very important in the history of modern walking robots because it demonstrated a walking machine capable to surpass obstacles and with good mobility in difficult terrains with versatile gaits. Nevertheless, it became clear that it was needed a computer control system for the coordination and control of the sequence of actuation of the leg joints.

The breakthrough development in the history of walking robots came in 1966, when a four-legged walking machine known as the "Phony Pony" (Fig. 2.6) was built by McGhee and Frank at the University of Southern California. This was the

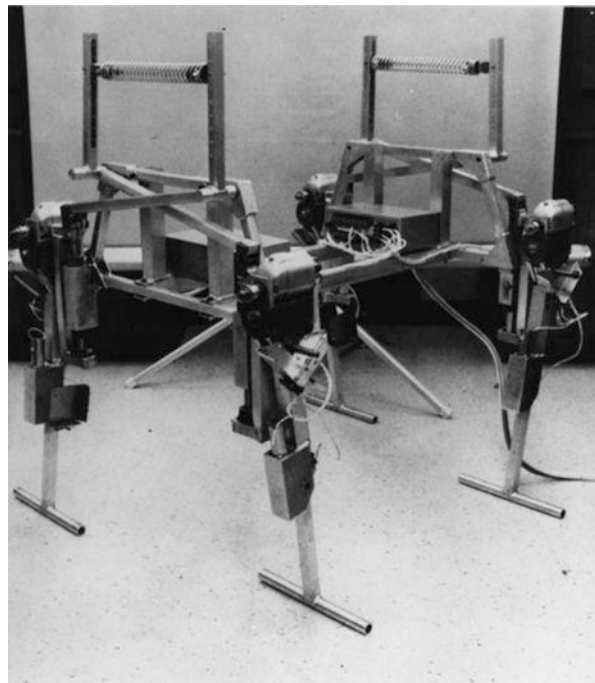
Fig. 2.5 General electric quadruped [3, 11]



first walking vehicle to walk under full computer control [13]. Phony Pony had two DOF in each leg, and the joint coordination was performed by the contemporary “digital computer” instead of cams or linkages. The leg mechanism had two links and two joints. Both joints were actuated by electric motors through a worm gear speed reduction system. The machine was powered externally through a cable. Phony Pony could walk with two different gaits: *the quadruped walk* and *the quadruped trot*. This was the big limitation of this walking machine that it could only walk in a straight line and not able to turn.

The research on biped locomotion, when compared with the multi-legged case, has advanced more slowly due to the difficulty in establishing a stable locomotion because biped robots are more demanding for their dynamic balance. However, development in robots with two legs occurred in much the same way as those with more legs [17]. Since the end of the 1960s, researchers at the Waseda University in Japan have developed a series of computer-controlled biped systems. In 1969, Ichiro Kato developed the biped robot WAP-1 at the Humanoid Research Laboratory. For its actuation, this robot had artificial rubber muscles, pneumatically actuated, and the biped locomotion was achieved through the playback of previously taught movements. Early bipeds had to be connected to large computational devices. WAP-1 used computers to alter artificial muscles connected to a twin-legged frame. The main initial limitation of this machine was its low speed, needing 90 seconds in order to complete a step. Latter advancements allowed reaching speeds near those achieved by human beings. Wap-2 and Wap-3 were

Fig. 2.6 Phony pony:
The first computer-controlled walking robot [3]



developed in 1970 and 1971, respectively. Wap-3 was able to move its center of gravity on the frontal plane so that it was able to walk not only on a flat surface, but it could also descend and ascend a staircase or slope and turn while walking. The three-dimensional walking and turning that Wap-3 achieved were the first in the world. It was directed by a controller-based memory. Kato went on to develop numerous other biped machines and is regarded as a one of the main pioneers in the biped robotics research. In 1973, Kato constructed a humanlike robot known as Wabot-I. It was the first full-scale anthropomorphic robot in the world and was highly sophisticated. It had a limb control system, a vision system, and a conversation system. It was estimated that it had the mental ability of a one-and-a-half-year-old child [17]. Kato developed a variety of robots in the 1980s and applied 16-bit microcomputer to design versatile control system for the bipeds. He also built biped robot for the first time in the world that could perform quasi-dynamic walking. In 1985 Kato and his group developed a new robot that could descend stairs and slight inclines. This is far harder to do with a biped than quadrupeds because of the decreased stability and complex balance issues. In 1989 Kato and his group developed a walking control method (implemented in the WL-12RIII) which enables stable walking under unknown external forces and moments by using “cooperation motion of a trunk and lower limbs.” This enabled increased speed of movement whilst ascending or descending stairs because of the added stability that this new system provided.



Fig. 2.7 The *big muskie* [3]

In 1969, Bucyrus-Erie Co. developed the *Big Muskie* (Fig. 2.7) for use in an open-air coal mine. It is perhaps the biggest off-road walking machine built so far and weighing around 15,000 ton. This machine had four hydraulically actuated legs. When it moved, the four legs raised the body and moved forward or backward one stride and then lowered the body on the ground. While the body remained on the ground, the legs lifted and moved to the next position. This motion was cycled by an electronic sequencer [3, 13].

In 1972, a group at the Institute Mihailo Pupin in Belgrade, Yugoslavia, built a pneumatically actuated biped exoskeleton to help paraplegics. It was controlled by analog computer [13].

In 1972, a six-legged walking machine was built by Petternella and his associates at the University of Rome [13]. It was actuated by electric motors and was similar to the Phony Pony in its control structure. They also attempted to establish interaction between the human operator and the walking machine.

Since 1972, Professor Kato at Waseda University, Japan, developed a series of computer-controlled bipeds [13]. These biped walking machines could operate at a very slow speed and could climb stairs under the control of an operator.

In 1974, a six-legged vehicle was built at Moscow Physico-Technical Institute in Russia. Subsequently in 1978, Okhotsimski and his colleagues described about the development of two six-legged walking machines [13]. One of these six-legged walking machines was controlled by analog computer and the other one was equipped with a scanning distance-measuring system. Both the machines were powered externally, and one of them could turn in its body length. The machines had insect-type legs with three DOF with one upper link and one lower link. The joints were actuated by motors and gears, and foot pad was attached on the lower link with a gimbal joint.

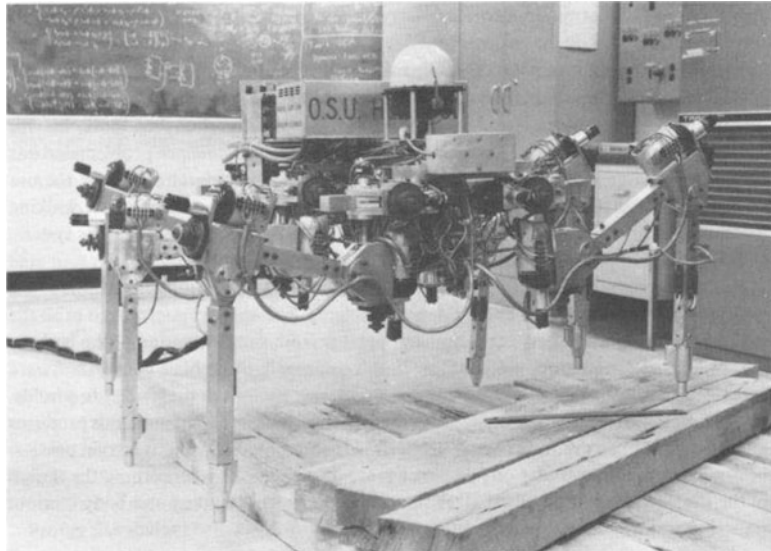


Fig. 2.8 The OSU hexapod [18]

In 1977, the OSU Hexapod was built by McGhee and his associates at the Ohio State University to study control algorithms for a walking machine [18] (Fig. 2.8). It was a six-legged walking machine and weighing about 300 pounds. It was fully controlled by a PDP 11/70 computer via an umbilical cable and was powered externally through a cable. Each leg of this vehicle had three DOFs and consisting of two links connected by joints, and each joint was actuated by an electric motor through a worm gear. The walking vehicle was later equipped with force sensors, gyroscopes, proximity sensors, and a camera system.

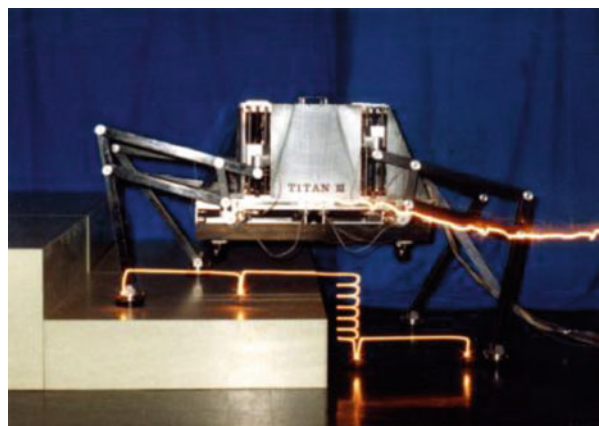
Matsuoka was the pioneer to develop a monopod walking robot, which performed locomotion through hops, with an objective to model the cyclic jumps in human locomotion in 1979 [3]. He formulated a model, consisting of a body and a weightless leg (to simplify the problem), and considered that the support phase duration was short when compared with the ballistic flightphase in which the feet lose contact with the ground. This gait, in which almost the entire cycle is spent on the transfer phase, minimizes the inclination influence during the support phase. His one-legged hopping machine could stand over an inclined table (10° with the horizontal), and an electrical solenoid gave a fast impulse to the foot in such a way that the support period was small. The machine hopped in place with a period of one hop per second and could walk forward and backward over the table.

Hirose and Umetani in 1980 built PV-II shown in Fig. 2.9, a four-legged walking machine, at Tokyo Institute of Technology, Japan [13]. Its weight was only 22 pounds and could walk at a very slow speed of the order of 0.8 inch per second. Its power consumption was very small of the order of only 10 W due to its small weight, sophisticated leg design, and slow average speed of locomotion. The leg

Fig. 2.9 PV-II walking robot [19, 20]



Fig. 2.10 TITAN-III [19, 20]



mechanism was a three-dimensional pantograph type, and the leg actuation was accomplished by DC motors and power screw speed reduction system. In addition, a passive ankle system was also included in the leg mechanism. PV-II was powered from external electrical energy source, and the control signals were also applied to it from an external computer via an umbilical cable. Its control system enabled it to maintain a horizontal body orientation. Contact sensors on each foot were used to detect obstacles in its path and contact with the ground. Later in 1984, an enlarged version of PV-II was built by them and named as TITAN-III (*Tokyo Institute of Technology, Aruku Norimono (walking vehicle)*) [19, 20]. The total weight of TITAN-III shown in Fig. 2.10 was 176 pounds and had four legs of about 4 ft long. The leg mechanism was of three-dimensional pantograph type and was built from composite materials. The latest walking robot in the TITAN series is the TITAN-XI built in 2008, a 7,000 kg hydraulic quadruped robot developed as a construction machine for drilling holes to reinforce steep slopes with rock or anchor bolts and thus preventing landslide. Its leg length is 3.7 m.

Vohnout at the Ohio State University built a one-legged walking machine, the Monopod, in 1982. It was a 20-inch high four-bar leg and was mounted on the inner frame of a three-wheeled cart. The inner frame was free to move vertically relative to the cart. The leg pushed the cart forward during the contact phase of its walking. The machine was controlled externally by a PDP 11/70 computer which was later replaced by an onboard Intel 8086 microprocessor-based microcomputer. The Monopod was built to test the energy efficiency of the four-bar leg. The tested data was compared to the data of the OSU Hexapod, and an improvement in specific resistance by a factor of 20 was obtained [13].

In 1982, a six-legged passive walking machine, the DUWE, was built by Brown at the Ohio State University [13]. The DUWE could walk in alternating tripod gait synchronizing each of the three legs by a pulley and wire system. The vehicle was controlled by an Apple II microcomputer. Although the leg structure was similar to that of the Monopod, the foot was lifted by shortening the driven crank via a toggle mechanism actuated by a solenoid.

The first self-contained walking machine was built by Sutherland in 1983 [13]. It was a hydraulically actuated six-legged vehicle and controlled by an onboard microcomputer. A gasoline engine was installed on board to give electric power supply to the computer as well as to drive a set of hydraulic pumps. Each leg of the machine had three DOF it could walk on smooth terrain and carry a human operator.

Odetics Inc. developed a six-legged “Functionoid” the ODEX-I in 1983 [13]. The weight of ODEX-I was only 370 pounds; however, it could lift up to 900 pound weight. This machine was powered by an onboard aircraft battery and was controlled by onboard computers that used to receive commands from a joystick via radio telemetry. The six legs, each with three DOF and designed as a planar modified pantograph mechanism, were mounted around the body.

Raibert at Carnegie-Mellon University built a hopping machine in 1983 [3, 13]. This hopping machine had only one leg and body structure that contained the actuators and several sensors to measure the body inclination angle, the hip angle, the leg width, the spring leg stiffness, and the ground contact. This machine was powered and controlled externally. This first prototype was limited to operate on a level surface and, therefore, could only move up and down, front and back, or rotate in the plane. A second hopping machine prototype, named PogoStick, had an additional hip joint to allow the leg to move sideways, as well as forward and backward. During operation, this robot balanced itself while hopping, moving at a maximum speed of 2.2 m/s.

Adaptive suspension vehicle (ASV), a very popular hydraulically actuated hexapod robotic platform with capability to adapt very rough terrain during locomotion, was developed at the Ohio State University, together with the University of Wisconsin and the Environmental Research Institute of Michigan, at the end of 1985 [3, 13, 18]. ASV had a total weight of 2,720 kg with 250 kg payload capacity. It was 5.6 m long and was powered by an internal combustion engine. The maneuvering and vehicle state supervision tasks were performed by an operator. The operator used to control the vehicle locomotion speed and direction through a

joystick, but the individual control of each leg was performed by a central computer. The ASV also had optical radar to study the terrain in front of it and to decide on the front foot placement. It could negotiate a maximum slope of 60 %, cross 1.8 m width ditches, climb vertical steps with 1.65 m maximum height, cross isolated walls of 1.35 m height, and reach a maximum speed of 2.3 m/s over regular terrain.

The project of developing a biped robot, known as the Honda Humanoid Robot, began in 1986, and the key ideas adopted for its development were “intelligence” and “mobility,” since the robot should coexist and cooperate with human beings [3, 21]. The development of the Honda Humanoid Robot was based on data retrieved from human locomotion. Honda’s idea was to create a robot that could be used in daily life, in contrast to a robot developed for a particular application, aiming its introduction in factories. Honda also specified three functions that had to be fulfilled: the locomotion speed should correspond to that of a human being (approximately 3 km/h), the robot structure should be capable of supporting arms with hands, and should be able to climb up and down stairs. The more advanced version of this robot, known as ASIMO (Advanced Step in Innovative MObility) model, was built in 2000, having 1.2 m height and 43 kg weight. The ASIMO has 26 DOF, is electrically actuated, and can hold 0.5 kg in each hand. It was a completely autonomous robot, in terms of processing capability and in terms of power (it transports on its back batteries that allow 15 min autonomy). It was intended to perform people attendance tasks and museum visit guiding, due to the integration of a vision and audition sensors set and a human gesture recognition system, allowing this humanoid to interact with human beings.

A hexapod robot named Genghis was built at MIT in 1989. Genghis was famous for being made quickly and cheaply due to construction methods. Genghis was a small six-legged robot that could walk, climb over obstacles, and follow people. It used four microprocessors, 22 sensors, and 12 servo motors. Rodney Brooks took the idea of a finite state machine and used it to build layered levels of behavior on Genghis.

Professor A. Halme at the Helsinki University of Technology, Finland, developed a hydraulically actuated six-legged walking machine, known as MECHANT (MECHanical ANT) in 1992 [22]. Its weight was about 1,100 kg and was driven by a 38 kW 2-cylinder ultra-light aero plane engines with air cooling. The hydraulic system was a traditional one including valve-controlled system with central pump, the work pressure being about 300 bars. The body was constructed of rectangular aluminum tubes which are welded together, forming a rigid structure. The leg mechanism was a two-dimensional pantograph with vertical rotation axis, thus having three DOF. The operator controlled the vehicle remotely by the joysticks via the radio link. The control system of MECHANT consisted of a computer network connecting seven onboard computers running under a commercial real-time operating system.

Another successful field robot, named DANTE, was developed by the CMU Field Robotics Center in 1993. DANTE was an eight-legged walking robot developed for the mission to collect data from a harsh environment such as those found on planetary surfaces. It descended into Mt. Erebus, Antarctica. The mission failed

when, after a short 20-foot decent, DANTE's tether snapped and it dropped into the crater. Later in 1994, DANTE-II was built. It was a more robust version of its predecessor and successfully descended into the crater of Alaskan volcano Mt. Spurr in order to gather and analyze high-temperature gases from the crater ground. DANTE-II was also an eight-legged robot and was electrically actuated. The power was supplied externally through an umbilical cable that also served as a communication structure and rescue cable. Besides contributing to volcano exploration advancement, another primary objective of this robot is to show the possibility of robotic exploration of extreme environments.

In 1997, a planar one-legged walking machine, known as ARL Monopod-I, was built by the Ambulatory Robotics Lab (ARL) at Canada. This planar monopod was inspired from the work of Raibert and was electrically actuated. It could attain a top running speed of 4.3 km/h. It was quite energy efficient and consumed only 125 W of electrical power. An improved version of ARL-I was built, known as ARL-II monopod, in 1999. ARL-II could attain a maximum running speed of 4.5 km/h with a total mechanical power expenditure of only 48 W. The ARL Monopod-II employed an electrical motor to actuate a lead screw, as well as a storage/recovery energy system through springs [3].

The design of the configuration of hopping machines' legs has been done as an approximation of the animal's legs. Moreover, many monopod robots that use the hopping principle for their locomotion also have feet with special geometry to maintain balance when stopped [3]. These robots allow jumping over obstacles or positioning themselves in places where available places for feet placement exist, without worrying about the static stability. In this connection it can be mentioned that in 1945, Wallace patented a "hopping" tank that could move on with one leg. During motion, it would lead to an erratic trajectory and, therefore, would be difficult to be shot by the enemy. Another potential application for these robots is the exploration of small celestial bodies like satellites, asteroids, comet nucleus, where legged or wheeled robots are not able to move successfully due to the reduced local gravity. An actual example is the vehicle ПРОП-Ф (Hopper), designed by the Russian Mobile Vehicle Engineering Institute, and sent in a space mission to Phobos in 1998. This 45-kg robot was able to move using hops, perform scientific experiments and transmit the collected data and the experimental results to the Earth through a radio communication channel.

The WABIAN (WAseda BIpedal humANoid) biped robot is another example of a biped robot that has been developed in Japan in 1997. The main objective of this robot development was the creation of an anthropomorphic robot sharing the same work space and presenting thought and behavior patterns similar to those of the human being. It was intended to achieve a robot able to interact in a natural way with humans, namely, being able to talk and to present emotions [3]. This biped robot, with 43 DOF, 136 kg weight, and 1.97 m height, was electrically actuated. The head had the capability to gather visual information (through a stereo artificial vision system) and audition. The electrical power was externally supplied; however, all the processing and computing system was integrated on the robot itself. To further increase the similarity with human beings, on this robot the hip joints

were antagonistically actuated and with variable stiffness, in a similar way to the human joint actuation (each human joint is actuated by two or more muscle groups that present characteristics identical to nonlinear springs). In terms of locomotion capabilities, this robot was able to move forth and back, dance in a dynamic way waving its arms and hips and to transport some load, using its arms.

A huge advancement has been made in the research on biped locomotion during the last decade in Japan partially due to the implementation of the HRP-Humanoid Robotics Program supported by the METI—Ministry of Economy, Trade and Industry of Japan between 1998 and 2002. The main objective of this program was similar to that followed in the development of the biped WABIAN. One example of a biped robot that has been developed under this program is the HRP-2 humanoid (Humanoid Research Project) [3]. This robot is able to move on irregular surfaces at 2/3rd of the normal human speed and is able to cross narrow passages, modifying its gait for that purpose. If the robot loses balance and falls, besides the fall being controlled in order to minimize eventual damage to the structure, it is capable of rising alone.

In 1999, Sony designed and manufactured a four-legged robotic pet, known as the AIBO (*Artificial Intelligence roBOt*, also means “love” or “attachment” in Japanese, can also mean “partner”). The AIBO was an inexpensive platform for artificial intelligence research, because it integrated a computer, vision system, and articulators in a package vastly cheaper than conventional research robots.

A hexapod Walking Harvester was developed by Plustech Oy Ltd (presently John Deere Forestry Oy) in 2000 for forestry work. This vehicle has three hydraulically actuated DOF on each leg and is fed from a diesel engine, allowing it to reach aimed maximum speed. For maneuvering, it needs a human operator who controls the machine through a joystick.

The SILO4 [23] walking robot is a medium-sized quadruped mechanism built at Instituto de Automatica Industrial, Spain, for basic research and development as well as an educational robot in 1999 and tested till 2003. The body of the SILO4 is a parallelepiped of about 310 mm × 300 mm × 300 mm. It contains all the drivers and electronic cards, as well as the force sensor amplifiers and a two-axis inclinometer that provides pitch and roll body angles. The structure of the body is made of aluminum, and the body’s weight, including electronics, is about 18 kg.

SCOUT-II has been designed and constructed at Ambulatory Robotics Laboratory, McGill University, Canada, in 2000. It is an under-actuated walking robot; therefore, its control is quite challenging. SCOUT-II is fully autonomous having on board power, computing, and sensing. Other features include an on board pan-tilt camera system and laser sensors.

BigDog is a dynamically stable quadruped robot created in 2005 by Boston Dynamics with Foster-Miller and funded by DARPA. It is 3 ft (0.91 m) long, 2.5 ft (0.76 m) tall, and weighs 240 pounds (110 kg), about the size of a small mule. It is capable of traversing difficult terrain, running at 4 mile/h (6.4 km/h), carrying 340 pounds (150 kg), and climbing a 35-degree incline. Locomotion is controlled by an onboard computer that receives input from the robot’s various sensors. Navigation and balance are also managed by the control system.

Professor Kenzo Nonami and his group at Chiba University, Japan, have worked for more than the last one decade for development of six-legged land mine detection and removal robot for *humanitarian demining* [24, 25]. They developed a series of robots called COMET (Chiba university *Operating Mine detection Electronics Tools*). In this series COMET-I, COMET-II, COMET-III, and COMET-IV have already been developed and successfully tested in various terrain conditions with various robust and intelligent control algorithms for its effectiveness in locomotion. COMET-I and II are electrical motor actuated, whereas COMET-III and COMET-IV are hydraulically actuated. The mass of COMET-I is about 120 kg, length of the body is 80 cm, width of the body is 120 cm, and the height is 80 cm. COMET-I has exhibited interesting results during locomotion in various terrains and motivated to develop a more advanced version after COMET-II after solving the drawbacks of COMET-I. COMET-II has a speed of locomotion of about 150 m/h which is ten times faster than COMET-I. Its mass is about 100 kg. In order to provide sufficient power to walk on uneven terrain with heavier payload (of the mine detection and removal tools), COMET-III has been hydraulically powered. Its weight is about 900 kg, 4 m long, 2.5 m wide, and 0.8 m high. Its prime mover is a 700 cc gasoline engine, and the driving force of the hydraulic system is 14 MPa.

2.3 Modern and Future Perspective of Walking Robot Research

The robot has to interact with the environment with one or more effectors that are suitable to perform the intended task. They are very important element of any robotic system, and their nature, capability, and mode of utilization give an identity and distinctiveness. In autonomous robotic systems, there are two basic ways of using effectors so that the point of action of the effector falls within the robot workspace: (1) to move the robot around (which results “locomotion”) and (2) to move other object around (which results “manipulation”). These actually divide present day robotics into two separate categories: (1) mobile robotics and (2) manipulator robotics. Many kinds of effectors and actuators can be used to move a robot around, like legs (for walking/crawling/climbing/jumping/hopping), wheels (for rolling), arms (for swinging/crawling/climbing), and flippers (for swimming). While most animals use legs to get around, legged locomotion is a very difficult robotic control problem, especially when compared to wheeled locomotion.

The main challenges [9, 19] those are still present for the development of autonomous walking robot are: (1) nonavailability of energy-efficient and high-performance actuators with high torque to weight ratio and high torque to volume ratio; (2) reliable and economical sensors; (3) lightweight but mechanically strong material for construction of the structure and mechanism; (4) fast, high computing power, and economical dedicated computer system that must be suitable for any type of hostile situation of nature; and (5) lightweight and onboard power source for long duration energy autonomy.

Another significant aspect of modern walking robotics research is the development of biologically inspired design that involves the idea of transferring the biological principles of nature to the robotic systems [26–34]. It has been observed that a large variety of efficient mechanical and physiological designs have evolved in nature in order to fit with the characteristics of a given physical environment and different locomotion modes. Animals seem to have evolved to be as fast as possible; to have the best possible acceleration, maneuverability, and endurance; and to have energy consumption as low as possible [1]. At a first glance, one may get tempted to mimic a legged animal while designing a walking robot. However, it is not possible to completely mimic a living system because the principle of energy supply, actuation, sensing, control, and intelligence of a biological system is entirely different from the artificial energy supply, actuation, sensing, control, and intelligence. Therefore, from engineering perspective the main focus of biologically inspired robotics is not to create a new generation of robots that imitate life but to use principles from nature to improve robotic systems [29]. As the concepts of the biological world are very hard to transfer to the walking machines, mainly due to the bottleneck in mechatronics, in the recent past many laboratories and their researchers were involved in the design and development of artificial locomotion systems with suitable modification of the principles observed in the biological world to accommodate the existing mechatronic technology. Therefore, the mechanical structures of the legs still comprise of several links connected by prismatic or rotational joints, with the proportion of the links or the location of the joints resemble to the living creatures [21]. Off course few attempts have been made to optimize the geometry of the leg mechanisms to match with the morphology and performance of living legged systems. However, due to the complexity of design and fabrication, the progress so far is very little [19, 35]. This is a future area of research where the robotics researchers should pay attention and many advanced technologies, like nanotechnology, micro electromechanical systems, single-chip computer, and smart materials, may help mankind to develop a walking robot that will resemble to the living legged systems.

Ever since, developments have mainly been driven to resemble physical aspects, although in the last few years, one of the main challenges in robotics has been to endow these machines with a grade of intelligence in order to allow them to extract information from the environment and use that knowledge to carry out their tasks safely. Although much progress has been made in the theoretical development of artificial intelligence, however, the applicability of most of the algorithms in real time is difficult or sometimes not feasible. The present trend to design intelligent robotic system is to impart prior knowledge with capability of learning in an integrated manner [9, 29, 35, 36]. Another important development in walking the robotics research during the last decade is the introduction of social behavior during the design of the control system. Therefore, the day is not very far when the walking robots will not only function as a machine but also blend themselves in our social environment and interact with people and play more important roles in our society [21].

The walking robotics research is still confined to the laboratory. The time is approaching when the commercial production of walking robot will start to commensurate with the future domestic, commercial, and industrial need. Obviously, like the industrial manipulator, this demand will have cumulative impact on further growth of the production of walking robot industry and reduce the cost of its production. Most of the innovations in the development of walking robots have occurred, so far, in Japan [17].

References

1. Carbone G, Ceccarelli M (2005) Legged robotic systems. In: Kordic V, Lazzinica A, Merdan M (eds) Cutting edge robotics. ARS International/pro literatur, Vienna/Mammendorf
2. Zielinska T (2004) Development of walking machines: historical perspective. In: Proceedings of the international symposium on history of machines and mechanisms. Kluwer Academic Publisher, pp 357–370
3. Silva M, Machado AT (2007) A historical perspective of legged robots. J Vib Control 13(9–10):1447–1486
4. Kajita S, Espiau B (2008) Legged robots. In: Siciliano B, Khatib O (eds) Springer handbook of robotics. Springer, Germany
5. Pfeiffer F, Josef S, Robmann T, Muchen TU (1998) Legged walking machines. In: Khatib O, Anibal TA (eds) Autonomous robotic systems. Springer, Germany
6. Boone G, Hodgins J (2000) Walking and running machines. MIT Encyclopedia of the Cognitive Sciences. <http://rm-f.net/~pennywits/MIT ECS/Entry/boone.html>. Accessed 4 June 2012
7. Stone WL (2005) The history of robotics. In: Kurfess TR (ed) Robotics and automation handbook. CRC, Boca Raton
8. Rosheim ME (1994) Robot evolution: the development of anthro robotics, 1st edn. Wiley, New York
9. Tesar D (1997) Where is the field of robotics going? Technical report of the robotics research group, The University of Texas at Austin
10. Rosheim ME (1997) In the footsteps of Leonardo. IEEE Robot Automat Mag 4:12–14
11. Raibert MH (1986) Legged robots. Commun ACM 29(6):499–514
12. Machado JAT, Silva M (2006) An overview of legged robots. <http://citeseerx.ist.psu.edu/viewdoc/summary?doi=10.1.1.106.8192>. Accessed 4 June 2012
13. Song SM, Waldron KJ (1989) The machine that walk: the adaptive suspension vehicle. MIT, Cambridge
14. Wallen J (2008) The history of the industrial robot. Technical reports from the Automatic Control group at Linköpingsuniversitet. <http://www.control.isy.liu.se/publications>. Accessed 4 June 2012
15. Garcia E, Jimenez MA, Santos PGD, Armada M (2007) The evolution of robotics research. IEEE Robot Automat Mag 14(1):90–103
16. Kar DC (2003) Design of statically stable walking robot: a review. J Robot Syst 20(11):671–686
17. RUN THE PLANET (2004) The history of walking robots. <http://www.runtheplanet.com/resources/historical/walkingrobots.asp>. Accessed 4 June 2012
18. McGhee RB (1985) Vehicular legged locomotion. In: Sirdis GN (ed) Advances in automation and robotics. JAI Press Inc., Greenwich
19. Hirose S (2001) Super mechano-system: new perspective for versatile robotic system. In: Rus D, Singh S (eds) Experimental robotics VII. Springer, Berlin, Heidelberg

20. Hirose S, Kato K (2000) Study on quadruped walking robot in Tokyo institute of technology – past, present and future. In: Proceedings of the IEEE international conference on robotics and automation, San Francisco, CA, pp 414–419
21. Hirai K (1997) Current and future perspective of Honda humanoid robot. In: Proceedings of the IEEE/RSJ international conference on intelligent robots and systems, Grenoble, pp 500–508
22. Hartikainen K, Halme A, Lehtinen H, Koskinen K (1992) MECANT I: a six legged walking machine for research purposes in outdoor environment. Technical reports 6, series B, Helsinki University of Technology, Automation Technology Laboratory
23. Santos PG, Garcia E, Estremera J (2006) Quadrupedal locomotion: an introduction to the control of four-legged robots. Springer, London
24. Nonami K, Huang Q, Komizo D, Fukao Y, Asai Y, Shiraishi Y, Fujimoto M, Ikeda Y (2003) Development and control of mine detection robot COMET-II and COMET-III. JSME Int J Ser C 46(3):881–890
25. Nonami K, Huang Q, Komizo D, Fukao Y, Asai Y, Shirashi Y, Fujimoto M, Ikeda Y (2002) Development of mine detection robot COMET-II and COMET-III. In: Proceedings of the 6th international conference on motion and vibration control. Saitama, pp 449–454
26. Kimura H, Tsuchiya K, Ishiguro A, Witte H (2006) Adaptive motion of animals and machines. Springer, Tokyo
27. Voth D (2002) Nature's guide to robot design. IEEE Intell Syst Mag 17:4–6
28. Beer R, Quinn RD, Ciel HJ, Ritzmann RE (1997) Biologically inspired approaches in robotics: what we can learn from insects. Commun ACM 40(3):30–38
29. Berns K (2002) Biologically inspired walking machines. In: Gini M, Shen WM, Torras C, Yuasa H (eds) Intelligent autonomous systems 7. IOS, Amsterdam
30. Hasslacher B, Tilden MW (1995) Living machines. Robot Autonom Syst 15(1–2):143–169
31. Pfeiffer F, Eltze J WHJ (1995) Six-legged technical walking considering biological principles. Robot Autonom Syst 14(2–3):223–232
32. Dillmann R, Albiez J, Gabmann B, Kerscher T, Zollner M (2007) Biologically inspired walking machines: design, control and perception. Phil Trans R Soc A 365:133–151
33. Quinn RD, Ritzmann RE (1998) Construction of a hexapod robot with cockroach kinematics benefits both robotics and biology. Connect Sci 10(3–4):239–254
34. NaikaK MM, Bardenc J (2010) Design, development and control of a hopping machine – an exercise in biomechatronics. Appl Bionics Biomech 7(1):83–94
35. Hirzinger G, Fischer M, Brunner B, Koeppe R, Otter M, Grebenstein M, Schäfer I (1999) Advances in robotics: the DLR experience. Int J Robot Res 18(11):1064–1087
36. Arikawa K, Hirose S (2007) Mechanical design of walking machines. Phil Trans R Soc A 365 (1850):171–183
37. Yokoyama K, Handa H, Isozumi T, Fukase Y, Kaneko K, Kanehiro F, Kawai Y, Tomita F, Hirukawa H (2003) Cooperative works by a human and a humanoid robot. In: Proceedings of the IEEE international conference on robotics & automation, Taipei, pp 2985–2991

Chapter 3

Design and Optimization of Hydraulically Actuated Hexapod Robot COMET-IV

Abstract The development of COMET-III resulted in a completely self-contained drive system that closely approximated a practical robot. However, various problems emerged in the course of research and development. In general, there was significant scope for improvement in terms of adaptability to terrain and speed of movement. For example, owing to an insufficient amount of oil and poor durability, sustained tripod walking could not be achieved, and the achieved walking speed was slow; the possible range of motion of the legs, which lacked the ability to move sideways or diagonally, was small, and the robot could not move omnidirectionally. In particular, the preeminence of legged robots as locomotive robots is ascribed to their superior capability of discrete walking in specific environments (such as minefields) and outstanding ability in general to adapt to the terrain. These capabilities enable legged robots to easily move over difficult and uneven terrain—even in environments wherein crawler robots and wheeled robots are incapable of motion. Therefore, there is an urgent need to overcome the fatal flaws in COMET-III—for example, in terms of terrain adaptability and speed of movement.

To this end, Nonami's team combined their various achievements to date and commenced the development of COMET-IV auxiliary robot, which is aimed at actual mine detection and removal [1–5]. This chapter describes the group's attempt to fundamentally review the basic specifications of a robot, such as the mechanism, gait, drive system, and control system, and approach the optimization-based design of COMET-IV—the hexapod dangerous-operations robot [6–18]. First, based on the conceptual design of legged robots, the superiority of COMET-IV was clarified in terms of system construction, and the overall design of the robot was arrived at. Then, a single-legged robot was constructed and tested for speed and load endurance for analyzing robot performance both theoretically and experimentally. Based on the obtained test results, the design of the robot leg mechanism—essential to a walking robot—was theoretically optimized by means of iterative Jacobian-analysis-based complex evaluations. Further, a practical hexapod robot system that uses walking control for navigating uneven terrain was established by implementing force control or impedance control of end-effectors at any attitude.

3.1 System Construction

3.1.1 Conceptual Design

3.1.1.1 Development Objectives

COMET-IV was designed to satisfy the following performance targets:

1. Move at a speed of 1 km/h.
2. Be able to negotiate upward or downward level differences, where the step height step is 1 m or the incline is 20° .
3. Be able to move in any direction (including sideways and diagonally).

These aspects of movement capability are crucial to the practical implementation of a locomotive robot. A new model with these capabilities was developed; however, the following specifications must also be adhered to when constructing an outdoor auxiliary robot for dangerous operations.

4. A medium-sized outdoor robot must weigh less than 1.5 t and be able to transport a 2-t load on a rack.
5. Must be resistant to hazardous materials and manage unforeseen accidents in an intelligent manner.
6. Must be able to operate continuously for long periods.

A dangerous-operations robot that satisfies the abovementioned performance criteria was to be built. However, this robot need not necessarily be an extension of COMET-III. Accordingly, after determining the type of movement for COMET-IV, its conceptual design was considered, and factors such as the power source, drive system, and leg mechanism were selected as follows.

3.1.1.2 Locomotion Mechanism Type

Various types of locomotion mechanisms can be imagined. However, they can be divided broadly into four categories in terms of their movement in environments where the ground is solid. These are as follows:

- Wheeled type
- Crawler type
- Legged type
- Special type (such as trunk type or hybrid)

The wheeled-type mechanism has characteristic advantages over other types of locomotion mechanisms, such as the fact that it allows for stable movement at high speeds, exhibits a high level of energy efficiency, is simple and easy to control, and can incorporate a whole wealth of automobile technology that has already been built. A limitation of the wheeled-type mechanism is that it is confined to moving on flat road surfaces; however, when certain amounts of level differences or steps exist, travel can be enabled by adding certain degrees of freedom to the wheeled mechanism.

Crawler robots are also known as caterpillar robots. The most significant feature of a crawler robot is that its multiple wheels do not make direct contact with the road surface because they are wrapped in circular caterpillar tracks. It can function in various terrain conditions because the caterpillar tracks mitigate the effects of unevenness of road surfaces. Crawler robots exert less pressure on the ground surface than wheeled robots because they have a large area of contact with the ground; in addition, crawler robots have strong surface grip. Other advantages are that they are highly capable of traveling over road surfaces and can, to a certain degree, traverse uneven ground and surmount level differences and ditches. However, because there is high resistance to track motion, owing to a large track-ground contact patch, this type of robot would damage floor surfaces if it has metal tracks. Furthermore, this type of robot is inferior to the wheeled robot in terms of energy efficiency. Both abovementioned types of locomotion mechanisms necessitate that there be continuous contact between the robot and the ground surface.

In contrast, because the points of contact between a legged robot and the ground surface are noncontiguous, the points at which this type of robot touches the ground can be controlled; moreover, the position and orientation of the robot body can be changed without changing these points. In addition, the legged robot has the highest level of adaptability to terrain, in that it can surmount level differences, step over ditches, and go up and down stairs. These characteristics give the legged robot an advantage over the wheeled and crawler robots in terms of movement in complex environments. However, the legged robot has several shortcomings: the numerous degrees of freedom in the joints, a mechanism that is more complex than those of the wheeled and crawler robots, difficulty in maintaining stable gait, and extremely poor energy efficiency. In addition, there are special types of robots such as trunk-type robots (snake robots) and hybrids that are composed of a combination of the abovementioned mechanisms.

For COMET-III, a legged–crawler hybrid design was adopted, in which the type of movement could be selected based on the use of the robot. An attempt was made to enhance movement efficiency. However, the weight of the crawler section was relatively high in proportion to the total robot weight, and this high weight decreased the robot's walking speed. With COMET-IV, the objective was to design and build a robot that exhibits excellent terrain adaptability and can soundly execute dangerous operations while protecting itself. Accordingly, we selected the legged robot mechanism and designed it such that the robot is capable of adapting to complex terrain and conducting safe operations while avoiding dangerous zones.

3.1.1.3 Number of Legs

Legged robots with two, four, and six legs have been studied in the past. Bipod robots are suited to narrow spaces; however, it is difficult to ensure their dynamic stability. While quadripod robots are statically stable, they have the least mobility. Although quadripod robots are mechanically superior to hexapod robots, they are inferior in terms of movement speed and movement algorithms because they cannot lift more than one leg at once. Hexapod robots can adopt various gaits depending on the conditions. There are also reports that substantiate the practical utility of six legs. These reports state that for a robot with a body of a given size, increasing the number of legs from four to six remarkably improves stability, whereas further increase in the number of legs does not improve stability that much. However, the increase from four to six legs makes the robot larger.

It is thus necessary to consider the form of the robot in the context of the environment in which it would be used because the characteristics of legged robots vary depending on the number of legs. The primary requirement from COMET-IV is that it should reliably manage unforeseen accidents as stipulated in development objective (5). Accordingly, if the possibility of failure of one of the legs due to an accident is considered, the redundancy inherent in a many-legged design is appropriate. A hexapod design, which can continuously perform stable static walking, is particularly suitable. The hexapod design can also achieve a wider variety of gaits than can a quadripod design and is relatively easy to control. Given that hexapod designs also have numerous other advantages (e.g., the results of a wealth of past research can be applied to the design process), the hexapod system was adopted for this project.

3.1.1.4 Power Source and Drive System

COMET-IV is intended to be a robot that is completely self-powered so that it can engage in continuous outdoor operations. Therefore, it will need its own built-in battery or engine. To achieve both a high level of terrain adaptability (as specified in the development objectives) and high-speed walking, the battery or engine must be of suitable size and output considering robot size. Power sources for moving robots must be considered with reference to a robot's shape, size, and the field in which the robot will be used. Indoor robots use either AC or DC power supply connected via a cable or a battery. In contrast, outdoor robots often draw direct power from a gasoline or diesel engine. The three principal types of drive systems used in robots are electric, pneumatic, and hydraulic. The use of an engine allows for the use of hydraulic drives—the engine drives a generator and the electricity generated is used to operate a hydraulic pump. Accordingly, it was decided that a hydraulic-drive system (which has the highest output-to-weight ratio among the three drive system types and can produce high output levels) would be used. An engine serving as the power source would drive this system in an indirect manner.

3.1.1.5 Form and Disposition of Legs

Next, the form and disposition of the legs were determined. The key factors in designing the leg mechanism are that it should have just enough drive torque and rigidity to support the body, and an adequate range of motion and drive speed. As with the robot arm, four different configurations were considered for the joint structure of the leg mechanism: cylindrical-coordinate type, polar-coordinate type, rectangular-coordinate type, and polyarticular type. Among these, the polyarticular structure is the most widely adopted leg mechanism for walking robots because it is the most effective at establishing an arbitrary position and attitude for the robot and highly adaptable to a wide variety of operations. With this type of drive configuration, the most straightforward arrangement is a serial link mechanism that drives each joint independently. Although inferior to a pantograph in terms of output, the polyarticular structure facilitates control and ensures that the range of motion is as wide as possible. In this case, the structure is the same as that of an excavator with a hydraulic cylinder serving as the actuator for each joint.

Next, three configurations for leg placement relative to the body of the robot were considered: insect-type, mammal-type, and radiation-type. Although the mammal-type configuration is suitable for high-speed straight-line walking, the robot body must be lengthened to generate a long stride. Although the radiation-type configuration is outstanding in terms of stability and omnidirectionality, it cannot achieve high walking speed. Because the insect-type configuration is outstanding in terms of static stability and omnidirectionality, and has a large range of movement for a comparatively small body, it was selected as the optimal configuration for this robot. Finally, the end-effector (foot) mechanism is required to function in a manner that the sole of the foot remains firmly planted on the ground—even when the leg is acting as a supporting leg and its joint angle changes. Accordingly, a mechanism connected to the ankle via a bearing in a universal joint and supported by a spring element was adopted from COMET-III. COMET-IV represents an attempt to improve adaptability to uneven ground by driving the robot's feet more actively. Based on the abovementioned points, we decided that the Komatsu PC02 Mini-Excavator, which has four degrees of freedom (for shoulder, boom, arm, and bucket), be adopted as the leg mechanism. This commercially available excavator features a polyarticular hydraulic-drive system that was optimized for construction work, is cheap, exhibits sufficient rigidity, and has been proven in the field. The Komatsu PC02 Mini-Excavator is light in weight and allows the desired range of movement to be obtained through selection of appropriate link length. For COMET-IV, the bucket section was replaced with the foot mechanism; the foot roll angle is driven actively. Situating the leg mechanisms in a bilaterally symmetrical fashion, as on an insect, allows us to limit the robot dimensions to approximately 2.3 m in length, 4.1 m in width, and 1.5 m in height. Therefore, effective use of the four degrees of freedom provides COMET-IV with the capability for other types of gait (notably, sideways walking) in addition to walking in the forward direction.

A conceptual design of COMET-IV was produced. However, research on similar outdoor hydraulic-drive walking robots is being pursued actively worldwide.

The adaptive suspension vehicle (ASV), shown in Fig. 3.1a, developed at Ohio State University is a large 3-t hexapod walking robot equipped with a cockpit and powered by an onboard gasoline engine. Each leg comprises a completely independent hydraulic system with three degrees of freedom, in which a two-dimensional pantograph rotates around the roll axis. The Walking Forest Machine manufactured by Plustech (shown in Fig. 3.1b) is a vehicle for deforestation operations in mountain forests. Similar to the ASV, the Walking Forest Machine has a mammalian leg mechanism, and as a manned robot, it can successfully traverse uneven ground. Recently, research has also been conducted on TITAN-XI, a 7-t quadripod slope-operations robot (shown in Fig. 3.1c). Many projects, however, have gone no further than the research stage, with development abandoned because of control difficulties, oversized mechanisms, or lack of utility. In essence, although legged robots can seemingly function effectively in environments wherein the locomotion mechanisms of crawler and wheeled robots are incapable of travel and are better at performing dangerous operations, they have virtually no record to establish their superiority as practical robots in terms of the abovementioned reasons. Thus, the foremost motivation for this research was to develop a truly practical robot to break this impasse. Based on lessons learned from the development of COMET-III and the other robots mentioned above, the most important considerations when developing COMET-IV (in addition to providing it with outstanding walking ability) were to make it as small and as light as possible, enhance its reliability, and to develop a simple control system.

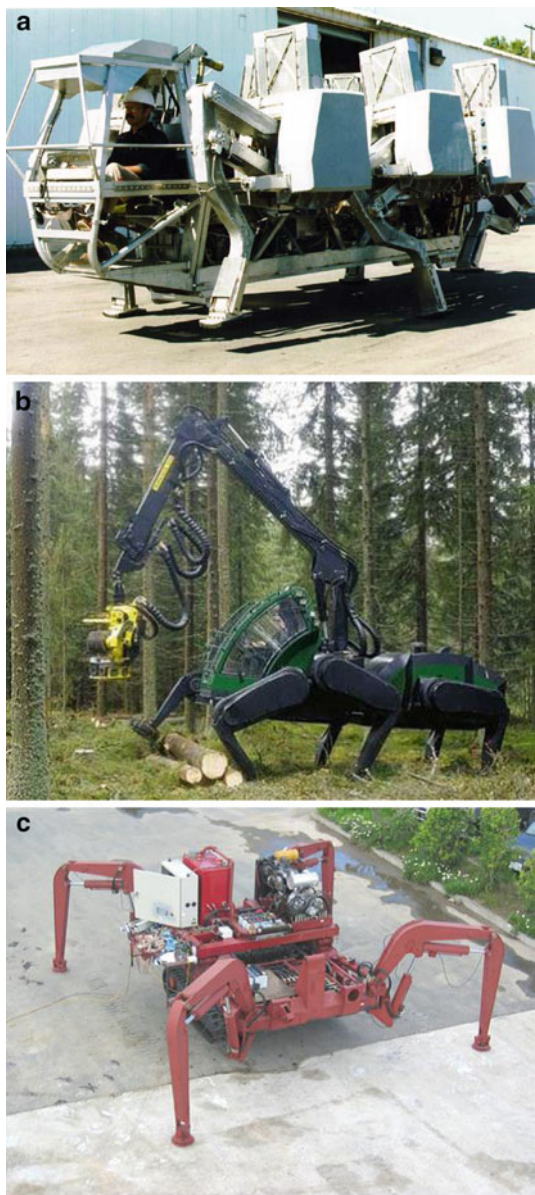
3.1.2 Overall Mechanical System Design

After the conceptual design was completed, the entire mechanical system for the actual robot was designed. Schematic diagrams of COMET-IV produced using DADS, a mechanical analysis software application, and robot dimensions are shown in Figs. 3.2 and 3.3, respectively. The development specifications of COMET-IV are listed in Table 3.1 in comparison with those of COMET-III. A hardware layout diagram is shown in Fig. 3.4. The objective was to ensure that COMET-IV is a completely independent robot. To this end, COMET-IV was equipped with a gasoline engine to serve as its power source and a generator for powering electronic systems such as the onboard computer. The engine also operates a variable-displacement hydraulic pump, to which it would be connected directly. The features of COMET-IV are described below.

1. *Less than 1.5 t weight achieved using housing with lightweight high-strength frame structure*

SUS304 stainless steel, which has a high degree of rigidity, was used as the principal structural material for the body of COMET-III. However, because the upper part of the body section opened wide, it was low in strength and prone to deformation. Therefore, the frame structure shown in Fig. 3.2 was adopted

Fig. 3.1 Hydraulic walking robot. (a) Adaptive suspension vehicle, (b) The walking forest machine, (c) TITAN-XI



because a closed box-like structure was needed to achieve the desired strength and robustness. This closed box-like structure is similar to the monocoque structure used for car bodies, and it is constructed from an aluminum alloy that is considerably lighter than SUS304. Therefore, the new design is significantly lighter. It is also important to build the robot to a size such that it can be transported on a 2-t truck.

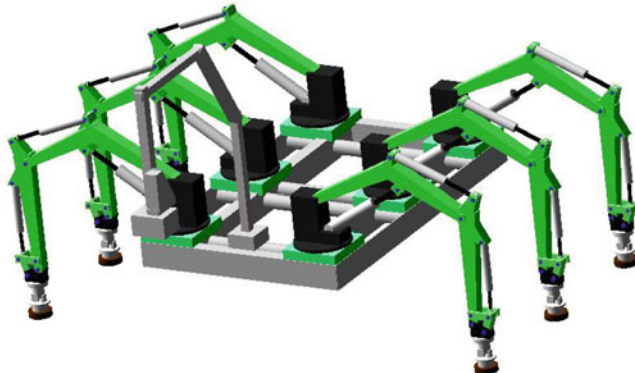


Fig. 3.2 Image of COMET-IV

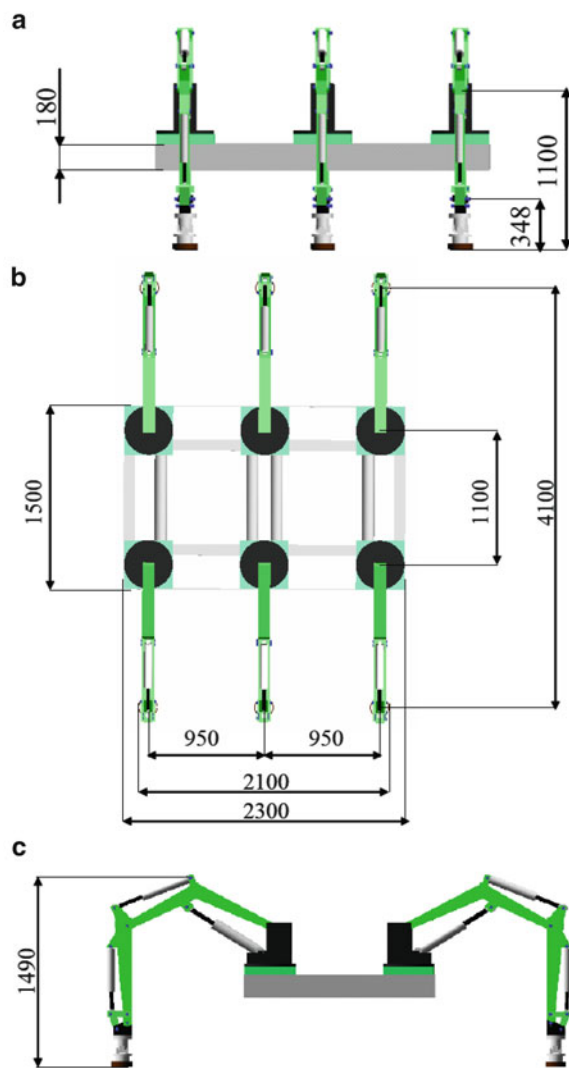
2. Construction of a load-sensing system using a variable-displacement hydraulic pump and a control valve

A load-sensing system is a system that includes power conservation circuits for minimizing energy consumption by regulating the pressure and flow rate in accordance with the load. The system is based on the principle of flow rate through an orifice. A load-sensitive valve (or LS regulator) is used to detect pressure drop across the orifice; this difference is converted to a feedback signal; this signal is used for controlling the pump's discharge rate and pressure so as to maintain a constant pressure drop across the orifice even under a varying load. For COMET-IV, we adopted a control scheme that combines a variable-displacement hydraulic pump and a control valve. A variable-displacement swash plate pump manufactured by Bosch Rexroth and a PSV proportional-control valve manufactured by Hawe (the same type of control valve that was used in COMET-III) were used. The control valve's maximum flow control rate is 80 L/min. Therefore, the system, which is designed to minimize energy loss in terms of both pressure and flow using load pressure feedback and the variable pump, is capable of significant energy saving and is suited for outdoor robots.

3. Adoption of a distributed control system that allows the engine and hydraulic system to independently control legs in two groups of three (left and right)

COMET-IV is equipped with two Robin engines made by Fuji Heavy Industries (22.7 ps, 3,600 rpm) and its output is 2.7 times higher than that of COMET-III. Designed for greater reliability and endurance, COMET-IV features a distributed autonomous system that allows its engine and hydraulic system to independently control the legs in two groups of three (left and right sides of robot). Hence, in the event of an emergency, if either control system malfunctions, the other functioning system will automatically take over so that the robot can still walk. As described above, a system that is highly efficient in terms of energy usage was constructed with the aim of allowing at least 4 h of continuous operation.

Fig. 3.3 Overview of COMET-IV. (a) Side view, (b) Top view, (c) Front view

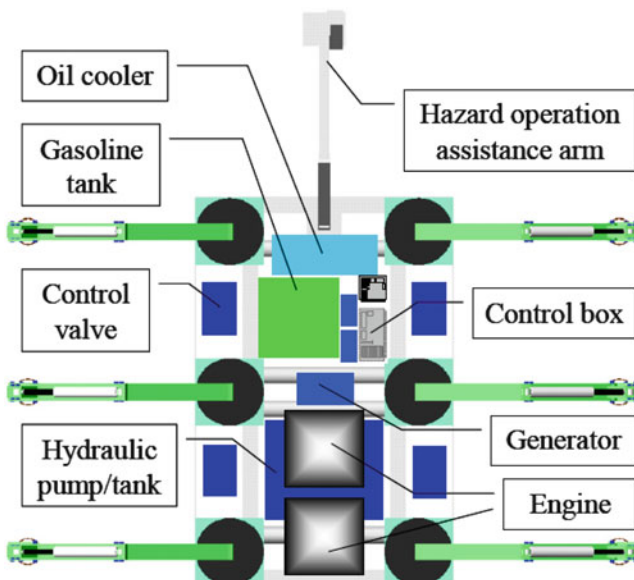


4. Onboard arm and gripper for dangerous operations

Attached to the front of the robot, COMET-IV's dangerous-operations arm and gripper enable it to support dangerous operations. Initially, it was suggested that either the six-axis hydraulic multifunction arm, which is currently being developed by the research group, or a commercially available electrical hand or arm would be used as the robot arm. This enables the robot to be used for hazardous operations such as mine detection and removal.

Table 3.1 Specifications of COMET-III and COMET-IV

	COMET-III	COMET-IV
Height (m)	0.87	1.49
Width (m)	2.56	4.10
Length (m)	1.60	2.30
Weight (kg)	1,100	1,500
Walking speed (m/h)	160	1,000
Engine size (cc)	653	720 × 2
Engine horse power (ps)	17	23 × 2

**Fig. 3.4** Hardware system of COMET-IV

5. Construction of an onboard remote-operations control system with a wireless unit

With existing technology, dangerous-operations support robots can only be semiautonomous. Simple walking tasks such as avoiding obstacles will be automated in COMET-IV; however, it will be remotely controlled by an operator who can view the robot on a monitor. Accordingly, this system will involve the construction of a remotely operated control system, featuring a built-in Scalance wireless unit made by Siemens and a channel for communication between a host PC and the target PC installed in the robot.

The actuation system for COMET-IV is shown in Fig. 3.5. The actuation principle is as follows: the generator is driven by the gasoline engine and supplies electricity to drive the control system; concurrently, the engine drives the variable-displacement

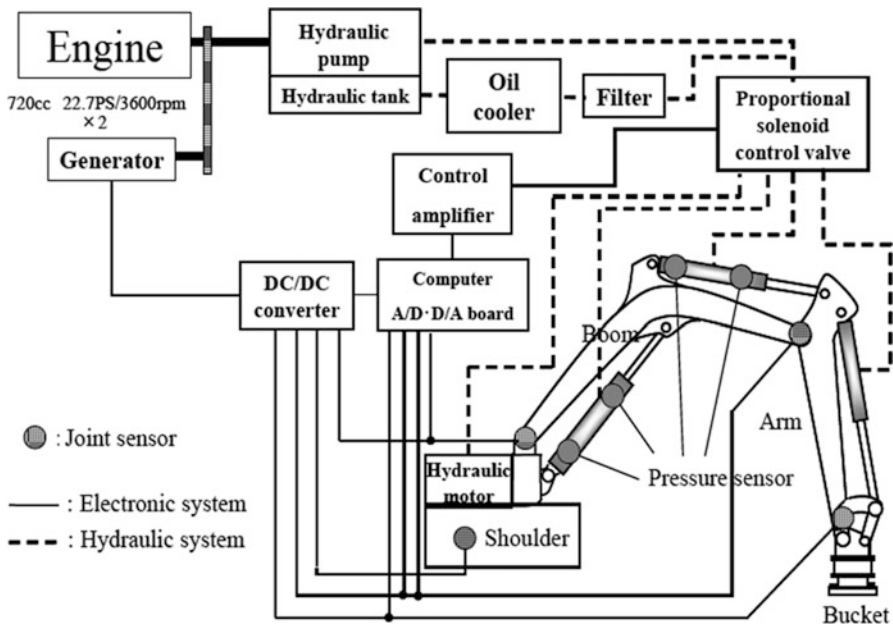


Fig. 3.5 Control system of COMET-IV

hydraulic pump. The oil pressure filter removes harmful impurities and contaminants from the oil, and the oil cooler prevents any increase in internal leakage flow resulting from an increase in oil temperature as well as problems such as friction or burning in the sliding parts of the equipment. The computer reads the angular signal transmitted from the rotary potentiometer on each joint via an A/D converter and calculates the control inputs. A built-in computer is used for control and calculation. The control algorithms were implemented using xPC Target for MATLAB/Simulink. The calculated control inputs are transmitted via an A/D converter and drive each actuator by displacing the spool on the proportional solenoid valve.

The spooling properties of the control rod were determined considering the pressure area differences that are characteristic of single-rod cylinders. The three joints other than the shoulder joint were designed with a counterbalance valve to prevent them from moving under their own weight. Part of the detailed hydraulic circuit for COMET-IV is shown in Fig. 3.6.

For leg force control, the installation of a force sensor in each foot would allow for the measurement of the reactive force in each leg and make it easy to construct a simple control system. (This method was used for COMET-III.). However, when considering walking in muddy water or under other unfavorable conditions, such installation would be inappropriate from the fault tolerance and noise immunity viewpoints. Also problematic is the fact that there would be offsets and mechanical

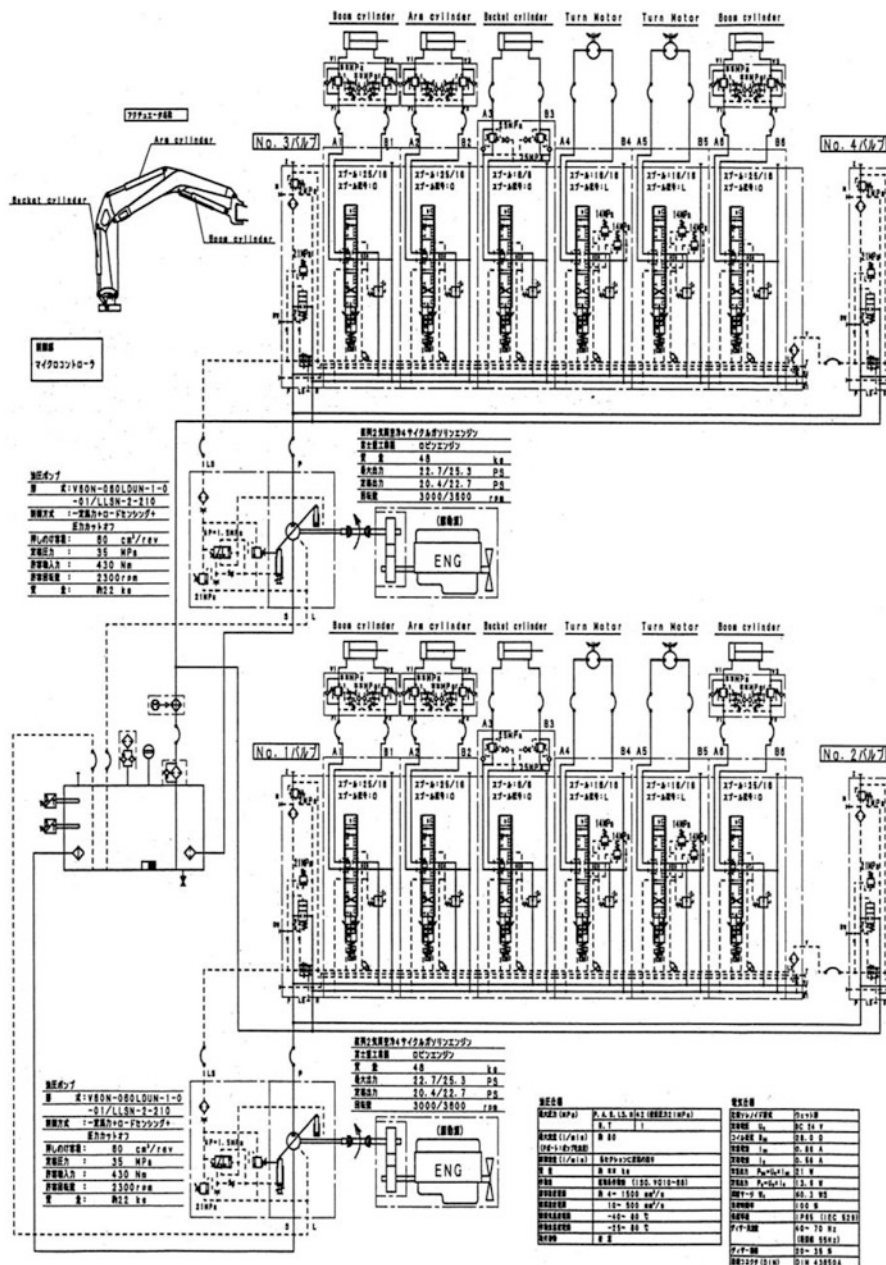


Fig. 3.6 Hydraulic circuit of COMET-IV

elements such as springs between the feet that are in contact with the environment and the sensors. Considering this collocation problem, it would be advisable to place the actuators and the sensors in the same place. Accordingly, in the case of COMET-IV, force control was achieved using a pressure sensor to measure the pressure in each hydraulic cylinder and deriving the force on each foot. Thus, it was possible to determine the load condition of each leg from the actuator. Given that there are no sensors in the foot mechanisms, the legs are lighter and may even be able to cope with watery swamps. Pressure sensors are divided into mechanical sensors and electronic sensors. Long-life, high-precision electronic sensors are further categorized as strain gauges and capacitance sensors based on the sensing method used. Strain gauges are more suitable for measuring high pressures. Therefore, we decided to use the AP-15S strain gauge sensor (Keyence), which features a single diaphragm. This sensor detects pressure directly using strain resistors made of thin-film semiconductors, which are integrated into the SUS diaphragm. With a rated pressure range of 0–20 MPa and a withstand pressure of 40 MPa, this sensor has a measurement resolution of 0.01 MPa.

3.2 Building a Single-Leg Model

Before building a hexapod system, we built a single leg and performed all evaluation tests to verify whether this leg delivered the desired performance. The developed leg and the related kinematic model are shown in Figs. 3.7 and 3.8. To perform the tests at the earliest, we used different hydraulic pumps and a different control valve system from that used in COMET-IV, but their performance was similar to that of the specified pumps; therefore, these components were suitable for evaluation purposes.

3.2.1 Leg Mechanism

We modeled COMET-IV's leg link mechanism on the PC-02 excavator, with four degrees of freedom—shoulder, boom, arm, bucket—and for the foot mechanism, we modified the bucket to make active drive possible. The shoulder uses a hydraulic motor, whereas the other three joints have direct hydraulic cylinders. Table 3.2 summarizes the link specifications for a commercial excavator. Here, from the viewpoint of manipulability, which is discussed later, the boom and arm + bucket link length were modified to make them almost proportional. The specifications of the hydraulic cylinders are identical, with a bore diameter of 40 mm, rod diameter of 25 mm, and pump pressure of 14 MPa.



Fig. 3.7 Single-leg model of COMET-IV

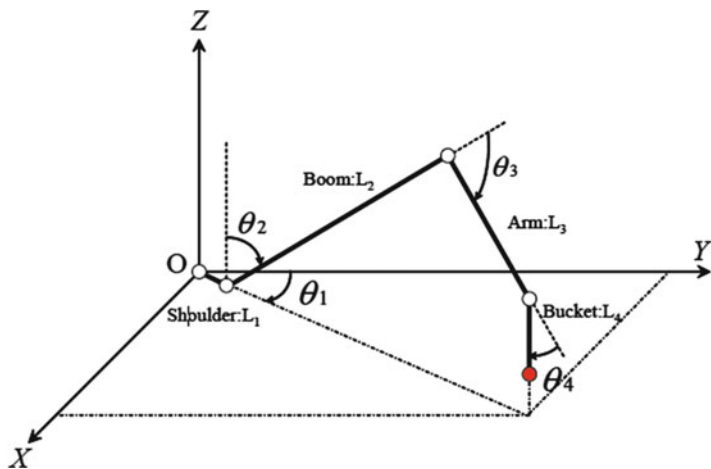


Fig. 3.8 Kinematic model of leg

Table 3.2 Link parameter of single-leg model

Link		
Shoulder	L_1 (m) 0.00	$-180.0 \leq \theta_1$ (deg) ≤ 180.0
Boom	L_2 (m) 1.13	$50.0 \leq \theta_2$ (deg) ≤ 142.6
Arm	L_3 (m) 0.77	$36.6 \leq \theta_3$ (deg) ≤ 150.8
Bucket	L_4 (m) 0.40	$-47.9 \leq \theta_4$ (deg) ≤ 103.0

3.2.2 Observations from the Evaluation Experiments

In the preliminary research, we used a single-leg model to conduct performance evaluations such as speed and load endurance tests. These results revealed that there are problems with speed and the ability to support its own weight when using an unmodified excavator as the leg mechanism.

In other words, the tracking limit of the walking trajectory is slow at 0.5 km/h, and there is insufficient joint torque on the boom and arm, which is the primary support for the body. We attempted to improve the walking speed by using a hydraulic pump with the appropriate discharge flow rate and by making appropriate changes to the spool properties of the control valve; however, improving the support capacity of the leg mechanism calls for a radical redesign. The following analysis explains leg mechanism optimization for achieving the desired self-support capacity and walking speed. When optimizing the design, we set the hydraulic pump pressure to 21 MPa to provide 1.5 times the thrust.

3.3 Kinematic Analysis

3.3.1 Forward Kinematics, Inverse Kinematics

Based on the COMET-IV leg mechanism model shown in Fig. 3.8, the forward kinematic equation can be calculated from the angle of each joint, $\Theta = [\theta_1 \theta_2 \theta_3 \theta_4]$ T, to the foot position $X = [x \ y \ z]^T$ as follows:

$$\begin{aligned} x &= -S_1(L_1 + L_2S_2 + L_3S_{23} + L_4S_{234}) \\ y &= C_1(L_1 + L_2S_2 + L_3S_{23} + L_4S_{234}) \\ z &= L_2C_2 + L_3C_{23} + L_4C_{234} \end{aligned} \tag{3.1}$$

where $\sin(\theta_i + \theta_j + \theta_k)$ is abbreviated as S_{ijk} and $\cos(\theta_i + \theta_j + \theta_k)$ as C_{ijk} .

In addition, the inverse kinematics equation used to calculate each joint angle from the foot position is expressed as follows:

$$\begin{aligned}\theta_1 &= \arctan\left(\frac{x}{y}\right) \\ \theta_2 &= \frac{\pi}{2} - \arctan\left(\frac{z-L_1}{\sqrt{x^2+y^2}}\right) - \arctan\left(\frac{L_3 \sin \theta_3}{L_2 + L_3 \cos \theta_3}\right) \\ \theta_3 &= \arccos\left\{\frac{x^2+y^2+(z+L_1)^2-L_2^2-L_3^2}{2L_2L_3}\right\} \\ \theta_1 &= \pi - \theta_2 - \theta_3\end{aligned}\quad (3.2)$$

However, the focus of this research was redundant systems with four DOF; therefore, the angle of each link cannot be determined uniquely. Thus, binding conditions are applied to maintain the bucket perpendicular to the surface at all times, and then, the angle of each joint is determined.

3.3.2 The Jacobian

The Jacobian is a matrix that linearly relates joint micro-rotation velocities to foot micro-movements. Using the Jacobian transposition matrix, we can express the relationships between power produced by the joint motor and cylinder and the torque with the resulting power generated at the foot. Upon analyzing the Jacobian, we determined the attitudes that produce the easiest movement or the highest power. The following equation can be used to define the Jacobian by applying a time differential to the equations expressing the relationship between joint angle and foot velocity (3.1):

$$\dot{X} = J\dot{\Theta} \quad (3.3)$$

where the elements of the Jacobian are as follows:

$$J = \begin{bmatrix} J_{11} & J_{12} & J_{13} \\ J_{21} & J_{22} & J_{23} \\ J_{31} & J_{32} & J_{33} \end{bmatrix} \quad (3.4)$$

$$J_{11} = \frac{\partial x}{\partial \theta_1} = -(L_2 S_2 + L_3 S_{23} + L_4 S_{234}) C_1$$

$$J_{12} = \frac{\partial x}{\partial \theta_2} = -(L_2 C_2 + L_3 C_{23} + L_4 C_{234}) S_1$$

$$J_{13} = \frac{\partial x}{\partial \theta_3} = -(L_3 C_{23} + L_4 C_{234}) S_1$$

$$J_{14} = \frac{\partial x}{\partial \theta_4} = -L_4 C_{234} S_1$$

$$J_{21} = \frac{\partial y}{\partial \theta_1} = -(L_2 S_2 + L_3 S_{23} + L_4 S_{234}) S_1$$

$$J_{22} = \frac{\partial y}{\partial \theta_2} = (L_2 C_2 + L_3 C_{23} + L_4 C_{234}) C_1$$

$$J_{23} = \frac{\partial y}{\partial \theta_3} = (L_3 C_{23} + L_4 C_{234}) C_1$$

$$J_{24} = \frac{\partial y}{\partial \theta_4} = L_4 C_{234} C_1$$

$$J_{31} = \frac{\partial z}{\partial \theta_1} = 0$$

$$J_{32} = \frac{\partial z}{\partial \theta_2} = L_2 S_2 + L_3 S_{23} + L_4 S_{234}$$

$$J_{33} = \frac{\partial z}{\partial \theta_3} = -(L_3 S_{23} + L_4 S_{234})$$

$$J_{34} = \frac{\partial z}{\partial \theta_4} = -L_4 S_{234}$$

This system is driven by direct hydraulic cylinders on three joints, but not on the shoulder joint. Thus, a Jacobian can be derived for expressing the relationship between the generative power of the hydraulic cylinder, F_{cyl} , and the torque around the torque shaft, Tang (torque gain G_T), as well as between the cylinder change velocity, V_{cyl} , and the velocity angle around the torque shaft, V_{ang} (angular velocity gain G_V). Here, each symbol and parameter value used are shown and listed in Fig. 3.9 and Table 3.3, respectively; H_i is the length of the cylinder that drives joint i .

[Shoulder]

A hydraulic motor drives the shoulder, and the following equation gives the torque at the joint, T_{sh} :

$$G_V(\theta_1) = G_T(\theta_1) = 1 \quad (3.5)$$

[boom]

From Fig. 3.9a, the length of hydraulic cylinder H_2 is

$$H_2^2 = l_{21}^2 + l_{22}^2 - 2l_{21}l_{22} \cos(\pi - \theta_2 + \delta_{21} - \delta_{22}) \quad (3.6)$$

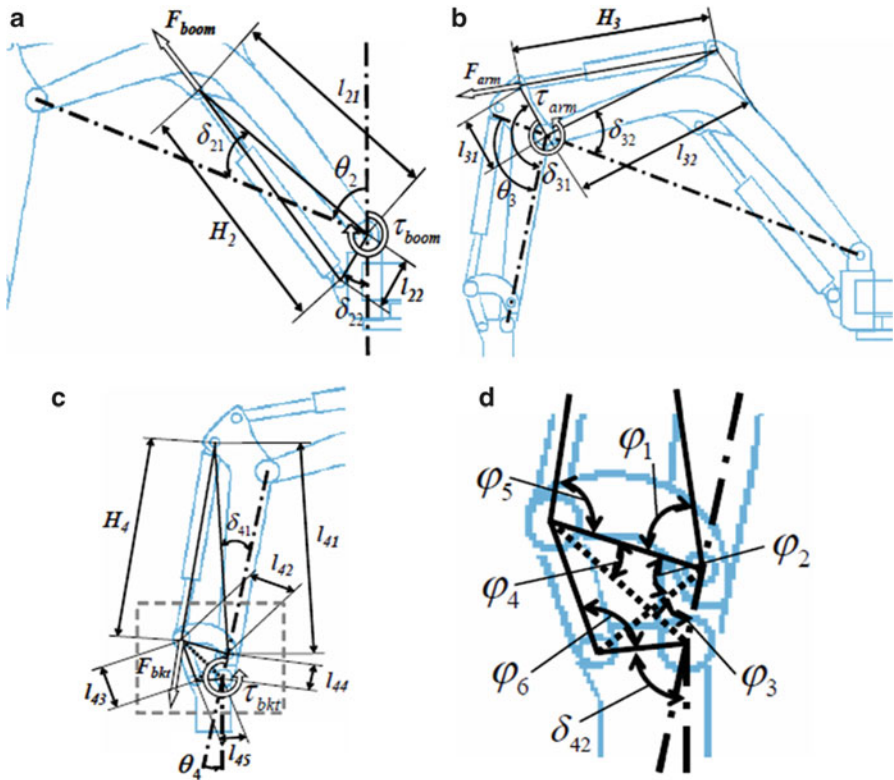


Fig. 3.9 Notation of the link mechanisms. (a) Boom, (b) Arm, (c) Bucket, (d) Bucket (zoom)

Table 3.3 Parameter of single-leg model

Parameter	Value	Parameter	Value	Parameter	Value
l_{21}	610 mm	l_{31}	155 mm	l_{41}	540 mm
l_{22}	170 mm	l_{32}	591 mm	l_{42}	133 mm
δ_{21}	17.8°	δ_{31}	140.0°	l_{43}	130 mm
δ_{22}	20.8°	δ_{32}	37.0°	l_{44}	71 mm
				l_{45}	100 mm
				δ_{41}	12.5°
				δ_{42}	60.0°

Upon application of the time differential,

$$H_2 \dot{H}_2 = -l_{21} l_{22} \sin(\pi - \theta_2 + \delta_{21} - \delta_{22}) \dot{\theta}_2 \quad (3.7)$$

This is the result, and the angular velocity gain, $G_V(\theta_2)$, is as follows:

$$G_V(\theta_2) = \frac{\dot{\theta}_2}{\dot{H}_2} = -\frac{H_2}{l_{21}l_{22} \sin(\pi - \theta_2 + \delta_{21} - \delta_{22})} \quad (3.8)$$

Then, the rotational torque, T_{boom} , of the shaft produced owing to thrust from the hydraulic cylinder, F_{boom} , is given as follows:

$$\tau_{\text{boom}} = -l_{21}F_{\text{boom}} \sin \psi_2 \quad (3.9)$$

where ψ_2 is expressed as follows:

$$H_2 \sin \psi_2 = l_{22} \sin(\pi - \theta_2 + \delta_{21} - \delta_{22}) \quad (3.10)$$

Thus, the torque gain $G_T(\theta_2)$, shown in Eqs. (3.9) and (3.10), changes to the following:

$$G_T(\theta_2) = \frac{F_{\text{boom}}}{\tau_{\text{boom}}} = -\frac{H_2}{l_{21}l_{22} \sin(\pi - \theta_2 + \delta_{21} - \delta_{22})} \quad (3.11)$$

From Eqs. (3.8) and (3.11), we get

$$G_V(\theta_2) = G_T(\theta_2) \quad (3.12)$$

[arm]

Following a procedure similar to that for the boom, the arm can be derived from Fig. 3.9b as follows:

$$G_V(\theta_3) = G_T(\theta_3) = \frac{H_3}{l_{31}l_{32} \sin(\pi - \theta_3 + \delta_{31} - \delta_{32})} \quad (3.13)$$

However,

$$H_3^2 = l_{31}^2 + l_{32}^2 - 2l_{31}l_{32} \cos(\pi + \theta_3 - \delta_{31} - \delta_{32}) \quad (3.14)$$

[Bucket]

From Fig. 3.9c, d, the torque gain $G_T(\theta_2)$ is

$$G_T(\theta_4) = \frac{F_{\text{bkt}}}{\tau_{\text{bkt}}} = \frac{1}{\sqrt{l_{42}^2 + l_{44}^2 - 2l_{42}l_{44} \cos(\varphi_2 + \varphi_3) \sin(\pi - \varphi_4 - \varphi_5)}} \quad (3.15)$$

However,

$$\alpha = \arccos \frac{l_{42}^2 + l_{43}^2 - l_{44}^2 - l_{45}^2 + 2l_{44}l_{45} \cos(\pi - \delta_{42} + \theta_4)}{2l_{42}l_{43}} \quad (3.16)$$

$$\varphi_2 = \arcsin \frac{l_{43} \sin \alpha}{\sqrt{l_{44}^2 + l_{45}^2 - 2l_{44}l_{45} \cos(\pi - \delta_{42} + \theta_4)}} \quad (3.17)$$

$$\varphi_6 = \arcsin \frac{l_{42} \sin \alpha}{\sqrt{l_{44}^2 + l_{45}^2 - 2l_{44}l_{45} \cos(\pi - \delta_{42} + \theta_4)}} \quad (3.18)$$

$$\gamma_1 = l_{43}l_{45} \cos(\varphi_6 + \delta_{12} - \theta_4) - l_{42}l_{44} \cos \varphi_2 \quad (3.19)$$

$$\gamma_2 = l_{43}l_{45} \sin(\varphi_6 + \delta_{12} - \theta_4) + l_{42}l_{44} \sin \varphi_2 \quad (3.20)$$

$$\varphi_3 = \arcsin \frac{l_{42}^2 + l_{44}^2 - l_{43}^2 - l_{45}^2}{2\sqrt{\gamma_1^2 + \gamma_2^2}} - \arccos \frac{\gamma_1}{\sqrt{\gamma_1^2 + \gamma_2^2}} \quad (3.21)$$

$$\varphi_1 = \pi - \delta_{41} - \varphi_2 - \varphi_3 \quad (3.22)$$

$$\varphi_4 = \frac{\arcsin(l_{44} \sin(\varphi_2 + \varphi_4))}{\sqrt{l_{42}^2 + l_{44}^2 - 2l_{42}l_{44} \cos(\varphi_2 + \varphi_3)}} \quad (3.23)$$

$$\varphi_5 = \pi - \arccos \frac{l_{42} + l_{41} \sin(\pi - \delta_{41} - \varphi_2 - \varphi_3)}{\sqrt{(l_{42} + l_{41} \sin(\pi - \delta_{41} - \varphi_2 - \varphi_3))^2 + (l_{41} \cos \varphi_1)^2}} \quad (3.24)$$

The length of hydraulic cylinder H_4 is

$$H_4 = \sqrt{l_{41}^2 + l_{42}^2 - 2l_{41}l_{42} \cos \varphi_1} \quad (3.25)$$

Then, with these conditions,

$$\beta_1 = \frac{\sqrt{l_{44}^2 + l_{45}^2 - 2l_{44}l_{45} \cos(\pi - \delta_{42} + \theta_4)} - l_{42} \cos \varphi_2}{l_{42} \sqrt{l_{44}^2 + l_{45}^2 - 2l_{44}l_{45} \cos(\pi - \delta_{42} + \theta_4)} \sin \varphi_2} \quad (3.26)$$

$$\beta_2 = \frac{\sqrt{l_{44}^2 + l_{45}^2 - 2l_{44}l_{45} \cos(\pi - \delta_{42} + \theta_4)} - l_{44} \cos \varphi_3}{l_{44} \sqrt{l_{44}^2 + l_{45}^2 - 2l_{44}l_{45} \cos(\pi - \delta_{42} + \theta_4)} \sin \varphi_3} \quad (3.27)$$

$$\beta_3 = \frac{l_{41}l_{42} \sin \varphi_1}{H_1} \quad (3.28)$$

$$\beta_4 = \frac{l_{44}l_{45} \sin(\pi - \delta_{42} + \theta_4)}{\sqrt{l_{44}^2 + l_{45}^2 - 2l_{44}l_{45} \cos(\pi - \delta_{42} + \theta_4)}} \quad (3.29)$$

The angular velocity gain $G_V(\theta_4)$ is expressed as follows:

$$G_V(\theta_4) = \frac{\dot{\theta}_4}{\dot{H}_4} = \frac{1}{(\beta_1 + \beta_2)\beta_3\beta_4} \quad (3.30)$$

The above equations can be combined to express the torque gain G_T and angular velocity gain G_V as follows:

$$G_T = \text{diag}[G_T(\theta_1), G_T(\theta_2), G_T(\theta_3), G_T(\theta_4)] \quad (3.31)$$

$$G_V = \text{diag}[G_V(\theta_1), G_V(\theta_2), G_V(\theta_3), G_V(\theta_4)] \quad (3.32)$$

Thus, the relationship between the foot force F_{foot} and cylinder thrust $F_{\text{cyl}} = [T_{\text{sh}} F_{\text{boom}} F_{\text{arm}} F_{\text{bkt}}]^T$ can be expressed as follows:

$$F_{\text{cyl}} = (JG_T)^T F_{\text{foot}} \quad (3.33)$$

Similarly, the relationship between the foot velocity V_{foot} and cylinder velocity $V_{\text{cyl}} = [\dot{\theta}_1 \dot{H}_2 \dot{H}_3 \dot{H}_4]^T$ can be expressed using a quasi-inverse matrix equation such as (3.34):

$$V_{\text{cyl}} = (JG_V)^+ V_{\text{foot}} \quad (3.34)$$

3.3.3 Manipulability

For performing a certain operation, a number of factors must be considered for designing the manipulator and determining the operating position and attitude within a workspace; one of the more important aspects is the amount of freedom of movement the foot attached to the end of the arm has in a given position and attitude. From the kinematics viewpoint, this ability to be manipulated can be quantified in terms of the manipulability ellipsoid and the manipulability measure; the leg mechanism can be analyzed using the degree of manipulability.

Consider a leg mechanism that has n degrees of freedom. The n dimension joint variable vector is q , and the foot position and attitude are expressed by the foot position vector, which is $r = [r_1, r_2, \dots, r_m]^T$ ($m \leq n$). Then, the geometric relationship between vectors q and r is given as follows:

$$r = f_r(q) \quad (3.35)$$

The relationship between the velocity vector v and joint velocity \dot{q} related to r is given as follows:

$$v = J(q)\dot{q} \quad (3.36)$$

Considering a set in which all feet v expressed using joint velocity \dot{q} satisfies a Euclidian norm $\|\dot{q}\| = (\dot{q}_1^2 + \dot{q}_2^2 + \dots + \dot{q}_n^2)^{\frac{1}{2}}$ where $\|\dot{q}\| \leq 1$, this will become an ellipsoid in m -dimensional Euclidian space. The highest foot speed can be achieved along the length of the major axis of this ellipsoid; the lowest foot speed can be achieved along the minor axis.

As this ellipsoid approaches a circle, the foot can move equally fast in any direction. Thus, this ellipsoid is considered to express the manipulability of the foot and is called the manipulability ellipsoid. The manipulability ellipsoid is expressed as follows:

$$v^T (J^+)^T J^+ v \leq 1, \quad \text{and} \quad v \in R(J) \quad (3.37)$$

Next, we determine the primary axis of the manipulability ellipsoid using J singular value decomposition. The following is the J singular value decomposition:

$$J = U\Sigma V^T \quad (3.38)$$

where U or V is an $m \times m$ or $n \times n$ rectangular matrix, the sum of which is found as follows:

$$\Sigma = \left[\begin{array}{ccccc} \sigma_1 & & & & \\ & \ddots & & & O \\ & & \ddots & & \\ O & & & \ddots & \\ & & & & \sigma_m \end{array} \right] \quad (3.39)$$

In addition, $\sigma_1, \sigma_2, \dots, \sigma_m$ is called a J singular value decomposition, and it consists of the $J^T J$ characteristic value $\{\lambda_i, i = 1, 2, \dots, n\}$ for those with a larger square root of λ_i up to m elements. In addition, by using u_i to express the i sequence vector of U , the primary axis of the manipulability ellipsoid can be determined from $\sigma_1 u_1, \sigma_2 u_2, \dots, \sigma_m u_m$. The most common measure of manipulability introduced by the manipulability ellipsoid is the ellipsoid volume. This is determined using $c_m w$. However,

$$w = \sigma_1 \sigma_2 \dots \sigma_m \quad (3.40)$$

$$c_m = \begin{cases} \frac{(2\pi)^{\frac{m}{2}}}{[2.4.6 \dots (m-2)]} \\ \frac{2(2\pi)^{\frac{m-1}{2}}}{[2.4.6 \dots (m-2)]} \end{cases} \quad (3.41)$$

Coefficient c_m is a constant when m is given; therefore, w is proportional to the ellipsoid volume. In addition, if we consider w as an index, it is called manipulability in attitude q . Manipulability w has the following qualities:

1.

$$w = \sqrt{\det J(q) J^T(q)} \quad (3.42)$$

2. When $m = n$, i.e., when there is no redundancy, w changes to the following:

$$w = |\det j(q)| \quad (3.43)$$

3. When $w \geq 0$, and $w = 0$,

$$\text{rank } J(q) < m \quad (3.44)$$

i.e., when in an anomalous attitude, and only in that case. Thus, we can interpret manipulability as an expression of one type of distance from anomalous attitude.

4. When $m = n$

$$|\dot{q}_i| \leq 1 \quad (i = 1, 2, \dots, m) \quad (3.45)$$

the entire set of v that can be expressed using the joint angle q and that satisfies Eq. (3.45) becomes a multifaceted parallelogram in m -dimensional space whose volume can be determined using $2mw$. This applies only when $m = n$, and it implies another w separate from the volume of the manipulability ellipsoid. In conclusion, I would like to discuss the relationship between force that the foot tip can apply to a target object and manipulability. This discussion assumes that the leg mechanism is not in an anomalous posture. The power that a static foot tip can apply to a target object is expressed as an m -dimensional vector f corresponding to v , where T represents the f -equivalent joint drive torque

$$\tau = J^T(q)f \quad (3.46)$$

The set of all f that can be expressed using a T and satisfying $\|\tau\| \leq 1$ forms an ellipsoid in m -dimensional Euclidian space:

$$f^T J(q) J^T(q) f \leq 1 \quad (3.47)$$

This is the force manipulability ellipsoid. The volume $\frac{c_m}{w}$ of the force manipulability ellipsoid is inversely proportional to w . In addition, the primary axis of the force manipulability ellipsoid is determined by using $\frac{u_1}{\sigma_1}, \frac{u_2}{\sigma_2}, \dots, \frac{u_m}{\sigma_m}$. Therefore, through comparison with the primary axis of the velocity manipulability ellipsoid, we found that the direction that produces the most power (in other words, along the longer semidiameter of the velocity manipulability ellipsoid) produces only a small amount of power, and conversely, in the direction that produces the most power, manipulability is bad.

3.4 Analysis of the Foot Mechanism

We retained the link mechanism of the commercial excavator without any modifications and designed the cylinder thrust, position, and other aspects as suited to the optimum leg mechanism of a walking robot. Here, we analyze the leg mechanism while eliciting the necessary conditions of self-support capacity, range of motion, and walking speed.

3.4.1 Definition of the Required Cylinder Force and Torque

Foot Reactive Force

Among other walking patterns, sideways walking is the main objective of COMET-IV. We selected the following three attitudes, which are considered to have the highest loads and determined the reactive force on each leg.

Attitude 1: Using three legs as support, start from the basic attitude and walk sideways on flat land with 70-cm strides.

Attitude 2: Using four legs as support, climb 1-m-high stairs.

Attitude 3: Using four legs as support, walk on a 20° gradient.

With three-legged support, we were able to elicit foot reactive force by resolving the statically determinate problem in the balance equation between the rectilinear moment and the vertical force. However, with four-legged support, redundancy appeared, resulting in a statically indeterminate problem. Here, we used the more rigorous angle of slope deflection method from the field of structure theory. In other words, in addition to the force and moment balance equation, we considered a test

that considered changes in the structure, thus making it possible to solve the statically indeterminate problem. The three selected attitudes are shown in Fig. 3.10. The reactive force for each foot is given beneath the supporting foot in the diagram (in kilograms). In addition, the robot's gross target weight was frozen to be 1,500 kg.

3.4.2 Jacobian Analysis

Here, the coordinates for each cylinder thrust (equation) and foot force (equation) are defined, as shown in Fig. 3.11. With these definitions, the relationship between the two forces can be expressed using the Jacobian J and torque gain G_T , formulas (3.48) and (3.49). Here, the torque τ_{mg} based on link weight is considered within the related equation:

$$F_{\text{foot}} = (J^T)^{-1} (G_T^{-1} F_{\text{cyl}} - \tau_{mg}) \quad (3.48)$$

$$F_{\text{cyl}} = G_T (J^T F_{\text{foot}} + \tau_{mg}) \quad (3.49)$$

In addition, we investigated the suitability of Jacobian-analysis-based methods by applying them to the one-legged model. As shown in Fig. 3.12, the pressure recorded by the pressure sensor and the cylinder's pressure receiver area are denoted by p and A , respectively; the supply and back pressure sides are denoted by subscripts 1 and 2, respectively. With a thrust efficiency of 1, thrust F_{cyl} is expressed by the following equation:

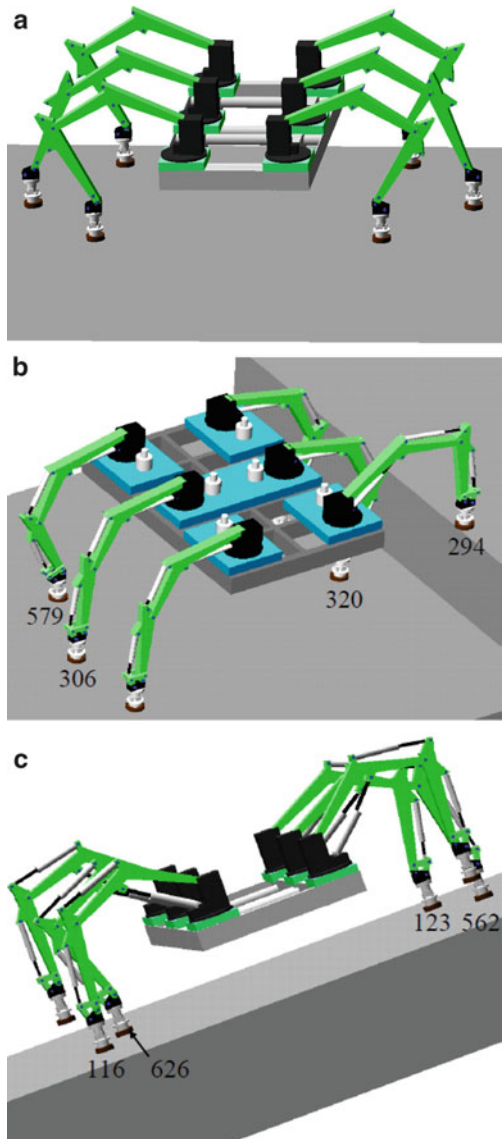
$$F_{\text{cyl}} = A_1 p_1 - A_2 p_2 \quad (3.50)$$

F_{cyl} is substituted in Eq. (3.48) to obtain F_{foot} . The value of the foot's force sensor, obtained for reference, is denoted by F_{fc} ; the values along the y - and z -axes are shown in Fig. 3.13. As can be seen, the results are closely matched, with a maximum variation of 5 %. This suggests that the Jacobian-analysis-based method is suitable for deriving the thrust on the leg mechanism and that it might be possible to achieve power control using only the pressure sensor. The use of the pressure sensor for leg control will be discussed later.

3.4.3 Analysis Results

Table 3.4 lists the calculated maximum thrust (F_{n1}) and torque (T_{n1}) values necessary for walking and the maximum thrust (F_p) and torque (T_p) capable of being generated by current commercial excavators. The terms "head" and "rod" refer to the head side

Fig. 3.10 Representative attitude of COMET-IV.
 (a) Attitude 1, (b) Attitude 2,
 (c) Attitude 3



or rod side of a single-rod cylinder. Furthermore, because $F_{n1} > F_p$ and $T_{n1} > T_p$ for both the boom and arm, extensive modification may be required. The analysis of the bucket shows that sufficient power is generated for walking on an incline; therefore, a redesign would not be necessary. As an example of the type of analysis, let us consider the case in which the z component of the power generated by the foot, F_{foot} , should be half the device weight, which is 7,500 N. Figure 3.14 shows the foot mechanism's possible range of motion, using the center of rotational force for the boom and arm

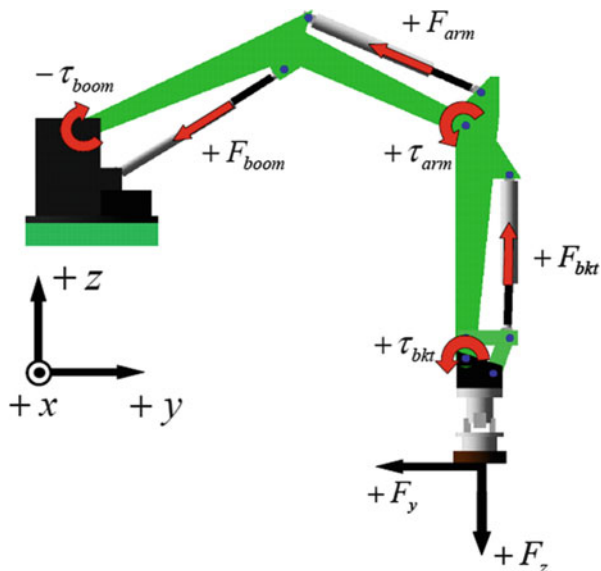


Fig. 3.11 Coordinate of COMET-IV leg

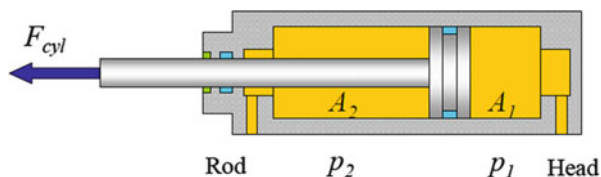


Fig. 3.12 Force of cylinder

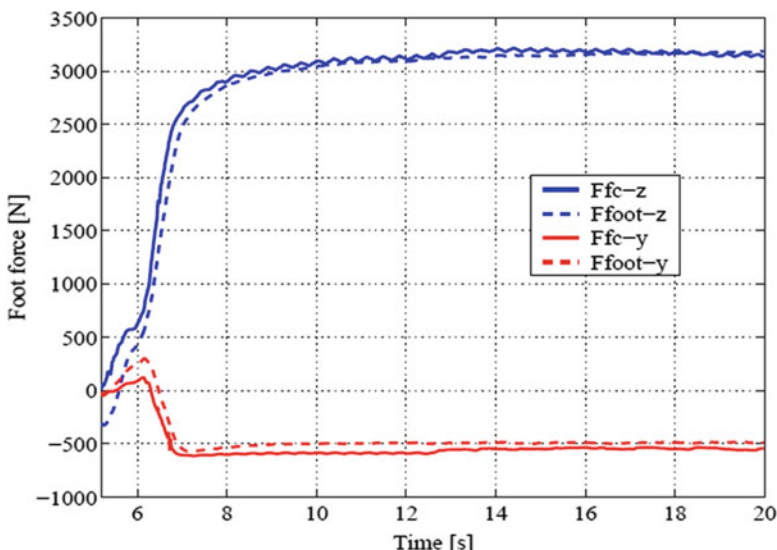
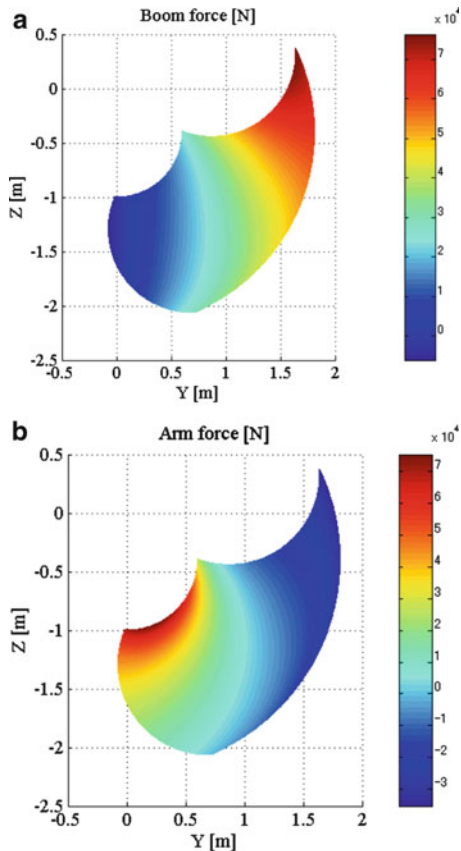


Fig. 3.13 Comparison of a measurement method of foot force

Table 3.4 Cylinder force analysis of single-leg model

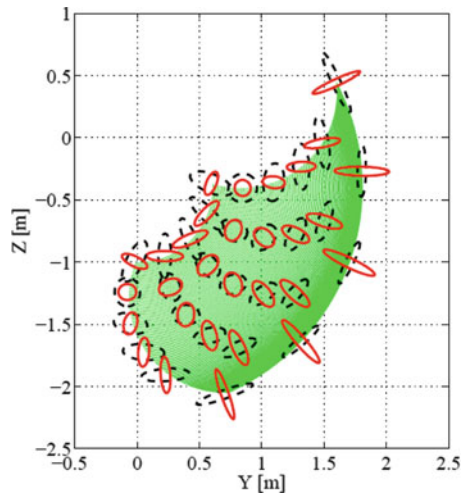
		F_{n1}, τ_{n1}		F_p, τ_p	
		Head	Rod	Head	Rod
Boom	F (N)	—	46,985	—	10,720
	τ (Nm)	—	-7,733	—	-1,822
Arm	F (N)	-15,593	22,560	-17,592	10,720
	τ (Nm)	-2,412	3,003	-2,726	1,661

Fig. 3.14 Necessary cylinder force. (a) Boom, (b) Arm



cylinders, which are necessary for support, as the starting point. From this figure, we can see that with regard to the boom, the further the foot moves from the main body, the greater is the force required; further, so long as the arm is in the range of $y = 0.8\text{--}1.2$ m and nearly perpendicular to the ground, the force required for arm movement is extremely small. In other words, the power required to lift the body is produced primarily from the rotational torque generated by the link mechanism, which

Fig. 3.15 Manipulability of single-leg model



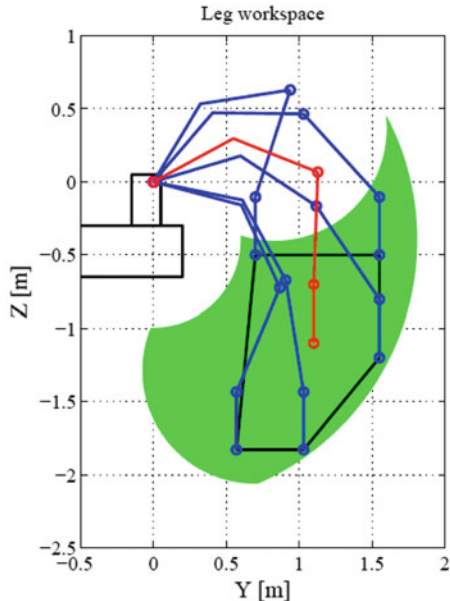
consists of the body, boom mechanism, and boom cylinder. Furthermore, when walking sideways (i.e., when a distance is created between the arm's center of rotation and the foot position), rotational torque from the arm is also necessary. Considering the above and that the boom link length is 1.13 m, the basic attitude was determined to be one in which the arm is almost perfectly perpendicular to the ground and the foot position (x, y, z) is almost at the center of the range of motion on the y, z -axes so that $(x, y, z) = (0, 1.1, -1.1)$.

Boom force required for the basic attitude is 45,802 N, whereas the current maximum possible force is 10,720 N, which is insufficient for supporting the body. Figure 3.15 shows the manipulability ellipsoid and operability ellipsoid for the single-legged model. Through the whole range of motion, the perpendicular length of the actual line of the operability ellipsoid is short. Therefore, the operability is insufficient from this viewpoint as well. The optimum leg mechanism design must consider loss of pressure in the transmission of oil along the conduit or within the controller valve, force efficiency of the cylinder, effects of oil compression, and other system failures. Therefore, we decided to ensure to incorporate a factor of safety (S) of 1.5.

3.4.4 Definition of the Necessary Workspace

Based on the analysis in the previous section, the cylinder positions were changed. When the joint torque was increased, the range of motion decreased. However, because the range of motion of the leg limits the scope usable for walking, as long as it is within a range that permits walking, any decreased in the range of motion will not affect the robot's walking ability. Thus, we set the necessary workspace, which is the minimum scope for walking, as follows. First, based on the 1-m-high

Fig. 3.16 Leg workspace of single-leg model



stair-climbing capability shown in Fig. 3.10b, the lower limit in the z direction was set to 2 points. Next, to conduct safe-landing actuation, the distance between the center of rotation of the boom and the base of the body was considered, and the upper limit in the z direction was set to 2 points. In addition, the necessary range in the y direction increased by 1 point, from 0.6 to 1.6 m. The limit on the scope of motion was set to 5, as shown in Fig. 3.16, and thus, the pentangle scope was set as the necessary range of motion. The thin line in the diagram represents the basic attitude.

3.4.5 Defining the Necessary Flow Rate and Walking Speed

The target walking speed for COMET-IV is 1 km/h. With a tripod stride of 70 cm, to achieve this goal a single cycle must be completed within 2.5 s. In addition, the oil flow at that time must be at a rate lower than the flow rate of the pump at maximum load. The maximum velocity, V_{\max} , was derived as per the following process.

Step 1 Determine walking trajectory of the foot of each leg and the foot velocity V_{foot} .

Step 2 Use relational expressions from Eq. (3.34) to find the cylinder velocity V_{cyl} for each cylinder.

Step 3 Calculate necessary flow Q for each leg considering the differential between the cylinder pressure receiver areas A_1 and A_2 based on positive and negative V_{cyl} .

Repeat the calculations for ($Q = AV_{\text{cyl}}$), and the V_{foot} value is the maximum foot velocity when the hydraulic power ($P \times Q$) equals the pump drive power. At that instant, the body velocity is at its maximum value, V_{\max} . However, for simplicity, the changes in the cylinder volume and the compression characteristics of oil were not considered in Step 3. As an example of analysis, Fig. 3.17a shows the walking trajectory and foot velocity for each leg of a tripod walking at a speed of 1 km/h, and Fig. 3.17b shows the results of converting that velocity to the speed of each joint cylinder. In addition, Fig. 3.18a shows the required flow at each joint when cylinder diameter is (boom: $\varphi 70-\varphi 35$, arm: $\varphi 55-\varphi 30$), and Fig. 3.18b shows the total required flow for the three legs on the right and left sides. The maximum value of the total required flow must be lower than the pump's flow rate at that instant.

3.5 Optimization of the Leg Mechanism

3.5.1 Optimization Process

Next, we performed optimization to find solutions that satisfied the required conditions derived by us. Complex machines such as robots and their leg mechanisms have many factors that require evaluation, and there is no unified method for evaluating these factors. The best method for creating a design manual is to turn all the objectives and processes into formulas and then use reverse analysis to find all the solutions at once. However, there are so many design factors for leg mechanisms that it would be very difficult to derive formulas for all of them. Consequently, in this design process, it would be difficult to arrive at unique solutions for all factors. Therefore, we took an eclectic approach by considering Jacobian analysis and investigating manipulability, cylinder specifications, buckling strength, practical installation location, safety ratios, etc. Then, by repeating the following steps, we arrived at the optimum solution:

Step 1 Increase thrust by using a cylinder with a wider diameter.

Step 2 Change cylinder location to improve joint torque.

Step 3 Select cylinder stroke that would satisfy the required range of operability.

Step 4 Calculate the necessary fluid flow and walking speed.

We repeated Steps 1–4 for range of motion, self-support, and walking speed until the optimum solution was determined. Here, we considered using a common JIS-standard hydraulic oil cylinder or a refined construction equipment cylinder for Step 1. The former was attractive in terms of price and availability. However, there were not many options in terms of cylinder diameter, and in many cases, the available options were deficient in terms of power, stroke length, etc. The latter

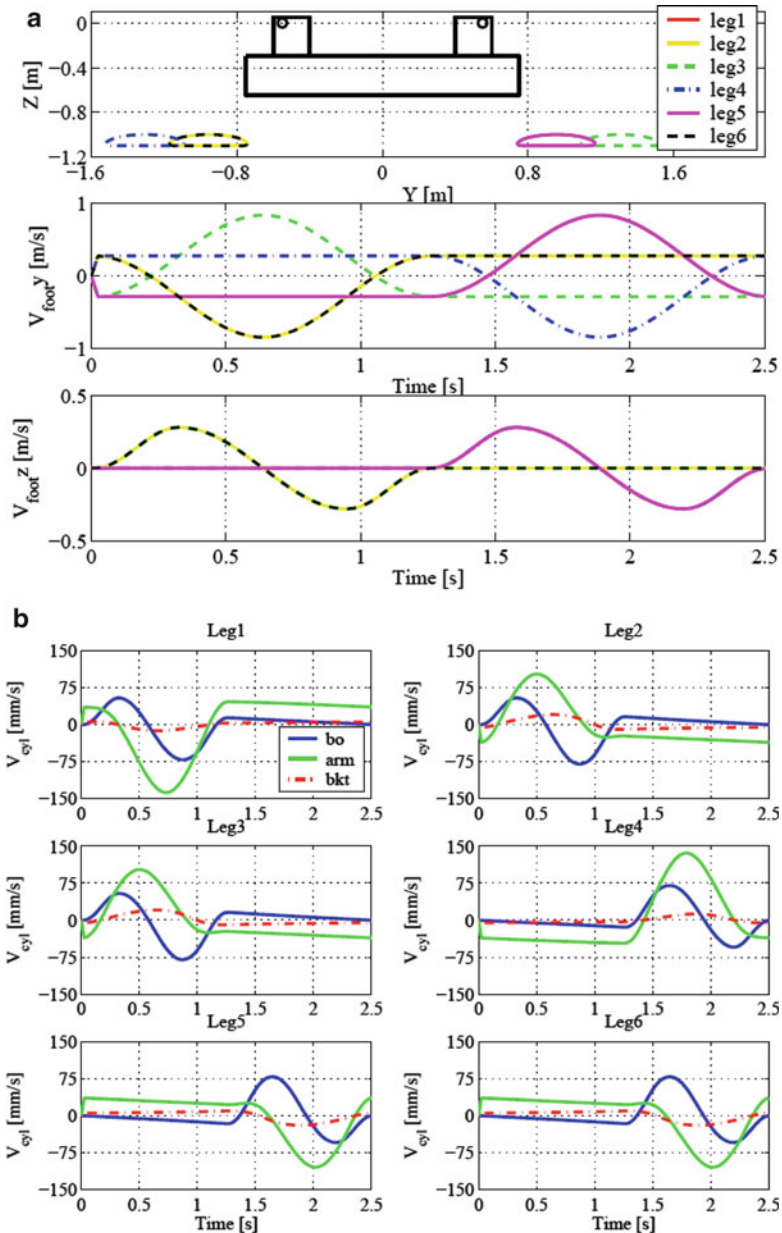


Fig. 3.17 Trajectory and cylinder velocity. (a) Step 1, (b) Step 2

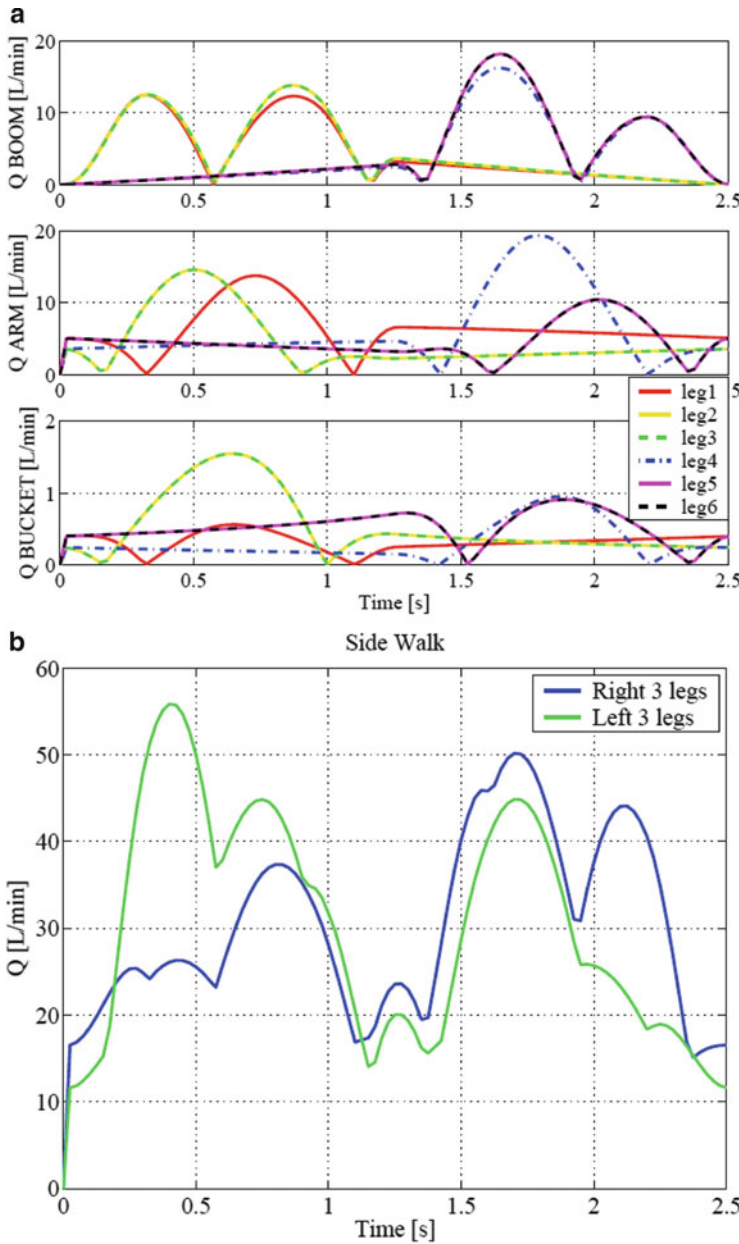


Fig. 3.18 Required flow. (a) Step 3–1, (b) Step 3–2

Table 3.5 Parameter of mechanism design ($S = 1.5$)

Stroke	l_{21} (mm)	δ_{21} (deg)	l_{22} (mm)	δ_{22} (deg)	F_n (N)	P (MPa)	Q (L/min)	V_{\max} (km/h)
260	613	15.0	0.207	22.1	38,344	19.93	45.2	0.840
270	660	13.8	0.215	21.3	36,880	19.17	47.0	0.862
280	675	12.7	0.223	20.5	35,559	18.48	48.8	0.884
290	690	11.7	0.230	19.8	34,460	17.91	50.3	0.900
300	707	10.6	0.240	19.0	33,036	17.17	52.5	0.916

cylinder type is slightly expensive, but it is compact, strong, highly reliable, and could easily withstand high pressures. Therefore, we used a construction equipment cylinder. For cylinder placement (Step 2), we considered placing the cylinder on the upper part of the boom mechanism such that the pressure-receiving area was effectively used on the large head side. We also considered installing two cylinders below the boom mechanism in a parallel configuration. However, the installation base for the former required heavy reinforcement, which increased weight. However, the latter required special installation and was not compact; therefore, we decided to install one cylinder at the bottom of the boom mechanism, similar to that in COMET-III. In this case, by increasing the distance between the center of rotation of the link and the cylinder, we were able to increase the torque; however, the cylinder speed and the range of motion decreased. Therefore, this tradeoff was given due consideration during the design process.

3.5.2 Optimization Results

In Step 1 of the abovementioned optimization process, consideration of the force and speed led to the conclusion that the optimum bore diameter of the boom was 70 mm (load diameter of 35 mm). Next, the cylinder stroke started at 260 mm—the lowest possible value of motion—and was increased in steps of 10 mm. Thereafter, the positioning of each cylinder was adjusted until they achieved the same range of motion, as summarized in Table 3.5. Here, in addition to each parameter, the required maximum force F_n , required maximum pump pressure P , and maximum velocity V_{\max} are listed. Assuming a force efficiency of 1, the force on the load side of a $\varphi 70-\varphi 35$ cylinder is shown in Eqs. (3.51)–(3.53); with a factor of safety of 1.5, the maximum force F_{\max} was determined to be 40,408 N. The required maximum pump pressure P was calculated using (equation). In addition, the output rating L_o of engine 1 was 22.7 ps (=16.7 kW); thus, the pump overall efficiency η was found to be 0.9. Considering these parameters, the oil force L_h under a pump flow rate of Q results in the following:

$$\frac{\pi(0.07^2 - 0.035^2)}{4} \times 21 \times 10^6 = 60613 \text{ N} \quad (3.51)$$

Table 3.6 Parameter of optimized design

		Before	After
Boom cylinder	l_{21} (mm)	610	675
	l_{22} (mm)	170	223
	δ_{21} (deg)	17.8	12.7
	δ_{22} (deg)	20.8	20.5
	Cylinder bore (mm)	40	70
	Rod diameter (mm)	25	35
	Stroke (mm)	250	280
Arm cylinder	l_{31} (mm)	155	175
	l_{32} (mm)	598	628
	δ_{31} (deg)	140	144
	δ_{32} (deg)	37	37
	Cylinder bore (mm)	40	55
	Rod diameter (mm)	25	30
	Stroke (mm)	270	270

$$P = \frac{\text{Required maximum thrust force } F_n}{\text{Maximum thrust force } F_{\max}} \times 21 \text{ MPa} \quad (3.52)$$

$$L_h = \frac{PQ}{60} = \eta L_a = 15.0 \text{ kW} \quad (3.53)$$

At a glance, it may seem that the longer the stroke, the smaller is the required maximum force F_n . However, as the stroke length increases, l_{21} increases as well; the result of this is that the leg mechanism becomes unshapely, cylinder buckles, and rotational center part needs additional reinforcement. In addition, a long stroke decreases precision and increases weight and cost. There are also tradeoffs between power and speed, and a long-stroke mechanism makes it difficult for the robot to achieve high speed. The net increase in V_{\max} is small, and therefore, increasing stroke length is not beneficial in terms of speed. Considering the above points, we decided to adopt a stroke length of 280 mm, which yields acceptable results in terms of power and speed. The arm can be evaluated in the same manner, and the final optimum solution is presented in Table 3.6. Figure 3.19 shows a diagram that compares the optimized leg with the stock leg. The load area ratio relative to the boom was 3.76, and the bore area ratio relative to the arm was 1.89 for a load area ratio of 2.17. In addition, to extract more joint torque, the distance between the cylinder and the joint was increased within reasonable limits.

Table 3.7 lists the enhanced self-support strength values. If the maximum force and torque required to walk are denoted by F_{n2} and τ_{n2} , and the maximum strength and torque obtained after optimization are denoted by F_o and τ_o , respectively, then the factor of safety (S) for the generated force is F_o/F_n , which must be higher than the 1.70—the factor of safety for the boom.

Considering potential system failure, the factor of safety of the necessary maximum force should be $S = 1.5$ or higher, and after optimization, there was

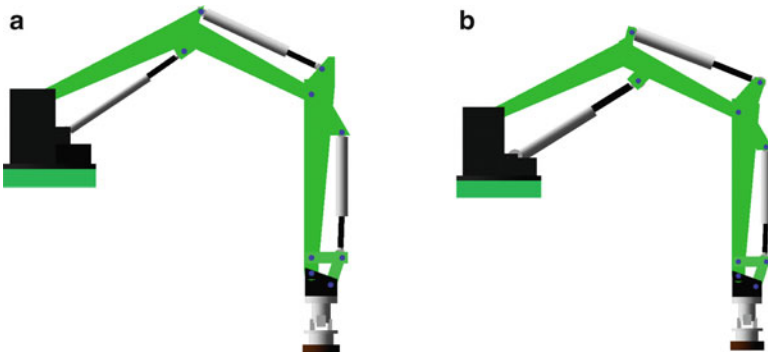


Fig. 3.19 Image of optimized leg. (a) Before, (b) After

Table 3.7 Cylinder force analysis of optimized leg

		$F_{n1,\tau_{n2}}$		F_{o,τ_o}	
		Head	Rod	Head	Rod
Boom	F (N)	—	35,559	—	60,613 ($S = 1.70$)
	τ (Nm)	—	-7,733	—	-13,516
Arm	F (N)	-13,831	20,164	-9,892 ($S = 3.60$)	35,048 ($S = 1.73$)
	τ (Nm)	-2,412	3,003	-8,731	6,133

sufficient self-support force available. Next, we compare manipulability before and after optimization.

Here, we envisioned the most frequently used gait, the tripod walk with 70-cm stride in the standard position (Fig. 3.10a), and investigated manipulability at three points in the trajectory.

At these three points, we used generation of speed in the y direction and generation of force in the z direction as indexes and compared the sum of the lengths of the ellipses L_w and L_f (Fig. 3.20). A comparison of the results obtained before optimization is shown in Fig. 3.21; the dotted line represents the manipulability ellipsoid, whereas the solid line represents the operability ellipsoid. Based on this, the sums of L_w before and after optimization were 1:0.865; likewise, a comparison of the L_f sums before and after optimization yielded a value of 1:1.290.

Thus, from the speed-evaluation parameter L_w , we concluded that it was difficult to generate speed. However, with a large increase in L_f , the leg mechanism could easily generate power while maintaining its speed. Figure 3.22 shows the new range of motion. In this figure, the blue line represents the range of motion after optimization, which covers the necessary workspace; this confirms that a sufficient range of motion was achieved. In addition, the analysis results show that the walking speed, which should be within 1–1.70 km/h, was 0.809–1.330 km/h, which is very close to the required walking speed of 1 km/h. Therefore, we were

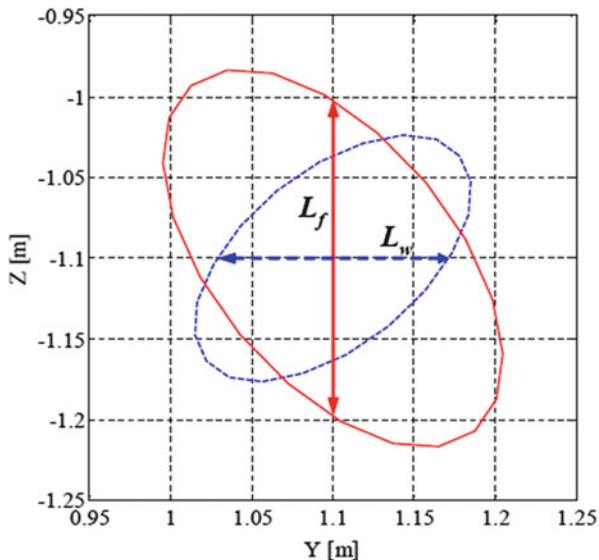


Fig. 3.20 Definition of L_w and L_f

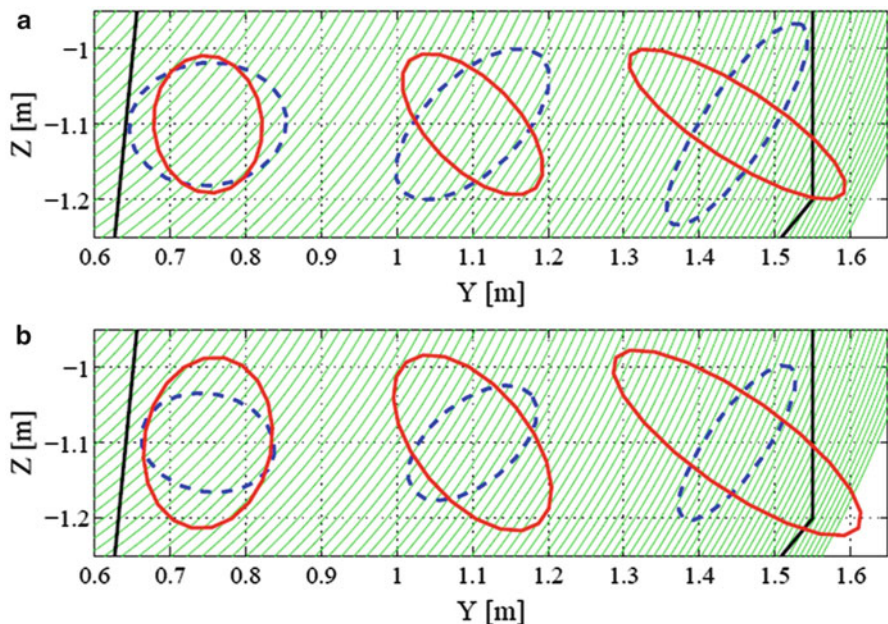
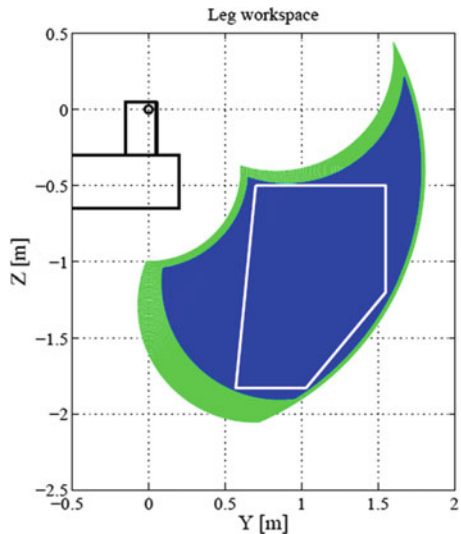


Fig. 3.21 Comparison of manipulability. (a) Before, (b) After

Fig. 3.22 Leg workspace of optimized leg



successful in designing an optimized leg mechanism that fulfills the desired walking speed requirement.

After arriving at the optimum leg mechanism design, we designed the entire COMET-IV system.

3.6 Exterior View of the Completed COMET-IV

The completed exterior view of COMET-IV is shown in Fig. 3.23. Figure 3.23a is a front view and b is a top view of COMET-IV which is a hydraulically driven hexapod robot that is designed to operate on extremely unstructured terrain such as daunting area and mountain area that contain rough terrain, soft terrain, and steep slopes. This robot is 2.5 m long, 3.3 m wide, 2.8 m high, and approximately two thousand kilograms weights. Two gasoline engines drive two hydraulic pumps. This research project started in 2005 by focusing on the main objective as mentioned until late 2011 that involves walking with the force/impedance control, fully autonomous navigation with laser mapping, tele-operation walking control, and several solutions on positioning precessions (Table 3.8). The current research issues are as follows:

1. *Locomotion on extremely unstructured terrain using force/impedance control*
In this task, force threshold-based walking trajectory is designed with support of optimal impedance control. The force on end-effector is reading a force delivery on each foot that calculated from pressure on the thigh and shank of the leg and torque on each joint. The target of the research is to create an

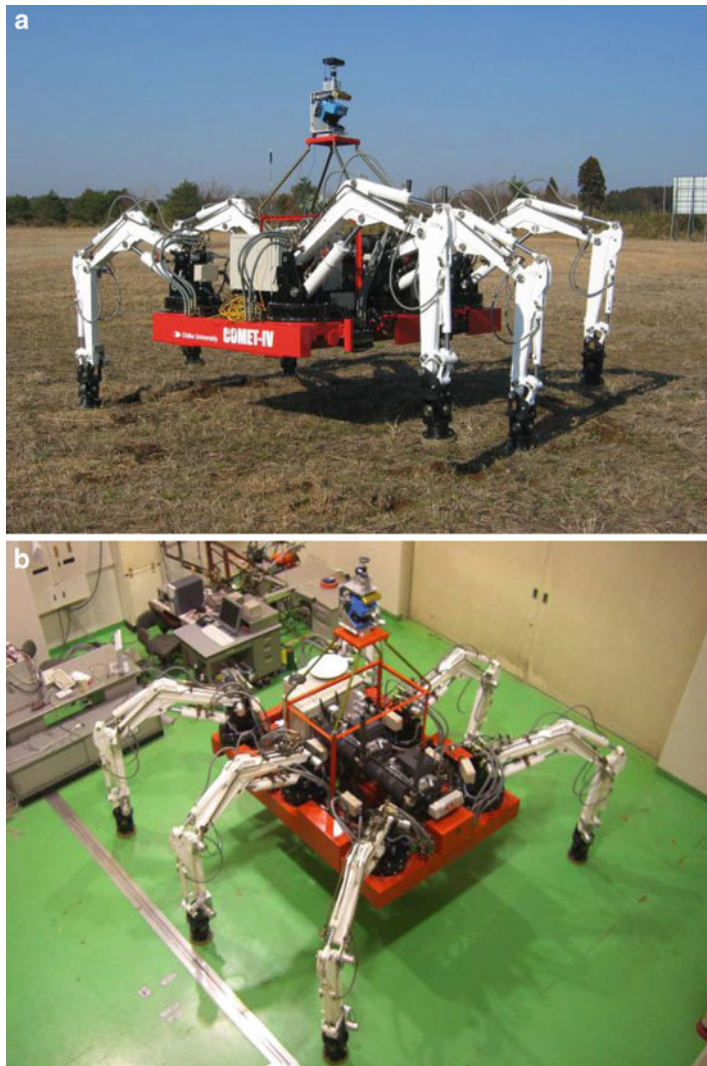


Fig. 3.23 Overview of COMET-IV. (a) Front view, (b) Top view

adaptive foot motion on each robot's leg that can compensate and differentiate the natural ground surfaces/changes, maintaining its body horizontal stable. In addition, in combination with three-dimensional mapping using laser range finder, the walking mode and planning is improved with precise foot stepping and obstacle/wall avoidance.

Table 3.8 COMET-IV hardware equipment

	Company	Product name (model number)
<i>Mechanics</i>		
Gasoline engine	Fuji heavy industries	Robin engine (EH72.25PS/3,600 rpm)
Generator	Mitsubishi motors	A001 TA1891A. 21 V. 1,200 W
Reduction gears	Harmonic drive systems	Harmonic drive CSF-40-160-2UH-SP
Bearing	Nippon Thompson	Crossed roller bearings (CRBC30025UU)
<i>Hydraulics</i>		
Hydraulic pump	Bosch Rexroth	A10V0 (28DFLR 78 L/min 2,750 rpm)
Proportioning solenoid valve	HAWE	PSV(PSV3S1)
Hydraulic cylinder	Nippon Kiki Kogyo	(Custom-built)
Hydraulic motor	Eaton fluid power	Orbit motor (J-08EBB-B)
Oil filter	Taisei Kogyo	Line filter (UL-10A)
Suction filter	Taisei Kogyo	Suction filter (SFT-10-150W)
Hydraulic oil	Japan energy	Hydlux (ISO VG 32)
<i>Electronics</i>		
CPU board	Kontron	CP306
Computer box	Kontron	CP-ASM3
A/D board	United electronic industries	cPCI/PXI (PDXI-MF-64-400-14H)
D/A board	United electronic industries	cPCI/PXI (PDXI-AO-32/16)
IEEE1394 board	ADTEX system science	Compact PCI (aPCI-8314)
Valve controller	HAWE	PLVC4
Potentiometer	Midori measurement instrument	Green pot (CPP-45/45B)
Pressure sensor	Keyence	AP-V80.AP-15S
Attitude sensor	Micro strain	FAS-A
WLAN access point	Siemens	Scalance (W788-2PRO)
WLAN client	Siemens	Scalance (W744-1PRO)
Emergency stop switch	Circuit design	WR-01, WT-02
Battery	The Furukawa battery	Standard battery (30A19L.R)

2. Three-dimensional mapping by laser range finder readings and obstacle avoidance

We are investigating ways to improve the robot's ability to avoid obstacles by using three-dimensional mapping data generated from data readings of the laser range finder.

3. Locomotion control on the steep slope

The task is toward achieving stable locomotion on a 20-degree slope (max inclination). The task is also used in the force threshold-based control

but solution is more focusing on giving the required stable (robot's body) walking on irregular steep slopes.

4. *High-speed locomotion*

The study is focusing on achieving one of the COMET-IV development objectives. The main task is focusing on achieving high-speed locomotion purposely for flat or smooth ground/surfaces.

5. *Gripper on foot*

Currently, we are upgrading the robot's leg structure with a gripper for sorting and removing rubbles operation. This modified structure will become a new line of COMET-IV research and is involved in enhancing the tele-operation control with combination of several previous progresses.

6. *Remote control*

This research area is related to the latest improvement of COMET-IV leg structure (gripper on foot), which is focusing to realize the targeted gripping task and enhancing the tele-operation control study. Currently, bilateral master-slave control became a main scope of study using with the force feedback.

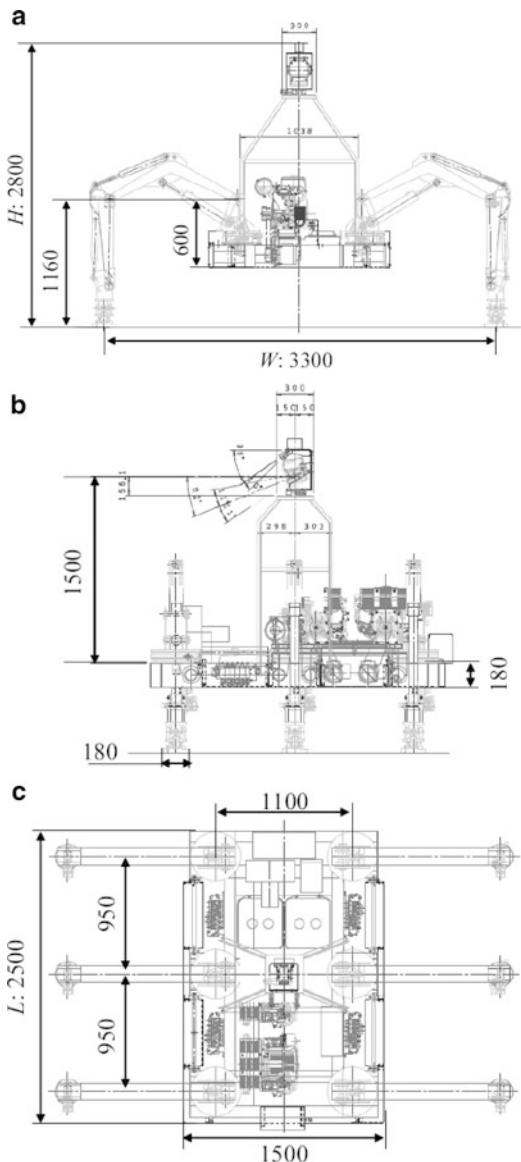
Figure 3.24 shows diagrams created using a three-dimensional CAD software suite, and Fig. 3.23 shows the exterior view of a fully assembled COMET-IV created from these diagrams. Eventually, the total weight of COMET-IV was 2,120 kg, around 600 kg more than the desired value.

7. *Fully autonomous walking navigation system*

In this section, we discuss the fully autonomous walking navigation system. The system algorithm is discussed in detail in a later chapter, so the discussion here will focus primarily on devices that constitute this system.

Figure 3.25 shows the arrangement of the primary devices used in the navigation system. A laser range finder is attached at a depressed angle at the top and center of the main unit and another laser range finder is attached horizontally to the front of the main unit; the former device is used to monitor the topography and detect any obstructions, whereas the latter device is used primarily for detecting obstructions. The information collected by these laser range finders, as well as that collected by the GPS, direction sensors, and attitude sensors, allows the robot to be aware of its location and attitude and create a dimensional map of the external environment. The GPS receiver, navigation computer, and attitude sensor are attached to the front of the robot body frame, and the GPS antenna is located on the body's central sensor mount frame. The direction sensor is mounted on top of the sensor mount unit, which is located at the top of the central part of the robot body.

Fig. 3.24 Drawing of COMET-IV. (a) Front view, (b) Side view, (c) Top view



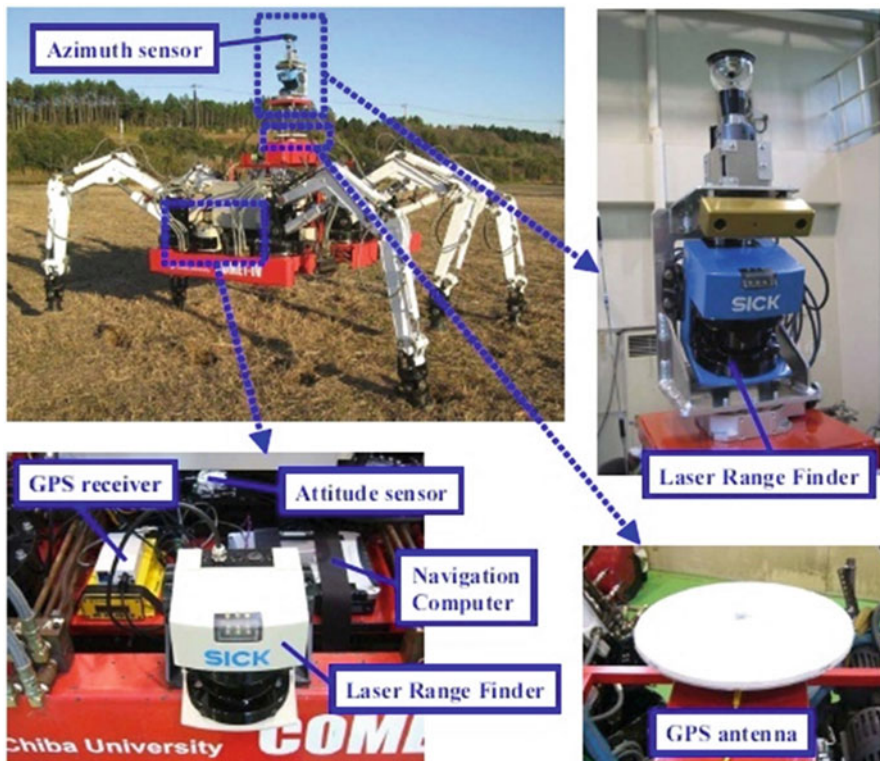


Fig. 3.25 Setup of autonomous navigation system

References

1. U.S. Department of State (1998) Hidden killers: the global demining crisis. U.S. Department of State Publication, Washington DC
2. International Committee of the Red Cross (1999) Landmines must be stopped: overview 1999. ICRC Publication, Geneva
3. Chesney R et al (2002) Terrain adaptive scanning of conventional mine detectors. In: IARP workshop on robots for humanitarian demining (Hudem'02), pp 69–74
4. Gonzalez de Santos P, Jimenez MA (1995) Generation of discontinuous gaits for quadruped walking machines. J Robotic Syst 12(9):599–611
5. Nonami K et al (2003) Development and control of mine detection robot COMET-II and COMET-III. JSME Int J Ser C 46(3):881–890
6. Ikeda Y, Nonami K (2004) Preview sliding mode walking control of hexapod robot COMET-III. Trans Jpn Soc Mech Eng C 70(700):3484–3492
7. McGhee RB, Jain AK (1972) Some properties of regularly realizable gait matrices. Math Biosci 13(1):179–193
8. Uchida H, Nonami K (2003) Feedback Force reference generation for attitude control of six leg walking robot. Trans Jpn Soc Mech Eng C 69(685):2315–2322

9. Raibert MH, Craig JJ (1981) Hybrid position/force control of manipulators. *Trans ASME J Dyn Syst Meas Control* 102:126–133
10. Nonami K, Tian H (1994) Sliding mode control. Corona, Japan
11. Lauda ID, Courtiol B (1974) Design of multivariable adaptive model following control systems. *Automatica* 10:483–494
12. Robotics Society of Japan (ed) (2005) Handbook of robotics. Corona, Japan
13. Song S-M, Waldron KJ (1988) Machines that walk – the adaptive suspension vehicle. MIT, Cambridge
14. The Walking Forest Machine. <http://www.plustech.fi/Walking1.html>
15. Hodoshima R et al (2005) Development of quadruped walking robot TITAN XI for steep slope operation. *J Robotic Soc Japan* 23(7):847–857
16. Heinrichs B et al (1997) Position-based impedance control of an industrial hydraulic manipulator. *IEEE Contr Syst Mag* 17(1):46–52
17. Nagata F et al (1997) Impedance control for articulated robot of critically damped condition with an object dynamics. In: Proceedings of the SICE 36th annual conference, pp 1119–1124, Tokushima, Japan
18. An HC, Hollerbach JM (1987) Dynamic stability issues in force control of manipulator. In: Proceedings of IEEE international conference on robotics and automation, pp 890–896, Raleigh, NC, USA

Chapter 4

Kinematics, Navigation, and Path Planning of Hexapod Robot

Abstract In Chap. 3, fundamental analysis on COMET-IV’s leg kinematics and dynamics has been briefly discussed. On further research progress on this robot, the developed kinematics and dynamics are exploited to be used for end-effector force on foot detection and overall COMET-IV stability for force-attitude control purposes. In COMET-IV research progress, the total force on foot is calculated for center of mass (CoM) identification as an input for robot attitude during walking session. This method is based on shoulder coordination system (SCS) kinematics on vertical position and total of force on foot for each touching leg on the ground. On the other hand, the designed force delivery on foot value is categorized phase by phase and threshold sensing method is applied for dynamic trajectory walking named *force threshold-based trajectory*. This method is done to achieve the novel end-effector force sensorless method that is applicable for large-scale legged robot that required expensive sensor on each leg’s tip.

4.1 COMET-IV Kinematics (Inverse/Direct) and Force Sensing

As previously mentioned, COMET-IV was designed with 4-DOF since it has four different links to each leg [1]. Corresponding to the mechanical structure design of the leg, each link has been set up in the laboratory with certain angle limitation as shown in Table 4.1. Thus the calculation of kinematics for this robot is based on the determined angle limitations and also on the shoulder point known as shoulder coordinate system (SCS), as shown in Fig. 4.1. SCS becomes the main kinematic for COMET-IV since there is no material movement on the frame of the body and the frame is not fragile (flat frame). Thus, the calculations of kinematics based on center of body (CoB) or body coordinate system (BCS) are calculated from SCS for each leg as proposed in [2], and this is shown in Fig. 4.2.

Table 4.1 Link angle configuration (limitations)

Joint	Link	Length (m)	Range (degrees)
Shoulder	1	0.00	$-120^\circ \leq \theta_1 \leq 60^\circ$ (legs 1–3) $-60^\circ \leq \theta_1 \leq 120^\circ$ (legs 4–6)
Thigh	2	1.13	$53^\circ \leq \theta_2 \leq 131^\circ$
Shank	3	0.77	$35^\circ \leq \theta_3 \leq 144^\circ$
Foot	4	0.39	$-56^\circ \leq \theta_4 \leq 108^\circ$

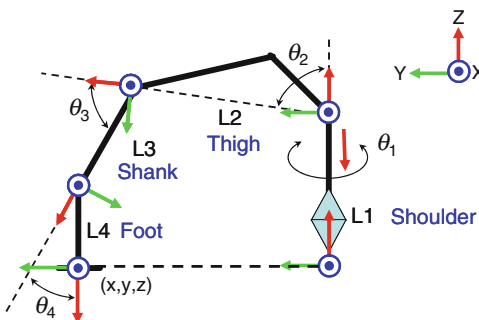


Fig. 4.1 Shoulder-based coordination system (one leg)

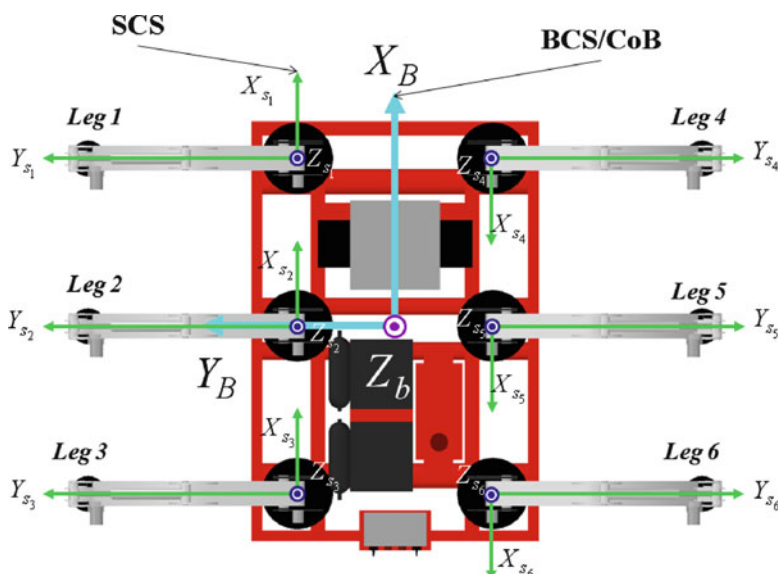


Fig. 4.2 Coordinate system used for COMET-IV

For control purposes, kinematics of each rotational joint angle is defined based on SCS as shown in Fig. 4.1, where $\Theta_{r_n} = [\theta_1 \ \theta_2 \ \theta_3 \ \theta_4]^T$ against the leg coordinates $\Gamma_{r_n} = [x_{r_n} \ y_{r_n} \ z_{r_n}]^T$ which are limited within the specific range as shown in Table 4.1. It should be noted that n represents the number of legs ($n = 1, 2, 3, \dots, 6$). The motion of each leg can be described using the following equations:

$$x_{r_n} = \Delta\theta_1(L_1 + L_2\Delta\theta_2 + L_3\Delta\theta_{23} + L_4\Delta\theta_{234}) \quad (4.1)$$

$$y_{r_n} = \Delta\Phi_1(L_1 + L_2\Delta\theta_2 + L_3\Delta\theta_{23} + L_4\Delta\theta_{234}) \quad (4.2)$$

$$z_{r_n} = L_2\Delta\Phi_2 + L_3\Delta\Phi_{23} + L_4\Delta\Phi_{234} \quad (4.3)$$

where $i = j = k = 1, \dots, 4$ denote leg's joint tags and L_i is a leg's link, as shown in Fig. 4.1, and $\theta_{ijk} = \sin(\theta_i + \theta_j + \theta_k)$ and $\Phi_{ijk} = \cos(\theta_i + \theta_j + \theta_k)$. The inverse kinematics is used to convert the leg coordinates (generated from trajectory sequences) to joint angles coordinates, which the latter coordinates are necessary to define the control input signal. The inverse kinematics of each joint are described using the following equations:

$$\theta_1 = \tan^{-1}\left(\frac{x_{r_n}}{y_{r_n}}\right) \quad (4.4)$$

$$\theta_2 = \frac{\pi}{2} \tan^{-1}\left(\frac{z_{r_n} - L_4}{\sqrt{x_{r_n}^2 + y_{r_n}^2}}\right) - \tan^{-1}\left(\frac{L_3 \sin \theta_3}{L_2 + L_3 \cos \theta_3}\right) \quad (4.5)$$

$$\theta_3 = \cos^{-1}\left(\frac{x_{r_n}^2 + y_{r_n}^2 + (z_{r_n} - L_4)^2 - L_2^2 - L_3^2}{2L_2L_3}\right) \quad (4.6)$$

$$\theta_4 = \pi - \theta_2 - \theta_3 \quad (4.7)$$

Corresponding to the inverse kinematics of each link (feedback from potentiometers), the force acting on the foot of leg- n ($n = 1 \dots 6$) can be calculated from the torque of each link via the Jacobian matrix (J) of the actual rotation of velocity ($\dot{\Theta}$) for each joint of the robot's leg and the leg axis velocity ($\dot{\Gamma}$). The Jacobian matrix of a leg is written as follows [3]:

$$J_n = J_{3 \times 4} = \frac{\partial \Gamma_{o_n}}{\partial \Theta_{o_n}} \quad (4.8)$$

For hydraulic-driven link, the force on each attached hydraulic cylinder must be considered. Therefore, in the case of COMET-IV, the force delivered to the foot through the torque of each link and the pressure of the cylinder found on the thigh and shank can be expressed as follows:

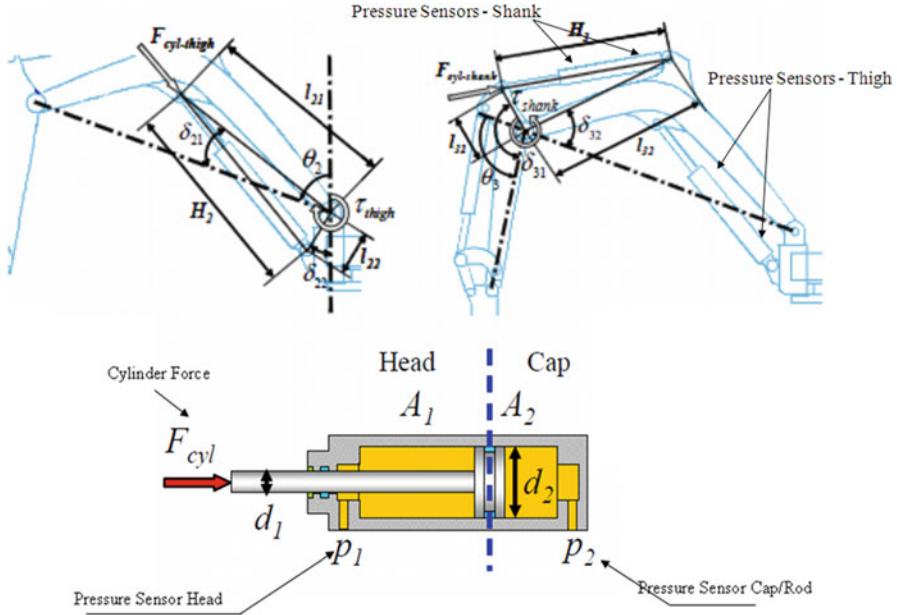


Fig. 4.3 Configuration of the hydraulic cylinder attached to the thigh and shank of the robot's leg

$$\mathbf{F}_{\text{foot}_n} = [F_x \quad F_y \quad F_z]^T = J_n^{-T}(\boldsymbol{\tau}_{\text{cyl}_n} + \boldsymbol{\tau}_{g_n}) \quad (4.9)$$

where $\boldsymbol{\tau}_{g_n} = \sum_{k=1}^3 J_k [0 \quad 0 \quad m_k g]^T$ and $\boldsymbol{\tau}_{\text{cyl}_n} = G_{\text{th}_n} F_{\text{cyl-th}_n} + G_{\text{sh}_n} F_{\text{cyl-sh}_n}$. m is the actual mass of the leg's joint for link- k . G_{th_n} and G_{sh_n} are the torque gains, based on Fig. 4.3 [3], and are calculated as follows:

$$G_{\text{th}} = \frac{l_{21}l_{22} \sin(\pi - \theta_2 + \delta_{21} - \delta_{22})}{H_2} \quad (4.10)$$

$$G_{\text{sh}} = \frac{l_{31}l_{32} \sin(\pi + \theta_3 + \delta_{31} - \delta_{32})}{H_3} \quad (4.11)$$

where

$$H_2 = \sqrt{l_{21}^2 + l_{22}^2 - 2l_{21}l_{22} \cos(\pi - \theta_2 + \delta_{21} - \delta_{22})}$$

and

$$H_3 = \sqrt{l_{31}^2 + l_{32}^2 - 2l_{31}l_{32} \cos(\pi + \theta_3 + \delta_{31} - \delta_{32})}$$

The fixed value for each vertical sub-links (l_{nm}) and sub-angles (δ_{nm}) is estimated in accordance with the actual dimensions of the COMET-IV legs [3]. Table 4.2 summarizes the values of l_{nm} and δ_{nm} .

Table 4.2 Torque gain values

Sub-links	Dimension (m)	Sub-angles	Angle (degree)
l_{21}	0.675	δ_{21}	12.7
l_{22}	0.223	δ_{22}	20.5
l_{31}	0.175	δ_{31}	144
l_{32}	0.628	δ_{32}	37

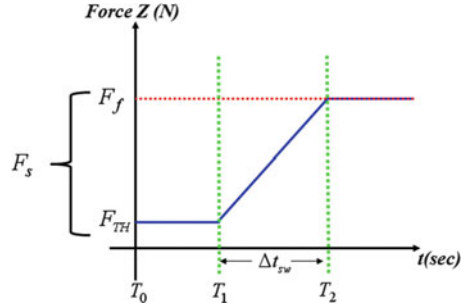
4.2 COMET-IV Center of Mass/Gravity

As discussed in Sect. 1.4, the stability of the legged robot depends on the position of CoM, whether or not it is within the *support polygon*. The CoM is effectively the same as the center of gravity (CoG) whenever the body is sufficiently rigid and the gravitational forces are uniform. However, in a nonuniform gravitational field, $\text{CoM} \neq \text{CoG}$ since CoM is now moving in the certain position. CoM is the point equivalent to the total body mass, or the point at which the weight of the body can be considered to act [4]. On the contrary, for a legged robot in motion, CoM is developed from the numbers of center of pressure (CoP) points [5]. In designing the locations of CoP in most legged robot with $k \leq 3$ configuration, determining zero moment points (ZMP) is essential for the stability of the robot as the mass is not stationary. On the contrary, in the case of legged robot with $k > 3$ configuration, the probability that the robot is statically stable is very high as the mass of the body is stationary. However, for flat or *table-like* structure such as COMET-IV, when it is walking on extremely uneven terrain using fixed trajectory position, body inclination happens and the situation could lead to instability. This instability can be traced to the changes in CoM since the position of the point where the weight of the body seemed to act changes with body inclination. For COMET-IV, real-time CoM ($B(t)$), which represents the robot's instantaneous body height based on SCS, can be determined using the following equations:

$$B(t) = \begin{cases} B_r - \frac{\sum_{i=a}^c z_{o_i}(t) F_{s_i}(t)}{\sum_{i=a}^c F_{s_i}(t)}; & \text{Walking} \\ B_r - \frac{\sum_{i=a}^6 z_{o_i}(t) F_{s_i}(t)}{\sum_{i=1}^6 F_{s_i}(t)}; & \text{Transient} \end{cases} \quad (4.12)$$

where $i = a, b$, and c are the tripod legs that touch the ground during walking and $i = 1, \dots, 6$ are the legs that touch the ground during the transient phases. $B_r = |Z_o - S_h|$ is the ideal body vertical position from shoulder to ground surface (standing up) based on SCS; for COMET-IV, $S_h = 0.78$ m is the normal height in the standing position, $Z_0 = -0.5$ m is a fixed initial value for the coordinates of each leg in the vertical axis (based on SCS), and B_r is calculated

Fig. 4.4 Static force generation, $F_s(t)$, based on a linear interpolation method



under the assumption that the average z_R is the same as the ideal body height (positive value). It should also be noted that z_o is the vertical position output of each leg, which is sensed using potentiometers on each joint of the leg (converted by direct kinematics as described in Sect. 4.3). On the other hand, F_s is the linear vertical static force acting on each leg and is calculated using a linear interpolation method [3] as shown in Fig. 4.4; this calculation method is used because each leg touches the ground at a different position during the support phase of the ETT module system (will be discussed later).

The $F_s(t)$ can be calculated by solving the equilibrium of forces and moment acting on the robot, which is expressed as follows:

$$\begin{aligned} W_g &= F_{sa}(t) + F_{sb}(t) + F_{sc}(t) \\ 0 &= (x_{r_a}(t) - x_G)F_{sa} + (x_{r_b}(t) - x_G)F_{sb} + (x_{r_c}(t) - x_G)F_{sc} \\ 0 &= (y_{r_a}(t) - y_G)F_{sa} + (y_{r_b}(t) - y_G)F_{sb} + (y_{r_c}(t) - y_G)F_{sc} \end{aligned} \quad (4.13)$$

Where $W_g = M_{bg}$ is the mass of the robot's body (in Newton) and $x_{r_a}(t), x_{r_b}(t), x_{r_c}(t)$, $y_{r_a}(t), y_{r_b}(t)$, and $y_{r_c}(t)$ are generated reference values for the leg motion according to SCS (as discussed in Sect. 4.3) from the ETT real-time state flow module (will be discussed later). Furthermore, $x_G = x_{cog} - l_{pp}$ and $y_G = y_{cog} - l_w$ are the center points of the robot, as shown in Fig. 4.5. Lastly, l_{pp} and l_w are the length of the robot's leg and half the width of the robot's body, respectively, both of which correspond to the structural dimensions of the actual robot.

By assuming that the center of gravity (CoG) coordination is equal to the CoB (ideal or zero), $x_G = -l_{pp}$, $y_G = -l_w$, and $F_s(t)$ can be expressed as follows:

$$F_{si}(t) = \begin{cases} F_{TH}, & T_0 < t < T_1 \\ F_{TH} + \frac{F_f(t) - F_{TH}}{\Delta t_{sw}}, & T_1 \leq t < T_2 \\ F_f(t), & t \geq T_2 \end{cases} \quad (4.14)$$

Where $i = 1, \dots, 6$ and $\Delta t_{sw} = 2s$ is the extra time that has been granted to COMET-IV in the ETT walking module to sense the hardness of the ground (for the first time) before it pushes its body up. Additionally, $F_f(t)$ is a moment and force equilibrium matrix, which can be expressed as follows:

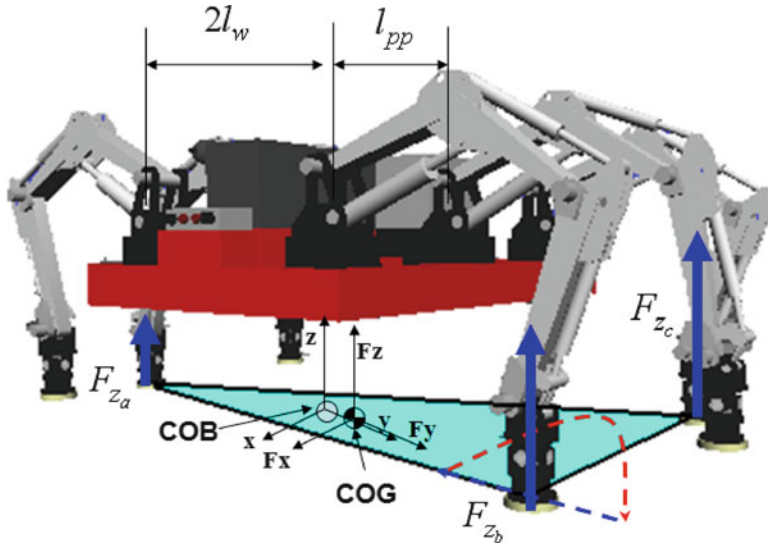


Fig. 4.5 Tripod force coordination/orientation and *support polygon*

$$F_{fi}(t) = I_3 H^{-1} F_g^T \quad (4.15)$$

where $F_g = [W_g \quad 0 \quad 0]$ and H is calculated as follows:

$$H = \begin{bmatrix} 1 & 1 & 1 \\ \text{sign}(q)x_{r_a}(t) & \text{sign}(q)(x_{r_b}(t) + l_{pp}) & \text{sign}(q)(x_{r_c}(t) + l_{pp}) \\ \text{sign}(q)(y_{r_a}(t) + l_w) & \text{sign}(q)(y_{r_b}(t) + l_w) & \text{sign}(q)(y_{r_c}(t) + l_w) \end{bmatrix}$$

In this case, note that a is considered as a center leg (Leg 2 or Leg 5) of the robot (see Fig. 4.5), and based on the BCS, $q = 1$ for legs 1–3 and $q = -1$ for legs 4–6. Figure 4.6 shows a sample of $F_{si}(t)$ generated in an experiment that was carried out with the proposed ETT module and with a tripod pattern on flat terrain (fundamental test).

4.3 Navigation and Path Planning Issues in Field Robotics Applications

Navigation is the process of monitoring and controlling the movement of a craft or vehicle from one place to another. For instance, a car is driven by a driver from a start point to a destination following direction and a map given by a navigation system. A car navigation system may suggest some routes for the driver to choose, whether to select a shortest distance but has to pay more for tolls or a long distance

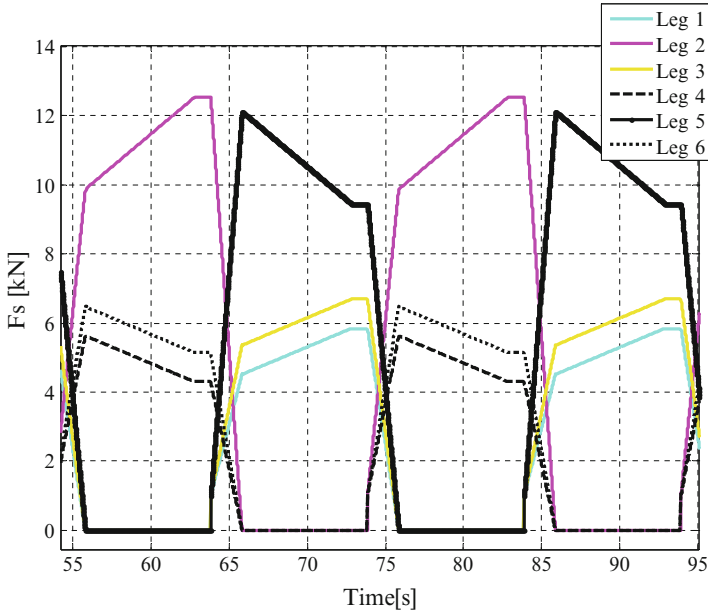


Fig. 4.6 Sample of $F_s(t)$ generated during an actual experiment

using toll-free road. Normally, the location of the car at any time in this period is determined based on global positioning system (GPS) data of the system. Similarly, in the case of a robot navigation system, a map either is given or is developed by the robot itself. Based on the map, the navigation system of the robot selects a shortest path and relays the information to a controller that drives the robot from a start point to a targeted destination, while avoiding obstacles. The location of the robot may also be traced using odometer or other sensors such as GPS. The robot may be controlled by an operator for a manual navigation and by a set of algorithm that is already uploaded into the robot computer for an autonomous navigation. However, there are many issues that haven't been resolved yet, especially when the proposed methods will be applied to a legged robot. Some of the issues that are going to be highlighted in this chapter are as follows:

1. Unknown environment exploration for a map building: As for current achievement [6–9], the mapping task is done by a wheeled robot, which has capabilities to move fast, immediate turning, and immediate stops. The wheeled robot can explore a big area and construct a map of unknown environment by itself and then plan a walking path after that.
2. Information associated in the map: The information is associated in the map developed by a wheeled robot, not included with obstacles height since the purpose of the map built is to navigate a robot from a start point to a destination point while avoiding those obstacles. Instead, a legged robot has capabilities to walk over, step on, ascending and descending obstacles. The capabilities can be

capitalized only if the information of the map is included with the height of the obstacles present in the environment.

3. Performing specific tasks: Most of the legged robots have been operated for specific tasks. For instance, the TITAN-IX [10] and ROBOCLIMBER [11] have been operated on mountain for slope consolidation and monitoring.
4. High operation cost: Most of the advanced robots, such as the BigDog and Athlete, have been equipped with many expensive sensors that make the robot movement very dynamic. However, it is desirable to use minimum quantity and less expensive sensors, but the robot can function well and achieve all designated tasks.
5. Blind navigation: Most of the legged robots in operations have been operated based on leg-sensing information, such as the BigDog [12] and ROBOCLIMBER, or they are controlled from a nearby remote place, where the operator controls the movement of the robot. This will not enable the robot to be autonomously navigated to a far place, unless the robots are equipped with several expensive sensors as mentioned above.

4.4 Movement Control Methods

For legged robot locomotion control, there are several methods that can be used to generate the trajectory movement, either by intelligent method such as [13, 14] or manually determined via teleoperation unit such as [15]. However the basic movement needs to be based on the defined kinematics that depends on robot structure configuration. With multi-DOF and multi-legged as COMET-IV system, the capability of movement can be achieved to omnidirectional movement. Omnidirectional here means the robot is capable of performing and operating with fixed movement; left, right, forward, and backward; centroid rotating, zigzag/flanking movement; and pedestrian lane changed movement as shown in Fig. 4.7.

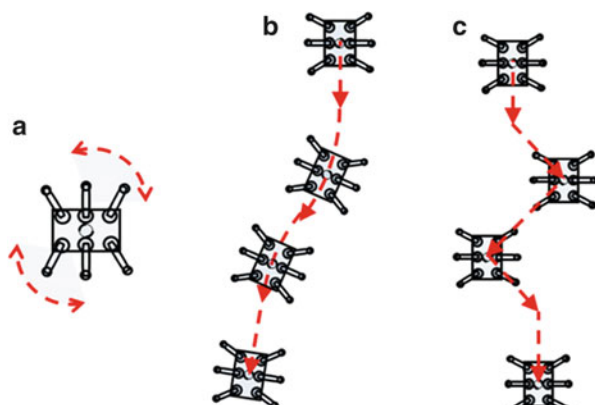


Fig. 4.7 Omnidirectional moving capability: (a) centroid rotating, (b) zigzag (flanking), (c) pedestrian lane change



Fig. 4.8 Section of COMET-IV trajectory generation module based on SCS

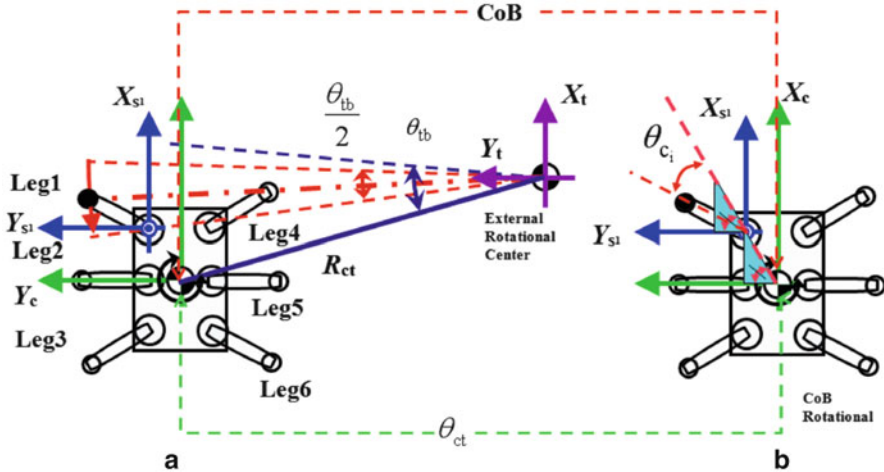


Fig. 4.9 Omnidirectional rotation moving concept: (a) external rotational center based and (b) proposed CoB rotational based

Moreover, with SCS and BCS approach in kinematics calculation, as discussed in Sect. 4.1, the trajectory system module/unit for multi-legged and multi-DOF robot as COMET-IV is defined as shown in Fig. 4.8.

Two methods can be done to perform omnidirectional movement for multi-legged robot system: external rotational center-based method and CoB rotational-based method. These methods can be chosen depending on the objective of the control structure design. As, for example, in COMET-IV progress, CoB rotational-based method is used for force control walking instead of external rotational center-based method, since CoB rotational-based module structure is less complicated in combination process with force-based motion that is discussed in Sect. 4.5. For external rotational center-based method as shown in Fig. 4.9a [16], the design and calculation are including the leg motion movement and based on the SCS and BCS as defined in Sect. 4.1. The shoulder position is determined with reference to the external point defined in Fig. 4.9a and calculated as Eq. (4.16) as follows:

$$\begin{bmatrix} X_{sf_1}(t) \\ Y_{sf_1}(t) \end{bmatrix} = \begin{bmatrix} R_{ct} \cos \theta_{ct}(t) - x_{ts_1} \\ R_{ct} \sin \theta_{ct}(t) - y_{ts_1} \end{bmatrix} \quad (4.16)$$

Where R_{ct} is the radius between robot CoB and defined external point or foot turning radius which is calculated as follows:

$$R_{ct} = \sqrt{X_{tf_1}^2(0) + Y_{tf_1}^2(0)} \quad (4.17)$$

and θ_{ct} is rotational angle input on CoB that is calculated as Eq. (4.18) as shown in Fig. 4.9a:

$$\theta_{ct}(t) = \frac{\theta_{tb}}{4} (\cos \frac{2\pi t}{T} - 1) + \tan^{-1} \frac{Y_{sf_n}(0) + y_{ts_n}}{X_{sf_n}(0) + x_{ts_n}} \quad (4.18)$$

where t is the update time (real time) (s), Y_{sf_n} is the initial position of y-axis for each foot based on SCS (m), X_{st_n} is the initial position of x-axis for each foot based on SCS (m), Y_{ts_n} is the position of y-axis for each foot based on BCS (m), and X_{ts_n} is the position of x-axis for each foot based on BCS (m).

Moreover, the traverse angle (θ_{tb}) of the robot's body in Eq. (4.18) needs to consider the range of the leg motion for one cycle of foot stepping with reference to the defined law as follows [16]:

$$R_{ct} \sqrt{2(1 - \cos \theta_{tb})} \leq r_b \quad (4.19)$$

Where $r_b = 2d_L$ is the line where the robot's CoB is moved after completing one cycle of foot stepping with reference to the defined horizontal workspace as shown in Fig. 4.10.

It is different to the CoB rotational-based method whereby the θ_{ct} can be defined directly with reference to Tables 4.3 and 4.4. The movement angle command input (θ_{c_n}) for this method is based on SCS as follows:

$$\theta_{c_n} = 0.5\theta_{ct} - \theta_{c_{o_n}} \quad (4.20)$$

where θ_{o_n} is the initial SCS-based angle for n -leg; normally 20° is used for side legs (legs 1, 3, 4, and 6) and 0° for center legs (legs 2 and 5) in COMET-IV. Therefore, for side movement (left, right, forward, backward) and zigzag/flanking movement, input is scheduled as Table 4.3 with reference to the defined law in Fig. 4.11:

$\theta_{m_s} = \{\theta_{c_{ct1}}; \theta_{c_{ct3}}; \theta_{c_{ct4}}; \theta_{c_{ct6}}\}$ and $\theta_{m_c} = \{\theta_{c_{ct2}}; \theta_{c_{ct5}}\}$ are the SCS angle control input for side legs and center legs, respectively, and each leg has a different starting point. Furthermore, for centroid rotating moving, θ_{ct} is scheduled as Table 4.4 corresponding to the defined law in Fig. 4.12 which is depending on the desired

Fig. 4.10 Horizontal workspace of each leg defined for safety omnidirectional movement

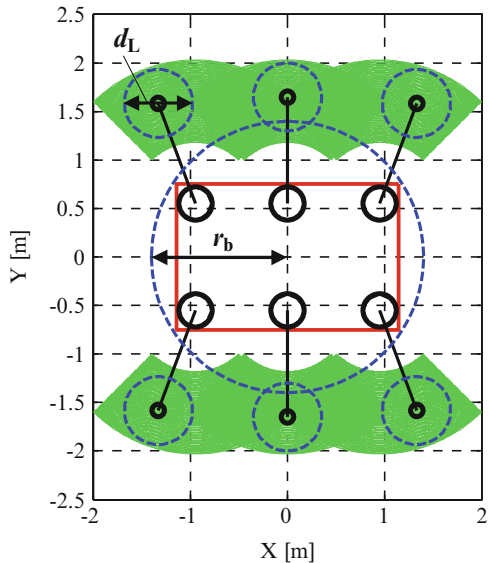


Table 4.3 SCS control input for side/zigzag moving

Side moving	θ_{ct}
Right	$0 < \theta_{m_s} < 180^\circ; 180^\circ < \theta_{m_c} < 360^\circ$
Left	$0 < \theta_{m_c} < 180^\circ; 180^\circ < \theta_{m_s} < 360^\circ$
Forward	$\theta_{m_s} = 180^\circ; \theta_{m_c} = 0^\circ$
Backward	$\theta_{m_s} = 0^\circ; \theta_{m_c} = 180^\circ$

Table 4.4 SCS control input for centroid rotating moving

Rotational moving	θ_{ct}
CW	$180^\circ < \theta_{135} < 360^\circ$ $0^\circ < \theta_{246} < 180^\circ$
CCW	$0^\circ < \theta_{135} < 180^\circ$ $180^\circ < \theta_{246} < 360^\circ$

direction of rotation, whether clockwise (CW) or counterclockwise (CCW). θ_{ct} input defined in Table 4.4 is the example for the tripod gait pattern mode.

As for summary, external rotational center-based method and CoB rotational-based method performed same movement, since both methods used the same kinematics coordination base structure. The selection of these methods is depending on the objective control strategy and structure design.

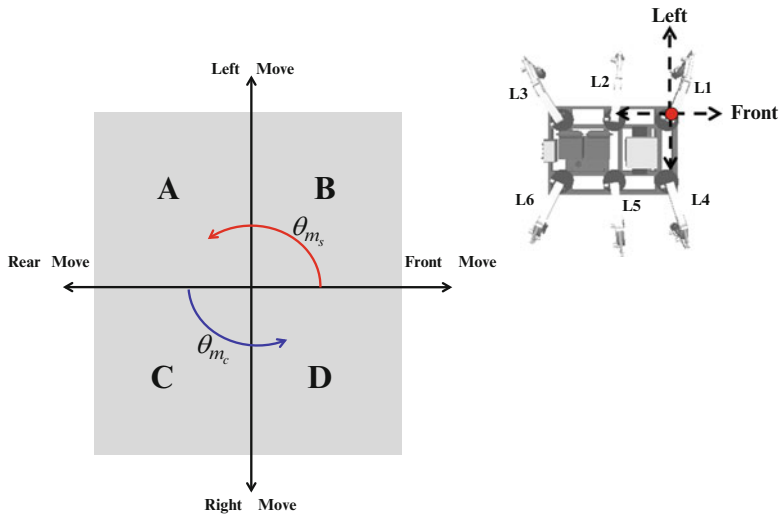


Fig. 4.11 Side/zigzag moving angle control inputs law based on SCS

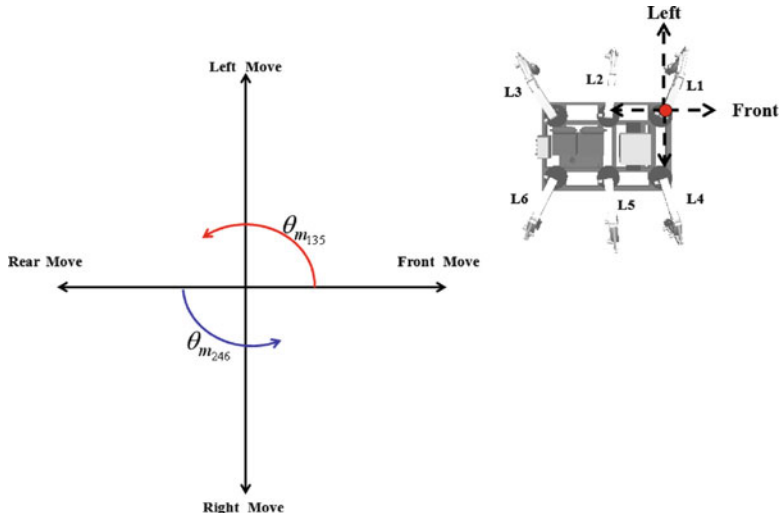


Fig. 4.12 Centroid rotating moving angle control inputs law based on SCS

4.5 Terrain Adaptive Foot Trajectory Using Force Threshold-Based Method

Such as hydraulically driven and heavy hexapod robot that is based on hydraulic cylinder pressures and angle rotational position feedback on its control system module, it is necessary to consider a force threshold method during initial touching in order to differentiate the stepping on uneven terrain. Applying force sensor on

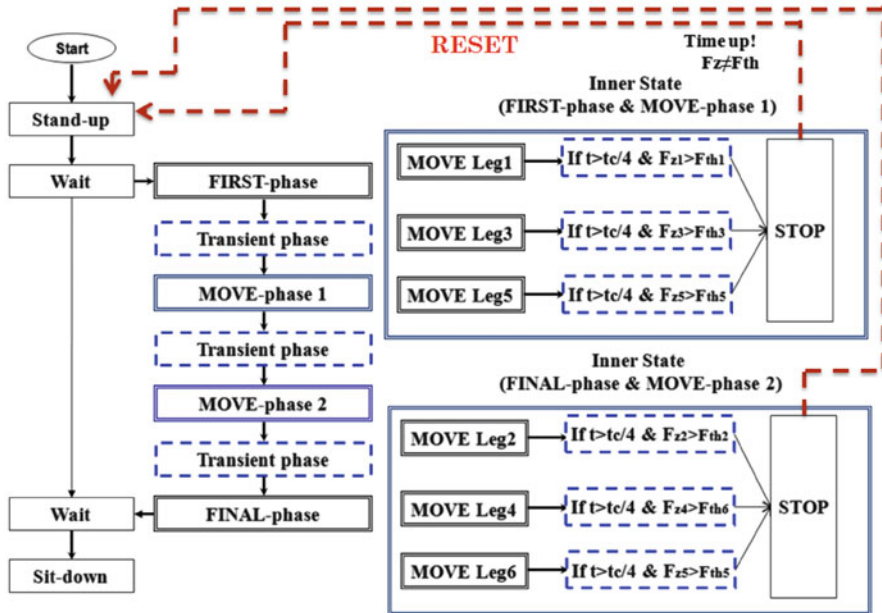


Fig. 4.13 General flow of ETT module for tripod walking pattern

each foot may become an alternative and easy solution, but it is costly and not practical since the value of hydraulic cylinder pressures is known. For hydraulically driven hexapod robot, the force threshold-based trajectory can be designed and combined with any gait patterns to perform stable walking on the uneven terrain. This trajectory gives an extra force each time a leg touches a terrain, hence giving the ability to the robot to sense the level of the terrain. As shown in Fig. 4.13, the force threshold-based method, named as environment-trailed trajectory (ETT) [17], is designed to stand alone as a module and used to filter the vertical feedback touching forces using logical bit {1, 0} for the control system module.

The vertical force for each leg (F_{z_0n}) denotes an external force and is one of the component of a vector of force delivery on the foot, $F_{\text{foot}} = \{F_{x_0}, F_{y_0}, F_{z_0}\}$, which is derived from the thigh and shank cylinder pressures and the torque acting on each joint of the leg. The vertical force can be calculated as follows:

$$F_{z_0n} = F_{\text{foot}}(z) = I_{1,3}F_{\text{foot}} \quad (4.21)$$

As expressed in Eq. (4.16), $I_{1,3} = [0 \ 0 \ 1]$ and F_{z_0n} is the feedback force acting on the leg; the leg is stopped from pushing the ground once the feedback force has reached the predetermined threshold force (F_{TH}) in the ETT module. For the modified ETT used in this study, only filtered F_{z_0n} is used in the front control system of the plant, as shown in Figs. 4.14 and 4.15 for experiment sample result.

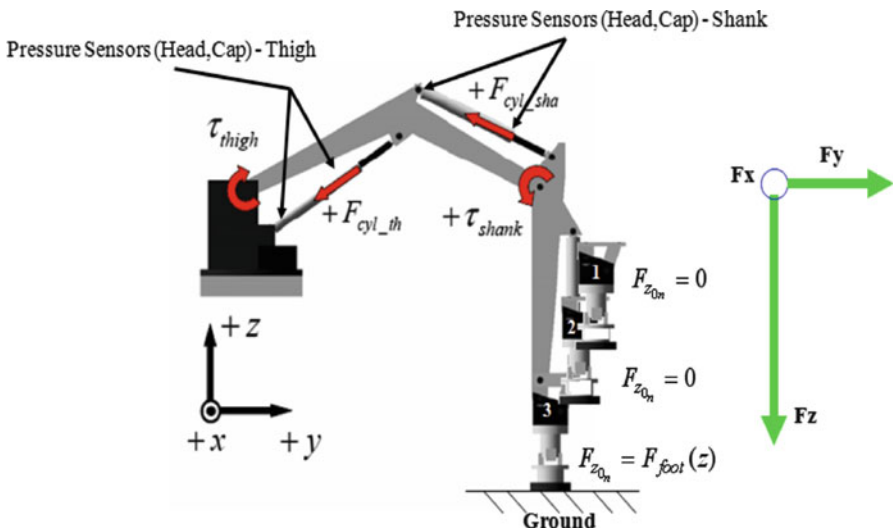


Fig. 4.14 Force delivery coordination for each leg of the robot and $F_{z_{on}}$ reading condition

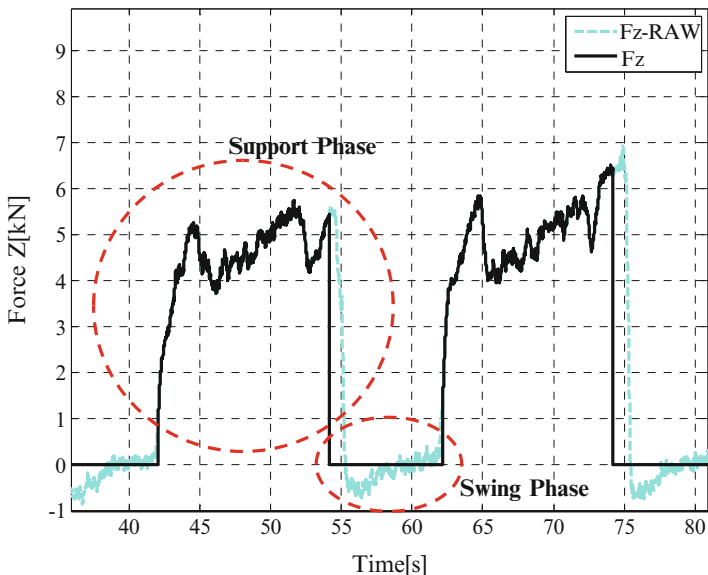
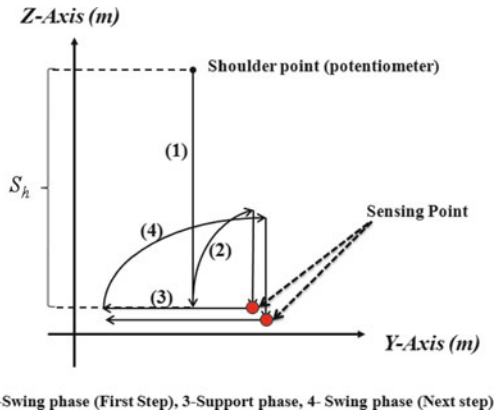


Fig. 4.15 Sample of $F_{z_{on}}(t)$ reading from an actual experiment; $F_z - RAW$ is a vertical force reading for all leg motion phases, and F_z is a vertical force reading only for the support phase (filtered by Bit 1 state from the ETT module)

Fig. 4.16 Example of foot point movement for force threshold-based trajectory based on SCS



1-Stand-up, 2-Swing phase (First Step), 3-Support phase, 4- Swing phase (Next step)

F_{TH} can be set up based on the total weight of the robot itself (for COMET-IV case, F_{TH} is set to 1 kN for each leg).

The setup F_{TH} value should be sufficient for each of the robot's leg to start patching and carry its body during a walking session. However, for the robot to achieve a stable walk when the ETT method is employed, three criteria are set and should be implemented:

1. The leg that has been moved must remain in contact with the ground until the movement for center of gravity ends. The leg should trail the pattern of the environment after it is in contact with the ground.
2. The maximum applied force should be reduced and controlled before starting the swing phase in the next step.
3. During the grounding period, the force must be directed vertically along each leg that touches the ground, and the total force should be approximately or equal to the weight of the robot's body.

All this criteria are important especially for static move-based walking robot using linear actuator with estimated force delivery on foot.

The foot trajectory pattern, as shown in Fig. 4.16, is designed with 90° vertical push down to the ground in order to get precise F_{z0} values. The example of equations for the motion as shown in Fig. 4.16 expressed using Eqs. (4.7)–(4.22) (e.g., the movement of Leg 2) [17] is as follows:

First phase

(Support phase: first stepping to the ground) $0 \leq t \leq \frac{T_c}{2}$

$$\begin{aligned} X_{s_n}(t) &= X_{0_n} + \frac{S_o}{4} \left(\frac{2t}{T_c} - \frac{1}{2\pi} \sin \left(\frac{4\pi t}{T_c} \right) \right) \cos \theta_n \\ Y_{s_n}(t) &= Y_{0_n} + \frac{S_o}{4} \left(\frac{2t}{T_c} - \frac{1}{2\pi} \sin \left(\frac{4\pi t}{T_c} \right) \right) \sin \theta_n \\ Z_{s_n}(t) &= Z_{0_n} \end{aligned} \quad (4.22)$$

Move phase 1

(Swing phase) $0 \leq t \leq \frac{T_c}{2}$

$$\begin{aligned} X_{s_n}(t) &= X_{0_n} + \frac{S_o}{2} \left(1 - \cos\left(\frac{2\pi}{T_c}t\right) \right) \cos \theta_n \\ Y_{s_n}(t) &= Y_{0_n} + \frac{S_o}{2} \left(1 - \cos\left(\frac{2\pi}{T_c}t\right) \right) \sin \theta_n \\ Z_{s_n}(t) &= Z_{0_n} + H_0 \sin\left(\frac{2\pi}{T_c}t\right) \end{aligned} \quad (4.23)$$

(Next step phase) $\frac{T_c}{4} \leq t \leq \frac{T_c}{2} + t_{\text{ex}}$

$$\begin{aligned} X_{s_n}(t) &= X_{s_n} \left(\frac{T_c}{4} - T_s \right) \\ Y_{s_n}(t) &= Y_{s_n} \left(\frac{T_c}{4} - T_s \right) \\ Z_{s_n}(t) &= Z_{s_n} \left(\frac{T_c}{4} - T_s \right) + H_0 \sin\left(\frac{4t - T_c}{T_c}\right) \end{aligned} \quad (4.24)$$

Move phase 2

(Support phase: stepping) $0 \leq t \leq \frac{T_c}{2} - 1$

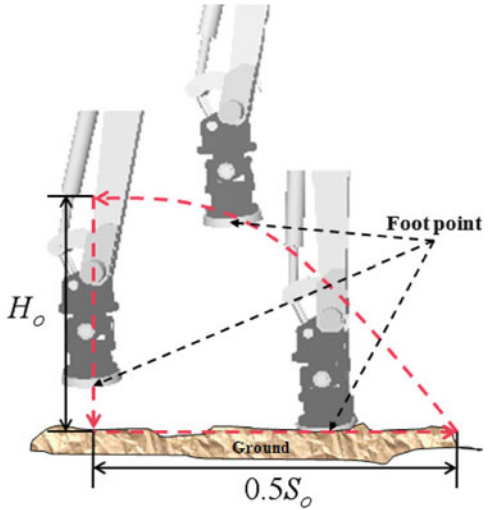
$$\begin{aligned} X_{s_n}(t) &= X_{0_n} - S_o \left(\frac{t}{T_c - 2} \right) \cos \theta_n \\ Y_{s_n}(t) &= Y_{0_n} - S_o \left(\frac{t}{T_c - 2} \right) \sin \theta_n \\ Z_{s_n}(t) &= Z_{0_n} \end{aligned} \quad (4.25)$$

Final phase

(Swing phase) $0 \leq t \leq \frac{T_c}{4}$

$$\begin{aligned} X_{s_n}(t) &= X_{0_n} + \frac{S_o}{4} \left(1 - \cos\left(\frac{2\pi}{T_c}t\right) \right) \cos \theta_n \\ Y_{s_n}(t) &= Y_{0_n} + \frac{S_o}{4} \left(1 - \cos\left(\frac{2\pi}{T_c}t\right) \right) \sin \theta_n \\ Z_{s_n}(t) &= Z_{0_n} + H_0 \sin\left(\frac{2\pi}{T_c}t\right) \end{aligned} \quad (4.26)$$

Fig. 4.17 Leg motion configuration for force threshold-based trajectory system



(Support phase: final stepping to the ground) $\frac{T_c}{4} \leq t \leq \frac{T_c}{2} + t_{\text{ex}}$

$$\begin{aligned} X_{s_n}(t) &= X_{s_n} \left(\frac{T_c}{4} - T_s \right) \\ Y_{s_n}(t) &= Y_{s_n} \left(\frac{T_c}{4} - T_s \right) \\ Z_{s_n}(t) &= Z_{s_n} \left(\frac{T_c}{4} - T_s \right) + H_0 \sin \left(\frac{4t - T_c}{T_c} \right) \end{aligned} \quad (4.27)$$

where T_c is the walking cycle time (s), t is the update time (real time) (s), t_{ex} is the extra period for given applied extra force (s), S_0 is the distance of foot placement for one cycle (m), and H_0 is the height of leg rising from the initial position (m).

$t_{\text{ex}} \geq 2s$ (depending on overall height of terrain levels) is given when an extra force is applied to the supported leg, and this is due to the joint angle limitations of the robot's leg and the trajectory cycle timing. The distance of foot placement for one cycle S_0 and the height of leg rising from the initial position H_0 are shown in Fig. 4.17. Also, one cycle here implies that the robot has completed the movements of all its legs based on tripod pattern. Note that all calculations are based on the SCS as described in Sect. 4.1, while every initial value of the axis $\Gamma_0 = \{X_0, Y_0, Z_0\}$ refers to the first signal that enters the phase module as described in Fig. 4.13. ETT module is tested for one leg (Leg 5) as shown in Fig. 4.18 before it is implemented for overall legs in walking event. The difference between ETT and fixed trajectory motion in terms of the output of the leg foot point motion based on SCS is shown in Fig. 4.19, and the value of the stepping level varies as it is dependent on the environment of the surface each leg set foot on when $F_{z_0} \geq 1 \text{ kN}$.



Fig. 4.18 Snapshots of one-leg tests on ETT module impact

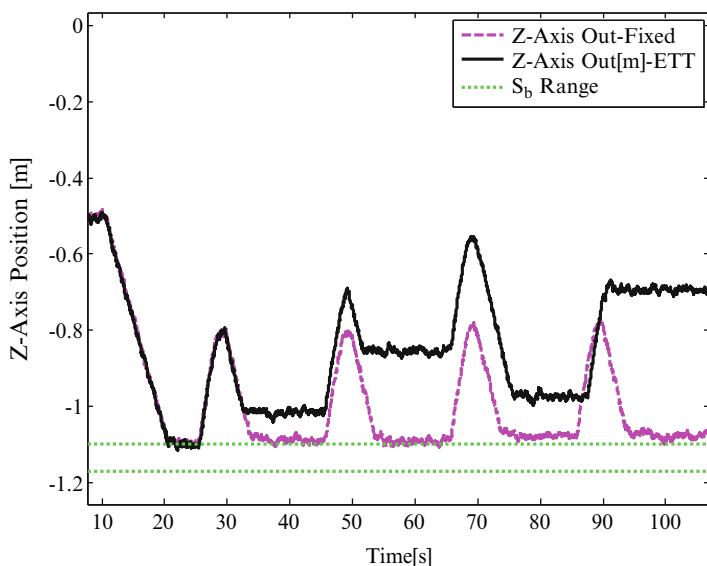


Fig. 4.19 Comparison between fixed walking and force threshold-based trajectory system (ETT) in leg foot point movement output based on SCS (experiment sample for Leg 5)

References

1. Oku M, Yang H, Paio G, Harada Y, Adachi K, Barai R, Sakai S, Nonami K (2007) Development of hydraulically actuated hexapod robot COMET-IV – The 1st report: system design and configuration. In: Proceeding of JSME conference on robotics and mechatronics 2007 (ROBOMECH 2007), Akita, pp 2A2–G01
2. Ohroku H, Irawan A, Nonami K (2009) A 3D modeling for hydraulic-drive hexapod walking robot using 3D geometric technique with distributed numerical model. Int J Automat Robot Auton Syst 9(1):23–31

3. Oku M, Koseki H, Ohroku H, Harada Y, Futagami K, Tran DC, Li L, Lin X, Sakai S, Nonami K (2008) Rough terrain locomotion control of hydraulically actuated hexapod robot COMET-IV (in Japanese). In: JSME conference on robotics and mechatronics 2008 (ROBOMECH 2008), Nagano
4. Aoyama H, Goto M, Naruo A, Hamada K, Kikuchi N, Kojima Y, Takada Y, Takenaka Y (2006) The difference between center of mass and center of pressure: a review of human postural control. *Aino J* 5
5. Byl K (2008) Metastable legged-robot locomotion. Massachusetts Institute of Technology, Cambridge
6. Schleicher D, Bergasa LM (2009) Real-time hierarchical outdoor SLAM based on stereovision and GPS fusion. *IEEE Trans Intell Transport Syst* 10(3):440–452
7. Ishikawa K, Amano Y, Hashizume T (2007) A mobile mapping system for precise road line localization using a single camera and 3D road model. *J Robot Mech* 19(2):174–180
8. Sakai A, Saitoh T, Kuroda Y (2010) Robust landmark estimation and unscented particle sampling for SLAM in dynamic outdoor environment. *J Robot Mech* 22(2):140–149
9. Chang HJ, George Lee CS, Lu YH, Hu YC (2007) P-SLAM: simultaneous localization and mapping with environmental-structure prediction. *IEEE Trans Robot* 23(2):281–293
10. Hodoshima R, Doi T, Fukuda Y, Hirose S, Okamoto T, Mori J (2007) Development of a quadruped walking robot TITAN XI for steep slope operation – step over gait to avoid concrete frames on steep slopes. *J Robot Mech* 19(1):13–26
11. Nabulsi S, Armada MA, Montes H (2006) Multiple terrain adaptation approach using ultrasonic sensors for legged robots. In: Proceeding of climbing and walking robots 2006 (CLAWAR 2006), Brussels
12. Raibert M, Blankespoor K, Nelson G, Playter R (2008) TheBigDogTeam BigDog: the rough terrain quadruped robot. In: Proceeding of 17th world congress, the international federation of automatic control, Seoul
13. Murata T, Yamaguchi M (2008) Multi-legged robot control using GA-based Q-learning method with neighboring crossover. In: Iba H (ed) Frontiers in evolutionary robotics. I-Tech Education and Publishing, Vienna, pp 342–352
14. Kohl N, Stone P (2004) Policy gradient reinforcement learning for fast quadrupedal locomotion. In: Proceeding of IEEE international conference on robotics and automation 2004 (ICRA 2004), Barcelona, pp 2619–2624
15. Ohroku H, Nonami K (2009) Omni-directional vision and 3D animation based teleoperation of hydraulically actuated hexapod robot COMET-IV. *Int J Autom Contr Syst Eng* 9(1):17–24
16. Futagami K, Harada Y, Oku M, Ohroku H, Lin X, Okawa K, Sakai S, Nonami K (2008) Real-time navigation and control of hydraulically actuated hexapod robot COMET-IV. In: Proceeding of the 9th international conference on motion and vibration control 2008 (MOVIC 2008), Munich
17. Irawan A, Nonami K (2011) Compliant walking control for hydraulic driven hexapod robot on rough terrain. *J Robot Mech* 23(1):149–162

Chapter 5

Position-Based Robust Locomotion Control of Hexapod Robot

Abstract Position-based locomotion control is a very popular technique in walking robot research. However, the actuation system of the robot may pose various challenges for smooth and stable locomotion of the walking robot. This chapter presents few nonlinear robust control techniques for the position-based locomotion control of a hydraulically actuated hexapod walking robot COMET-III. This chapter starts with a general description of position control-based locomotion control of walking robot. Then the various nonlinearities of the hydraulic actuation system have been described in brief. Finally, two sliding model-based locomotion control techniques and a robust adaptive fuzzy control-based locomotion control technique of COMET-III in the position control-based framework have been presented with real-time experimental results.

5.1 Introduction

Locomotion control is the most important control task of a walking robot. Locomotion control of a walking robot involves an ordered movement of the leg joints so that some of the legs support the body and at the same time push the body in the forward direction, while some legs are in swing motion for placing their foot on a new foothold position. This ordered movements of the leg joints are to be repeated for the continuous locomotion of the robot over a terrain. Therefore, the variable that is of utmost importance during the locomotion control of a walking robot is the angular position and angular velocity of the leg joints. The leg mechanisms of the walking robots are very similar to the serial manipulator and are constructed from rigid members or links. Therefore, the legs of the walking robot can be kinematically described by Denavit–Hartenberg (D–H) notation using the joint variable and fixed link parameters. The foot position can be calculated by forward kinematics using the joint angles data and the other D–H parameters of the leg mechanisms.

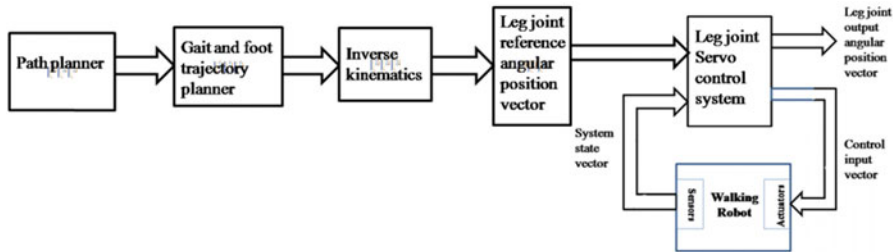


Fig. 5.1 Schematic diagram of position-based locomotion control of walking robot

For autonomous locomotion control of the walking robots, at first the path of the robot is planned from the map of the surroundings and the terrain assuming the robot as a point mass (i.e., mass concentrated at the center of gravity of the robot body). The map is either computed beforehand from the sensor data, like vision sensor, laser range finder, and SONAR, or online from the SLAM (simultaneous localization and mapping) technique. After the path of the robot has been planned, the next task is to find out the permissible foothold position for rough terrain locomotion. Accordingly some correction of the previously planned body path may be required. Now, the next task is to plan the foot trajectory keeping in mind the terrain condition. If the terrain is flat then some regular gait, like wave gait, is preferred. Then the foot trajectory can also be a fixed and predetermined one. The various aspects of path and trajectory planning have already been discussed in the previous chapter. After the foot trajectory has been found in the Cartesian task space of the foot, the next task is to get the corresponding joint angle trajectory in the angular space by inverse kinematics. Finally, the locomotion control system of the walking robot must accurately track the joint angle position trajectories of the legs of the walking robot for the proper foot placement at the desired foothold position very accurately. Therefore, the position-based locomotion control of the walking robot is actually a tracking control problem of the desired joint angle trajectories. The position control-based locomotion control of walking robot is the oldest and widely used technique in the walking robot motion control. However, in critical situations like very rough terrain locomotion or locomotion through dangerous terrain, the foot trajectory tracking should be very accurate; otherwise, there will be accident or loss of static stability of the robot arising out of the accumulation of large tracking error. The entire process of position-based locomotion control has been explained at Fig. 5.1.

5.1.1 Locomotion Control Techniques

The walking robot is a good example of nonlinear MIMO system. Therefore, the locomotion control of hexapod walking robot is a very interesting and challenging control problem. As the robot legs are similar to robot manipulator, the hexapod

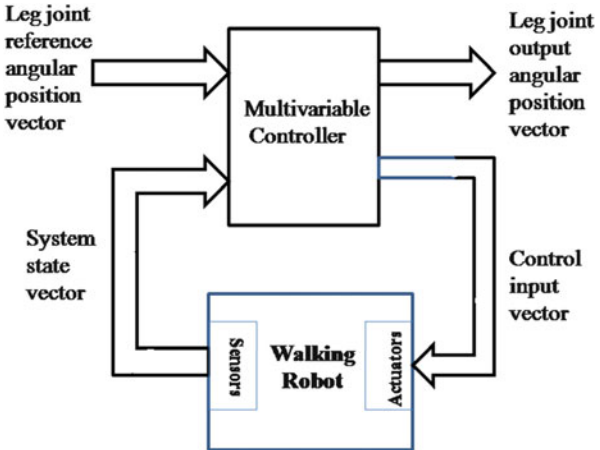
walking robot can be thought of as a complex robotic system of six parallel manipulators coordinating with each other as per the desired foot trajectories depending upon the terrain conditions. Therefore, most of the time the design of the servo control system, which forms the lowest control level in a hierarchical control that are often found in autonomous mobile and walking robots, is inspired from the control methods already applied for the industrial manipulators. Depending upon the implementation point of view, the locomotion control of a walking robot may be broadly categorized as the following.

5.1.2 *Centralized Control*

In centralized control, the controller computes the control input vector needed to actuate all the joints simultaneously for tracking the desired joint angle trajectories. Multivariable control theory can be best utilized in this case. State-space technique is quite useful for the development of centralized control system, because both the nonlinearities and coupling can be considered with state-space technique. Centralized control is normally implemented in a single high-end computer. The main advantage of centralized control is that the control input vector is calculated, even by the sequential computing platforms, at once after performing some linear algebraic manipulation on the matrices describing the state model and the state vector. Therefore, there is no time delay between the applications of the control inputs at the different joint actuators of the robot leg. As a result the shaking motion of the whole robot body caused by the asynchronous actuation of the joints due the delay of application of control input at various leg joints is absent and the walking of the robot is smooth and stable.

Centralized control of robotic manipulator is commonly performed by computed torque control technique [1]. However, being a model-based control technique, the computed torque control requires a very accurate model of the manipulator which is very nonlinear and dynamically coupled, and the model parameters should be calculated in real-time for the implementation of the algorithm. It is quite difficult to determine the model of the robot manipulator very accurately and as a result the tracking performance deteriorates. The state model of a walking robot is very similar to that of the robot manipulator, and it is also very nonlinear and dynamically coupled and the model parameters should be calculated in real-time for the implementation of the algorithm. Therefore, these model uncertainties will cause poor tracking performance of the desired leg joint trajectories, which result into poor tracking performance of the desired foot trajectories and the problems associated with the calculation of model parameters in real-time in centralized walking control. Various robust control techniques are available now to address the problems associated with model uncertainty and reduction of computational loading. The schematic diagram depicting the concept of centralized control is shown in Fig. 5.2.

Fig. 5.2 Centralized control of walking robot



5.1.3 Distributed Control

In centralized control, all the computation required for the generation of control input vector is performed in a single computer. Therefore, the computing power, computing speed, and hardware resources required by the central computer may be quite huge and economically impractical. In distributed control, instead of a central controller, there are individual controllers for controlling the motion of each leg or each leg joint. Distributed control may be implemented in a single high-end computer or on distributed computing platform consisting of different smaller computers connected in network. There may be a supervisory controller to coordinate the functioning of the individual controllers or the individual controllers may cooperate with each other through some communication network. Nowadays, distributed control is becoming popular for the drastic reduction in the cost of the embedded computers and equipments needed for establishing communication network.

In one configuration, each leg can be treated as a multivariable MIMO plant, and control input vector is generated by a computer dedicated for controlling that leg only. One supervisory controller is implemented in a dedicated supervisory computer which coordinates the overall motion control of each leg as per the desired/required gait for locomotion control over a particular terrain. In this scheme, one very high-end and costly computer is not required, and the control can be achieved with few low-cost computers after connecting them into a network. Although the inaccurate tracking problem occurs due to model uncertainty of the leg model and real-time computation of the model parameters, however, the problem can be largely mitigated by using various robust control techniques. This control scheme is quite useful when the leg joints have to move faster for achieving dynamically

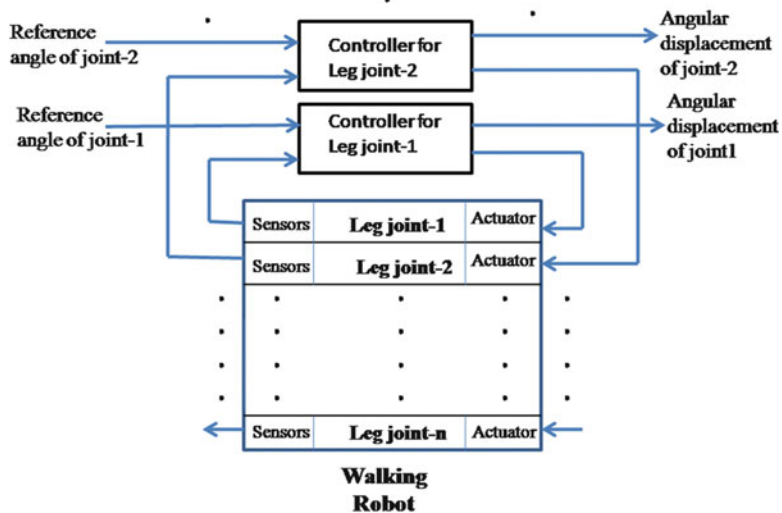


Fig. 5.3 Distributed control of walking robot

stable locomotion of the walking robot during high-speed walking or running. The schematic diagram of this type of control configuration has been depicted in Fig. 5.3.

In another control configuration, the dynamic coupling between various leg joints of the walking robot is neglected. Then each joint of the leg is considered as a Single Input - Single Output (SISO) plant. Then joint model is experimentally identified or mathematically modeled and some type of robust control law is implemented for controlling the motion of each joint. This is a very simplified control scheme and known as *independent joint control* in robotics literature [1]. As the dynamic couplings are neglected, this control scheme is only applicable for statically stable locomotion control of walking robot during very low-speed locomotion. As the computational load has been reduced substantially after neglecting the dynamic and parameter varying terms in the robot model, the independent joint control scheme can be implemented on a single computer with moderate computational resources. In that case the control inputs for actuating the leg joints will be calculated sequentially, and the computation time of the control law for each joint should be small enough so that the total computation time is much smaller than the sampling time; otherwise, the locomotion may become unstable. If the control algorithm is quite lengthy and takes much computation time, then it is better to employ a networked distributed computing platform with small computers or microcontrollers for each joint and one supervisory computer to coordinate the functions of the individual leg joint controller. The schematic diagram of this type of control configuration has been depicted in Fig. 5.3.

5.2 Challenges of Position-Based Locomotion Control of Hydraulically Actuated Hexapod Robot

There are few challenges associated with position-based locomotion control of hydraulically actuated hexapod robot. The first is the presence of a high level of nonlinearities in the system. The robot is actuated by hydraulic cylinders for the generation of linear motion and hydraulic motors for generation of rotational motion. In addition to the dry friction at the bearings of the joints, there is a high degree of viscous friction present in the system. This friction forces fetch nonlinearities in the system model and is a cause of much loss of precious onboard power. There are other sources of nonlinearities, like dead zone of the proportional electromagnetic valves, saturation of electrohydraulic valve controllers, and time delay in the hydraulic fluid flow. Moreover, the hydraulic actuators are subjected to non-smooth and discontinuous nonlinearities due to directional changes of valve opening and frictions. The presence of dead zone of the proportional electromagnetic valves causes large tracking error. This is due to the fact that a part of the control effort is always lost within the dead zone for its insensitivity over this range of operation, which is quite obvious from its characteristics shown in Fig. 5.4.

The problems of nonlinearities are aggravated by the parameter variation of the system. The characteristic of the hydraulic fluid changes with temperature. Therefore, the accuracy of the locomotion will vary over the season and also with the duration of the operation of the robot. Because the hydraulic fluid becomes hot after the robot starts, the locomotion and the characteristic of the fluid change with increase in temperature. A hydraulically actuated leg mechanism experiences a large amount of model uncertainties including the large changes in the load on the foot, large variation of parameters (like bulk modulus), oil leakage, and air bubbles. Therefore, it is very difficult to determine an accurate model of hydraulically actuated actuator.

The effect of mechanical vibration, due to the onboard internal combustion engine, is another challenge that is invariably encountered during the operation of a hydraulically actuated walking robot. As the input power requirement is quite large for hydraulically actuated walking robot, battery cannot supply this power. Therefore, the onboard power supply for the hydraulically actuated walking robot is normally internal combustion engine. The vibration of the internal combustion

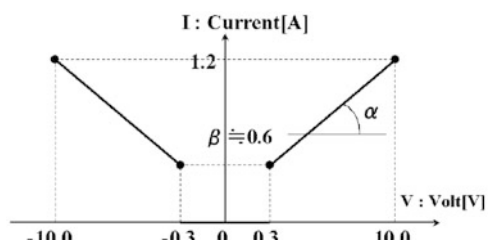


Fig. 5.4 Proportional electromagnetic valve characteristics

engine during its operation affects the performance of the actuators and sensors. Thus, the overall locomotion performance is affected by the vibration.

The overall model of a hydraulically actuated robot is quite complex [2–5]. Therefore, there are good amount of nonlinearities and uncertainties associated with the model. Thus, the control system should be able to cope with the challenges posed by the nonlinearities and model uncertainties. In such a situation linear controllers like PID will not give good locomotion control performance. We have to look for robust control techniques [6, 18] to improve the tracking performance of the robot during locomotion control [2–5].

5.3 Independent Joint Control-Based Locomotion Control of Hydraulically Actuated Hexapod Robot

In centralized control, the overall MIMO model is taken and the control law is developed employing the principles of multivariable control theory. The control input comes in the form of a vector. The equation of motion of the legs is a second-order nonlinear differential equation and is of the following form:

$$M(q)\ddot{q} + C(q, \dot{q})\dot{q} + g(q) = \tau \quad (5.1)$$

where for a leg mechanism of n number of joints, q is the $n \times 1$ joint angle displacement vector, \dot{q} is the $n \times 1$ joint angular vector, $M(q)$ is the $n \times n$ symmetric positive definite inertia matrix of the leg mechanism, $C(q, \dot{q})q$ is the $n \times 1$ centripetal and Coriolis vector, and $g(q)q$ is the $n \times 1$ gravity force vector. The overall dynamic model of a hexapod walking robot has been derived in Chap. 4 and has the following functional form:

$$\dot{X} = F(\dot{X}, X, U, t)X + HU \quad (5.2)$$

where the state vector X consists of the angular position (q), angular velocity (\dot{q}), angular acceleration of the leg joints (\ddot{q}), linear velocity of the robot body in the forward direction (V_x), linear velocity of the robot body in the lateral direction (V_y), linear velocity of the robot body in the vertical direction (V_z), roll angle of the body (Ψ_{roll}), pitch angle of the body (Ψ_{pitch}), and yaw angle of the body (Ψ_{yaw}); the matrix F is symmetric matrix but the terms of this matrix are nonlinear functions of the state variables, H is the control input distribution matrix, and U is the control input vector.

It can be observed that for field applications, the speed of operation of the hydraulically actuated robots is not very high due to several constraints like large amount of hydraulic fluid carried by the robot, large amount of friction force at the piston and cylinder assembly, and heavy and bulky body. Therefore, if the robot is operated at a high locomotion speed, there will be large amount of power loss due

to friction and frequent starting and braking operation of the hydraulic actuators. Consequently, there will be large amount of wear and tear of the robot actuation system, its structure, and the assembly, which may ultimately result into substantial damage of the robot. In other words, hydraulically actuated hexapod walking robots are designed for only walking, and not for running, galloping, or trotting. Therefore, hydraulically actuated hexapod walking robot can be considered as a statically stable walking machine and operating at low locomotion speed. As a result, the joint velocity of each leg is also quite small because of the low-speed locomotion of the walking robot. Therefore, the dynamic coupling terms like inertia, centrifugal, and Coriolis forces can be neglected for all practical purposes. If the weight of the leg mechanism is quite high, then the gravitation terms should be considered; otherwise, it can also be neglected. After neglecting the dynamic coupling terms among the leg joints, each joint can be modeled as a SISO plant. Then the control task has been transformed into a servo control problem for each leg joint, where the servo control law can be designed for each leg joint independently considering the SISO model of each leg joint. This is in fact quite interesting that in statically stable walking robots, we can control each joint of the legs independently, keeping a synchronism with each other as required by the desired gait for the desired locomotion plan, if the objective of locomotion control is only to maintain the static stability of the robot while walking. This methodology is called independent joint control in the robotics literature [1]. It is also one type of distributed control and can be implemented in a very simple manner. As the nonlinear and coupling force terms are neglected, for the design of the control law for the individual joints, it only needs the model of the joints. Identification of the model of the individual joints is quite easy and the derived model can be simplified further by model reduction. Independent joint control can be implemented in a single high-end computer; in that case no external communicating devices are necessary to communicate among the individual controller. It can also be implemented in individual embedded computers and in that case external communicating device are necessary to communicate among the individual controller. In the rest of the chapter we will discuss about the locomotion control of hydraulically actuated hexapod robot employing independent joint control technique.

5.4 Robust Control Techniques for Locomotion Control of Hydraulically Actuated Hexapod Robot

As hydraulically actuated robotic systems possess large amount of nonlinearities and uncertainties, the SISO model derived for each leg joint after neglecting the dynamic coupling terms is also quite nonlinear in form and contains substantial amount of uncertainties. Moreover, it may be necessary to perform model reduction for the sake of convenience of controller design, which further adds to the model uncertainty. Therefore, robust control techniques, applied in the independent joint

Fig. 5.5 Humanitarian de-mining robot COMET-III



control framework, would be a prudent choice of locomotion control strategy of statically stable hydraulically actuated hexapod walking robot. There are several robots control techniques reported in the literature [7] that promises robust tracking performance and stability upon satisfaction of some conditions like bound of model uncertainty. In this chapter we will present three case studies of position-based robust locomotion control of hydraulically actuated hexapod walking robot COMET-III. At first we will present a model-based nonlinear robust control of COMET-III by Preview Sliding Mode Control. Then we will present another model-based nonlinear robust control of COMET-III by Model Reference Sliding Mode Control of COMET-III. Finally, we will present a soft computing-based intelligent control approach for the design and implementation of nonlinear robust control of COMET-III, known as robust adaptive fuzzy control.

5.4.1 Technical Description of COMET-III and Its Model Identification

The humanitarian de-mining robot COMET-III is a six-legged walking robot with each leg having three degrees of freedom which ensure stable walking on rough terrains [2]. The picture of COMET-III is shown in Fig. 5.5. The driving force is based on the hydraulic power of 14 MPa pressure to generate sufficient hydraulic power to walk over irregular terrain [2], with the payload of the de-mining tools, with good speed of locomotion [4]. The shoulder joints of each leg are driven by hydraulic motors. The thigh and shank joints of each leg are driven by hydraulic cylinders. Therefore, the angular positions of the hydraulic motors are measured by rotary potentiometers and the positions of each cylinder are measured by the linear potentiometers. The schematic diagram of COMET-III leg mechanism and its controller electronics is presented in Fig. 5.5. COMET-III can also locomote itself by rubber crawler drive by hydraulic motors. The locomotion speeds by the walking mode of legs and running mode of the crawler are 300 m and 3 km per hour,

Fig. 5.6 Schematic diagram of COMET-III leg mechanism and its controller electronics

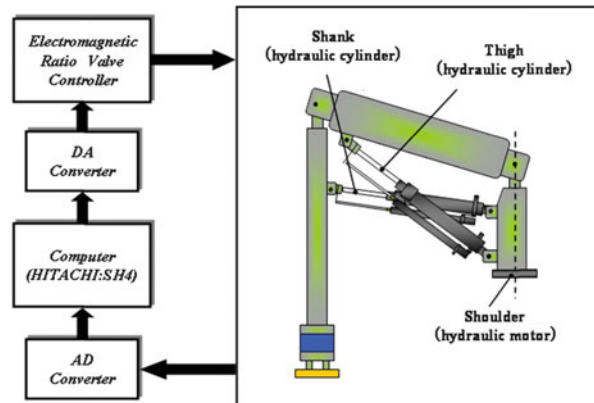


Table 5.1 Hardware specification of COMET-III

Hydraulic pump Engine	140 kg/cm ² , 17 L/min 5.53 cm ³ , Max output 22 ps/35.00 rpm Max torque 4.5.5 kg/fm
Material	Aluminum alloy, SUS304
Crawler	Rubber crawler
Hydraulic tank	40 L
Gasoline tank	20 L
Control valve	25.
Thigh cylinder	$\varphi 25 \times 250$ st, Max speed 280 mm/s
Shank cylinder	$\varphi 30 \times 175$ st, Max speed 300 mm/s
Leg turn	Max angle ± 80 deg, 5.9 deg/s
Weight	Frame + crawler + engine + hydraulic Unit = 1,000 kg, legs = 32 kg \times 5.
Computer	SH4 (clock frequency 198 MHz) \times 3

respectively. COMET-III can climb up a slope of 30° by crawler as well as by legs (Fig. 5.6). Table 5.1 summarizes the main features of COMET-III.

Here, we will restrict our discussion on the locomotion control of COMET-III for backward-forward walking with tetrapod gait [8]. The schematic diagram of the tetrapod gait is shown in Fig. 5.7. The gait command is issued by the operator by teleoperation over a wireless serial data link. Three embedded computers (SH4) are connected in TCP/IP to form a local area network. This enables simple and faster distributed control architecture. The locomotion control algorithm is executed by the SH4 computer-2, while SH4 computer-1 is entrusted with the task of the teleoperation and the SH4 computer-3 is entrusted with the task of manipulation of the mine detection and removal (or mine marking) arms. The gait command is received by SH4 computer-1 from the user over the wireless serial link and is passed to the SH4 computer-2 over TCP/IP network. From the gait command

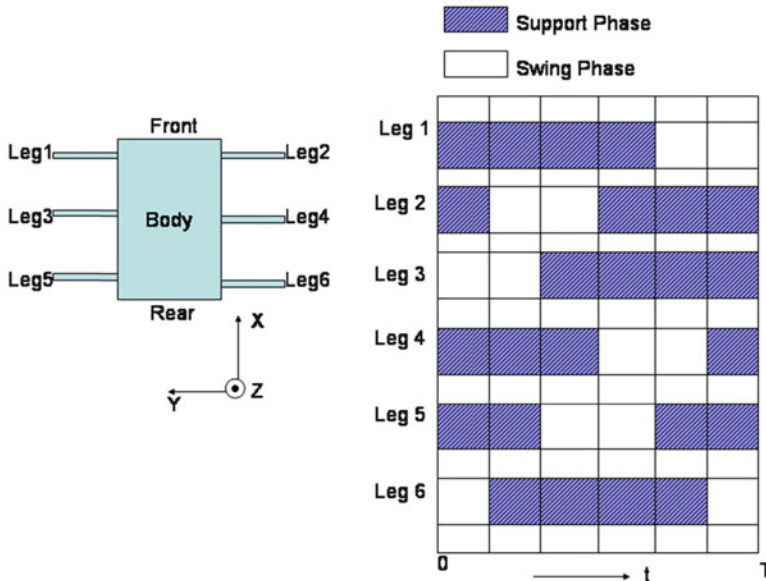


Fig. 5.7 Schematic diagram of tetrapod gait of COMET-III

received it first generates reference trajectory in the Cartesian task space. Then the task space trajectory is converted to joint space trajectory for each joint of all the legs. This joint space trajectory becomes input command to the controllers of each joint. The control architecture of COMET-III is shown in Fig. 5.8.

Since a hydraulic-drive system contains several nonlinear and uncertain factors, theoretical determination of an accurate mathematical model is difficult. Therefore, we have determined the model of each joint by closed-loop identification technique. We have applied simple proportional control during closed-loop identification as shown in Fig. 5.9. Identification of the model has been performed with the following assumptions:

1. The variation of the moment of inertia of the leg links, the gravity, and other influences are regarded as disturbances.
2. The right and left pressurized areas of the single rod piston are equal.
3. The mathematical models of legs are identical.

The leg joint models have been found as a second-order system with a time delay. Padé approximation has been performed on the model for ease of control system design, and after the approximation the model takes the following form:

$$G(s) = \frac{\alpha\omega_n^2}{s^2 + 2\zeta\omega_n s + \omega_n^2} \frac{1 - \frac{1}{2}sT}{1 + \frac{1}{2}sT} \quad (5.3)$$

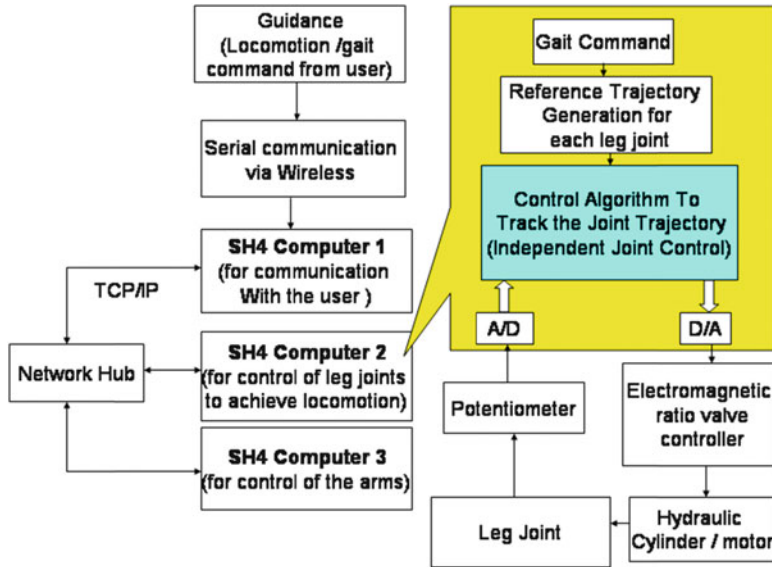


Fig. 5.8 Control architecture of COMET-III

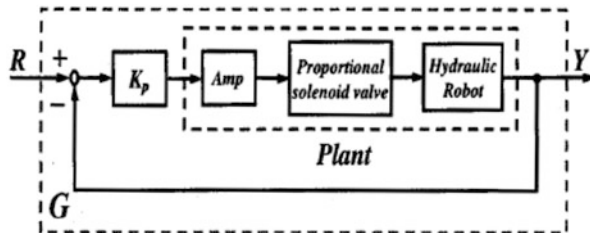


Fig. 5.9 Closed-loop identification of model of leg joints of COMET-III

where

$$\{\alpha, \zeta, \omega_n, T\}_{\text{shoulder}} = \{1.000, 1.500, 2.000, 0.300\}$$

$$\{\alpha, \zeta, \omega_n, T\}_{\text{thigh}} = \{1.000, 2.928, 4.477, 0.200\}$$

$$\{\alpha, \zeta, \omega_n, T\}_{\text{shank}} = \{1.000, 3.028, 5.507, 0.200\}$$

For the purpose of the development of advanced control law it is convenient to transform the transfer function model of Eq. (5.3) into its corresponding nominal state variable model as follows:

$$\dot{x} = Ax + Bu$$

$$y = cx + Du \quad (5.4)$$

where $x \in \mathbb{R}^n$ is the state vector and $u \in \mathbb{R}^m$ is the control input, and for COMET-III $n = 2$ and $m = 1$, the A and C matrix for the shoulder, thigh, and shank are as follows:

Shoulder:

$$A = \begin{bmatrix} 0 & 1 & 0 \\ 0 & 0 & 1 \\ 0 & -5.4.27 & -15..02 \end{bmatrix}, C = [4.500 \quad -0.450 \quad 0]$$

Thigh:

$$A = \begin{bmatrix} 0 & 1 & 0 \\ 0 & 0 & 1 \\ 0 & -299.5 & -35..50 \end{bmatrix}, C = [4.009 \quad -0.401 \quad 0]$$

Shank:

$$A = \begin{bmatrix} 0 & 1 & 0 \\ 0 & 0 & 1 \\ 0 & -393.5. & -43.41 \end{bmatrix}, C = [5..05.5 \quad -0.5.07 \quad 0]$$

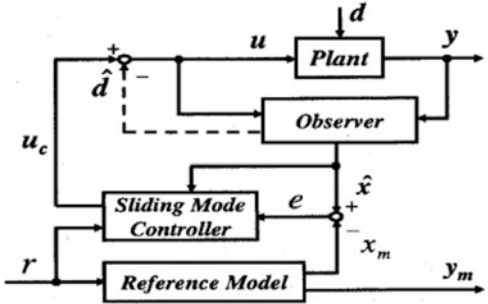
The remaining B and D matrices are the same for the shoulder, thigh, and shank as given below:

$$B = \begin{bmatrix} 0 \\ 0 \\ 1 \end{bmatrix}, D = 0$$

5.4.2 Model Reference Sliding Mode Control

Good walking control is not possible with PID controller because of the nonlinearity, parameter variation, and uncertainties associated with system model of hydraulically actuated walking robot COMET-III [2]. Sliding mode control is a popular control methodology that possesses the attractive properties like robustness against disturbances, model uncertainties, and parameter variation and has been successfully applied for robust control of various mechanical systems [4, 9]. Under sliding mode control, the system status is constrained to the switching hyperplane by the high-speed switching of feedback gain and to the origin along the hyperplane. Since the system behaviors are dominated by only the characteristics of the hyperplane,

Fig. 5.10 Schematic block diagram of MRSMC for COMET-III



sliding mode control is extremely robust against parameter behaviors and disturbances and is very effective for the position control of a hydraulically actuated system [3, 4]. In this section we will present the design and real-time implementation of the robust walking control of COMET-III with Model Reference Sliding Mode Control (MRSMC) [6, 10]. In this framework, at first a reference model is selected that exhibits ideal or desired dynamic and steady-state performances. The output and the states of both reference model and the actual plant are compared for the same reference input and the errors are combined to form an error dynamic model. Now, a sliding mode controller is designed such that these errors attain zero state or slides to the origin in the error state space along a sliding manifold. This ultimately results into a control action such that the performance obtained from the actual plant is quite similar to that of the performance obtained from the reference plant model (which is actually the desired performance). The schematic diagram of the MRSMC for COMET-III is shown in Fig. 5.10.

A disturbance observer has been incorporated in the inner loop in order to achieve good performance.

A. Design of MRSMC

The reference model may be selected as

$$\begin{aligned}\dot{x}_m &= A_m x_m + B_m r \\ y_m &= C_m x_m\end{aligned}\tag{5.5}$$

where x_m represents the desired state trajectory, and the coefficient matrices of the reference state model A_m , B_m , and C_m can be chosen from the desired locations of the eigenvalues for a desired dynamic and steady-state response of the system. Now, the error state can be found from Eqs. (5.4) and (5.5) as follows:

$$e = x - x_m$$

$$\begin{aligned}\dot{e} &= \dot{x} - \dot{x}_m \\ &= (Ax + Bu) - (A_m x_m + B_m r) = A_m e + (A - A_m)x + Bu - B_m r\end{aligned}\quad (5.6)$$

Now, in order to maintain the matching condition, let us consider the following:

$$A_m - A = BK_1, \text{ and } B_m = BK_2 \quad (5.7)$$

Therefore, the error dynamic equation becomes

$$\dot{e} = A_m e - B(K_1 x + K_2 r - u) \quad (5.8)$$

where

$$K_1 = B^+(A_m - A) \text{ and } K_2 = (-C_m A_m^{-1} B)^{-1} [4] \quad (5.9)$$

The error dynamic model (5.8) would be used for the design of the sliding mode controller. Let us consider the following sliding surface:

$$\sigma = S e = S(x - x_m) \quad (5.10)$$

Then,

$$\dot{\sigma} = S \dot{e} = S[A_m e - B(K_1 x + K_2 r - u)] \quad (5.11)$$

Therefore, the equivalent control can be written as

$$u_{\text{eq}} = -(SB)^{-1} S A_m e + K_1 x + K_2 r \quad (5.12)$$

The closed-loop error dynamic model is obtained after substitution of the equivalent control input from (5.12) into the error model (5.8) as shown below:

$$\dot{e} = [I - B(SB)^{-1} S] A_m e \quad (5.13)$$

Now, suppose there is a feedback gain F such that

$$F = S = B^T P \quad (5.14)$$

Here, we can assume that $SB > 0$, and the matrix $Q > 0$, then P can be determined by solving the following algebraic Riccati equation:

$$P A_m + A_m^T P - P B B^T P + Q = 0 \quad (5.15)$$

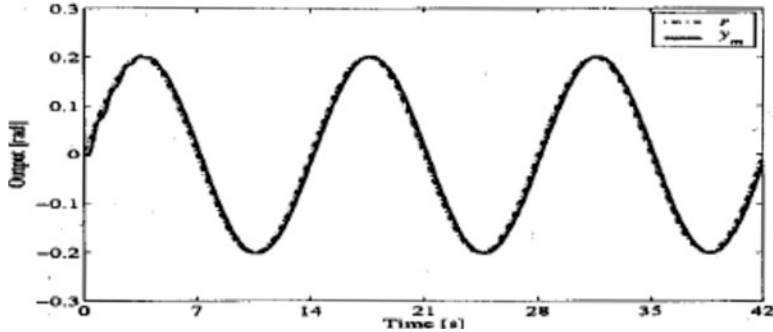


Fig. 5.11 Sinusoidal response of the reference model

Now, the sliding mode control input can be written as a combination of a linear term and a nonlinear term as follows:

$$u = u_l + u_n \quad (5.16)$$

where we can write

$$u_l = -(SB)^{-1}(SA_m - \Phi S)e + K_1 x + K_2 r$$

$$u_n = -\rho_n(SB)^{-1} \frac{P_2 \sigma}{\|P_2 \sigma\| + \delta_n}, \sigma \neq 0$$

where the term δ_n is used for chattering reduction and the gain $\rho_n > 0$. The matrix P_2 is to be determined from the following Lyapunov equation:

$$P_2 \Phi + \Phi^T P_2 = -I \quad (5.17)$$

B. Experimental results of the locomotion control with MRSMC

During implementation of the MRSMC in COMET-III, the form of the matrix A_m of the reference model has been chosen as

$$A_m = \begin{bmatrix} 0 & 1 & 0 \\ 0 & 0 & 1 \\ -k_1 & -k_2 & -k_3 \end{bmatrix} \quad (5.18)$$

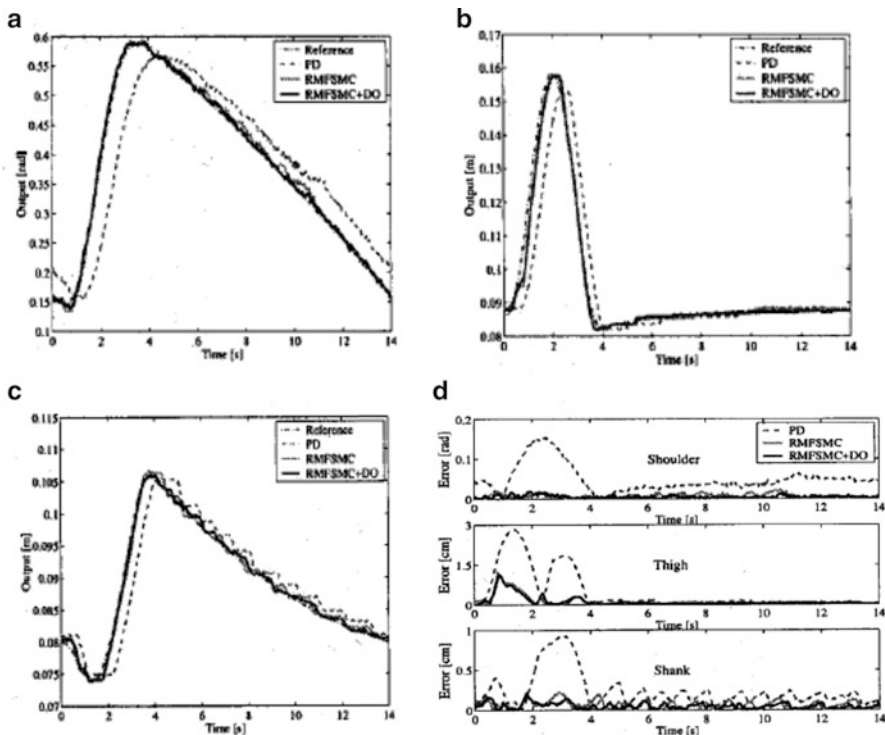
Here we will present the tracking performances with the proposed controller. Fig. 5.11 shows the sinusoidal response of the reference model.

Table 5.2 shows the design parameters of the reference models and MRSMCs for the shoulder, thigh, and shank joints of the COMET-III legs:

Figures 5.12a, b and 5.2c show the trajectory tracking performance of the shoulder joint, thigh joint, and shank joint respectively. The output tracking

Table 5.2 Design parameters of MRSMC and observer for COMET-III

Shoulder	$S = [27.447\ 8050\ 955.8]$
SMC	$\Phi = -8, P_2 = 0.0525, \rho_n = 5.0, \delta_n = 0.4$
A_m	$k_1 = 800, k_2 = 70, k_3 = 15$
Observer	$L = [0.2211.47 \times 10^{-3} - 1.17 \times 10^{-2}$
Thigh	$S = [995..079\ 543.153]$
SMC	$\Phi = -8, P_2 = 0.0525, \rho_n = 7.0, \delta_n = 0.3$
A_m	$k_1 = 5,000, k_2 = 300, k_3 = 35.5$
Observer	$L = [0.248 - 3.29 \times 10^{-4} - 4.0 \times 10^{-3}$
Shank	$S = [830.5\ 41.120.999]$
SMC	$\Phi = -9, P_2 = 0.0555., \rho_n = 5.0, \delta_n = 0.2$
A_m	$k_1 = 1.3 \times 10^4, k_2 = 394, k_3 = 43$
Observer	$L = [0.15.4 - 3.13 \times 10^{-4} - 8.10 \times 10^{-4}]$

**Fig 5.12** Experimental results with load: (a) trajectory tracking performance of the shoulder, (b) trajectory tracking performance of the thigh, (c) trajectory tracking performance of the shank, and (d) output error

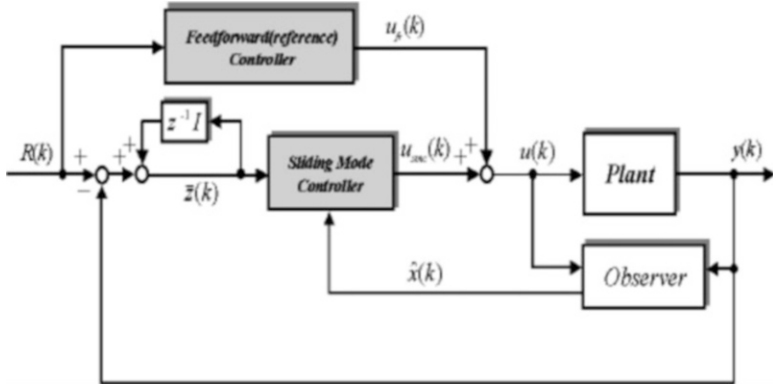


Fig. 5.13 Block diagram of Preview Sliding Mode Control

errors are shown in Fig. 5.12d. The tracking performances have also been compared with that of PD controller and with the application of disturbance observer (DO)

5.4.3 Preview Sliding Mode Control

Because of the strong nonlinear characteristic of the hydraulic system, conventional control methods like PID control produce the flattery delay at the output. In the unknown environment of minefield, the robot leg must follow correctly the walking orbit. The sliding mode control has strong robustness to parameter change or disturbance; however, mere feedback compensation results in actuator saturation and steady-state deviation by the time delay remains. Therefore, we have incorporated a preview feedforward control input corresponding to the future target value of a reference orbit to compensate the flattery delay. In this section, we will present the design and real-time implementation of a preview sliding mode controller [11, 12], which incorporate the advantages of both sliding mode control and preview control, for the improvement of the walking control performance of COMET-III (Fig. 5.13).

A. Design of the preview sliding mode control law

The system can be expressed by the following discrete-time state and output equations:

$$x(k+1) = Ax(k) + Bu(k) \quad (5.19a)$$

$$y(k) = Cx(k) \quad (5.19b)$$

An error signal is defined by the following equation:

$$\mathbf{e}(k) = \mathbf{R}(k) - \mathbf{y}(k) \quad (5.20)$$

For an optimum Type 1 servo system, the enlarged system shown in Eq. (5.21) is used. Δ represents the first order difference:

$$\begin{bmatrix} \mathbf{e}(k+1) \\ \Delta x(k+1) \end{bmatrix} = \begin{bmatrix} \mathbf{I}_m & -\mathbf{C}\mathbf{A} \\ 0 & \mathbf{A} \end{bmatrix} \begin{bmatrix} \mathbf{e}(k) \\ \Delta x(k) \end{bmatrix} + \begin{bmatrix} -\mathbf{C}\mathbf{B} \\ \mathbf{B} \end{bmatrix} \Delta \mathbf{u}(k) + \begin{bmatrix} \mathbf{I}_m \\ 0 \end{bmatrix} \Delta \mathbf{R}(k+1) \quad (5.21)$$

or

$$X_0(k+1) = \Phi X_0(k) + \Gamma \Delta \mathbf{u}(k) + \Gamma_R \Delta \mathbf{R}(k+1) \quad (5.22)$$

where the reference orbit until the M_R number of preview steps in the future is known. An enlarged system containing the following future reference orbit signal is then created.

$$\begin{bmatrix} X_0(k+1) \\ X_R(k+1) \end{bmatrix} = \begin{bmatrix} \Phi & \Gamma_{PR} \\ 0 & \mathbf{A}_R \end{bmatrix} \begin{bmatrix} X_0(k) \\ X_R(k) \end{bmatrix} + \begin{bmatrix} \Gamma \\ 0 \end{bmatrix} \Delta \mathbf{u}(k) \quad (5.23)$$

or

$$\bar{X}_0(k+1) = \bar{\Phi} \bar{X}_0(k) + \bar{\Gamma} \Delta \mathbf{u}(k) \quad (5.24)$$

where

$$X_R(k) = \begin{bmatrix} \Delta \mathbf{R}(k+1) \\ \Delta \mathbf{R}(k+2) \\ \vdots \\ \Delta \mathbf{R}(k+M_R) \end{bmatrix}, \quad \Gamma_{PR} = [\Gamma_R \quad 0 \quad \dots \quad 0], \quad \mathbf{A}_R = \begin{bmatrix} 0 & \mathbf{I}_m & 0 & \dots & 0 \\ \vdots & \ddots & \ddots & \ddots & \vdots \\ & & & & 0 \\ \vdots & & & \ddots & \mathbf{I}_m \\ 0 & \dots & \dots & \dots & 0 \end{bmatrix}$$

If the control input in Eqs. (5.23) and (5.24) is to stabilize the system such that $\mathbf{e}(k)$ may become 0 in a steady state, then this control problem can be solved as an optimum regulator problem, where the following quadratic-form cost function may be defined:

$$\mathbf{J} = \sum_{k=-M_R+1}^{\infty} \left[[X_0^T(k) \quad X_R^T(k)] \begin{bmatrix} \mathbf{Q} & 0 \\ 0 & 0 \end{bmatrix} \begin{bmatrix} X_0(k) \\ X_R(k) \end{bmatrix} + \Delta \mathbf{u}^T(k) \mathbf{H} \Delta \mathbf{u}(k) \right] \quad (5.25)$$

where \mathbf{Q} is a semi-positive definite matrix and \mathbf{H} is a positive definite matrix. Now, the following control input can be determined by using this kind of future information and solving the above optimal control problem as

$$\Delta \mathbf{u}(k) = \bar{\mathbf{F}}\bar{X}_0(k) = \mathbf{F}_0\mathbf{X}_0(k) + \sum_{j=0}^{M_R} \mathbf{F}_R(j)\Delta\mathbf{R}(k+j) \quad (5.26)$$

where

$$\begin{aligned}\bar{\mathbf{F}} &= [\mathbf{F}_0 \quad \mathbf{F}_R] \\ \mathbf{F}_0 &= -[\mathbf{H} + \boldsymbol{\Gamma}^T \mathbf{P} \boldsymbol{\Gamma}]^{-1} \boldsymbol{\Gamma}^T \mathbf{P} \boldsymbol{\Phi} \\ \mathbf{F}_0(0) &= 0 \\ \mathbf{F}_R(j) &= -[\mathbf{H} + \boldsymbol{\Gamma}^T \mathbf{P} \boldsymbol{\Gamma}]^{-1} \boldsymbol{\Gamma}^T (\boldsymbol{\xi}^T)^{j-1} \mathbf{P} \boldsymbol{\Gamma}_R (j \geq 1) \\ \mathbf{P} &= \mathbf{Q} + \boldsymbol{\Phi}^T \mathbf{P} \boldsymbol{\Phi} - \boldsymbol{\Phi}^T \mathbf{P} \boldsymbol{\Gamma} [\mathbf{H} + \boldsymbol{\Gamma}^T \mathbf{P} \boldsymbol{\Gamma}]^{-1} \boldsymbol{\Gamma}^T \mathbf{P} \boldsymbol{\Phi}\end{aligned}$$

Then the sliding mode servo system is extended to the preview sliding mode servo system by the following procedure. At first, a sliding mode controller and a hyperplane are designed, and the control input $\mathbf{u}(k)$ is obtained in order to realize a regulator that forces state $\bar{X}_0(k)$ tend to zero.

Let us consider the following switching function:

$$\bar{\sigma}(k) = \bar{S}\bar{X}_0(k) = 0, \quad \bar{S}\bar{\Gamma} > 0 \quad (5.27)$$

In general, we can calculate the linear input and nonlinear input for sliding mode control [9] as shown in Eqs. (5.28) and (5.29):

$$\Delta \bar{\mathbf{u}}_{eq}(k) = -(\bar{S}\bar{\Gamma})^{-1} \bar{S}(\bar{\Phi} - \mathbf{I})\bar{X}_0(k) \quad (5.28)$$

$$\Delta \bar{\mathbf{u}}_{nl}(k) = -\eta(\bar{S}\bar{\Gamma})^{-1} \bar{\sigma}(k) \quad (5.29)$$

For asymptotic stabilization, η is greater than 0 and smaller than 2. For chatter-free sliding mode control, η is greater than 0 and smaller than 1. By using \bar{F} of Eq. (5.25) in place of \bar{S} for a switching hyperplane, equivalent control input and nonlinear input are designed as given in Eqs. (5.30) and (5.31):

$$\begin{aligned}\Delta \bar{\mathbf{u}}_{eq}(k) &= -(\bar{S}\bar{\Gamma})^{-1} \bar{S}(\bar{\Phi} - \mathbf{I})\bar{X}_0(k) \\ &= -(\mathbf{F}_0\boldsymbol{\Gamma})^{-1} \left[\mathbf{F}_0(\boldsymbol{\Phi} - \mathbf{I})\mathbf{X}_0(k) + \{\mathbf{F}_0\boldsymbol{\Gamma}_R - \mathbf{F}_R(1)\}\Delta\mathbf{R}(k+1) \right. \\ &\quad \left. + \sum_{j=2}^{M_R} \{\mathbf{F}_R(j-1) - \mathbf{F}_R(j)\}\Delta\mathbf{R}(k+j) \right]\end{aligned} \quad (5.30)$$

and

$$\begin{aligned}\Delta \bar{\mathbf{u}}_{nl}(k) &= -\eta(\bar{\mathbf{S}}\bar{\mathbf{T}})^{-1}\bar{\boldsymbol{\sigma}}(k) \\ &= -\eta(\mathbf{F}_0\mathbf{\Gamma})^{-1}\left[\mathbf{F}_0\mathbf{X}_0(k) + \sum_{j=2}^{M_R}\mathbf{F}_R(j)\Delta\mathbf{R}(k+j)\right]\end{aligned}\quad (5.31)$$

Therefore, the overall control input as given in Eq. (5.32) consists of the sum of two independent control input terms derived in Eqs. (5.30) and (5.31):

$$\Delta\bar{\mathbf{u}}(k) = \Delta\bar{\mathbf{u}}_{eq}(k) + \Delta\bar{\mathbf{u}}_{nl}(k) \quad (5.32)$$

B. Experimental results of the locomotion control with Preview Sliding Mode Control law

This section gives the experimental results of the locomotion control of COMET-III with PSMC. The results are compared with that of the conventional PD controller. When mounting the controller on an actual machine, the state is estimated using an observer because the quantity of the state cannot be measured directly. The full-order observer is applied in this study. The number of preview steps has been taken as $M_R = 15$, and the operation time has been set to 50 ms considering the computing speed for the calculation of inverse kinematics in order to determine a reference value and the PSMC operation. The weight matrixes $\mathbf{Q}_{\text{shoulder}}$, $\mathbf{Q}_{\text{thigh}}$, $\mathbf{Q}_{\text{shank}}$, $\mathbf{H}_{\text{shoulder}}$, $\mathbf{H}_{\text{thigh}}$, and $\mathbf{H}_{\text{shank}}$ were designed as follows:

$$\mathbf{Q}_{\text{shoulder}} = \text{diag}[200 \quad 10 \quad 10 \quad 100]$$

$$\mathbf{Q}_{\text{thigh}} = \text{diag}[20000 \quad 10 \quad 10 \quad 100]$$

$$\mathbf{Q}_{\text{shank}} = \text{diag}[10000 \quad 10 \quad 10 \quad 100]$$

$$H_{\text{shoulder}} = H_{\text{thigh}} = H_{\text{shank}} = 0.4$$

By trial and error, the observer gains $\mathbf{L}_{\text{shoulder}}$, $\mathbf{L}_{\text{thigh}}$, and $\mathbf{L}_{\text{shank}}$ were designed as follows:

$$\mathbf{L}_{\text{shoulder}} = \begin{bmatrix} -1.0057 \\ 7.4849 \times 10^{-3} \\ -7.9884 \times 10^{-5} \\ 3.9912 \times 10^{-4} \end{bmatrix}$$

$$\mathbf{L}_{\text{thigh}} = \begin{bmatrix} -1.0012 \\ 1.1015 \times 10^{-2} \\ -2.5095 \times 10^{-5} \\ 1.2787 \times 10^{-4} \end{bmatrix}$$

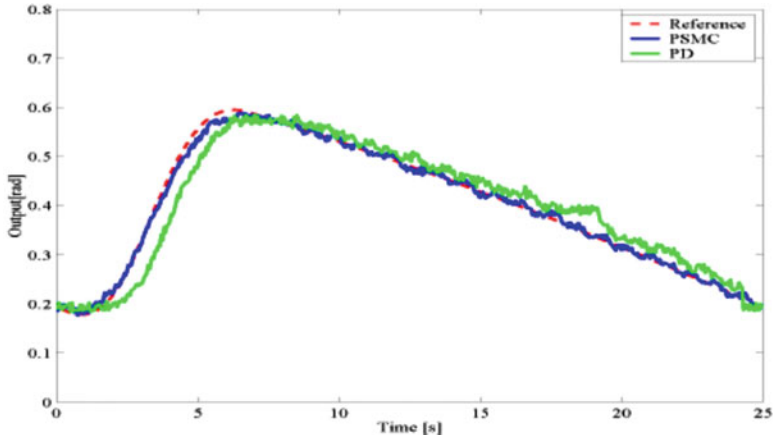


Fig. 5.14 Tracking performance of PSMC of shoulder joint

$$L_{\text{shank}} = \begin{bmatrix} -1.0001 \\ 7.0988 \times 10^{-4} \\ -1.7545 \times 10^{-7} \\ 1.3818 \times 10^{-5} \end{bmatrix}$$

Setting a high value for η is very dangerous because it not only causes chattering to occur but also triggers equipment damage or sudden pressure surges in high-pressure hydraulic-drive systems. In addition, a high-frequency band ignored in modeling the object of control may be excited to cause spillover or other oscillation. However, minimizing the η value reduces the sliding speed and causes the robustness of sliding mode to be lost. Therefore, by trial and error, η_{shoulder} has been set to 0.2, η_{thigh} has been set to 0.8, and η_{shank} has been set to 0.3 for the experiment.

Figures 5.14 and 5.15 show the trajectory tracking performance at each joint for a tetrapod walking gait at a cycle of 25 s. These results show that PSMC has both phase characteristics that are much improved from PD control and a very good tracking performance. The PSMC is able to track the reference orbit, irrespective of parameter variations (Fig. 5.16). It can be observed from these tracking results that even under PSMC, the tracking performance deteriorates at about 5–9 s. This is probably because control input to the plant is small and the influences of the dead zone shown in Fig. 5.4 appear to be large. Figure 5.17 shows the absolute differences between the reference orbits and the one-cycle orbits of the front left leg calculated from the measured response waveform data of each joint according to the forward kinematics of the leg mechanisms. The coordinate system is that of the ground. Here the x -axis is defined as the forward direction, the y -axis is defined as the horizontal direction, and the z -axis is defined as the vertical direction. For comparison, the orbit tracking performance

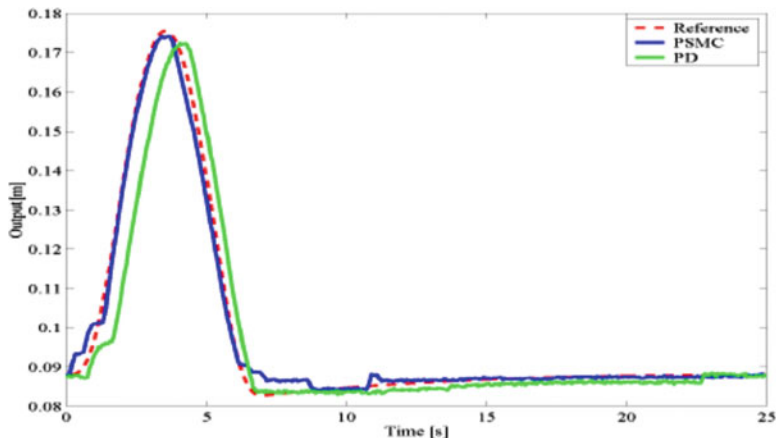


Fig. 5.15 Tracking performance of PSMC of thigh joint

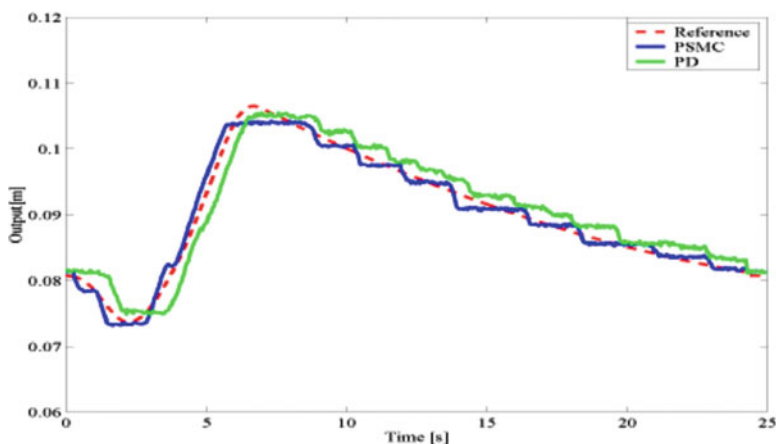


Fig. 5.16 Tracking performance of PSMC of shank joint

by the conventional PD control is also introduced. Judging from these results, the y -axis reference orbit is constant with almost no differences between PSMC and PD control. By improved phase characteristics, however, PSMC ensures accurate positioning on the x -axis and z -axis and the accuracy of leg-end orbit has been clarified. Under PD control, the error between a leg-end orbit and a reference orbit can be up to 3.3 cm. Therefore, this conventional control method is extremely dangerous if used to guide a robot through a minefield. These results verified the effectiveness of PSMC.

5.4.4 Robust Adaptive Fuzzy Logic Control-Based Intelligent Control for Locomotion Control of Hydraulically Actuated Hexapod Robot

There has been a growing interest toward adaptive fuzzy control for their smaller processing time compared to the classical adaptive controllers and their capability to approximate any higher order nonlinear systems by applying a set of *IF–THEN* rules. Being a model-independent and heuristics-dependent control strategy, it can successfully handle the situations where uncertainty is involved in the system model. Wang [13] proved that fuzzy systems are universal approximators and the

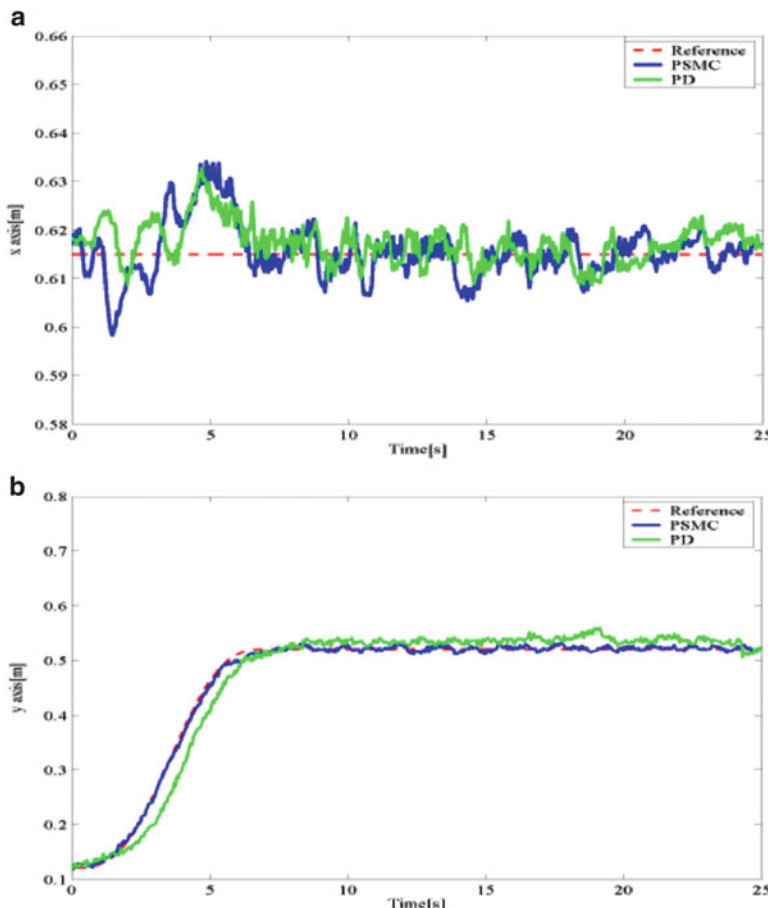


Fig. 5.17 Experimental results of foot trajectory tracking control performance in Cartesian space: (a) x-axis, (b) y-axis, (c) z-axis, and (d) tracking error

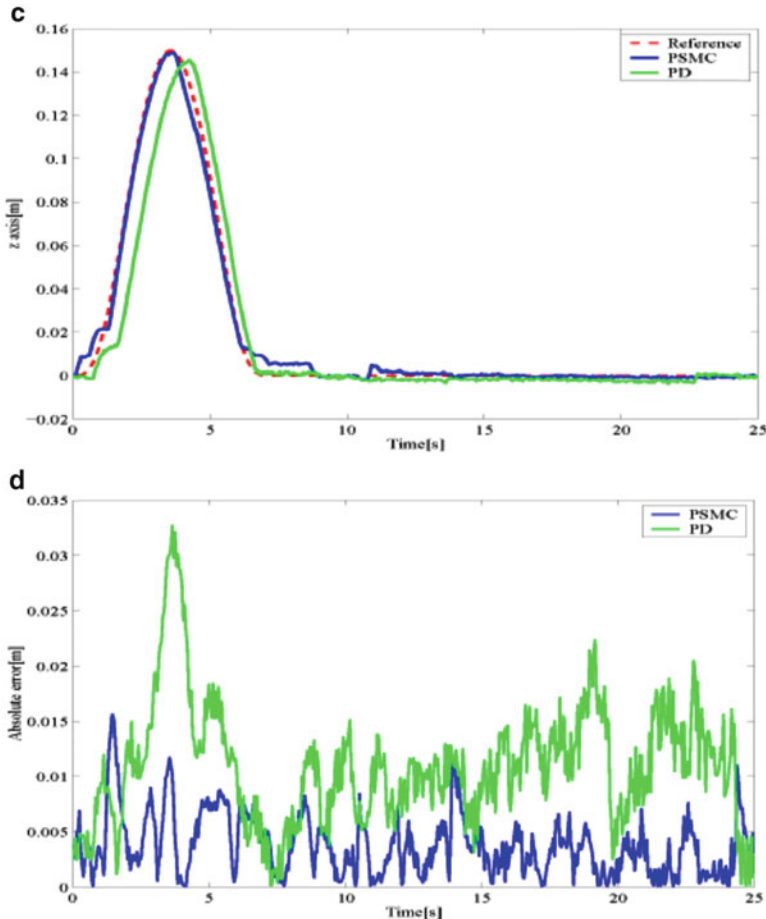


Fig. 5.17 (continued)

output of the system can be represented as a linear combination of the fuzzy regressor or *Basis Function*. This was indeed a breakthrough in the history of fuzzy systems. This discovery inspired many researchers to apply fuzzy control techniques in nonlinear system [14].

An accurate linear parameterizing model for the design of a classical adaptive control is very difficult to obtain when there is uncertainty in the system model. Fuzzy logic-based technique, being a model-independent approach, can be successfully applied in such situations because it does not require the parameterization

model. We will see later that the fuzzy model of the direct adaptive fuzzy controller in terms of the Basis Function is naturally represented in the same form of a linear parameterization model. However, since the fuzzy representation is approximate in nature, it may be insufficient to achieve desired tracking accuracy with mere adaptive fuzzy control. Further, the approximation error crept into the feedback loop makes it difficult to guarantee the stability of the closed-loop system [14, 15]. This necessitates the development of a robust adaptive fuzzy control law.

In this section we will present the locomotion control of a hydraulically actuated hexapod robot COMET-III by robust adaptive fuzzy control in conjunction with hydraulic dead zone compensation technique within independent joint control framework. When independent joint control method is applied in COMET-III robotic systems, parameter varying terms are considered as disturbances to the system. When controlling the joints to follow the desired trajectory, delay due to flow of oil and dead zone of the proportional electromagnetic control valve pose a serious problem. Here, a hydraulic dead zone-compensated robust adaptive fuzzy control law is presented for controlling the hydraulically actuated leg joints to achieve an accurate foot trajectory tracking. The adaptation law is designed by Lyapunov synthesis method and the dead zone compensation signal is designed by one-step-ahead [5] control principles.

A. Design of Robust Adaptive Fuzzy Control Law

Adaptive fuzzy controllers fall into two categories: direct adaptive fuzzy controller and indirect adaptive fuzzy controller. In the direct adaptive fuzzy control, the fuzzy rules are directly incorporated into the controller itself; thus, the rules describe the control input—making it easier to implement—whereas, in indirect adaptive fuzzy control, the fuzzy rules describe the plant and then the control input is derived from that plant description.

Here we have proposed direct robust adaptive fuzzy control law and it has two components. One is responsible for feedback control and this part of the control law is responsible for handling parameter variation and various uncertainties associated with the controlled object. The other component is to solve the problem of the time delay in the output response that is caused by the hydraulic oil flow and the dead zone of the proportional electromagnetic control valves [16]. We will present these components in the following subsections.

First we consider the n th order nonlinear dynamic system of the following form:

$$x^n = f(x, \dot{x}, \dots, x^{(n-1)}) + g(x, \dot{x}, \dots, x^{(n-1)})u \quad (5.33)$$

$$y = x$$

where f is an unknown but bounded continuous function, g is assumed to be a known function, and $u \in R$ and $y \in R$ are the input and output of the system, respectively. Let $\underline{x} = (x, \dot{x}, \ddot{x}, \dots, x^{(n-1)})^T \in R^n$ be the state vector of the system which is assumed to be available. The control objective is to force the output y to follow a given bounded reference signal y_m under the constraint that all signals must be bounded. Hence, we have determined a feedback control law based on fuzzy logic systems and also an adaptation law for adjusting the parameters of the fuzzy logic systems [17, 18] to satisfy the following conditions:

- (i) The closed-loop system must be globally stable in the sense that all variables must be uniformly bounded.
- (ii) The tracking error $e = y - y_m$ should be as small as possible under the constraint in (i).

Then our design objective is to apply an adaptive fuzzy control algorithm so that the following asymptotically stable tracking is achieved:

$$e^{(n)} + k_1 e^{(n-1)} + \dots + k_n e = 0 \quad (5.34)$$

where the polynomial $h(s) = s^n + k_1 s^{n-1} + \dots + k_{n-1} s + k_n$ is a Hurwitz polynomial and is represented by the characteristic of Eq. (5.34). The roots of the $h(s)$ should lie in the open left half of the s-plane via the adequate choice of $K = (k_1, k_2, \dots, k_n)$. In Eq. (5.34) if we incorporate the parameter error $\underline{\phi} = \underline{\theta} - \underline{\theta}^*$, where $\underline{\theta}$ is the actual parameter and $\underline{\theta}^*$ is the estimated parameter, then the error differential equation takes the following form:

$$e^{(n)} = -k_1 e^{(n-1)} - k_2 e^{(n-2)} - \dots - k_n e + K \underline{\phi}^T \xi(\underline{x}) \quad (5.35)$$

where K is a positive constant and $\xi(\underline{x})$ is an arbitrary but known signal.

Figure 5.18 shows a general description of adaptive fuzzy control system [13–15]. An adaptive fuzzy system is defined as a fuzzy logic system equipped with a learning algorithm where the fuzzy system is constructed from a set of fuzzy IF–THEN rules using fuzzy logic principles, and the learning algorithm adjusts the parameters of the fuzzy system based on the training information. The fuzzy logic system performs a mapping from $U \in R^n$ (universe of discourse of input fuzzy sets, in fuzzy logic literature) to $V \in R$ (universe of discourse of output fuzzy sets, in fuzzy logic literature). It comprises four components: fuzzifier, fuzzy rule base, fuzzy inference engine, and defuzzifier [13–15, 17]. In case of an adaptive fuzzy system, an additional block called “adaptation block” is necessary that changes the parameters of the fuzzy controller. Here we have considered that the fuzzy rule base consists of M number of rules for a multi-input single-output fuzzy system and has the following form:

$$R^l : \text{If } x_1 \text{ is } F_1^l \text{ and } \dots \text{ and, } x_n \text{ is } F_n^l \text{ then } y \text{ is } G^l \quad (5.36)$$

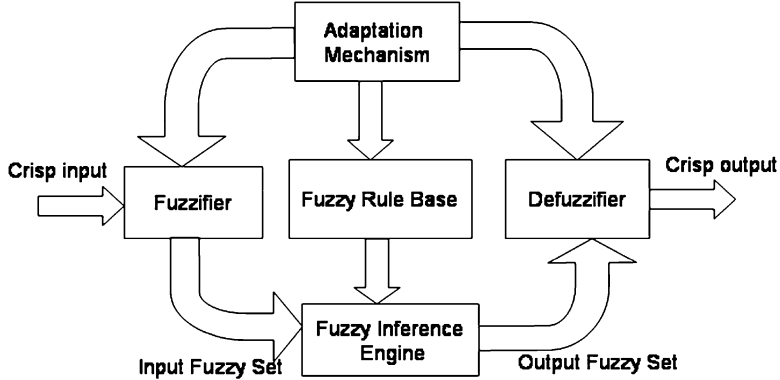


Fig. 5.18 Adaptive fuzzy systems

where $\underline{x} = (x_1, x_2, \dots, x_n)^T \in U$ and $y \in V \subset R$ are the input and output variables of the fuzzy system, respectively, F_i^l and G^l are fuzzy sets and are characterized by linguistic terms like “BIG” and “SMALL,” and $l = 1, \dots, M$. By using singleton fuzzifier, product inference, and center-average defuzzification, the fuzzy logic system can be expressed as

$$y(\underline{x}) = \frac{\sum_{l=1}^M y^{-l} (\prod_{i=1}^n \mu_{F_i^l}(x_i))}{\sum_{l=1}^M (\prod_{i=1}^n \mu_{F_i^l}(x_i))} \quad (5.37)$$

Here y^{-l} is the point where μ_G^l achieves its maximum value; therefore, we can assume $\mu_G^l(y^{-l}) = 1$. Then Eq. (5.35) can be written as [5]

$$y(\underline{x}) = \underline{\theta}^T \underline{\xi}(\underline{x}) \quad (5.38)$$

where $\underline{\theta} = (y^{-1}, \dots, y^{-M})^T$ is the parameter vector and $\underline{\xi}(\underline{x}) = (\xi^1(\underline{x}), \dots, \xi^M(\underline{x}))^T$ is called as *Basis Function*[13] and is defined as

$$\xi(\underline{x}) = \frac{\prod_{i=1}^n \mu_{F_i^l}(x_i)}{\sum_{l=1}^M (\prod_{i=1}^n \mu_{F_i^l}(x_i))} \quad (5.39)$$

There are two main reasons for using the fuzzy logic system of Eq. (5.38) as the basic building block [5, 14] for adaptive fuzzy controller. First, the fuzzy logic system in the form of (5.38) has been proved as universal approximator in [13], i.e., for any given real continuous function f on the compact set U , there

exists a fuzzy logic system in the form of (5.38) such that it can uniformly approximate f over U to an arbitrary accuracy. Therefore, the fuzzy logic system of (5.38) is qualified as the basic building block of adaptive controllers of nonlinear systems. Second, the fuzzy logic system (5.38) is constructed from fuzzy IF-THEN rules of (5.35) using some specific fuzzy inference, fuzzification, and defuzzification strategies. Therefore, linguistic information about a physical system can be directly incorporated in the controllers. It must be noted here that the form of Eq. (5.38) is just the same as the linear parameterization model [19].

If both $f(x)$ and $g(x)$ in Eq. (5.33) are known and there are no external disturbances, then the control law of (5.40) can be applied to the nonlinear system (5.33) to asymptotically achieve the error dynamic Eq. (5.34):

$$u = \frac{1}{g(\underline{x})} [-f(\underline{x}) + y_m^{(n)} + \underline{k}^T e] \quad (5.40)$$

However, the functions $f(x)$ and $g(x)$ are actually not known; therefore, the control law (5.40) could be approximated by fuzzy logic system of the form represented in (5.38). Then the control law is

$$u = \underline{\theta}^T \underline{\xi}(\underline{x}) \quad (5.41)$$

In Eq. (5.41) the elements of the parameter vector of the controller $\underline{\theta} = (y^{-1}, \dots, y^{-M})^T$ are varied based on some adaptation law to cope with uncertain plant parameter variation. Here we will develop an adaptation scheme that will render the overall system to be endowed with robustness and at the same time with faster adaptation to plant parameter variation. We can develop an adaptation law in the same line as discussed in [19], because after approximation of the system (5.33) by fuzzy technique, the system takes the form of linear parametric model that is required by the classical adaptive control.

Let us consider the following adaptation law:

$$\dot{\underline{\theta}} = -\gamma \underline{\xi}(\underline{x}) B^T P \underline{\theta} \quad (5.42)$$

where γ is the adaptation rate and P is a symmetric positive definite matrix and is the solution of the following Riccati-like equation:

$$PA + A^T P + Q - \frac{2}{r} PBB^T P + \frac{1}{\rho^2} PBB^T P = 0 \quad (5.43)$$

where r is a positive weighing factor and ρ is an attenuation level. A and B matrices are given as

$$A = \begin{bmatrix} 0 & 1 & 0 & \dots & 0 \\ 0 & 0 & 1 & \dots & 0 \\ 0 & 0 & 0 & \dots & 0 \\ \dots & \dots & \dots & \dots & \dots \\ -k_n & -k_{n-1} & -k_{n-2} & \dots & -k_1 \end{bmatrix}, B = \begin{bmatrix} 0 \\ 0 \\ \vdots \\ 1 \end{bmatrix} \quad (5.44)$$

Now due to the approximation error caused by the fuzzy system, modification of the adaptation law is necessary [5] so that the system does not become unstable due to large approximation error. We will modify Eq. (5.42) with a leakage term [19], called continuous switching leakage. Then the modified adaptation law is

$$\dot{\underline{\theta}} = -\gamma \xi(\underline{x}) B^T P \underline{e} - \gamma \sigma_s \underline{\theta} \quad (5.45)$$

where σ_s is called continuous switching function and is represented as

$$\sigma_s = \begin{cases} 0 & \text{if } |\theta(t)| < M_0 \\ \sigma_0 \left(\frac{|\theta(t)| - M_0}{|\theta(t)|} \right) & \text{if } M_0 \leq |\theta(t)| \leq 2M_0 \\ \sigma_0 & \text{if } |\theta(t)| > 2M_0 \end{cases} \quad (5.46)$$

where σ_0 and M_0 are design constants. The constraints for the design of σ_0 and M_0 are $\sigma_0 > 0$, $M_0 \geq |\theta^*|$, and $|\theta(0)| \leq M_0$. During implementation, these design constants are chosen by various trial and errors. The advantage of using the continuous switching leakage is that the adaptation law is not a discontinuous one.

B. Design of Electrohydraulic Dead Zone Compensator

The system of (5.33) assumes that there is no time delay associated with it, with this assumption the tracking error is expected to be in the neighborhood of zero [5]. However, when dealing with hydraulic systems this assumption should be relaxed. Therefore, even if stability of the system could be achieved due to bounded closed-loop signals, the overall tracking performance is not good due to the presence of flattery delay [4] in the output. One may be tempted to increase the feedback gain to get better performance, but mere feedback compensation results into actuator saturation, also the steady-state deviation by time delay remains. Here we have proposed to add one compensatory signal with the control input (5.41) so that it eliminates the effect of time delay caused by the hydraulic system. The delay compensation signal is designed from the principles of one-step-ahead control method [5]. Here we estimate the control input necessary at the next sampling ($u_{\text{est}}(k + 1)$) step from the reference and the output at the present sampling instant k . If we design a control input that is proportional to this $u_{\text{est}}(k + 1)$, it is very effective in eliminating the delay from the sampling instants $k = 1, 2, \dots, \infty$. This is because we are driving the system that would be at the instant $(k + 1)$ to the instant k .

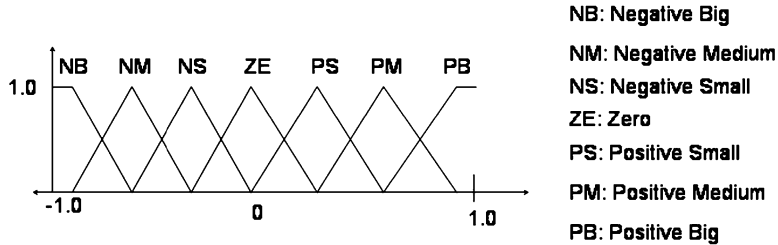


Fig. 5.19 Input/output membership functions with normalized base

Therefore, the hydraulic delay compensation control input can be written in the following form:

$$u_{hyd}(k) = \eta[r(k + 1) - y(k)] \quad (5.47)$$

where $u_{hyd}(k)$ is the hydraulic delay compensation control input at the k th sampling instant, $r(k + 1)$ is the reference at the $(k + 1)$ th instant, $y(k)$ is the output at the k th instant, and η is a design constant. The value of η is chosen by trial and error during real-time implementation.

Then the overall control input in the discrete form can be written as

$$u(k) = -\theta^T(k) \xi(-x(k)) + u_{hyd}(k) \quad (5.48)$$

C. Real-time Implementation of the Robust Adaptive Fuzzy Control Algorithm in Embedded System

The first step is to choose a suitable membership function among the pool of known membership functions for the real-time implementation of the proposed adaptive controller. In our case we have chosen symmetric triangles with equal width and 50 % overlap with neighboring triangle as the membership functions, because it is the most natural and unbiased type of membership function [13]. Implementation of these types of membership functions is also easier because fewer computations are involved and suitable for embedded systems. The input and output membership functions for the feedback controller with normalized bases are shown in Fig. 5.19.

In order to implement the controller represented by Eq. (5.41), we considered that ξ is a function of error $e = y - y_m$ and rate of change of error \dot{e} . The parameters of the controller (θ) are chosen as the center of each output membership functions. Thus, during adaptation the center points of each output membership functions are changed following the robust adaptation law presented in Eq. (5.45). This effectively makes the output membership functions crowded in the same direction as the filtered error signal P_e and as a result produces less control input if the error is less and larger control input if the error is larger; thus, the system can track the parameter variation at a much faster rate.

Fig. 5.20 FAM table for PI-like fuzzy controller

$\Delta e \setminus e$	NB	NM	NS	ZE	PS	PM	PB
NB	NB	NB	NB	NM	NS	NS	ZE
NM	NB	NM	NM	NM	NS	ZE	PS
NS	NB	NM	NS	NS	ZE	PS	PM
ZE	NB	NM	NS	ZE	PS	PM	PB
PS	NM	NS	ZE	PS	PS	PM	PB
PM	NS	ZE	PS	PM	PM	PM	PB
PB	ZE	PS	PS	PM	PB	PB	PB

We have implemented the controller represented by Eq. (5.41) as a simple proportional integral (PI)-like fuzzy controller. The fuzzy rule base of such controller is represented as fuzzy associative memory (FAM) table and is given in Fig. 5.20.

The source code is written in C language and compiled in exeGCC, a GNU C compiler for SH series applications. The compiled object file <filename>.mot is downloaded to the SH4 FlashROM by the development system provided by M/s Kyoto Micro System for the embedded application with Compact-PCI type SH4 microcomputers.

D. Experimental Results

Walking control experiments have been conducted on COMET-III with the dead zone-compensated robust adaptive fuzzy controller. As already mentioned tetrapod gait has been implemented for forward and backward walking of COMET-III. Here, we have assumed that the ground does not have much obstacles and roughness and it is slightly slippery. The actual experiment has been conducted over very smooth vinyl floor which is little bit slippery in nature. The experimental data showing the tracking performance of the reference joint trajectories when COMET-III is walking are shown in Figs. 5.21, 5.22, and 5.23 for the shoulder, thigh, and shank, respectively. For comparison the data from PID control is also plotted on the same axis. For successful implementation of any fuzzy controller, the most challenging part is to estimate the maximum swing of the input and output signals of the fuzzy controller. This is important because if the interval over which the fuzzy sets are defined does not match properly with the range of signal variation, the performance of the fuzzy controller will be ambiguous. When working with the state variables like error and rate of change of error, the situation is more complex. This is because during the tuning between the fuzzy set interval and the actual error signal swings, as they are becoming closer, the error further decreases. Thus, it needs lots of trial and error while tuning the fuzzy set intervals with the actual signal swing. In order to facilitate this tuning process we defined the input fuzzy

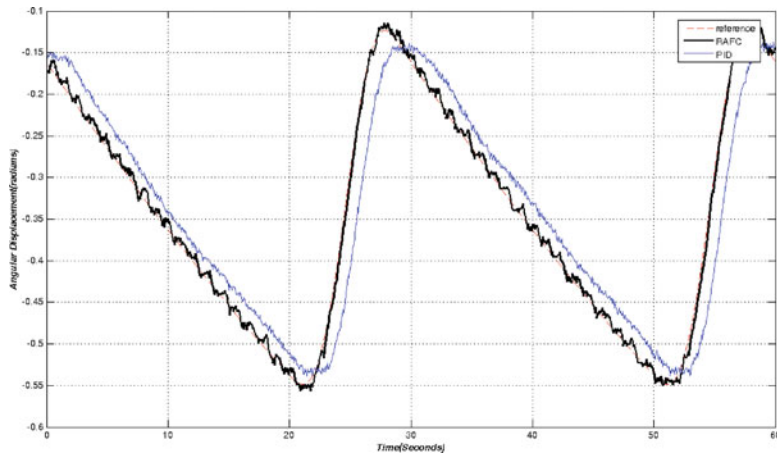


Fig. 5.21 Tracking performance of shoulder joint

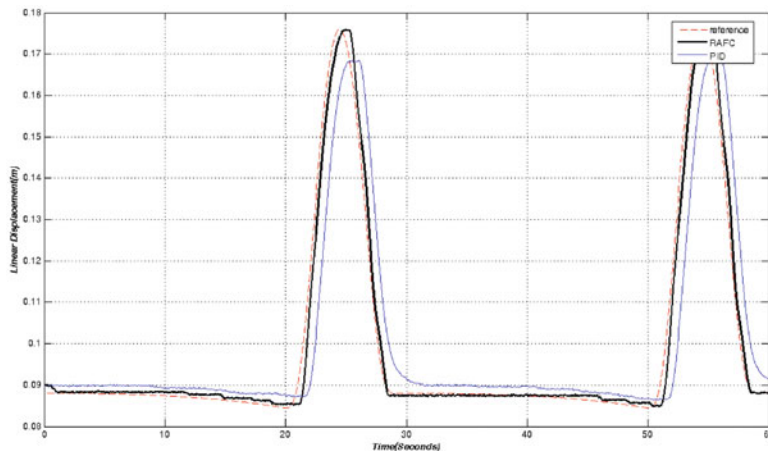


Fig. 5.22 Tracking performance of thigh joint

sets over a normalized interval of $(-1 - +1)$ and the input signals are multiplied by scale factors. As we have taken fuzzy singletons as the output fuzzy sets of the controller, we took a liberty of choosing the interval from $(-3 - +3)$ so that all the seven number of membership functions are unit distance apart. During experiment we have chosen the scale factors for the input error signal of 14.5, 25, and 15.0 for the shoulder, thigh, and shank joint, respectively. The scale factors for the input rate of change of error signal are 1, 2, and 10 for the shoulder, thigh, and shank joint, respectively. The output scaling factors are taken as 0.25, 0.475, and 0.14, respectively. These values are arrived after several experimental trials.

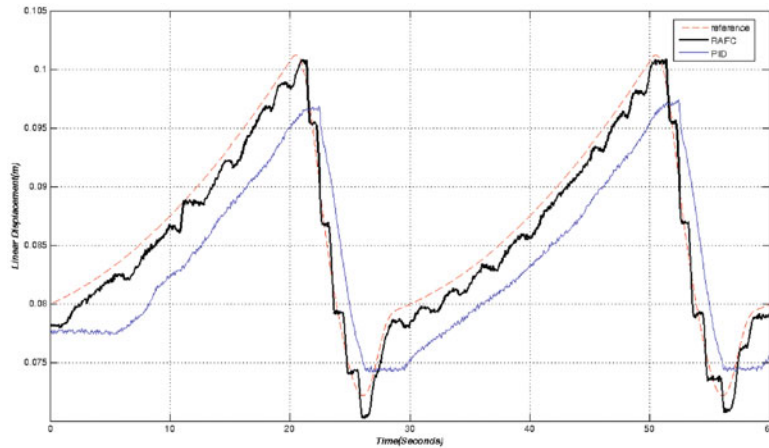


Fig. 5.23 Tracking performance of shank

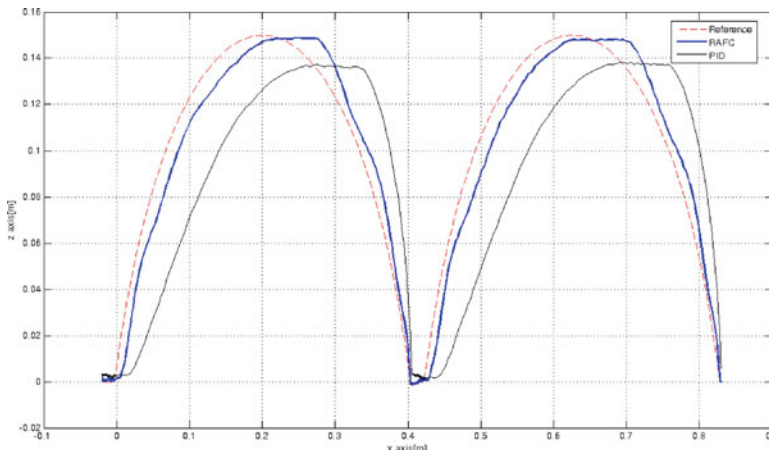


Fig. 5.24 The foot trajectory in the X-Z plane

The associated foot trajectory in Cartesian coordinate is shown in Fig. 5.24.

From Figs. 5.21, 5.22, and 5.23 it is evident that the proposed controller is quite effective for eliminating much of the flattening time delay caused by the hydraulic system.

References

1. Spong MW, Vidyasagar M (1989) Robot dynamics and control. Wiley, Singapore
2. Nonami K, Huang Q, Komizo D, Fukao Y, Asai Y, Shiraishi Y, Fujimoto M, Ikeda Y (2003) Development and control of mine detection robot COMET-II and COMET-III. JSME Int J Series C 45(3):881–890

3. Sugai H, Nonami K (2005) Reference model following sliding mode control for hydraulic mine detection hexapod robot. *Trans JSME* C72(721):2829–2837 (in Japanese)
4. Nonami K, Ikeda Y (2004) Walking control of COMET-III using discrete time preview sliding mode control. In: Proceedings of the IEEE/RSJ international conference on intelligent robots and systems, Sendai, pp 3219–3225
5. Barai RK, Nonami K (2007) Locomotion control of a hydraulically actuated hexapod robot by robust adaptive fuzzy control and dead zone compensation. *Robotica* 25(3):259–281
6. Slotine J, Li W (1991) Applied nonlinear control. Prentice Hall, Englewood Cliffs
7. Sage HG, Mathelin MFD, Ostertag E (1999) Robust control of robot manipulators: a survey. *Int J Control* 72(15):1498–1522
8. Song SM, Waldron KJ (1989) The machine that walk: the adaptive suspension vehicle. MIT, Cambridge
9. Nonami K, Tian T (1994) Sliding mode control. Corona Publishing Co Ltd, Tokyo (in Japanese)
10. Utkin VI, Guldner J, Shi J (1999) Sliding mode control in electromechanical systems. Taylor & Francis, Abingdon
11. Tsuchiya T, Egami T (1992) Digital preview control, Industrial Library. Sangyo-Tosyo, Tokyo
12. Sato T, Tsuchiya T, Egami T (2001) Digital preview sliding mode servo system and its characteristics. *J Inst of Syst Control Info* 14(12):582–592
13. Wang LX, Mendel JM (1992) Fuzzy basis functions, universal approximation, and orthogonal least-square learning. *IEEE Trans Neural Netw* 3(5):807–814
14. Park JH, Seo SJ, Park GT (2003) Robust adaptive fuzzy controller for nonlinear system using estimation of bounds for approximation errors. *Fuzzy Sets Syst* 133(1):19–35
15. Wang LX (1993) Stable adaptive fuzzy control of nonlinear systems. *IEEE Trans Fuzzy Syst* 1(2):145–155
16. Corbet T, Sepehri N, Lawrence PD (1995) Fuzzy control of a class of hydraulically actuated industrial robots. *IEEE Trans Control Syst Technol* 4(4):419–425
17. Mudji RK, Pal NR (2000) A self-tuning fuzzy pi-controller. *Fuzzy Sets Syst* 115(2):327–338
18. Wang XS, Su SY, Hong H (2001) Robust adaptive control of a class of nonlinear systems with unknown dead-zone. In: Proceedings of the 40th IEEE conference on decision and control, pp 15.27–15.32
19. Ioannou PA, Sung J (1995) Robust adaptive control. PTR Prentice Hall, Upper Saddle River

Chapter 6

Force-Based Locomotion Control of Hexapod Robot

Abstract As a part of motion control categories as discussed in Chap. 1, force and impedance control play a main role in legged/walking robot walking on unstructured or uneven terrain. With active suspension configuration (legs), the strong role of legged/walking robot design is capable of passing through any uneven terrain as long as the obstacles are not achieved its maximum or minimum overall body height, if compare to the wheel-type robot. Therefore, force or impedance control is needed to make a dynamic response on each leg in order to identify the different level of the terrain or any sudden changes on the terrain. Moreover, this control is very crucial on the hidden area that could not be identified by a vision system via pre-scanning and localization.

6.1 Position-Based Force Control for Hydraulically Driven Hexapod Robot Walking on Rough Terrain

6.1.1 Case Study: Hydraulically Driven Hexapod Robot Walking on Rough Terrain Issue

Fixed trajectory motion is not suitable to be applied in COMET-IV or any hydraulically driven hexapod robot for walking/operation on rough terrain [1]. As discussed in Chap. 5, ETT is designed as a preperception of each robot's leg to trace the current level of the stepped terrain during walking period. However, applying ETT module alone in the robot system attributes to other problems, which include causing the body to horizontally incline, a situation known as force redundancies, and causing instability of the robot body's posture angles (roll(ϕ) and pitch(θ)), as shown in Fig. 6.1a.

On the other hand, if fixed trajectory motion is applied in a robot walking on an uneven terrain, such as shown in Fig. 6.1b, one or more legs that are hanging during the support phase might suddenly drop causing a large vibration while the robot is walking.

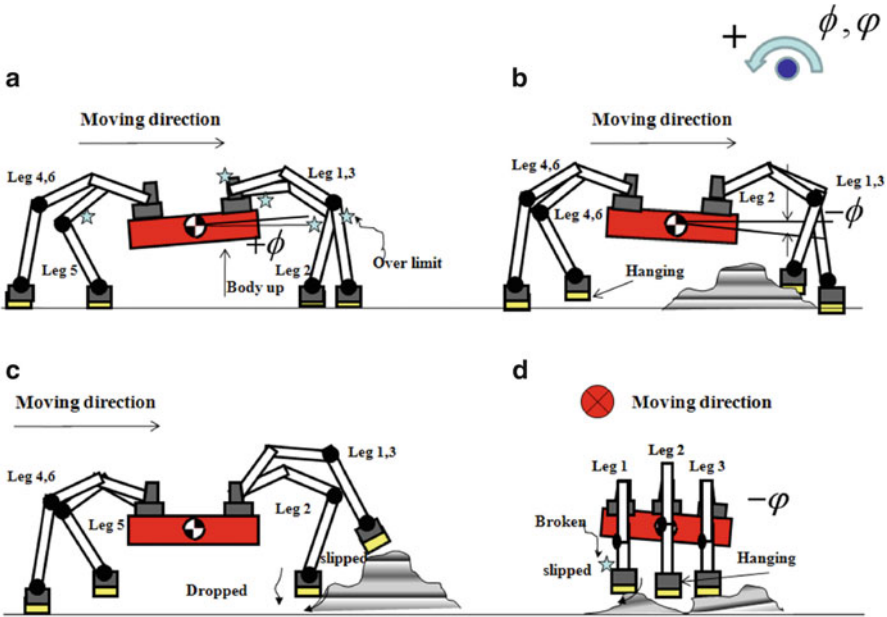


Fig. 6.1 Focus case studies for robot walking on rough terrain, (a) Leg(s) stiffed over limit, (b) Leg(s) hanging, (c) Leg(s) slipped, (d) Leg(s) hanged and slipped

When an unexpected vibration occurs in the overall robot system, such as in the case above, it will automatically trigger the programmable logic valve controller (PLVC) units to shutdown, stopping the robot. Leg slipped as shown in Fig. 6.1c is also part of the problem that can cause same effect as in Fig. 6.1b. This incident will happen if the foot stepped about less than 56 % on the ground or slope surfaces of the hard rock are wet (slipping) as shown in Fig. 6.2. The same things happened from the left-side view as shown in Fig. 6.1d where the roll angle of the body is disturbed.

Furthermore, the scenario above not only will shutdown the PLVC units but will also trigger the ETT module to do a *reset action* by resetting all the legs of the robot to the standing position state as previously shown in Fig. 6.3. Example of a situation where *reset action* is triggered while a robot is walking is shown in Fig. 6.3 and the related measurement waveforms are shown Fig. 6.4. This *reset action* is taken for safety reasons due to the limitations of the links of COMET-IV which has been previously determined and applied in studying COMET-IV, as shown in Fig. 6.5. However, there is a possibility that the robot will overturn or even topple to the ground when the reset action is triggered; hence, one key point to consider when developing the control system is to limit the action from occurring as much as possible when the robot is walking on a rough terrain.

For the hexapod robot designed with hydraulically driven locomotion, 4-DOF, equipped with counterbalances and hexapod configuration, makes it statically stable when walking on flat or almost flat terrain and can cope with small uneven

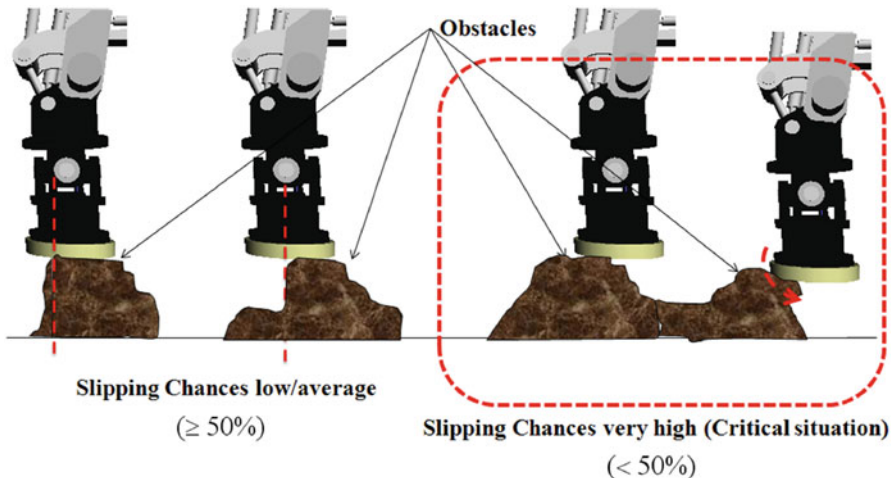


Fig. 6.2 Probability of foot slipping during stepping on the hard obstacle

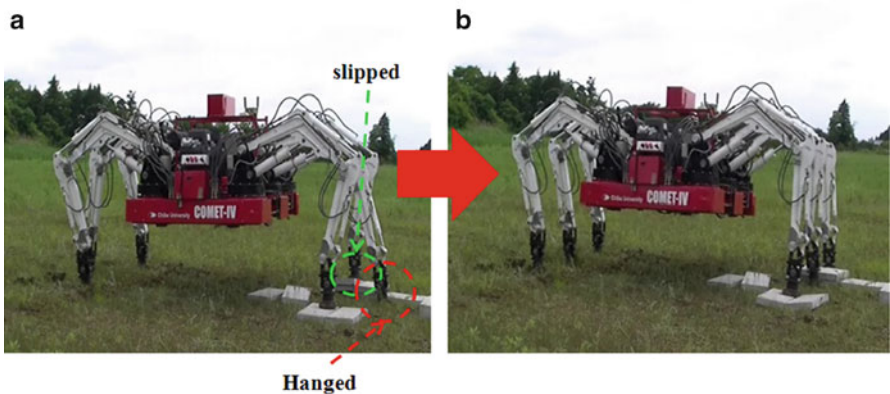


Fig. 6.3 Problem encountered during real-time operation of robot walking on rough terrain; (a) hanging and slipping, (b) reset action

surface ($\cong 10$ cm) at a speed of 16 s/cycle. However, the main objective of developing this kind of heavy hexapod robot is for operation on a large-scale uneven terrain and this is made possible using ETT, where the ETT is designed to distinguish the stepping positions of the robot's foot while it walks on a large-scale uneven terrain. As discussed in Sect. 4.5, the use of ETT module alone is not sufficient to stabilize such a hydraulically driven hexapod robot and attribute to the force redundancies scenario with reference to the second stability criteria that has been outlined in Sect. 4.5. This occurrence could happen whenever the robot's body is pushed (front) by the supporting legs during the walking period. As mentioned in Sect. 4.5, $F_{TH} = 1$ kN is set for each leg but the raw feedback response of $F_{zo}(t)$

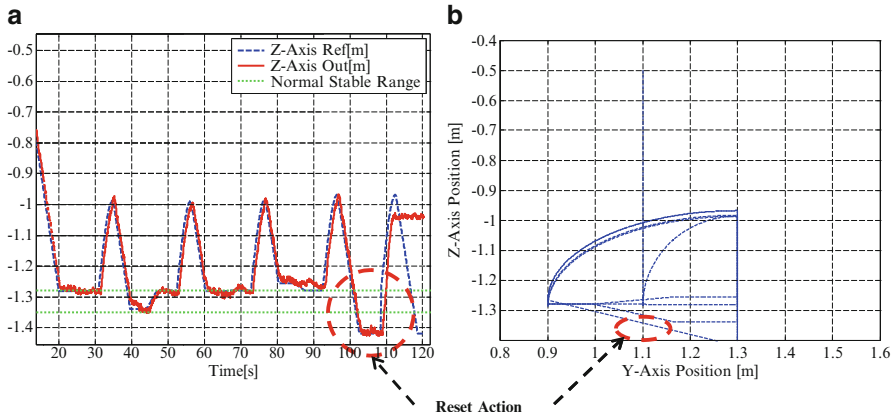


Fig. 6.4 Sample of experimental results for z-axis motion (foot point) of leg 6 when slipping occurred during stepping on an obstacle; (a) z-axis motion foot, (b) z-axis motion versus y-axis motion

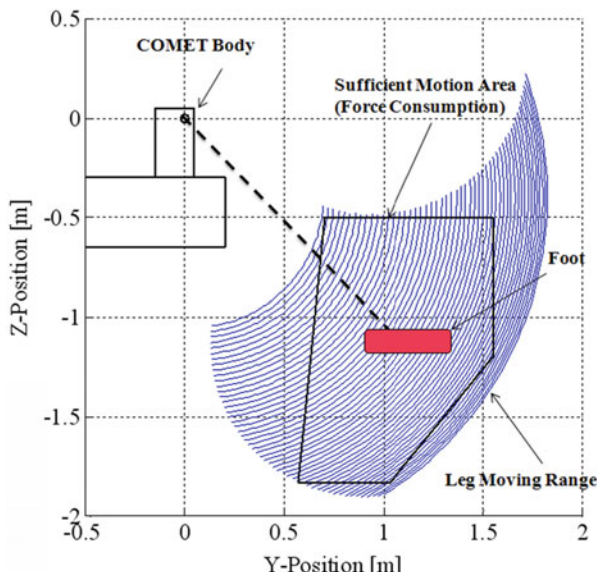


Fig. 6.5 Stable swing and footing range for COMET-IV walking

from each leg changes with every gait sequence. The $F_{z_o}(t)$ response in the legs on one side of the robot is more likely to increase, while that of the legs on the opposite side decreases (hydraulic cylinder actively actuated). During the swing phase of a leg, whenever the ETT module detects $F_{z_0}(t) = 1 \text{ kN}$, the leg is stopped from swinging. Therefore, when and where (in the z-axis) one leg is stopped from swinging is different from that of any other legs. The vertical force feedback used for ETT is not only from the force applied when the leg touches the ground but also

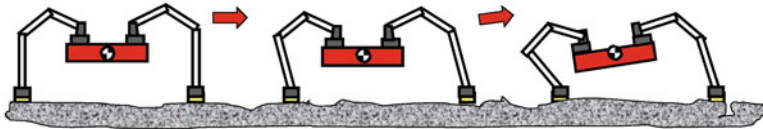


Fig. 6.6 Force redundancies factor; robot body's inclining uptable for every each step of walking sequences (based on COMET-IV system)

the force delivered to the foot every time the leg moves since it is derived from the total amount of pressure in the hydraulic cylinder of the thigh and shank and also the torques in each joint of the leg. For the case of rough terrain, this redundancies scenario affect the overall robot stability by giving its body inclining up every each step sequences as shown in Fig. 6.6.

As a solution to this problem, several force controllers are proposed and designed in with respect to the case studies of walking on rough terrain. For the case where the robot is required to walk on rough terrain, position-based force control is selected as the control system on the reference signal since the main input of the control valve is in position of each joint angle.

6.1.2 Compliant Control Using Pull-Back Method and Logical Attitude-Level Terrain Changes Switching for ETT Module

In order to provide stable walking and maintain the body on the secured horizontal level, motion control unit needs to be designed. This motion controller consists of force control and decision control that are based on the changes of kinematics motion of ETT module. The motivation for designing the controller is to solve the kinematics motion problem in ETT which is too static and hence causes force redundancies during walking on rough terrain or almost flat terrain. The design of the controller is focused on the generation of ETT module signals that are derived from support phase and swing phase signals. Proportional, integral, and derivative (PID) control is used for position controller in this study, and the gain values K_p , K_i , and K_d for each joint are the same as that used in fixed trajectory walking. Figure 6.7 shows the general flow of the compliant controller for ETT [1], and it will be described in detail in this section.

In ETT state sequences, stability control needs to be designed to meet the second criterion described in Sect. 4.5. ETT indirectly provides the information on environment height levels via support phase signal as in Eqs. (4.22) and (4.25) of Sect. 4.5. $z_{s_n}(t)$ probably generates a different value every time each foot touches the ground, and thus, every $z_{s_n}(t)$ signal can be used as a feedback response for the control of each leg. At this point, force control can be created by means of $z_{s_n}(t)$ feedback. This position-based force control concept can be done by creating *pull-back* action

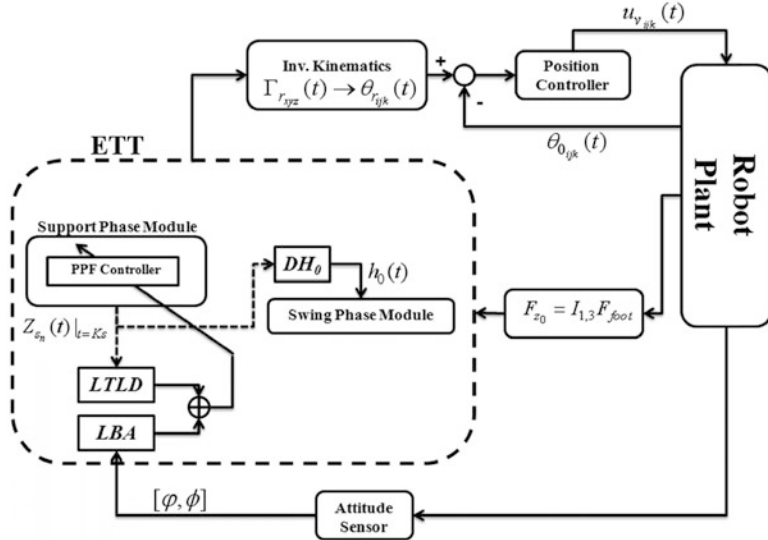


Fig. 6.7 Division of motion control module derived from ETT

for unnecessary force that is applied when the foot is going through the step phase. As shown in Fig. 6.8, the period during the support phase signals is generated can be divided into three clusters, namely, *sensing period*, *action period*, and *preparation period* [1].

During *sensing period*, it is possible to conduct a measurement process of the leg as it is just touching the ground but still away from the center of gravity of foot point because at this point the leg is not being used to fully support the body. The second cluster is called the *action period* because at this point some changes in the signal could be done (if any) since the foot is at the center of gravity and the leg is used to fully support the body weight during walking event. Finally, the *preparation period* is used to determine the possible stable position for each foot before commencing the swing phase. Therefore, a specific controller can be designed to function during the *action period* and the *preparation period* since both periods play major roles in stabilizing the robot during walking event.

According to the analysis of ETT module signals, the flat terrain or almost flat terrain can be identified in the first step movement (on flat terrain) where each leg will be pushed in the same range, and this conclusion can be expressed as follows:

$$S_b = \begin{cases} z_0 + S_h & ; S_{b_{\min}} \\ z_0 + S_h + \ell_x & ; S_{b_{\max}} \end{cases} \quad (6.1)$$

This z -axis motion range is determined from the combination of fixed walking trajectory position value ($S_{b_{\min}}$) and maximum pushing position by each leg in ETT

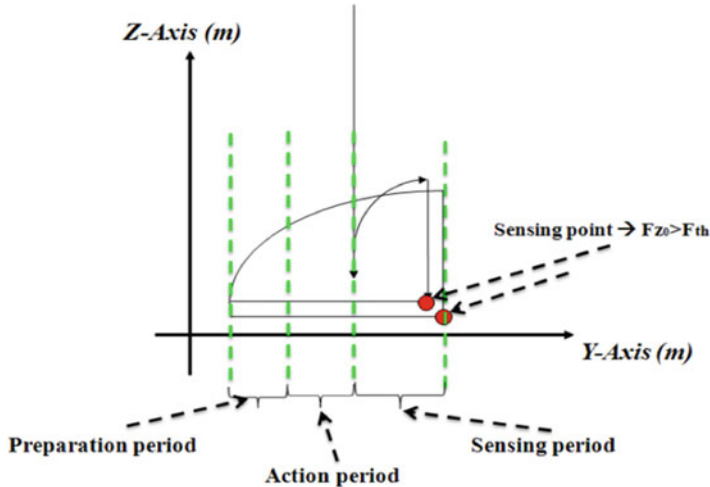


Fig. 6.8 ETT module support phase clusters

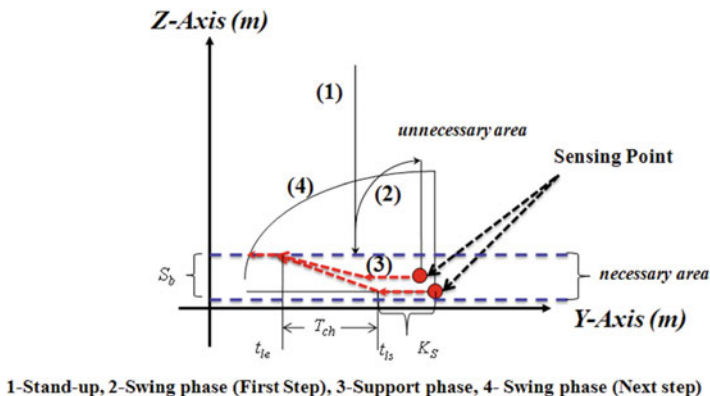


Fig. 6.9 Timing and *pull-back* control mechanism in PPF controller during support phase

($S_{b\max}$) where the maximum pushing range, $l_x = -0.7$ m, corresponds to the value obtained from several experimental study in the laboratory [1]. As shown in Fig. 6.9 is S_b range is indicated as *unnecessary area* to apply extra force (on the thigh and shank) during walking. Thus, force control must be designed and applied to bring back or *pull back* the leg motion to the necessary fixed position, $z_{s_n}(t) = S_{b\min}$.

Concerning the $z_{s_n}(t)$ feedback, the *pull-back* action can be done gradually using the proposed controller described in Fig. 6.9. This controller is named *pull-back* position-based force (PPF) control [1], where the controller will perform the *pull-back* action whenever it detects the value of $z_{s_n}(t)$ within the determined S_b range. The gradient pull-back slope period (T_{ch}) and length of a pull-back slope period (K_s)

are design parameters that can be tuned to decide the timing for a stable *pull-back* action. The PPF controller elements are derived and added to the z -axis support phase signal generation in ETT such as in Eqs. (4.22) and (4.25) in Sect. 4.5. Taking the z -axis signal generation in Eq. (5.5) and dividing it into three separated time clusters [1] will result in the following equations:

$$Z_{s_n}(t) = \begin{cases} z_{0_n}; & 0 \leq T_a \\ \Delta m + h; & T_a \leq t \leq T_b \\ z_{sh}; & T_b \leq t \leq \frac{T_c}{2} \end{cases} \quad (6.2)$$

where

$$T_a = \frac{(T_c - 2)K_s}{2}; \quad T_b = T_a + T_{ch};$$

and

$$\Delta m = \frac{z_{sh} - z_{0_i}}{t_{l_e} - t_{l_s}}; \quad h = Z_{0_i} - t_{l_s} \Delta m$$

where the designed timing division is indicated as T_a , T_b , and T_c in parallel determined the range of period for each defined cluster in Fig. 6.8. When heavy hexapod robot is walking on minor rough or soft terrain, PPF controller is applicable and stable to use since the $Z_{s_n}(t)$ lies within the S_b range. However, in the case of large-scale uneven rough terrain such as discussed in Sect. 6.2.1, the controller is unstable when performing *pull-back* action for every step of walking since S_b is a fixed value and this means that the applied forces (thigh and shank) are not always in the *necessary area*. For example, if *pull-back* action is applied when the robot is walking onto a higher terrain, the body will be drastically pushed up thus inclining the body and it may even overturn. Therefore, to overcome the problem, an ON-OFF switch for the *pull-back action* is designed and proposed, and its principle is illustrated in Fig. 6.10.

This switching function is named as Logical Terrain Level Detection (LTLD) [1]. In order to include the control of the robot body's posture, a logical attitude control, namely Logical Body Attitude (LBA) control [1], is proposed and is used in combination with LTLD. The design of LBA is based on the division of COMET-IV body's posture angles and legs as shown in Fig. 6.11. The posture angles are based on BCS and right-handed Euler angles along the dotted line as shown in the figure. The relation between robot body's posture angles and vertical motion of each leg is defined as in Table 6.1 where the positive (+) and negative (-) poles indicate whether the robot's body is inclining upward or inclining downward, respectively, out of the stable range of the robot body's posture angle (commonly defined via heuristic method in laboratory).

As shown in Table 6.2, both LTLD and LBA logical behaviors are combined and matched in order to design a particular logical switching control to activate

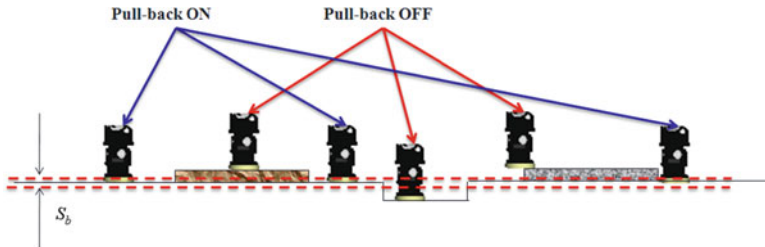


Fig. 6.10 Fundamental concept of compliant switching for stepping on uneven terrain

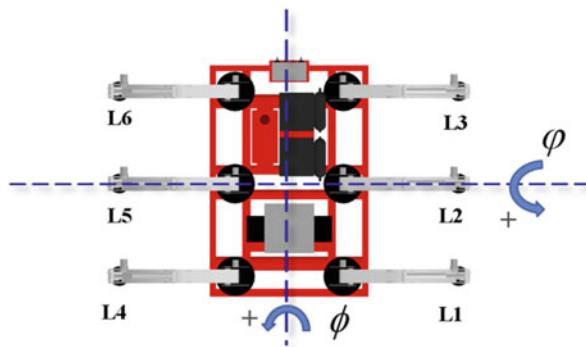


Fig. 6.11 Euler angle orientation for COMET-IV based on BCS

Table 6.1 Leg height position with changes of robot body's posture angles

Attitude angle	Poles	Leg 1, 3, and 5 positions	Leg 2, 4, and 6 positions
φ	+	L1 < L3,L5	L4 < L2,L6
	-	L3 < L1,L5	L6 < L2,L4
φ	+	L5 < L1,L3	L2 > L4,L6
	-	L5 > L1,L3	L2 < L4,L6

pull-back action for each leg. With reference to the table, a truth table for compliant switching function of PPF controller can be created for each leg of the robot: $R_n = D_n + A_n$.

Thus, after De Morgan's law simplification, Boolean expression for the compliant switching mechanism of PPF controller can be expressed as follows [1]:

$$R_1 = D_1 + [K \bullet (p \bullet r + \bar{p}) + M \bullet (\bar{p} + \bar{r})] \quad (6.3)$$

$$R_2 = D_2 + [(L + N) \bullet (\bar{p} \bullet \bar{r} + p \bullet r + \bar{p})] \quad (6.4)$$

$$R_3 = D_3 + [K \bullet (p + r + \bar{p} \bullet \bar{r}) + M \bullet (\bar{p} + r + \bar{p} \bullet \bar{r})] \quad (6.5)$$

Table 6.2 LTLD and LBA logical behavior definition

	Input/output	Bit	Definition
A_n	ϕ	1	$\phi > 1^\circ$
		0	$\phi < -1^\circ$
	ϕ	1	$\emptyset > 1^\circ$
		0	$\emptyset < -1^\circ$
	$[\varphi, \emptyset]$	NC	$-1^\circ < [\varphi, \emptyset] < 1^\circ$
		1	$S_{b_{\min}} \ll Z_{s_i} _{K_s}^0 \ll S_{b_{\max}}$
	D_n	0	$S_{b_{\min}} > Z_{s_i} _{K_s}^0; S_{b_{\max}} < Z_{s_i} _{K_s}^0$
		1	ON Pull-back
R_n		0	OFF Pull-back

Table 6.3 Attitude counter definition for tripod walking pattern

a_c	Status	Leg (support)	Leg (swing)
K	Walk	2, 4, 6	1, 3, 5
L	Walk	1, 3, 5	2, 4, 6
M	Transition	1, 2, 3, 4, 6	—
N	Transition	1, 2, 3, 4, 6	—

$$R_4 = D_4 + [(L + N) \bullet (p + \bar{r})] \quad (6.6)$$

$$R_5 = D_5 + [K \bullet (p + r) + M \bullet p] \quad (6.7)$$

$$R_6 = D_6 + [(L + N) \bullet (p + r)] \quad (6.8)$$

where p and r represent φ and ϕ , respectively, and D_n is the proposed detection level where $D = 0$ indicates $Z_{s_n}(t)|_{t=K_s}^0$ is out of S_b . On the other hand, $a_c\{\text{K, L, M, N}\}$ indicates the attitude counter ($a_c = 1$ is ON and $a_c = 0$ is OFF) that has been decided in the ETT module state flows with reference to the tripod cycles as shown in Table 6.3. The output of LBA is pre-calculated based on the attitude counter in the table and is shown in Fig. 6.12.

In order to provide better stable walking on rough terrain and more dynamic on ETT motion planning, swing rising controller is designed. As shown in the swing phase equations in Sect. 4.5, swing raising distance or height (H_0) is fixed to 0.3 m (COMET-IV system) from the ground for all step sequences. When walking on an actual rough terrain, instability in the robot can occur if the legs make too huge a swing when stepping up to a higher ground or if the swing is too small when stepping down to a lower ground. Moreover, the ETT module system could activate the *reset action* if a constant value of H_0 is used for robot walking on uneven terrain, plotted from the results of a short experiment as shown in Fig. 6.13. Cycle period “time out” can also cause the module to activate the reset action if the robot is stepping up onto a terrain whose level is too high (from the graft at running time between 110 and 130 s).

Therefore, a better approach is to change H_0 dynamically based on the height of the terrain after the leg touches the ground. This means the final $z_{s_n}(t)$ value in the

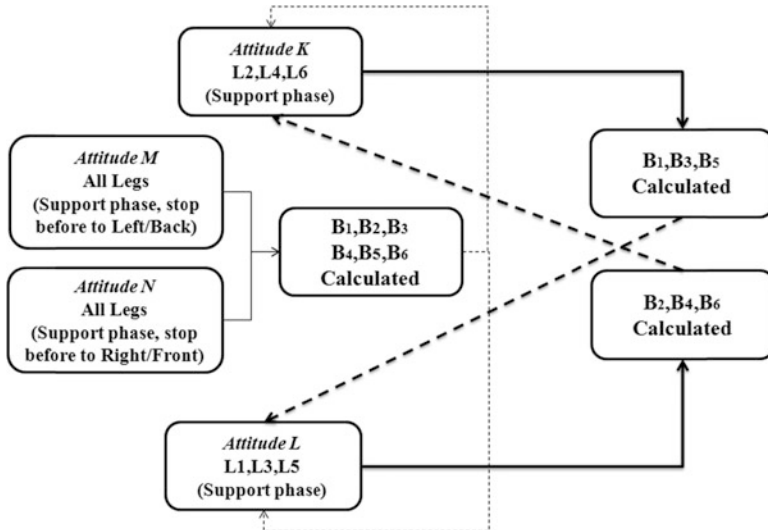


Fig. 6.12 LBA action by sequence of tripod walking attitude counter

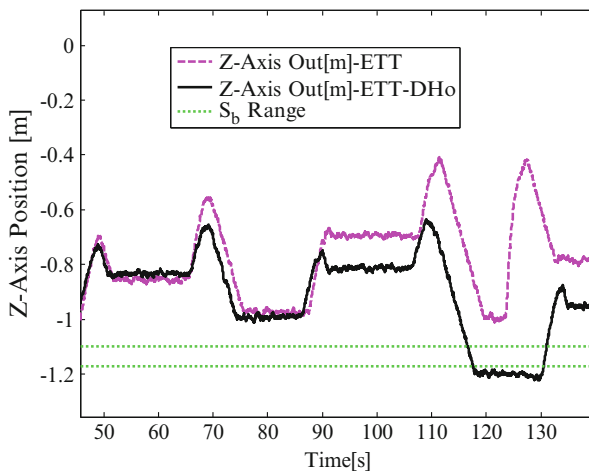


Fig. 6.13 Difference between ETT-PPF with and without DH_6 (sample of z-axis position output for leg 1)

support phase is used to estimate the percentage of the height of the terrain touched by each leg. Then, this percentage can be used to perform swing raising control via the proposed dynamic H_0 (DH_0) method [1] represented by $h_0(t)$ which can be expressed as follows:

$$h_0(t) = \begin{cases} H_0 - \gamma_{ci}H_0 + \lambda; Z_{s_i}(t) > S_{b_{\max}} \\ H_0 + \gamma_{ci}H_0 + \lambda; Z_{s_i}(t) < S_{b_{\min}} \end{cases} \quad (6.9)$$

where γ_{ci} is rate of support phase height changes for each leg calculated as follow:

$$\gamma_{ci} = \begin{cases} \frac{S_{b_{\max}} - Z_{s_i}(t)}{S_{b_{\max}}}; Z_{s_i}(t) > S_{b_{\max}} \\ \frac{S_{b_{\min}} - Z_{s_i}(t)}{S_{b_{\min}}}; Z_{s_i}(t) < S_{b_{\min}} \end{cases}$$

and λ is a design compensator based on acceptable range of H_0 (for COMET-IV, $0.3 \text{ m} > h_0(t) > 0.1 \text{ m}$) which was decided after conducting laboratory test. $h_0(t)$ is used only in the swing phase of a moving mode after it has been calculated in the support phase signal in the same a_c period. For example, $h_0(t)$ is used only in *MOVE-phase 1*, swing phase in Eq. (4.18) which is pre-calculated in *FIRST-phase* through Eq. (4.17) or *MOVE-phase 2* through Eq. (4.20). As shown in Fig. 6.13, the vertical leg axis moving point is stable (reset is avoided) when *DH₀* method is used compared to the conventional method. This method can control the rise of the swing even though the foot of the robot stepped on a terrain that is about 0.4 m higher than the $S_{b_{\min}}$ level or a terrain that is about 0.1 m lower than the $S_{b_{\max}}$ level.

6.1.3 Experiment and Verifications

Proposed position-based force control technique is verified via real hydraulically driven hexapod robot, COMET-IV, corresponding to the case studies discussed in Sect. 6.2.1. The discussions are covered from the fundamental test to the real situation test on the field. For the case study of walking on the rough terrain, the targeted field area contains major hard surfaces such as bricks and cliffs. In the fundamental test, the purpose of setting up the obstacles are related to the distance of tripod stepping in order to evaluate the reaction of each designed controller when the height of the environment is changed, as shown in Fig. 6.14. In this experiment, the performances of ETT with PPF controller (ETT–PPF), ETT with PPF controller and LTLD–LBA (ETT–PPF–LTLD–LBA), and ETT without both controllers (ETT) are evaluated and compared. The experiment is run with $S_h = 0.78 \text{ m}$; the height is sufficient for COMET-IV walking on a surface whose height varies less than 60 cm from the ground level. After some simulations and dummy testing (trial and error tuning), $T_{ch} = K_s = 3$ is set for each leg, which is considered as stable values for ETT with PPF controller. Since the evaluation of the proposed controller is on its high stability performance, hence, in such a critical situation the shoulder movement is set to OFF during all the experiments.

First of all, the discussion will describe the effectiveness of *pull-back* action using PPF controller with ETT in terms of the vertical force performance and z-axis position of the robot's leg as shown in Fig. 6.15. The *pull-back* action is performed

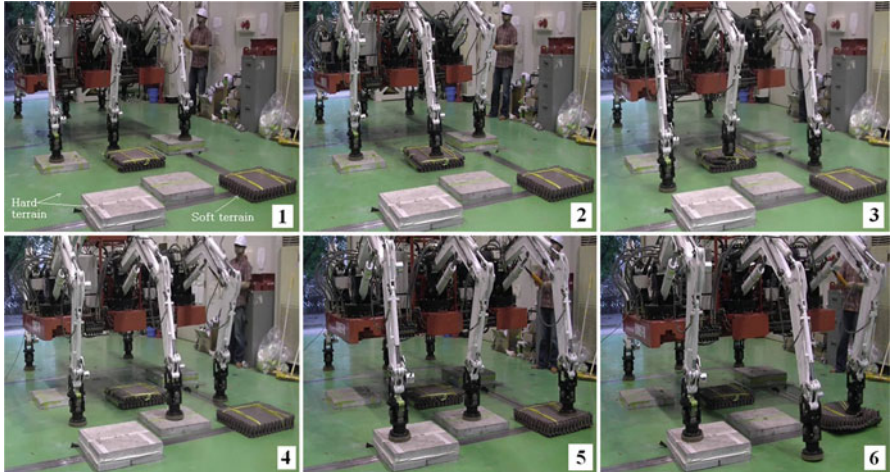


Fig. 6.14 Snapshots of fundamental test

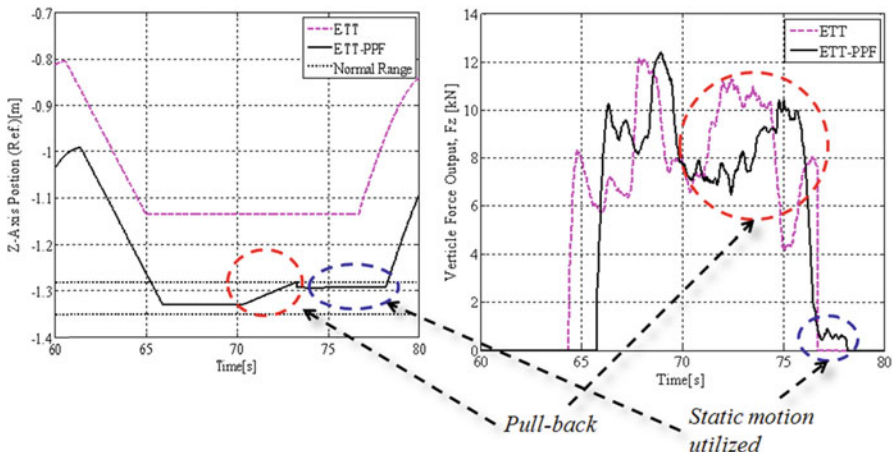


Fig. 6.15 Pull-back action by PPF controller in vertical force and z-axis foot point movement reference performance

on a linear slope during z -axis support phase signal and it affects F_{z_6} utilized during the foot placement. In this situation, the initial applied force of approximately 8 kN gradually increases to approximately 10 kN before reducing to nearly F_{TH} value at the start of the swing phase. At this instant the robot's body is slightly lowered, and also the support phase signal is reduced to static motion value ($S_{b,\min}$) as shown in Fig. 6.15. From the result it shows that statically compliance is performed on each of the robot's leg by controlling and eliminating the applied extra force when it steps into the unnecessary area.

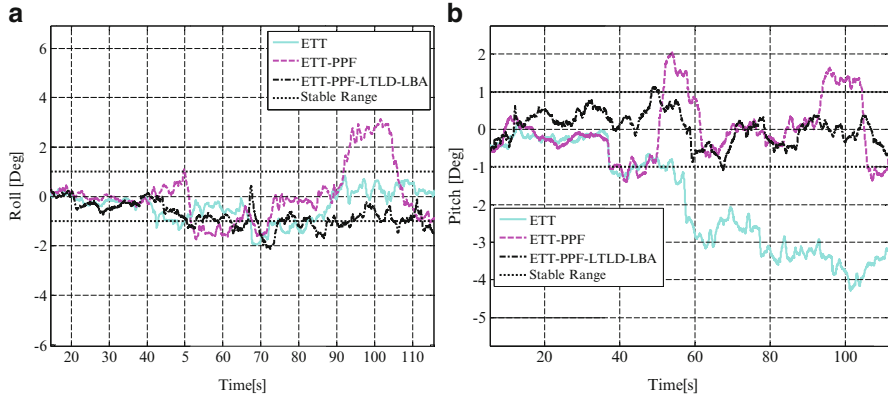


Fig. 6.16 Robot's body posture angles; (a) roll angle, (b) pitch angle

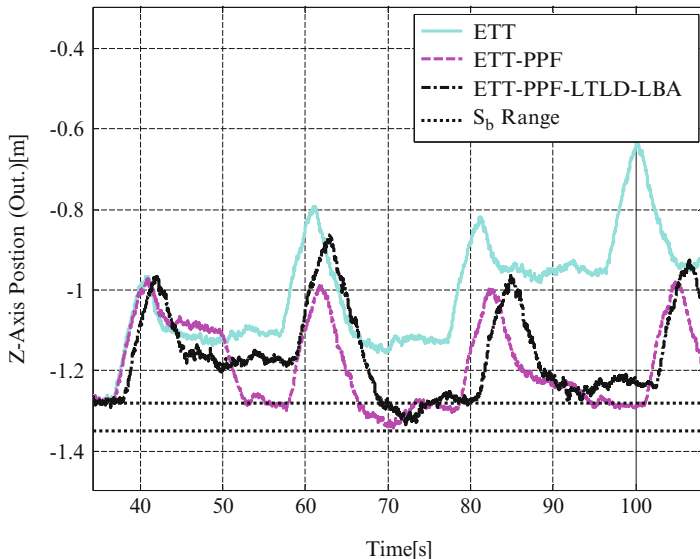


Fig. 6.17 Position of foot point on the z-axis (sample data of leg 3)

As shown in Fig. 6.16, for walking on rough terrain, the robot's body attitude is more stable when ETT module is used in conjunction with PPF controller with LTLD and LBA. If only ETT module is used, the robot walking on a rough terrain is unstable because the foot stepping point signal (based on SCS) increases linearly as shown in Fig. 6.17 and consequently proportionally causes the overall robot's body height to incline downward and causes role angle of the body twisted to negative rotation as shown in Fig. 6.16b. However, in COMET-IV walking with ETT-PPF test, the robot attitude performances are in stable range, but unnecessary *pull-back* action occurred when walking on high-level terrain as shown in Fig. 6.17, thus

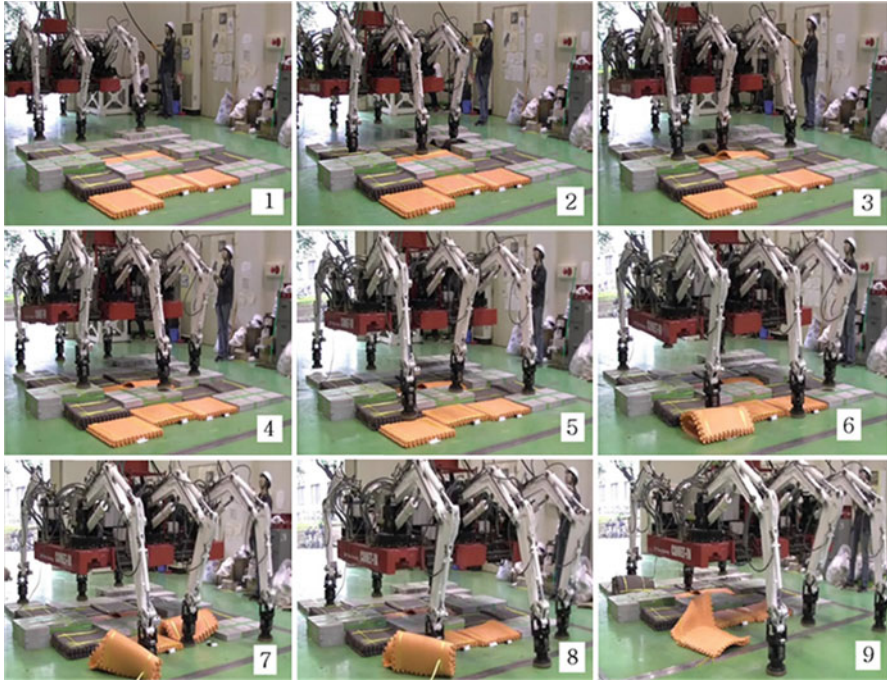


Fig. 6.18 Snapshots of COMET-IV operation during long-distance walking test

affecting the overall robot's body attitude as shown in Fig. 6.16. This means the recovery behavior is achieved with the use of the compliant controller in ensuring the horizontal stability of the robot. The stability is increased when DH_0 is added in the long-distance walking on the uneven and rough terrain as shown in Fig. 6.18.

COMET-IV with PPF-LTLD-LBA- DH_0 shows less inclination and swing in terms of body attitude with reference to the body attitude results as shown in Figs. 6.19 and 6.20, respectively. Moreover, the performance shows that PPF-LTLD-LBA with DH_0 , the probability of tracking the *necessary area*, is higher than PPF-LTLD-LBA without DH_0 .

As a summary, when COMET-IV walks on uneven and rough terrain, the proposed PPF controller with LTLD-LBA and DH_0 can stabilize the robot's motion in terms of force utilization control and body attitude stabilization although a shoulder of each leg is OFF (not moving). With the PPF controller making the switching decision, the combination of LTLD and LBA provides good compensation between the current event (during foot step) scenario and the previous event (during foot swing) in terms of body posture and leg vertical position. In addition, as noted in the results from the long-distance walking test, the PPF controller is more effective when supported with LTLD-LBA and is more sensitive when DH_0 is applied. In real field situations, COMET-IV will face not only rough terrain but also extremely soft terrain such as soft sandy soil or swampy ground. However, the

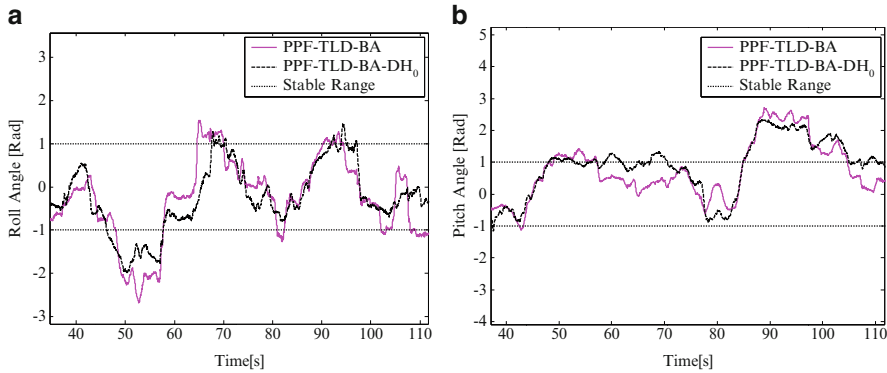


Fig. 6.19 Robot's body posture angles; (a) roll angle, (b) pitch angle

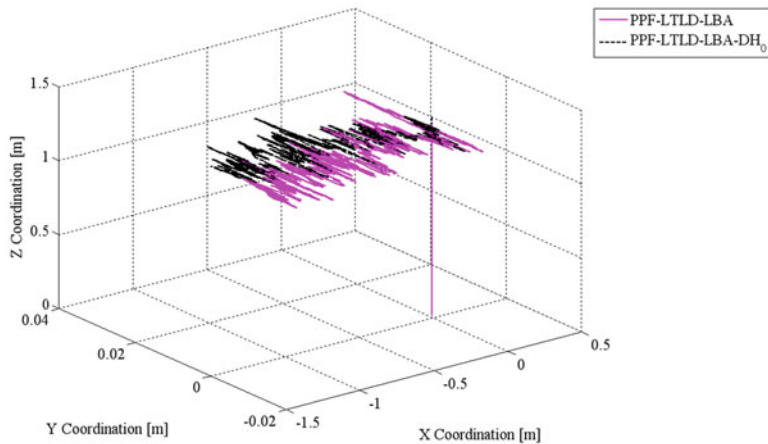


Fig. 6.20 Robot's BMC performance

soft terrain setup in this experiment cannot fully represent the natural extreme soft terrain. Therefore, the next section will focus on the robot fully walking on extremely soft terrain with the use of the proposed dynamic control.

6.2 Impedance Control for Hydraulically Driven Hexapod Robot

Based on the case studies discussed in previous sections, an active impedance control needs to be applied to the vertical motion of each leg of a hexapod robot when it is walking on soft terrain so that the *push-pull* motion [2] can be realized. With the specified number of DOF, COMET-IV is more flexible than other

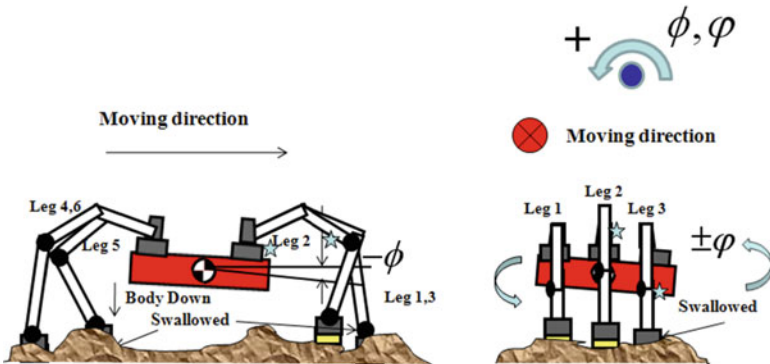


Fig. 6.21 Case study of a robot walking on extremely soft terrain

hydraulically driven robot systems discussed earlier making it possible to apply a dynamic control, such as impedance control, even though the leg configuration is $n = 6$. In this case, the motivation for implementing impedance control is to provide the aforementioned motion by taking the advantages of the flexibility of the robot's legs itself. Multi-legged robot research and development works such as Katharina [3], RHex [4], and OSU Hexapod [5] have proposed and applied some form of dynamic controls, including impedance control, to make a robot more adaptable with the actual ground, especially sandy soil, by taking advantages of the leg's flexibility.

6.2.1 Case Study: Hydraulically Driven Hexapod Robot Walking on Soft Terrain Issue

Large-scale dynamically changing environments and extremely soft terrain can make a heavy robot such as COMET-IV horizontally unstable especially when tripod walking pattern is applied. Increasing the number of support legs at a time may increase the stability but will cause decay in walking, especially for hydraulically driven and heavy robot such COMET-IV. Specifically, sandy soil, mud, wet sand, and peat—all of which are likely to be encountered in the target application area—are considered as soft terrain in this study. For uneven ground with soft surfaces, as shown in Fig. 6.21, COMET-IV needs to maintain a horizontally stable attitude for angles (roll (ϕ) and pitch (\emptyset)) in the range of $-1.5^\circ \ll [\phi, \emptyset] \ll 1.5^\circ$, with reference to the body coordinate system (BCS). In particular, to maintain a stable attitude when COMET-IV is walking on the soft ground, an extra angle of $\pm 6.5^\circ$ is added to the stable range for the robot walking on rough terrain. This estimated extra limit is added to the stable attitude range as the probability of the robot's leg suddenly dropping as it touches the soft ground is very high when the range specified for walking on a hard surface is used, and this problem will affect the attitude sensor (sensitivity).

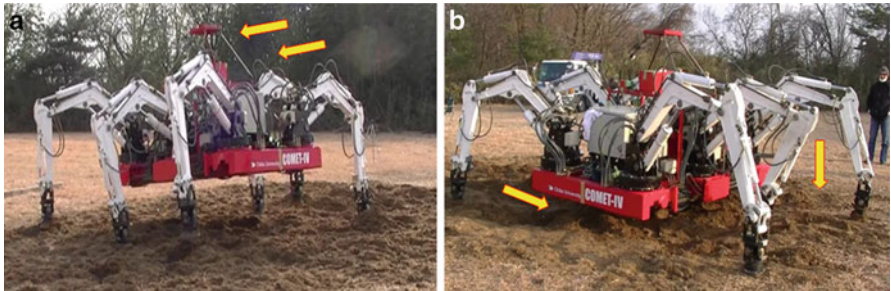


Fig. 6.22 A horizontally unstable robot body: (a) rotationally unstable, (b) horizontally unstable (foot sunk into the ground)

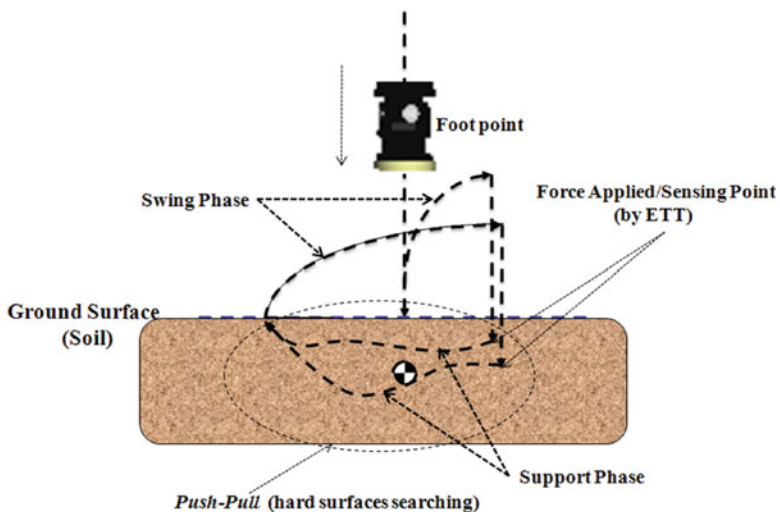
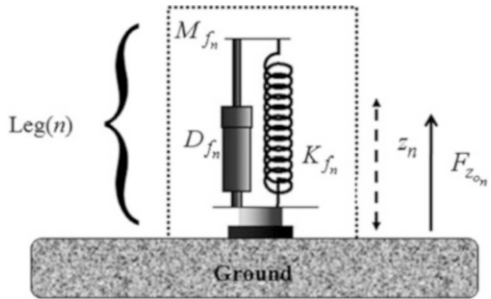


Fig. 6.23 Ideal desired motion of the robot's foot equipped with a *push–pull motion*

Overlimitations on the legs' motion are highly possible in the situation shown in Fig. 6.22. These incidents could result in the damage of the angle shaft or at least to the coupler between the potentiometer and joint shaft of the leg; ultimately, such damage would interrupt command execution. The robot's foot can sink into the ground when the robot is walking on extremely soft terrain. Consequently, with every step, the robot's body will fall toward the ground as can be clearly seen in Fig. 6.22b. Moreover, this “fallen” case is due to the force redundancies factor that reacted downward inclination when the robot is walking on the soft terrain. Thus, a dynamic control system needs to be designed in order to address this problem, such as the proposed dynamic *push–pull motion* to each foot (on the support phase period), as shown in Fig. 6.23. This dynamic motion will ensure that each leg will always be on a sufficiently hard surface of the soft ground during the entire

Fig. 6.24 Equivalent elastic model for the vertical motion of a robot's leg



period in which the robot is walking. Moreover, it could stabilize the robot's body since no major surface changes will be felt after the robot's foot steps on a relatively hard surface of the soft ground.

6.2.2 Impedance Control Schemes for Hexapod Robot

Hexapod robot generally is statically stable in legged robot stability principle and static control type is more preferable for this legged robot configuration. However, predetermination mechanisms and formulations is difficult for legged robot to perform desired stable walking in the actual practice through unknown environment. Therefore, particular dynamic control with compliant method needs to be done for hexapod robot to ensure the overall walking stability and avoid overturning attribute from over dynamic signal. In this section, impedance control design and implementation for hexapod robot is introduced with two different schemes named single-leg impedance control and center of mass-based impedance control [2]. For the design of the single-leg impedance controller, the vertical force acting on an individual leg is considered and represented as a combination of vertical motion and reaction. The impedance model for the interaction between the robot's leg and the ground can be defined as an equivalent elastic model, as shown in Fig. 6.24.

In Fig. 6.24, $n = 1, \dots, 6$, and the filtered vertical force on the foot ($F_{z_{0n}}$) is as described in Sect. 4.5. Thus, the impedance equilibrium (at real time (t) and sampling time $T_s = 10$ ms) for each of the robot's legs can be expressed as follows:

$$-F_{z_{0n}}(t) = M_{f_n} \ddot{z}_n(t) + D_{f_n} \dot{z}_n(t) + K_{f_n} z_n(t) \quad (6.10)$$

where z_n denotes the virtual vertical position for each leg. The M_f value for each leg is chosen to be a constant value of 16.66 kg with reference to each leg's actual weight and the total weight of the robot's body ($\cong 3$ tons), since the leg stiffness gain (K_f) plays a major role in the impedance output (the robot's leg moves very slowly ($\ddot{z}_n \cong 0$)). On the other hand, the damping or viscosity coefficient (D_f) is

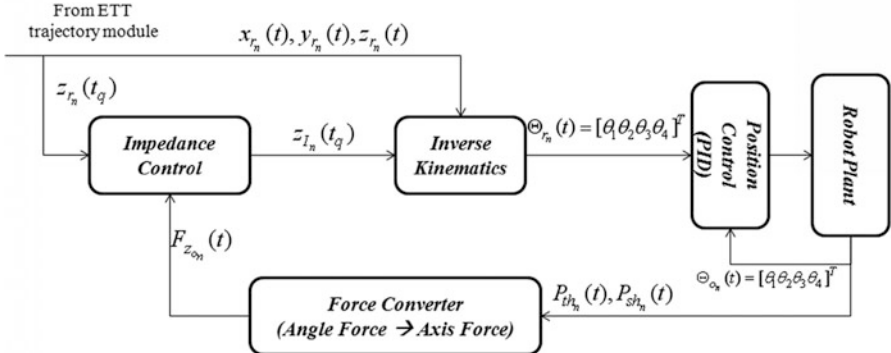


Fig. 6.25 Implementation of single-leg impedance control on the hydraulically driven hexapod robot

determined based on the vibration theory for spring–mass dampers by rearranging Eq. (6.10) using Newton’s law, as follows:

$$\ddot{z}_n + \left(\frac{D_{f_n}}{M_{f_n}} \right) \dot{z}_n + \left(\frac{K_{f_n}}{M_{f_n}} \right) z_n = 0$$

Ultimately, the natural frequency and damping ratio for the impedance model can be written as follows:

$$\omega_0 = \sqrt{\frac{K_f}{M_f}}, \zeta = \frac{D_f}{2\sqrt{M_f K_f}}$$

In order to control the oscillation in the control input, critical damping (free vibration with damping) is chosen, where $\zeta = 1$. Thus, D_f for the controller can be expressed as follows:

$$D_{f_n} = 2\sqrt{K_{f_n} M_{f_n}} \quad (6.11)$$

Thus, new z -axis motion with impedance control for each leg (Z_{l_n}) during the support phase period (t_q) can be determined as follows:

$$z_{l_n}(t_q) = z_{r_n}(t_q) + z_n(t) \quad (6.12)$$

where z_{r_n} is a reference for the z -axis motion of leg- n . A schematic overview of the single-leg impedance control developed for the hydraulically driven hexapod robot is shown in Fig. 6.25. $P_{th_n}(t)$ and $P_{sh_n}(t)$ are feedback pressure readings for the cylinder actuator of the thigh and shank, respectively, for leg- n .

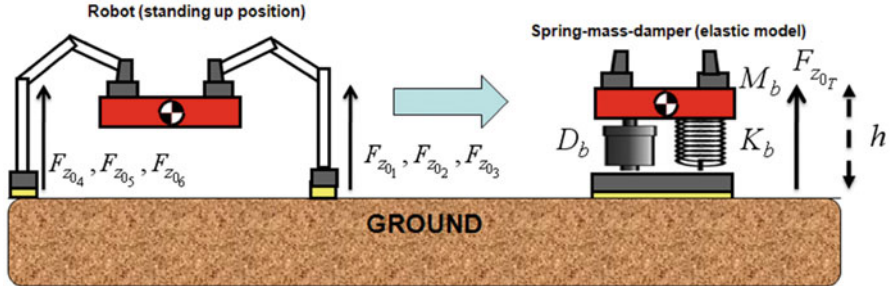


Fig. 6.26 Equivalent elastic model of the robot's body

Table 6.4 Calculation of the total vertical force based on the tripod walking pattern

Status	Supported legs	$F_{z_{0T}}$
Walk	1, 3, 5	$F_{z_{0T}} = F_{z_{0,1}} + F_{z_{0,3}} + F_{z_{0,5}}$
Walk	2, 4, 6	$F_{z_{0T}} = F_{z_{0,2}} + F_{z_{0,4}} + F_{z_{0,6}}$
Transient	All	$F_{z_{0T}} = \sum_{n=1}^6 F_{z_{0,n}}$

It is different for center of mass-based impedance control principle. Like walking on soft terrain, regular walking with hard stiffness (legs) creates an unstable orientation of the body's attitude and contributes to critical changes in the overall average height of robot's body. According to the force redundancies cases discussed in Sect. 6.1.1, changes of average body height are due to the changes of foot stepping motion. These results indicate the need to derive another form of impedance model that is based on the body height performance in terms of total forces acting on the support legs, as shown in Fig. 6.26. Thus, with reference to Fig. 6.26, impedance equilibrium can be written as follows:

$$\ddot{F}_{z_{0T}}(t) = M_b \ddot{h}(t) + D_b \dot{h}(t) + K_b h(t) \quad (6.13)$$

where $M_b = 224$ kg is the actual mass (weight) of the robot and D_b is the total damping, which is determined using the same approach as is used for single-leg impedance control. K_b is the total stiffness of the body from the shoulder to the ground (total stiffness of supported legs); this is a positive tuning parameter. $F_{z_{0T}}$ is the total vertical force acting on the legs touching the ground, and it is calculated based on the tripod walking pattern shown in Table 6.4.

Furthermore, the virtual vertical position of the robot's body height (h) (impedance output) from Eq. (6.13) is divided equally (based on COMET-IV configurations and force delivery on the foot for each leg) to each one of the robot's legs and is expressed as follows:

$$h_n(t_q) = \begin{cases} \frac{h(t)}{3}; & \text{Leg 1, 3, 4, 6} \\ \frac{2h(t)}{3}; & \text{Leg 2, 5} \end{cases} \quad (6.14)$$

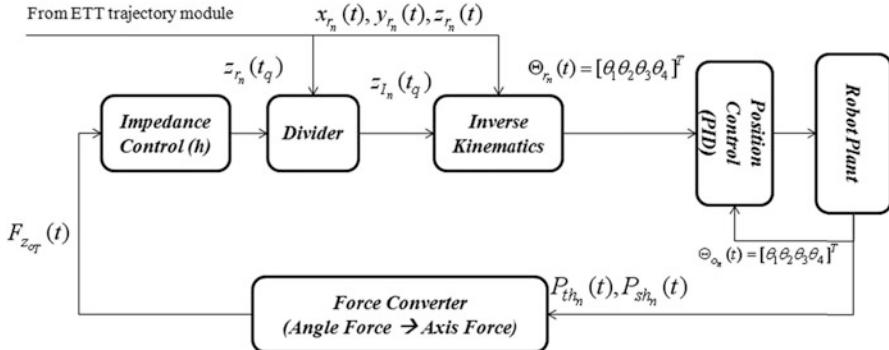


Fig. 6.27 Implementation of the proposed center of mass-based impedance control on the hydraulically driven hexapod robot

Thus, the new z -axis position reference for each leg at t_q can be written as follows:

$$z_{l_n}(t_q) = z_{r_n}(t_q) + h_n(t_q) \quad (6.15)$$

The proposed center of mass-based impedance control is described by the schematic diagram of Fig. 6.27.

For statically stable legged robot with linear actuator such as COMET-IV, impedance control is not enough on giving compliant and stable walking. Therefore the proposed design of compliant switching mechanism discussed in Sect. 6.1.2 is reused and customized for both schemes of impedance controller. By changing the *ON Pull-back to Reset* and *OFF Pull-back to No Reset*, the implementation is carried out in accordance with Fig. 6.28.

There is an impedance signal during action periods when the robot's legs are near or on the COG. Furthermore, T_{ch} , K_s , t_{le} , and t_{ls} are used to determine the appropriate instant for applying the impedance controller and resetting its action. Figure 6.29 shows sample data from a fundamental experiment that verified this mechanism's action for use in impedance control.

6.2.3 Experiment and Verification

The experiment is conducted almost same as discussed in Sect. 6.2.3 but the setup environment is less rough surface and material as shown in Fig. 6.30.¹

¹ The crane shown in this figure is just for backup and safety purposes in the laboratory (it is not attached to the robot body). It is handled by a licensed student.

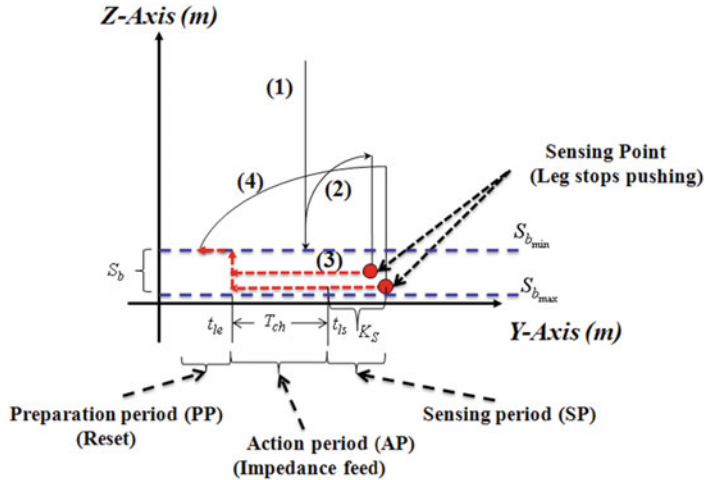


Fig. 6.28 Proposed cluster and time tuning for the implementation of the proposed impedance controller on hydraulically driven hexapod robot, together with the compliant switching mechanism

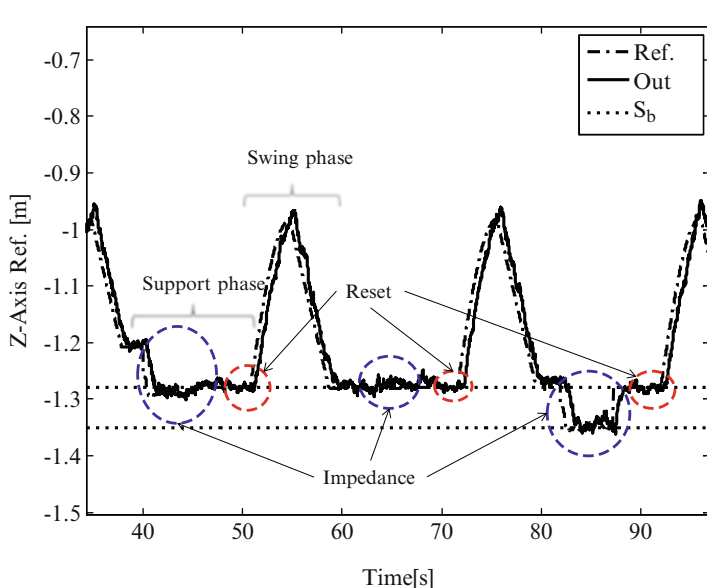


Fig. 6.29 Experimental results for motion along the z -axis (sample data for leg 1 motion)

An artificial major soft terrain area (representing actual soft ground) is set up in the laboratory with three layers of $4.2 \times 2.98 \times 0.02$ m rubber plate to represent the base of soft ground with randomly placed bricks (maximum density: 0.2 m/brick) and multiple rubber pads placed one on top of the other. The walking experiments

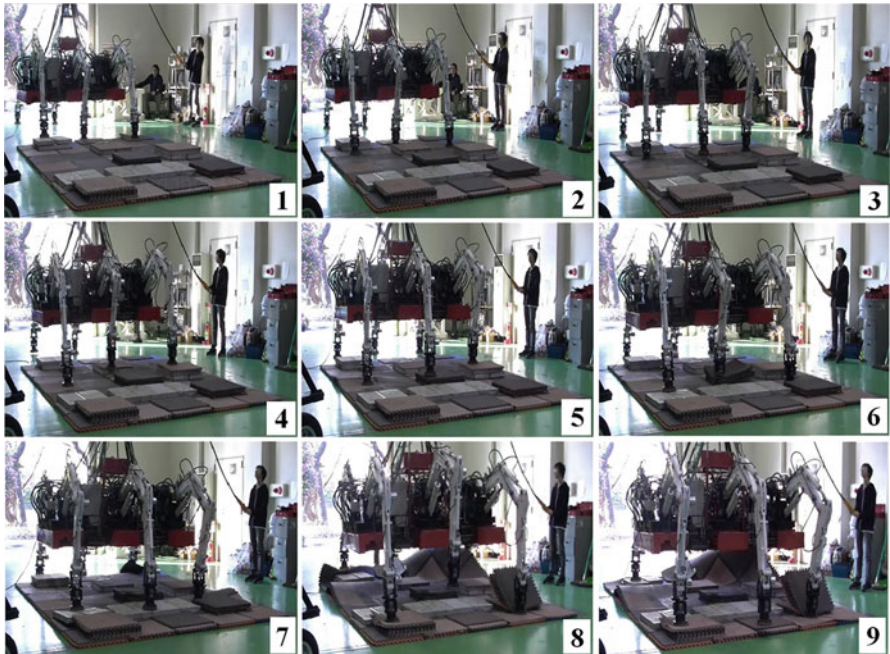


Fig. 6.30 Laboratory test setup (snapshots of COMET-IV in operation)

were performed three times (right to left side walking) using three different methods: the PPF–LTLD–LBA with DH_0 (PPF), the single-leg impedance control (LImp), and mass-based impedance control (MImp). As shown in Fig. 6.31, changes in the foot placement signal attributed to impedance cause the vertical force feedback to increase and decrease. This means that a reverse/forward force is applied at the foot closest to the center of gravity in order to stabilize the robot's body and help it to adapt to the environment. Furthermore, this behavior suited with the proposed compliant walking mechanism on giving stable stepping control although robot is walking on almost flat and soft surface as shown in vertical leg foot motion in Fig. 6.32.

According to the overall stability performances as shown in Figs. 6.33 and 6.34, robot walking/operating with both LImp and MImp performed stable walking (in stable range) if compared to robot walking/operating with PPF. In this situation, LImp performed better results if compared to other methods whereby robot's roll and pitch posture angles are major in setup stable range as shown in Fig. 6.33. The instability of robot walking/operating with PPF on the soft surface can be seen clearly in BCM plot as shown in Fig. 6.34 whereby the robot's body is inclining down on each every step of walking.

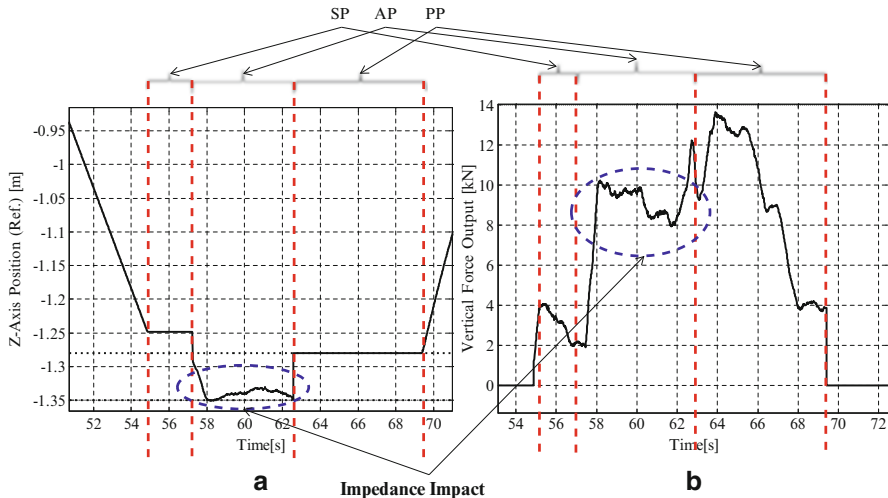


Fig. 6.31 Push–pull motion caused by the proposed impedance controller: (a) foot point motion along the z -axis foot point, (b) $F_{z_o}(t)$ performance (experimental results for leg 2)

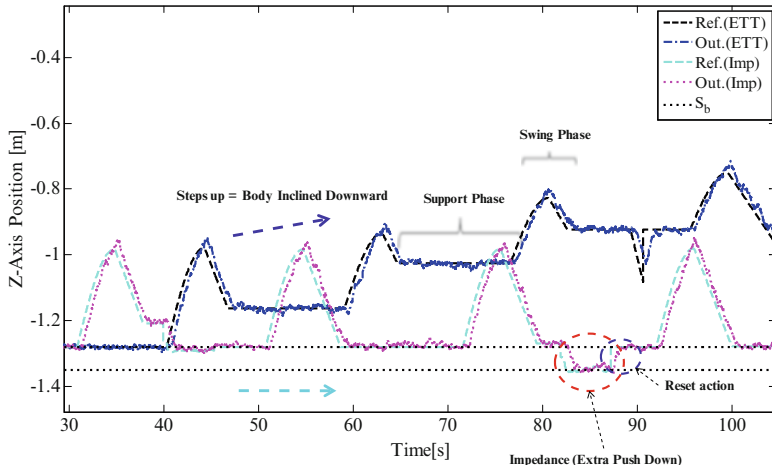


Fig. 6.32 Impact of Impedance control on giving stable position of the foot point on the z -axis with support of compliant switching mechanism (experimental results for leg 2)

Therefore, it can be concluded that the implementation of proposed impedance control schemes combined with a compliant control mechanism and an ETT walking module is suitable for COMET-IV system and configuration. In addition, LImp performed better results although a bit difficult on tuning process if compare

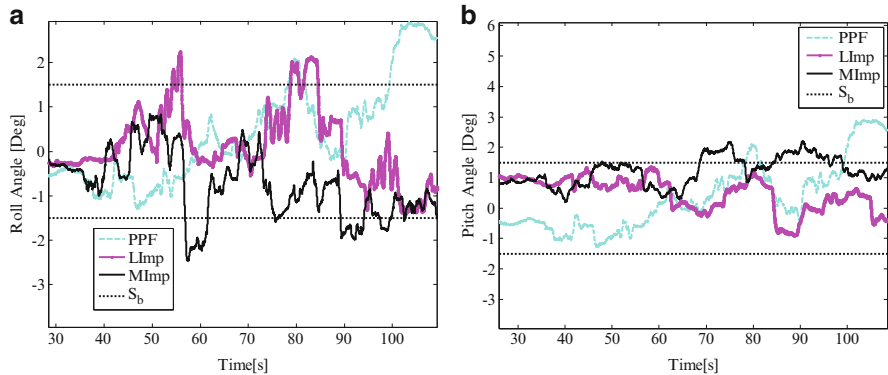


Fig. 6.33 Robot's body posture angles; (a) roll angle, (b) pitch angle

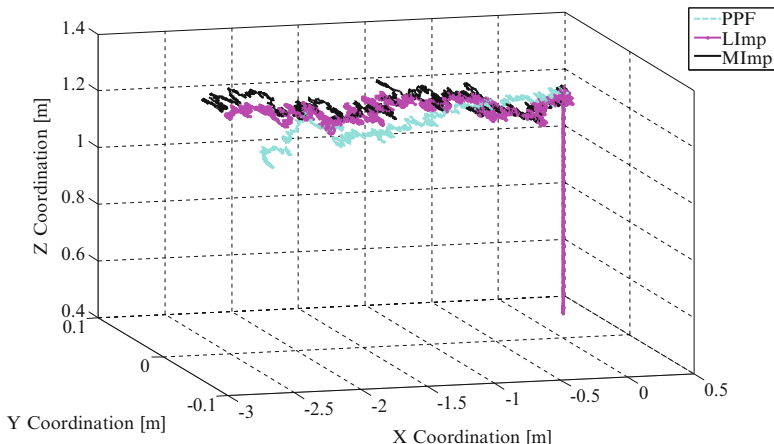


Fig. 6.34 Robot's BMC performance

to the MImp. However, both schemes have potential to be improved and optimized by using the robot's attitude criteria. The adaptive approach on both impedance control scheme is discussed in the next chapter.

References

- Irawan A, Nonami K (2011) Compliant walking control for hydraulic driven hexapod robot on rough terrain. *J Robotics Mechatronics* 23(1):149–162
- Irawan A, Nonami K (2011) Optimal impedance control based on body inertia for a hydraulically driven hexapod robot walking on uneven and extremely soft terrain. *J Field Robotics* 28 (5):690–713

3. Schneider A, Schmucker U (2006) Force sensing for multi-legged walking robots: theory and experiments part 2: force control of legged vehicles. In: Buchli J (ed) Mobile robotics, moving intelligence, IntechOpen
4. Altendorfer R, Koditschek DE, Holmes P (2004) Stability analysis of a clock-driven rigid SLIP model for RHex. *Int J Robotics Res* 23(10):1001–1012
5. Klein CA, Olson KW, Pugh DR (1983) Reliable, use of force and attitude sensors for locomotion of a legged vehicle over irregular terrain. *Int J Robotics Res* 22(1):3–17

Chapter 7

Impedance Control and Its Adaptive for Hexapod Robot

Abstract Impedance control should be generally applied for most robot when contacts some environment to achieve “softness of contact” between the end-effector of robot and the environment. This chapter proposes several algorithms such as impedance control implementation for hexapod robot COMET-IV. Also, in the case of heavyweight and large-scale-structured robot, inclinometers from attitude angles should be designed to control the long-term attitudes of the body, not to prevent shaking caused by changes in support of the legs. Moreover, this shaking is considered as a natural scenario since the robot is using hydraulic system and automotive engine. Therefore, only attitude errors that are over the acceptable limit will be included in the adaptive calculation.

7.1 Optimization of Impedance Control Using Virtual Forces from the Body’s Moment of Inertia

Impedance model has potential to be improved in according to three parts in its model, controller input part (force feedback), controller output part (current impedance value), and its parameters value as shown in Fig. 7.1. Therefore, for COMET-IV system, optimization has been designed on those mentioned parts based on the robot body posture angles or attitude, instead of using environmental characteristic as done in [1, 2]. Lehtinen has summarized that for the large-scale robot with hexapod configuration, attitude feedback can be used as a torque correction on each leg from the calculation of attitude error that has been filtered by particular dead zone [3]. This is similar to the stable range of posture angle for walking on extremely soft terrain that has been defined and discussed previously in Sect. 6.2.

For this adaptive type, inclinometers are derived from moment of inertia of the robot’s body with optimization from Linear Quadratic Regulator (LQR) to correct the impedance control input (for single-leg impedance control) and output (center of mass-based impedance control) directly [4]. As discussed in Sect. 7.4.1, unstable walking on extremely soft terrain contributes to the body swing, which in turn

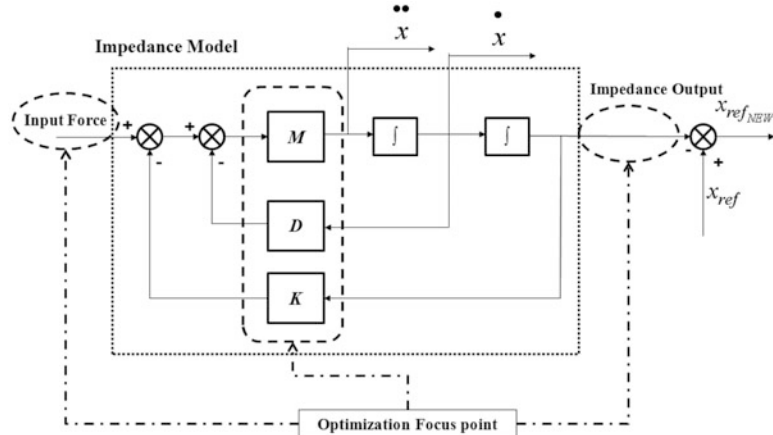


Fig. 7.1 Basic impedance model and command optimization focus points

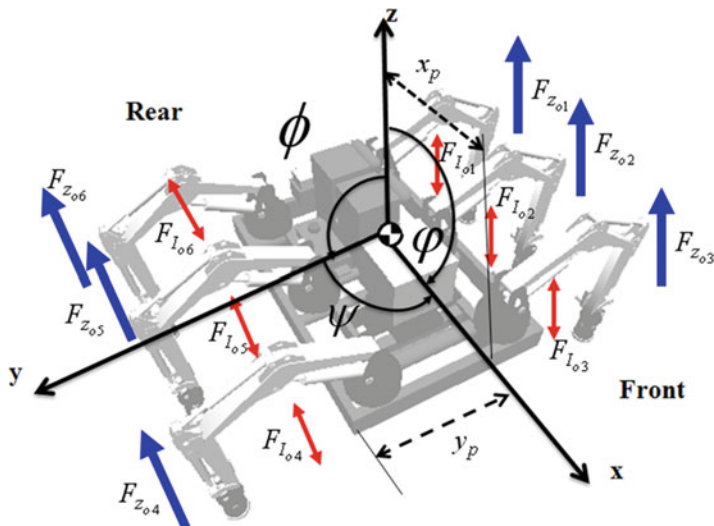


Fig. 7.2 The vertical forces acting on each leg and Euler angles (right hand rotation) along the particular axis based on the BCS (COMET-IV System)

affects the body posture angles or attitude: roll(φ) and pitch(\emptyset) as well as yaw(Ψ). However, the scope of impedance control described in this study will not be covered for Ψ case since it has been considered in navigation-based walking control in vision-based [5] and teleoperation research studies for COMET-IV [6]. Therefore, in order to include both rotational angles, φ and \emptyset , in the control system, it is necessary to derive a virtual force (two-way arrows) for each leg from the moment of inertia acting on the robot's body as shown in Fig. 7.2. The moment of inertia of

the robot's body can be calculated from the real-time (t) changes of robot posture angles ($\varphi(t)$ and $\dot{\varphi}(t)$) and center of mass during walking phases. It is different to the vertical force defined in Chap. 4 which is specifically derived from the torques for each leg's links and hydraulic's cylinder pressures attached to the thigh and shank on each leg as described in Chap. 4.

Let's consider the robot in the moving phase. The equilibrium of the moment of inertia is written as follows:

$$\begin{aligned} M_b \ddot{B}(t) &= F_{I_a} + F_{I_b} + F_{I_c} \\ I_r \ddot{\varphi}(t) &= x_a(t)F_{I_a} + x_b(t)F_{I_b} + x_c(t)F_{I_c} \\ I_p \ddot{\phi}(t) &= y_a(t)F_{I_a} + y_b(t)F_{I_b} + y_c(t)F_{I_c} \end{aligned} \quad (7.1)$$

where $I_r = 1015.7 \text{ kg m}^2$ and $I_p = 457.3 \text{ kg m}^2$ are the moments of inertia acting on the robot's body (solid cuboids). These values correspond to the actual structural dimensions of COMET-IV [7]. From the values of the robot body's moment of inertia values (according to φ and ϕ), the body's rotational angles, and center of mass error ($B(t)$), the virtual force acting on each leg ($F_{I_n}(t)$) can be determined by rewriting Eq. (7.7) in the state-space model, as follows:

where $\dot{x} = [B \quad \varphi \quad \phi \quad \dot{B} \quad \dot{\varphi} \quad \dot{\phi}]^T$ with

$$A = \begin{bmatrix} 0 & 0 & 0 & 1 & 0 & 0 \\ 0 & 0 & 0 & 0 & 1 & 0 \\ 0 & 0 & 0 & 0 & 0 & 1 \\ 0 & 0 & 0 & 0 & 0 & 0 \\ 0 & 0 & 0 & 0 & 0 & 0 \\ 0 & 0 & 0 & 0 & 0 & 0 \end{bmatrix}, \quad B = \begin{bmatrix} 0 & 0 & 0 \\ 0 & 0 & 0 \\ 0 & 0 & 0 \\ M_b^{-1} & M_b^{-1} & M_b^{-1} \\ x_a(t)/I_r & x_b(t)/I_r & x_c(t)/I_r \\ y_a(t)/I_p & y_b(t)/I_p & y_c(t)/I_p \end{bmatrix} \quad (7.2)$$

The derived virtual force or force corrector for each support leg can be considered as a control input $u_f(t) = [F_{I_a}(t) \quad F_{I_b}(t) \quad F_{I_c}(t)]^T$. Subsequently, taking into consideration the actual system configuration, state feedback law of LQR control [8] is used to optimize the virtual forces from robot body's moment of inertia as follows:

$$u_f(t) = -K_l x(t) \quad (7.3)$$

in order to minimize the quadratic cost function as follows:

$$J = \int_0^\infty [x(t)^T Q x(t) + u_f(t)^T R u_f(t)] dt \quad (7.4)$$

where K_l ($l = 1, 2, 3$) is the gain derived from the solution of algebraic Riccati's equation (S) as subject to the Eq. (7.8) as follows:

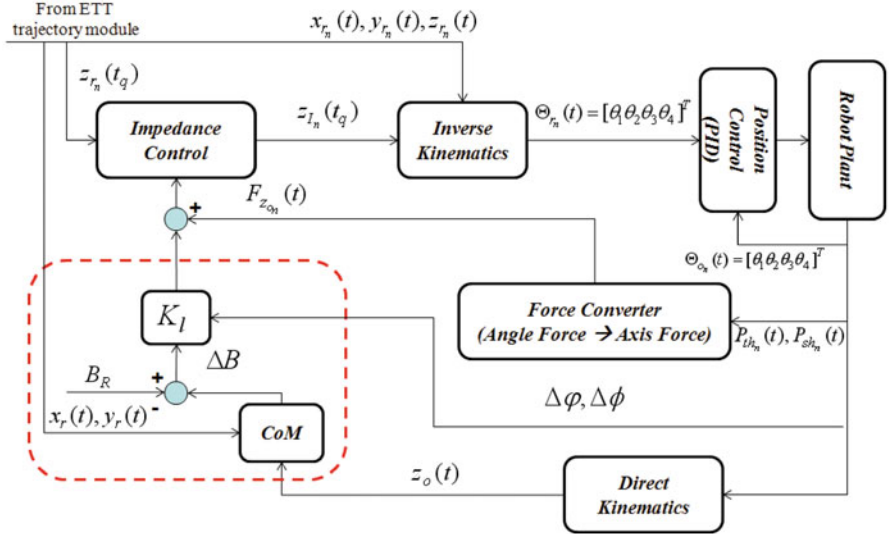


Fig. 7.3 Proposed optimal control (inside the *dotted line box*) for single-leg impedance

$$\begin{aligned} A^T S + S A - S B R^{-1} B^T S + Q &= 0 \\ \rightarrow K_l &= R^{-1} B^T S \end{aligned} \quad (7.5)$$

Thus, in single-leg impedance control, optimization is performed via control input, as follows:

$$-(u_f(t) + F_{z_n}(t)) = M_f \ddot{z}_n(t) + D_f \dot{z}_n(t) + K_f z_n(t) \quad (7.6)$$

where the impedance control for each leg (u_{I_n}) is proportional not only to F_{z_n} but also to the difference of F_{I_n} . This method is done in order to accumulate all forces acting on each leg and filtered indirectly via impedance model individually. The target on the output of the impedance control for each leg is to have an optimal virtual position of z-axis from the feedback responses of F_{z_n} and F_{I_n} . Figure 7.3 shows a flowchart of the proposed optimal control (inside the dotted line column) that has been adapted for single-leg impedance control. F_{I_n} is directly correcting F_{z_n} only during touching period (t_q). A different approach was followed for the center of mass-based impedance control, as shown in Fig. 7.4, in which LQR is applied on the control output, as follows:

$$z_{I_n}(t_q) = Z_{r_n}(t_q) + h_n(t_q) + \alpha_n u_{f_n}(t_q) \quad (7.7)$$

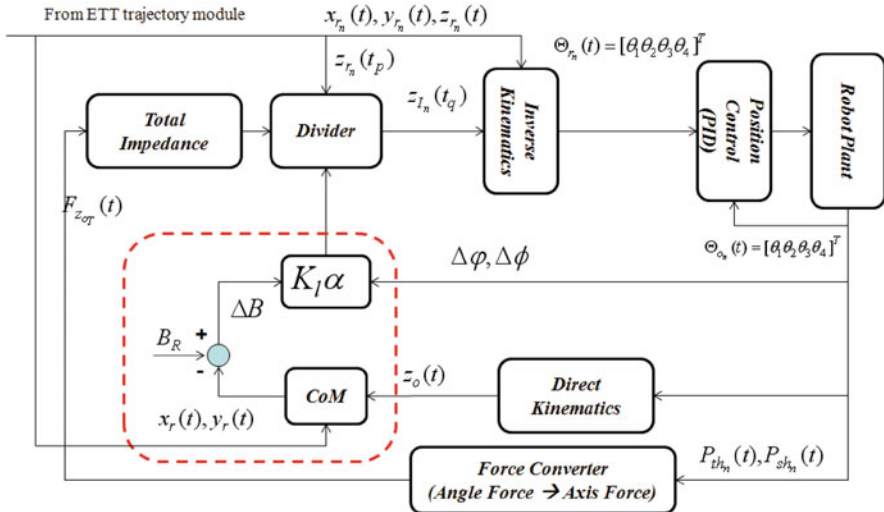


Fig. 7.4 Proposed optimal control (in the *dotted line box*) for center of mass-based impedance control

where α is the compensator gain for the control input that depends on the ratio of static stand-up height to static force (since the optimal control input is in Newton) and is written as follows:

$$\alpha = \frac{S_h}{F_{TH}} \beta \quad (7.8)$$

where $S_h = 0.78$ m is the initial setup value for the standing height of the robot, which is based on SCS, and β is the positive tuning gain or compensator. This approach will directly change the impedance output of the center of mass-based impedance control by creating a tunable inverse stiffness for virtual force on each leg in parallel as shown in Eq. (7.13). The target is to get the fast response from the robot body's posture angles (error) on changing the virtual position of z-axis instead of accumulating F_{z_n} and F_{I_n} .

7.1.1 Experiment and Verification

As for verification purposes, the experiment is done on the actual wide field area as shown in Fig. 7.5. After several tests in laboratory, optimal single-leg impedance control (LAImp) and optimal center of mass-based impedance control (MAImp) is extended for further experiment on the actual wide field due to its performances and safety consideration. Furthermore, in this experiment, LAImp and MAImp is compared with the proposed PPF controller with LTLD-LBA and DH_0 discussed

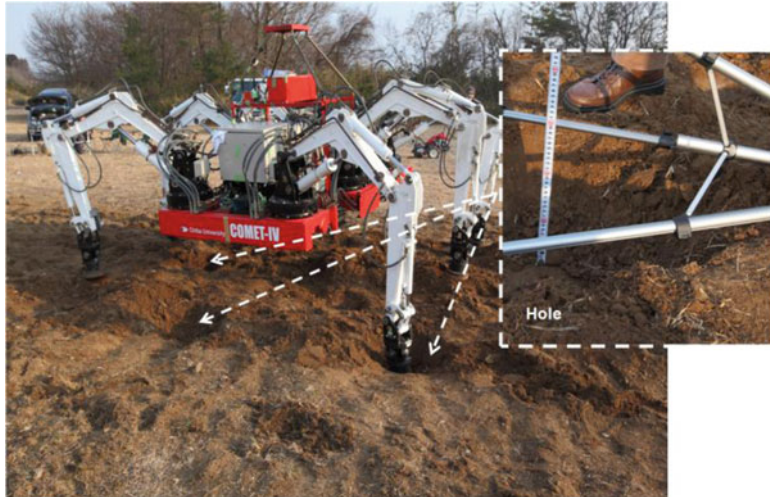


Fig. 7.5 Field test setup

in Chap. 6. As shown in Fig. 7.5, the field test area comprised of 10×10 m of relatively rough and uneven terrain with extremely soft surfaces, cliffs with a maximum height of 20 cm, and holes with a maximum depth of 30 cm. The walking experiments were repeated three times (walking from right to left) using three different control schemes, namely, the PPF controller (PPF-LTLD-LBA-DH₀), LAImp, and MAImp, as shown in Fig. 7.6.

According to the laboratory tests, the difference in control output/input are observed between proposed impedance with and without its adaptive as shown in Figs. 7.7, 7.8, and 7.9. When compared to LImp, LAImp exhibits obvious differences in the amplitude of z_n that is observed for different walking modes (Fig. 7.7a). These differences are related to the force feedback of the controller, as shown in Fig. 7.7. The same behavior is observed in the case of MImp and MAImp, shown in Fig. 7.7b, where the impedance control input u_{f_n} affects the motion along the z -axis (support phase) via impedance output h_n corresponding to the body height, as shown in Fig. 7.9.

The effect of these improvements obviously can be seen during the walking tests as shown in Fig. 7.6. There is a significant difference in the attitude performance of the robot when it is walking under optimal impedance control and when it is walking under PPF control, as shown in Figs. 7.10, 7.11, 7.12, and 7.13. Based on the overall field performance, the PPF controller experiences difficulty in helping the robot to regain its stability when the controller is combined with the compliant switching mechanism and the ETT.

As a consequence, body height is reduced and swinging is observed, even when the robot is walking only for a relatively short distance as shown in Fig. 7.10. The robot was stopped after operating for 150 s for safety reasons. This same behavior was observed when the robot was walking only with ETT module. MAImp

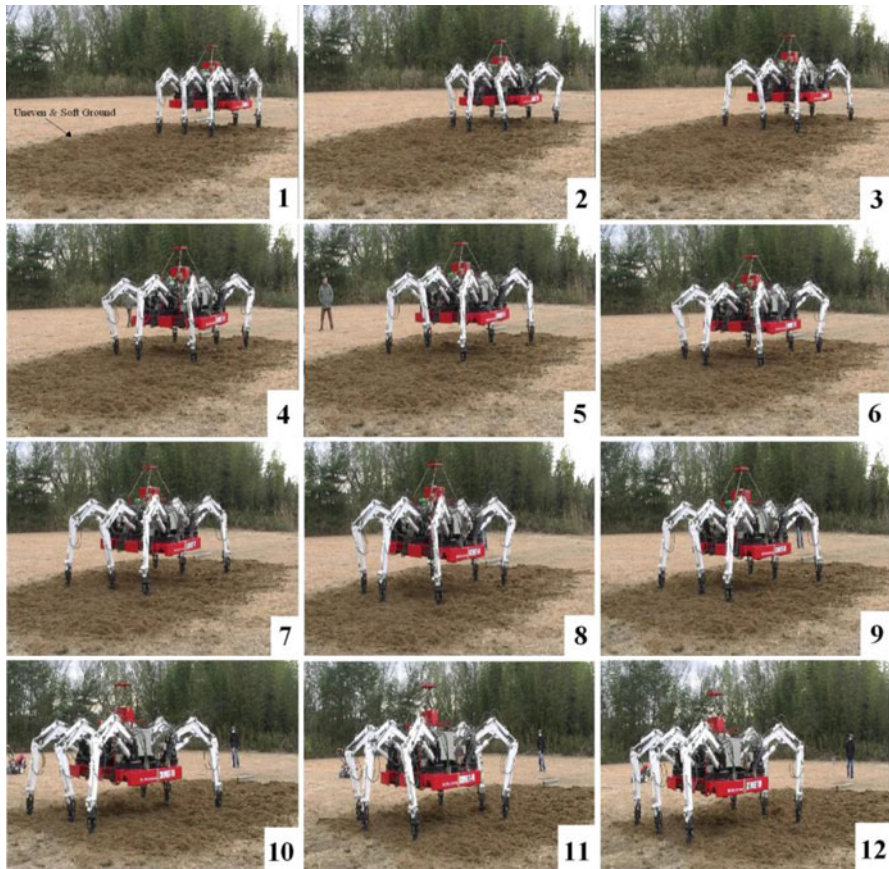


Fig. 7.6 Snapshots of COMET-IV in operation during the field tests

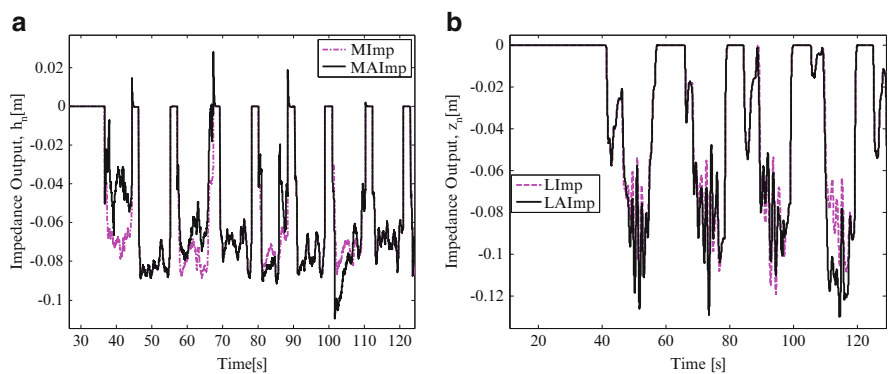


Fig. 7.7 Experiment result for impedance control outputs (sample of Leg 1); **(a)** LImp versus LAImp, **(b)** MImp versus MAImp

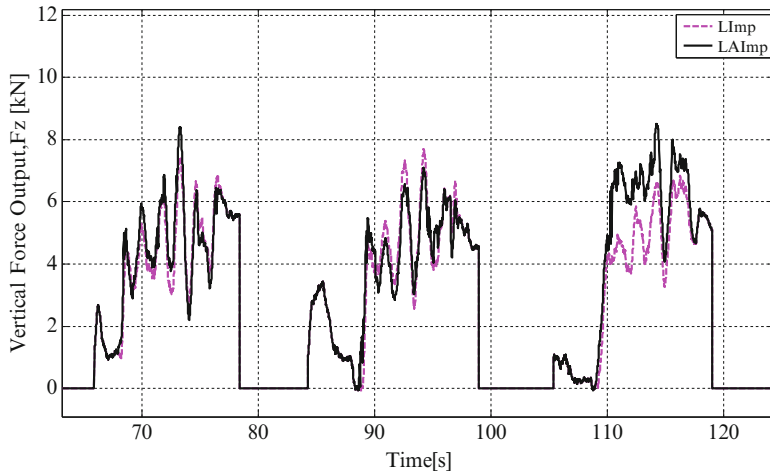


Fig. 7.8 The difference between $F_{z_o}(t)$ with optimal control and without optimal control for LImp (sample data of leg 1)

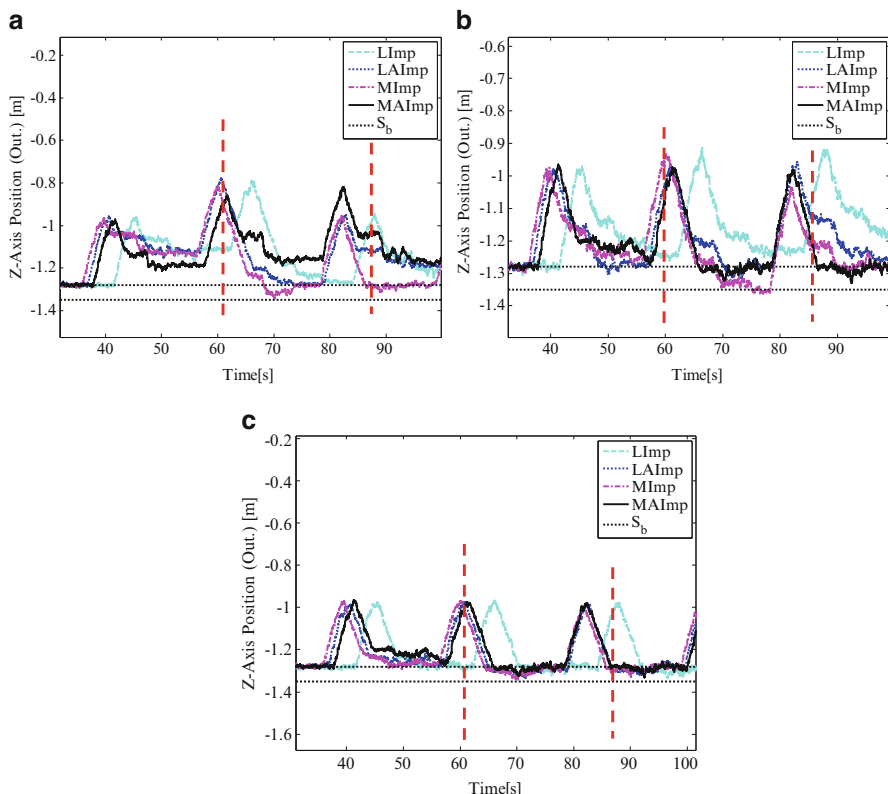


Fig. 7.9 Position of the foot point on the z-axis: (a) leg 1, (b) leg 3, and (c) leg 5

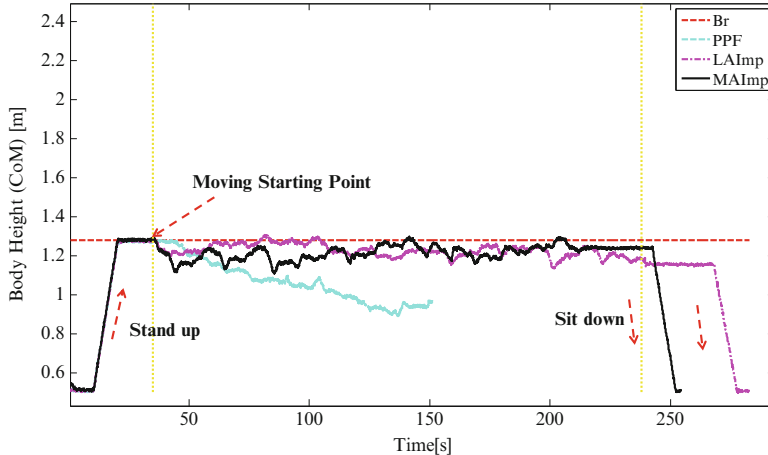


Fig. 7.10 Robot's body height output performance

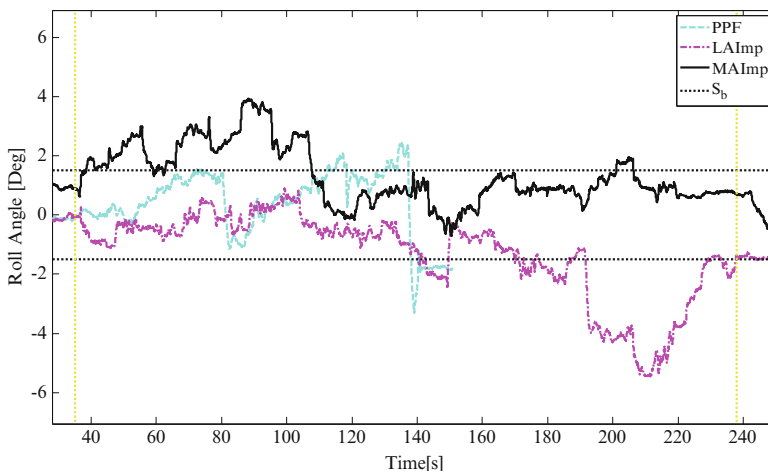


Fig. 7.11 Roll angle of the robot's body

outperformed LAImp in this field test, as can be clearly seen in the robot's body rotational feedback, as shown in Figs. 7.11 and 7.12. Between the start point and end point of walking (vertical dotted line), MAImp was successful in helping the robot to recover its initial position, and it performed faster than LAImp. This pattern can be observed in the rotational angles shown in Figs. 7.11 and 7.12. With respect to the average body height—which is defined by the center of mass, as shown in Fig. 7.10—MAImp performs slightly better than LAImp when it comes to the robot recovering its body height until the end of walking (when it sits down). With respect to the BMC point, both MAImp and LAImp allowed the robot to recover after

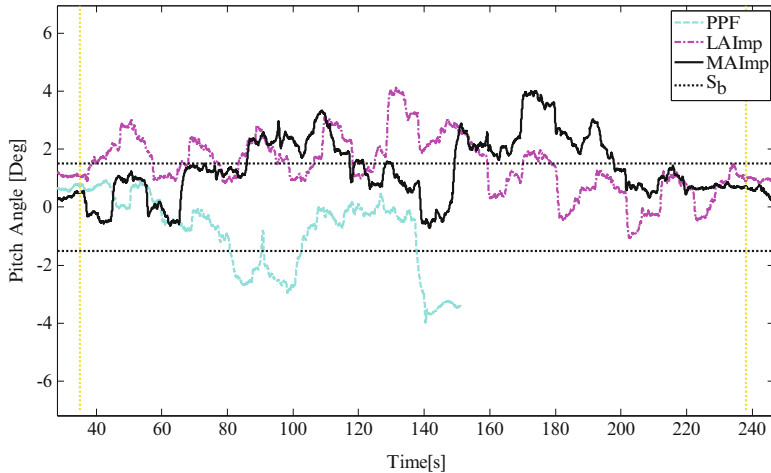


Fig. 7.12 Pitch angle of the robot's body

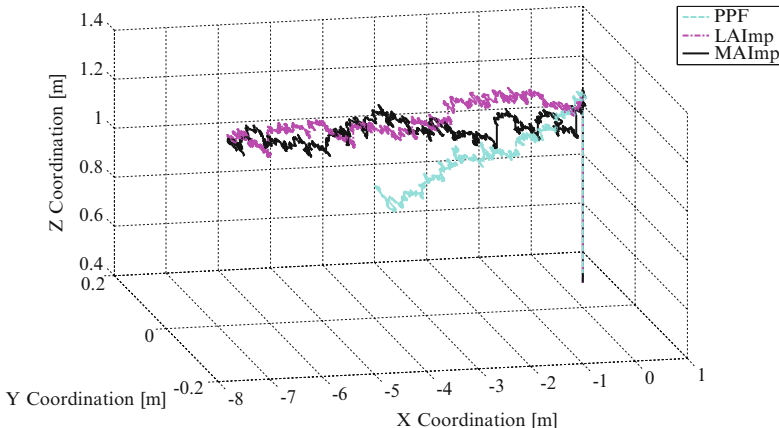


Fig. 7.13 Robot's BMC output performance

horizontally swinging between 2 and 5 m from its stand-up position (see X coordination in Fig. 7.13).

Through a series of laboratory tests, it was shown that single-leg impedance control and center of mass-based impedance adapted with robot body's attitude feedback as proposed LAImp and MAImp. According to the field tests, the best results were obtained when the robot was walking under the MAImp. In addition, MAImp allows easy tuning of the controller's parameters, and thus less time is spent on the tuning process. Moreover, the tuning setup from the fundamental test was adequate for MAImp was used in the outdoor locomotion test by performing more stable performance. This approach provided dynamically balanced

impedance acting on each supported leg's vertical motion. This led to a decrease of the $B(t)$ factor. However, the performance of LAImp could be improved with additional fine tuning of the control parameters such that they suit the environment in which the robot is walking. Based on the overall results, the problem on small vibration during some foot placement whenever impedance is applied became another issue that need to be investigated. The revealed of *push-pull* motion seems attributes to another unstable situation for this statically stable and hydraulically driven hexapod robot especially when leg stepped on rough surfaces.

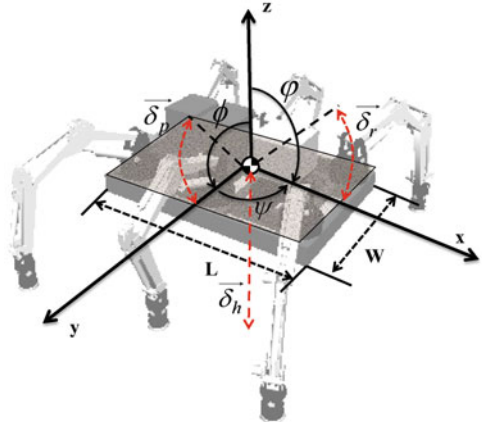
7.2 Optimization of Impedance Control by Self-Tuning Stiffness Using Logical Body's Attitude Control

Fine-tuning and trial-and-error tuning approaches are insufficient to guarantee the stability of applied impedance control, and it is difficult to implement, especially in a heavy and multi-legged robot system. Therefore, as an alternative of the optimization approaches, impedance parameters can be actively varied to compensate for the current response of the robot. Most of the published reports on the optimization criterion for impedance parameters are based indirectly on the changes of the derived elastic model of a predetermined environment, such as the skin structure for the massage system reported in [9] and estimating calculation via system identification and mathematical methods such as reported in [2, 10, 11].

The focus of most current research in robotic control is on the manipulator system that implements the dynamic control especially for redundant cases, but body posture is not a major concern in this kind of robot making its overall stability a secondary focus. Hence, it is difficult to apply the same approach to walking robots, especially in determining the changes in the environment parameters and using model reference approach, unless the robot is fully provided with a complete mathematical model and a vision unit. In fact, it is very difficult to have a complete mathematical model or analytical method approaches for hydraulically driven robot (large amount of model uncertainty) especially on determination of parameters with high degree of accuracy [12]. Therefore, in this adaptive approach, the logical changes of robot's body attitude response become the main criteria of the design. It is possible and also reliable to consider the logical robot's body posture current stability as a criterion for changing the impedance control parameters [13]. This is so since the unstable body attitude for the multi-legged robot is reflected to the current surface condition that the robot is stepping on.

As discussed earlier in this chapter, stiffness parameter for each leg (K_{f_n}) is the tuning parameter whereby $z_{I_n}(t_q) \propto K_{f_n}^{-1}$ is related to the derivation of Eqs. (6.10)–(6.12) and the kinematics motions of the robot described in Sect. 4.5. Corresponding to the horizontal stability defined for walking on extremely soft terrain in Sect. 6.2.1, the robot's body stable rotational range should be $-1.5^\circ \ll [\varphi, \emptyset]$

Fig. 7.14 Robot body's attitude calculation for self-tuning stiffness



$\ll 1.5^\circ$, and the average robot's body height error should be zero or very close to zero. Therefore, the adaptive law for varying K_{f_n} can be expressed as follows [13]:

$$K_{f_n} \propto [\delta_h, \delta_r, \delta_p]^{-1} \quad (7.9)$$

where $\delta_h = B(t)$ in this calculation, while δ_r and δ_p are the arc motion errors of robot's rotational posture angles when both angles at $-1.5^\circ > [\varphi, \emptyset]$ or $[\varphi, \emptyset] > 1.5^\circ$ as shown in Fig. 7.14 as follows:

$$\delta_r = 0.5L\varphi \quad (7.10)$$

$$\delta_p = 0.5W\psi \quad (7.11)$$

Moreover, in order to ensure the change in gradient of K_{f_n} is proportional to the criterion mentioned earlier, the exponential changes of the magnitude vectors can be expressed as follows:

$$K_{f_n} = K_{f_{o_n}} - p_c \chi = K_{f_{o_n}} - p_c (e^{-V_a} - 1) \quad (7.12)$$

where K_{f_o} is the initial stiffness value for each leg (predetermined) and V_a is a total error for the robot's body attitude feedbacks which can be written as follows:

$$V_a = \delta_h + \sqrt{\delta_r^2 + \delta_p^2} \quad (7.13)$$

p_c is a positive tuning parameter for changing the range of stiffness and proposed cost function $\chi \rightarrow 0$ whenever $V_a \rightarrow 0$. The value of magnitude vector of posture angles in Eq. (7.19) only applies to the disturbed leg(s), a leg which is lower or higher (vertical position) than the other legs during the support phase period. For the undisturbed legs, $V_a = \delta_h$ is used since the range of K_f for these legs is only

Table 7.1 Relation of robot's body rotational angles and leg position (logical truth table)

Attitude angle	Body angles	Legs position	Poles	C_a	C_b	C_c
K	φ	L1 < L3,L5	1	1	NC	NC
		L3 < L1,L5	0	NC	NC	1
	\emptyset	L5 < L1,L3	1	NC	NC	1
		L5 > L1,L3	0	1	1	NC
L	φ	L4 < L2,L6	1	NC	1	NC
		L6 < L2,L4	0	1	NC	NC
	\emptyset	L2 > L4,L6	1	NC	NC	1
		L2 < L4,L6	0	NC	1	1

Note: NC is Non-connection state

proportioned to the δ_h rates. Therefore, a switching function is designed to control this situation with reference to the Euler angle of the robot in Fig. 6.14 and the robot's attitude counter as discussed in Sect. 6.2.2. The truth table between changes in rotational angles and leg positions is determined as shown in Table 7.1.

C_a , C_b , and C_c shown in Table 7.1 denote the logical attitude control outputs of the three supported legs for the desired switching of V_a used in Eq. (7.18) but ignoring the transition state M and N. Thus, the Boolean expressions for C_a , C_b , and C_c can be simplified via De Morgan's laws and expressed as follows[13]:

$$C_a = K \bullet (\bar{r} + rp) + L \bullet \bar{p} \quad (7.14)$$

$$C_b = K \bullet p + L \bullet (\bar{r} + rp) \quad (7.15)$$

$$C_c = K \bullet (\bar{r} + rp) + L \bullet (p + r\bar{p}) \quad (7.16)$$

where NC (no changes) state is represented by $bit = 0$ and p and r are represented logical input for φ and ϕ , respectively, with reference to the range $-1.5^\circ \ll [\varphi, \emptyset] \ll 1.5^\circ$. Thus, self-tuning stiffness with logical attitude control for each leg of the robot is written as follows [13]:

$$K_f(t_c) = \begin{cases} K_{f_{on}} + p_c(e^{-V_a} - 1) & C_a = 1/C_b = 1/C_c = 1 \\ K_{f_{off}} + p_c(e^{-\delta_h} - 1) & C_a = 0/C_b = 0/C_c = 0 \end{cases} \quad (7.17)$$

where tuning reference and relation are due to the $z_{R_n} \propto K_{f_n}^{-1}$. The flow of the proposed self-tuning impedance control is shown in Fig. 7.15.

7.2.1 Experiment and Verification

The experiment is conducted in laboratory under the same operation as discussed in Sect. 6.1.2 but more environment setup as shown in Fig. 7.16 and with *physical solution*. The purpose of the experiments carried out in the laboratory is to investigate the performance of the derived impedance controllers with proposed self-tuning

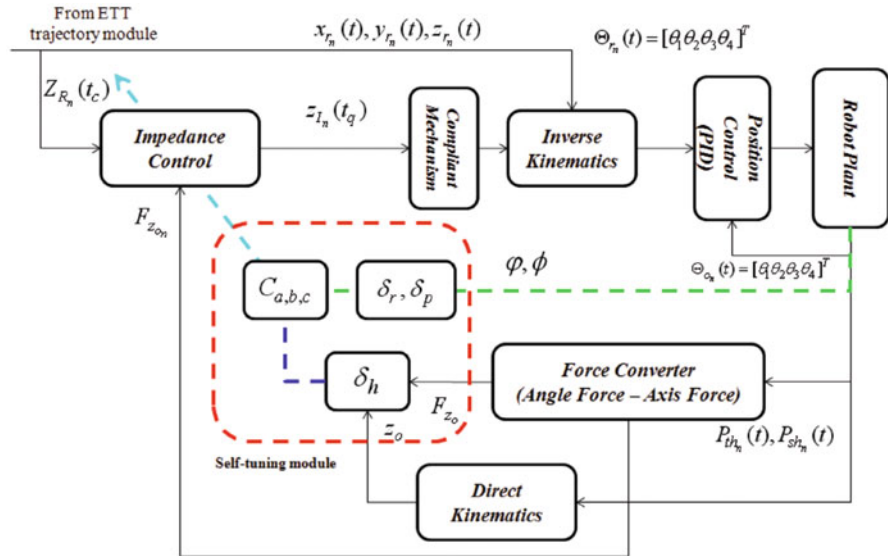


Fig. 7.15 Proposed implementation of self-tuning impedance control in robot control structure

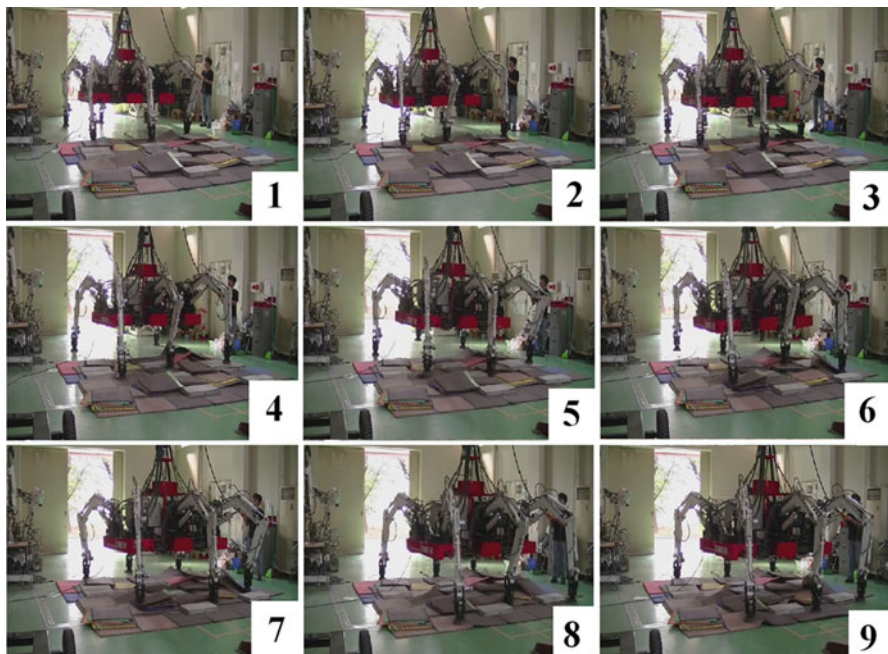


Fig. 7.16 Laboratory test setup (snapshots of COMET-IV in operation)

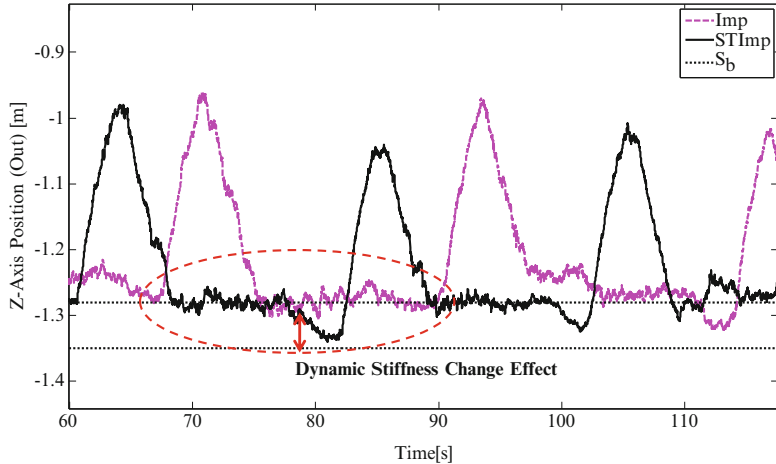


Fig. 7.17 Position of foot point on the z -axis between impedance control with and without self-tuning stiffness (sample data of leg 2)

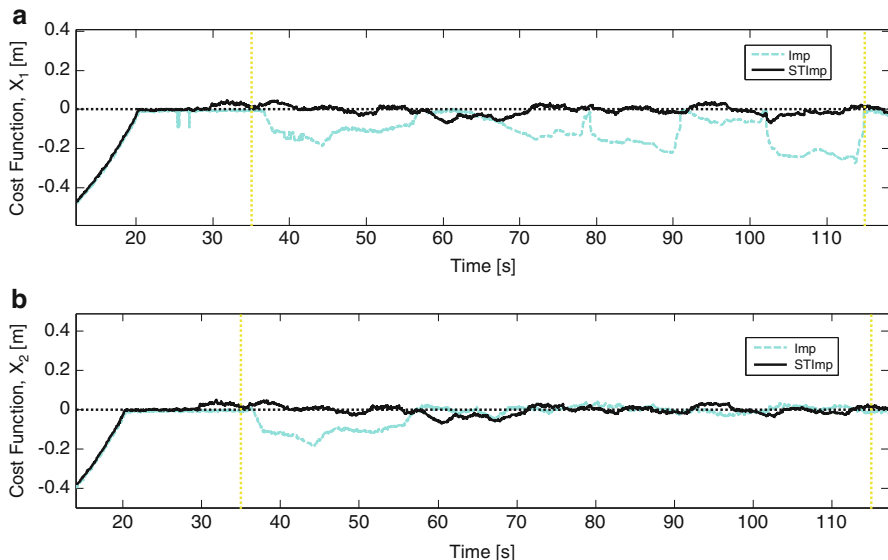


Fig. 7.18 Changes of cost functions X

stiffness corresponding to the COMET-IV attitude feedback. In this experiment, robot walking with proposed self-tuning impedance control (STImp) is compared with the robot walking with manual tuning single-leg impedance control scheme (Imp). As shown in Fig. 7.17, dynamic stiffness changes performed impulse signal to the foot stepping signal, and it is different for different steps. The difference is due to the criterion changes as shown in Fig. 7.18 that affect the value of K_{f_n} leg as shown in Fig. 7.19.

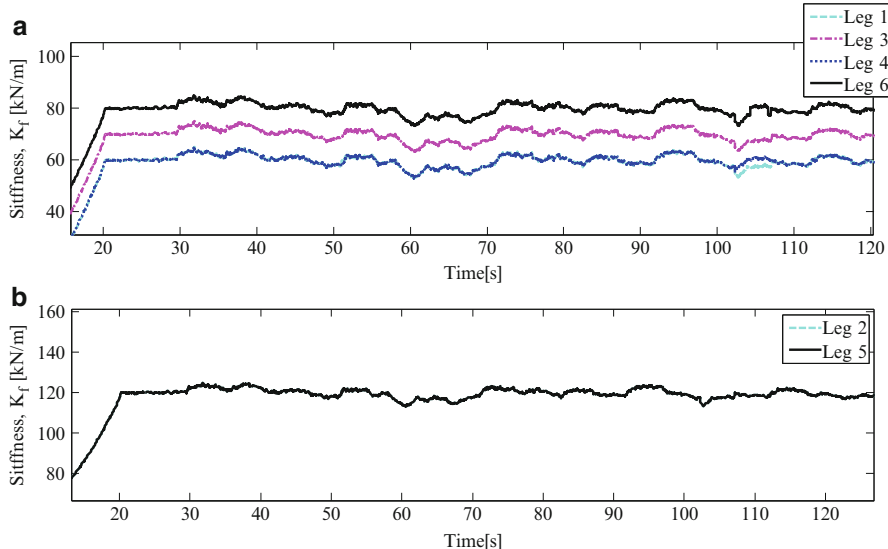


Fig. 7.19 Sample of robot's leg stiffness during walking period, (a) sample for leg 1, 3, 4, and 6 (b) sample for leg 2 and 5

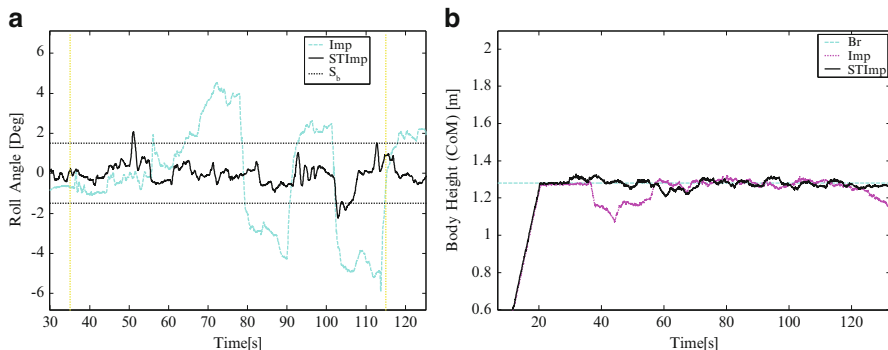


Fig. 7.20 Sample of robot's body attitude performance (a) roll angle (b) robot's body height

The average performance of $\chi_1 = e^{-V_a} - 1$ and $\chi_2 = e^{-\delta_h} - 1$ for STImp running is almost zero. However, although χ_2 is almost zero for both Imp running and STImp running (after 16 s), χ_1 for Imp running worsens with each step and adversely affecting its χ_1 and χ_2 . Therefore it can be concluded that the overall performance of STImp running is much better than that of Imp running. Furthermore, from the stiffness changes as shown in Fig. 7.19, the motion of the side legs (Leg 1, 3, 4, and 6) affects the changes of the body rotational angle (in this running emphasis is on roll angle control), thus playing a major role in balancing action of the robot as shown in Fig. 7.20. The implementation of STImp can be assumed performing

better performances which is almost similar as LAImp and MAImp with reference to the environment setup in Fig. 7.16 and physical configuration that has been used in this experiment. Moreover, this experiment also shows that LImp need to be tuned again after physical configuration is changed to perform stability on COMET-IV walking operation. In addition, STImp also performs hard swinging/shaking to the robot especially after COMET-IV stepping on the hard floor in the laboratory. Therefore, on the next section, the discussion will be focusing on the investigation and solution to reduce the swinging/shaking on COMET-IV walking with impedance control.

7.3 Impedance Forces Input Optimization Using Fuzzy Logic Control

As previously discussed, applying *push–pull* motion on the robot's foot that comes in contact with the surface became a main objective so as to ensure soft motion during walking. However, the application of the *push–pull* motion causes unwanted oscillation of the robot's body. The oscillation is due to the uncertainty of the measured inputs, such as the pressure from the hydraulic cylinder, signal from the potentiometers that are attached to the joint of every leg, and the attitude sensor signal due to shaking of the robot's body. All these uncertainties affect the impedance output signal from each leg, which subsequently affect the position control input and consequently causing the robot's body to shake and swing while walking. Furthermore, the situation will interfere with the operation of the hydraulic motor on the robot's shoulder causing it to overdrive and this again will affect the feedback input. This scenario will indirectly disturb the CoM tracking error and the attitude control calculation in general. On the other hand, too much oscillation on the feedback inputs, such angle position and force on cylinders, will cause oscillations on the force feedback input of the impedance controller.

The oscillations will cause the controller output to oscillate, which will affect the signal from the reference input, as shown in Figs. 7.21 and 7.22. Moreover, since the z-axis position is affected by the unwanted oscillations, this will give a negative impact on the leg position control input session due to unsolved inverse (leg's rotational angle reference signals determination) and direct kinematics (measured leg's axis signal determination) sessions. Therefore, the *push–pull* motion should be changed to be more in “step signal” curve whereby performing *push* or *pull* motion in one step as shown in Fig. 7.23. This impedance control is suitable to be implemented for the final position control input of COMET-IV since the robot is a statically stable robot and using linear type actuators (each leg). With this improvement, with the range (*push* or *pull*) changing dynamically and being proportional to the overall stability of the robot system, it is expected that leg motion is smoother than using the proposed adaptive impedance controls as discussed in the previous sections.

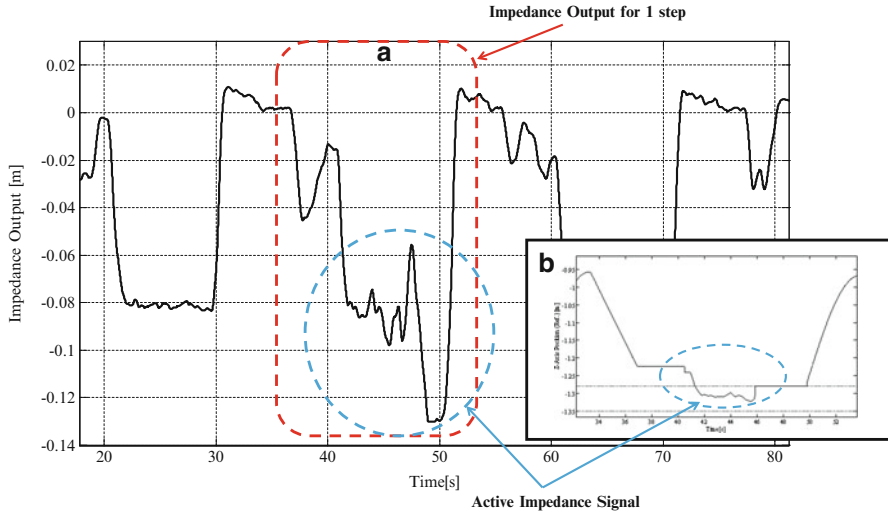


Fig. 7.21 Relation between impedance output and z -axis reference signal (vertical foot point motion); (a) impedance output, (b) z -axis reference signal (experiment sample for leg 3)

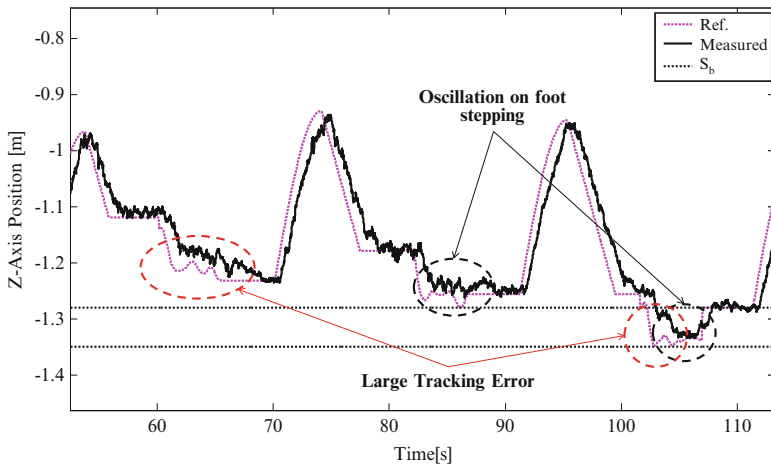


Fig. 7.22 Z -axis position (Experiment Sample for Leg 3)

In the derivation of F_{I_n} , all forces that acts on the robot system axes have been included, therefore it is possible to replace $F_{z_{0n}}$ with F_{I_n} as the input for each impedance controller of each leg. In order to optimize the input variables, the continuous fuzzy model proposed by [14] is used via fuzzy IF-THEN rules. FLC has been developed in various style and inference mechanisms, such as mamdani fuzzy models [15], TSK models [14, 16], and tsukamoto models [17]. These models could be freely selected depending on the system requirements and study needs.

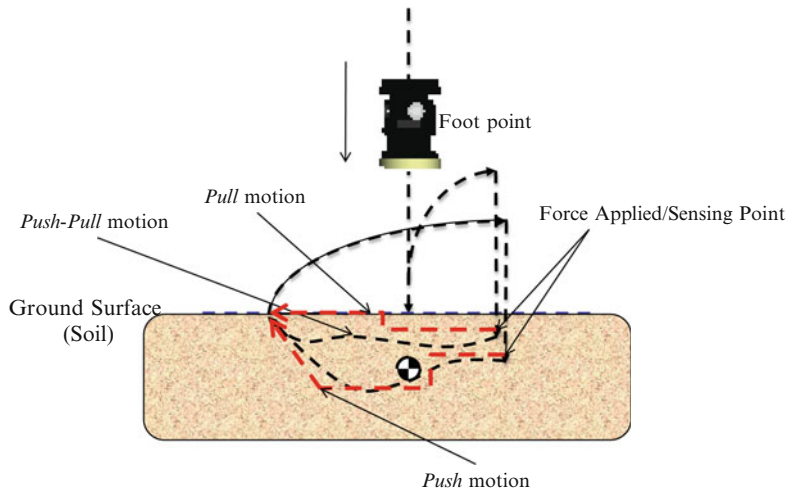


Fig. 7.23 Proposed push–pull and pull motion on robot foot

However, the real-time system control structure, such as applied in COMET-IV, TSK-FLC is more preferable since it is compatible with polynomial input variables (real-time input feedback), and it can be easily defined on inferred structure (minimum or product operator). Considering the fuzzy rule base consists of i th rules for multi-input single-output (MISO) fuzzy system have the following form [18]:

$$\text{if } x_1 \text{ is } M_1^i \text{ and } \dots \text{ if } x_k \text{ is } M_k^i \text{ then } H^i \quad (7.18)$$

where $x_k \in \Re^k$ is the system state variables, M_k^i are the fuzzy sets, and H^i are the outputs that are characterized in linguistic terms: SMALL (S), MEDIUM (M), and BIG (B) for both positive (P) and negative (N) coordination. The final output, or crisp output of the fuzzy system (ξ), for one attitude feedback parameter is inferred as follows (using singleton fuzzifier with minimum operator of the antecedent part of the rules (Π) and the center of mass method for defuzzification):

$$\xi_s(t) = \frac{\sum_{i=1}^{I^2} \epsilon [\prod_{a=1}^2 \mu_a(\lambda_a \dot{v}_s(t))] }{\sum_{i=1}^{I^2} \prod_{a=1}^2 \mu_a^i(\lambda_a \dot{v}_s(t))} \quad (7.19)$$

where I^2 is the number of rules fired out from the total of i th rules that present in the rule base for a set of inputs, λ_a is the feedback compensators for $\dot{v}(t)$ input variables (must satisfy $\dot{v}(t) > 1$), ϵ is the scaling factor for each defined membership function:

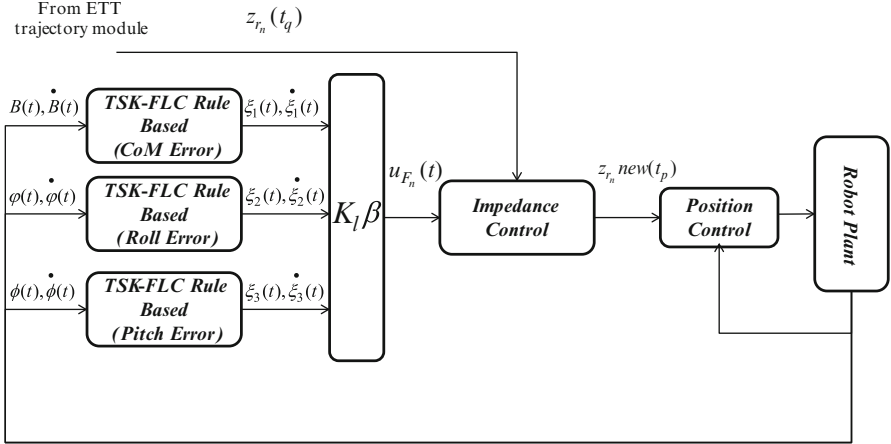


Fig. 7.24 Proposed improvement on optimal impedance control TSK-FLC

{NB = $-\varepsilon$, NM = -0.5ε , NS = -0.25ε , PS = 0.25ε , PM = 0.5ε , PB = ε }, and $\mu_a(\dot{v}(t))$ is the membership function value for the $\dot{v}(t)$ input variables, where $\dot{v}(t)$ represents different values for different s , where $s = 1: \dot{v}_1(t) = [B(t) \quad \dot{B}(t)]$, $s = 2: \dot{v}_2(t) = [\varphi(t) \quad \dot{\varphi}(t)]$ and $s = 3: \dot{v}_3(t) = [\phi(t) \quad \dot{\phi}(t)]$. Therefore, the control law for the impedance controller input (force inputs) can be written as follows:

$$u_F(t) = -K_l \xi(t) \quad (7.20)$$

where K_l ($l = 1, \dots, 6$) is the gain derived from the solution of Algebraic Riccati's equation (S) subjected to Eq. (7.8) with new state variables: $\dot{\xi}(t) = [\dot{\xi}_1(t) \quad \dot{\xi}_2(t) \quad \dot{\xi}_3(t) \quad \dot{\xi}_1(t) \quad \dot{\xi}_2(t) \quad \dot{\xi}_3(t)]^T$ making:

$$\dot{\xi} = A\xi + Bu \quad (7.21)$$

Thus, the new impedance controller form for each leg can be expressed as follows:

$$\beta u_{F_n}(t) = M_{f_n} \ddot{z}_n(t) + D_{f_n} \dot{z}_n(t) + K_{f_n} z_n(t) \quad (7.22)$$

Furthermore, to generalize the range of the controller input, adaptive compensator (β) defined in Eq. (7.14) of Sect. 7.2.1 is used. The schematic diagram for the proposed improvement of optimal impedance control using TSK-FLC is shown in Fig. 7.24.



Fig. 7.25 Fundamental experiment setup

7.3.1 Experiment and Verification

The experiment is focused on evaluating how far the proposed optimal impedance control with TSK-FLC could reduce the robot's body swinging and shaking during walking period, thus increasing its stability. Moreover, it also done to verify the potential of proposed CoB-based omnidirectional movement combined with ETT module on giving survival walking on extreme uneven terrain.

As previous experimental discussed in Sects. 6.1.3 and 6.2.3, this experiment is done fundamentally in the laboratory, and the environment is setup as shown in Fig. 7.25. Approximately 30-cm multilayer hard paper plates (package box type) are used as the targeted soft object that will be stepped on by COMET-IV during the walking operation, and the rest of the surface is the existing hard surface. The aim of the experiment is to verify the usability of the proposed optimal impedance control when the robot walks on mixed rough and soft terrains. The walking experiments were performed twice (walking right to left) using two different methods: first, using the proposed optimal single-leg impedance control using vertical force delivery on foot and LQR (LImp) and second, using the proposed optimal single-leg impedance control with TSK-FLC and LQR (FZImp). Both controllers are running with established force-based trajectory module named environment trailed trajectory (ETT) and with tripod walking pattern. As shown in Fig. 7.26, changes in the foot placement signal attributed to impedance is different for the different methods, where no jittering (support phase motion only) on reference control signal during support phase is noted when FZImp is used. This is the due to the effect of the impedance output signal from FZImp, as shown in Fig. 7.27.

Moreover, this non-jittering or smooth dynamic motion gives positive impact on position control precision performances as shown in Fig. 7.28, thus affecting the overall body stability of COMET-IV that can be represented by roll angle results as shown in Fig. 7.29.

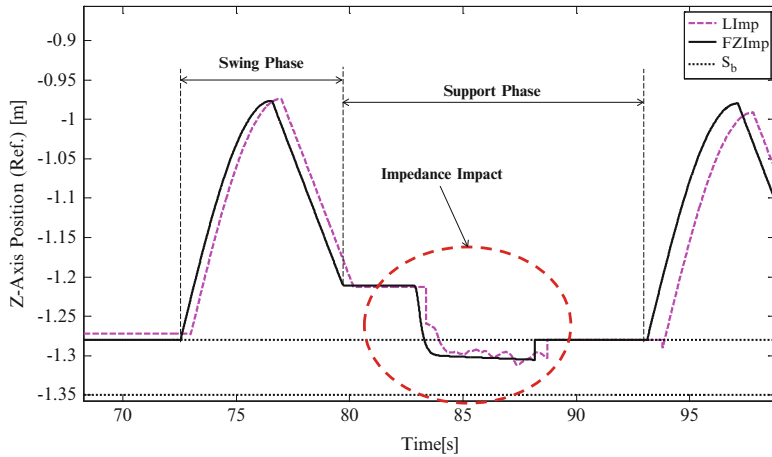


Fig. 7.26 Dynamic motion on support phase caused by impedance control (foot point motion reference along the z-axis foot point)

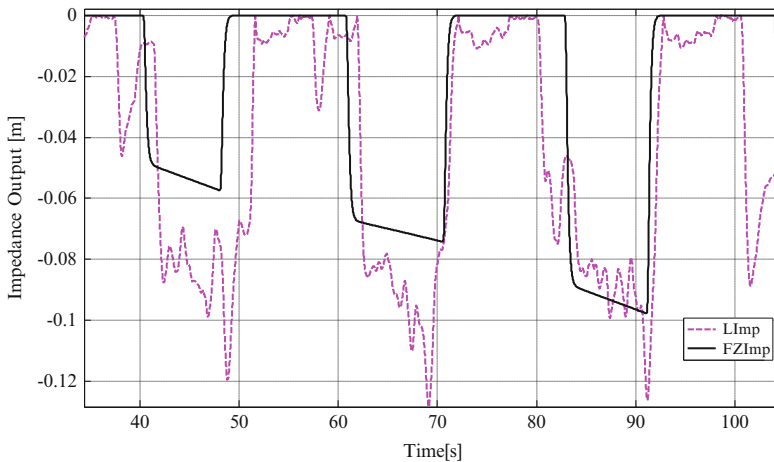


Fig. 7.27 The difference in impedance output between LImp and FZImp (sample of experiment for leg 1)

The experiment is extended to operate COMET-IV with FZImp in more extreme terrain such as rotating on an obstacle with 70 cm height as shown in Fig. 7.30 and walking down the 60-cm-high cliff as shown in Fig. 7.33. These experiments are done to evaluate the potential of COMET-IV to perform rotating movement between the pits of obstacles and walking down on large-scale unstructured terrain that may exist on the application target area such as mountain and afterquaked area. For rotating on the 70-cm obstacle test, the experiment is done using two methods of proposed impedance controls; FZImp and STImp. The obstacle

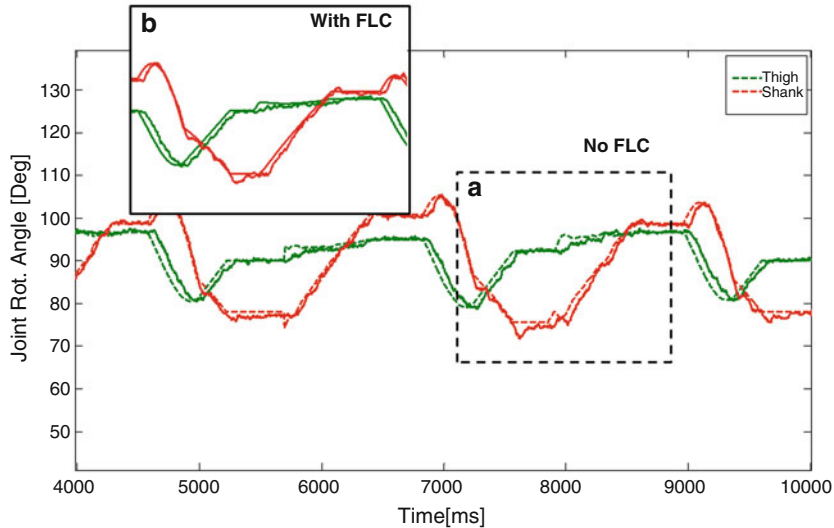


Fig. 7.28 Impact of proposed impedance on position control (leg angle motion control); (a) walking operation with LImp, (b) walking operation with FZImp (sample of experiment results for leg 1)

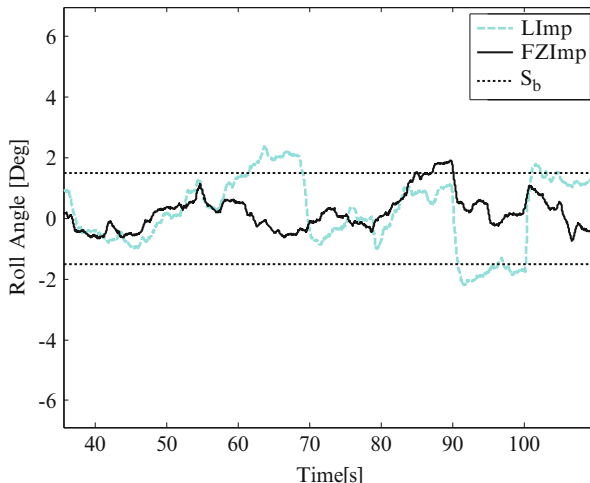


Fig. 7.29 Robot's body posture (experiment sample of roll angle results)

dimension is predetermined via proposed Grid-based Walking Assistant for Legged Robot (GWALR) [19] to vary S_b value during walking session.

As shown in Figs. 7.30 and 7.32, the results shows that robot with FZImp successfully performed stable rotating and stepping finishing on the 70-cm-high

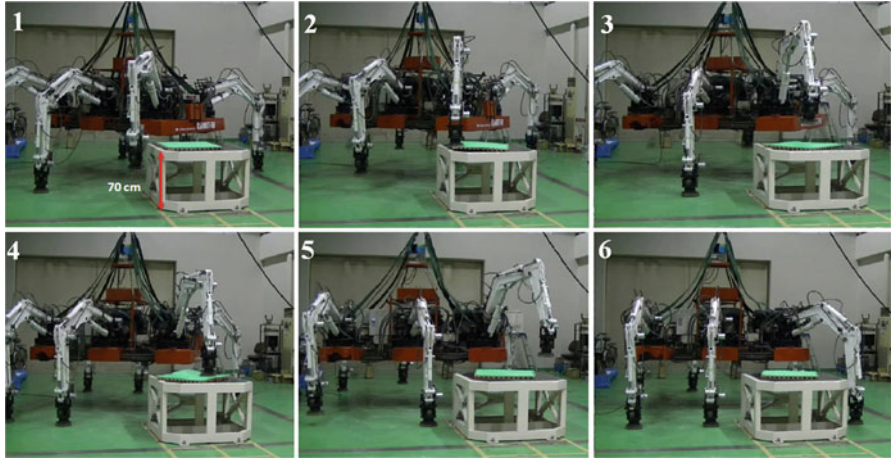


Fig. 7.30 Snapshots of COMET-IV omnidirectional with proposed optimal impedance control test by rotating on the obstacle with 70 cm height

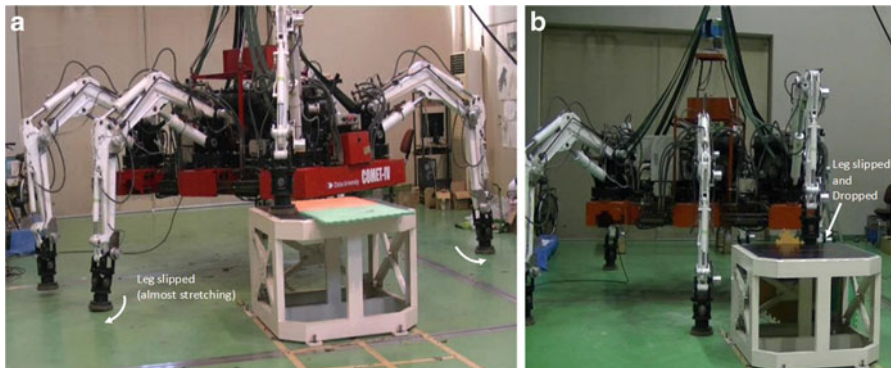


Fig. 7.31 Slipped problem (friction) during rotating session; (a) fault on other legs, (b) fault on overall CoB turning

obstacle with fixed setup value of H_o and S_o for Leg 1, 2, and 3. It is different to the rotating test with STImp as shown in Fig. 7.31, whereby several problems occurred which is mainly on imprecise foot stepping and leg slipping that are causing robot's CoB out of targeted circle as shown in Fig. 7.32. Moreover, this slipping also made overall robot's rotating movement unstable especially when robot's body hardly dropped as shown in Fig. 7.31b. Thus, CoM having a very small support polygon or out of support polygon, which is not reliable (in stability) for statically stable hexapod robot such as COMET-IV.

For walking down the 60-cm cliff, the purpose of experiment is to evaluate the potential of COMET-IV with FZImp walking on almost fully and extremely rough

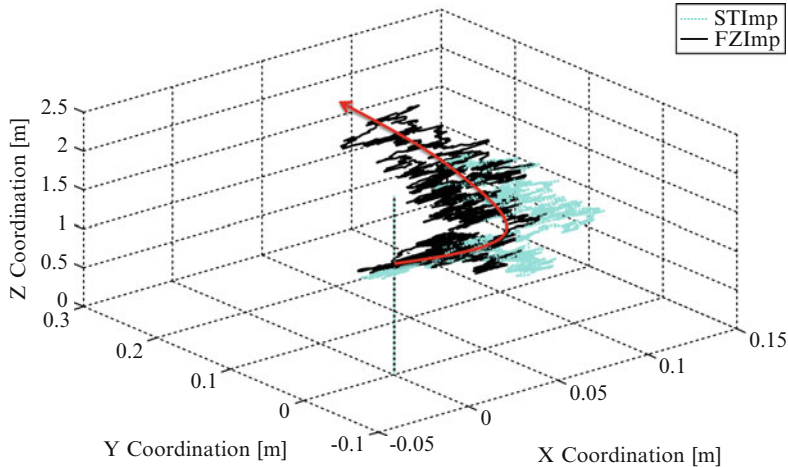


Fig. 7.32 Robot's BMC output performance

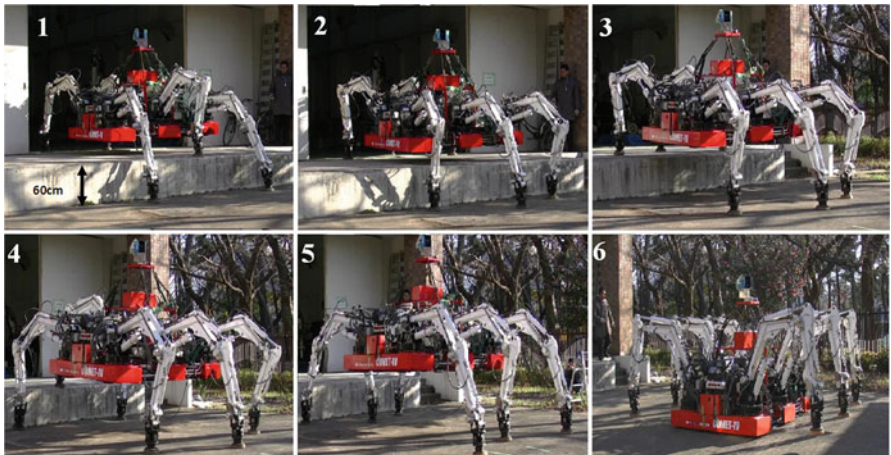


Fig. 7.33 Snapshots of COMET-IV in operation during walking down the 60-cm-high cliff tests

terrain as shown in Fig. 7.33. The experiment is done in two times with two different distance of stepping (S_o) determined by grid-mapping method proposed in [20].

In addition, $t_{ex} = 6$ s is set according to height of terrain and considering the enough cycle time for tripod sequence in ETT generation. As shown in Fig. 7.34, although one of the legs is on the end of cliff (dotted circle), the robot constantly holds the step and maintains the stability, thus making it to successfully walk down/descend through the cliff. In this situation, the critical moment can be seen on the second trial with $S_o = 0.9$ as shown in Fig. 7.34b.

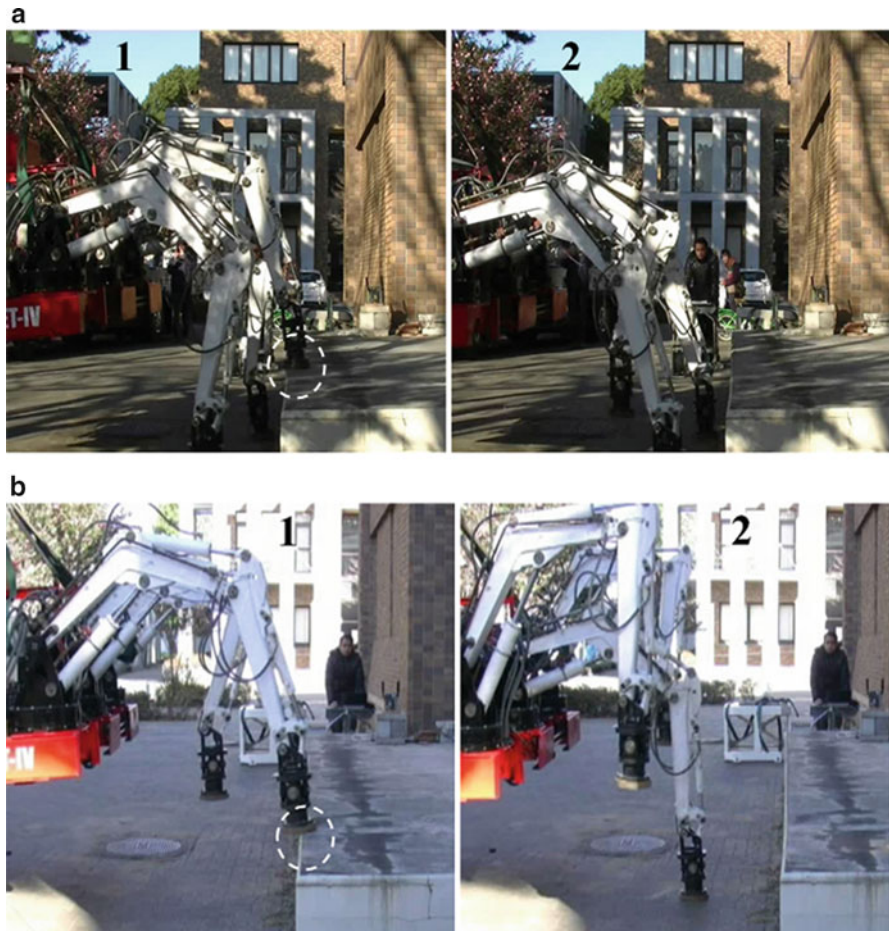


Fig. 7.34 Situation during finishing part walking down the cliff, (a) first trial with $S_o = 1.2$, (b) second trial with $S_o = 0.9$

Furthermore, BMC performance shows that the robot body almost follows the ideal path with FZImp. This is obviously can be seen in Fig. 7.35, whereby the robot constantly keeps the walking on the path about 0.02 m on Y -axis coordination. The difference is identified between walking with $S_o = 0.9$ and walking with $S_o = 1.2$ when the robot starts walking down the cliff as circled and marked in Figs. 7.35, 7.36, and 7.37. Walking setup with $S_o = 1.2$ performed out of the ideal path line (red line), since there have different force reaction regarding different value of S_o as shown in Fig. 7.36. Robot walking setup with $S_o = 0.9$ shows pushing motion is under control (foot in setup *stable range*) if compared to the walking setup with $S_o = 1.2$. These results are related to the robot's body attitude response as shown in

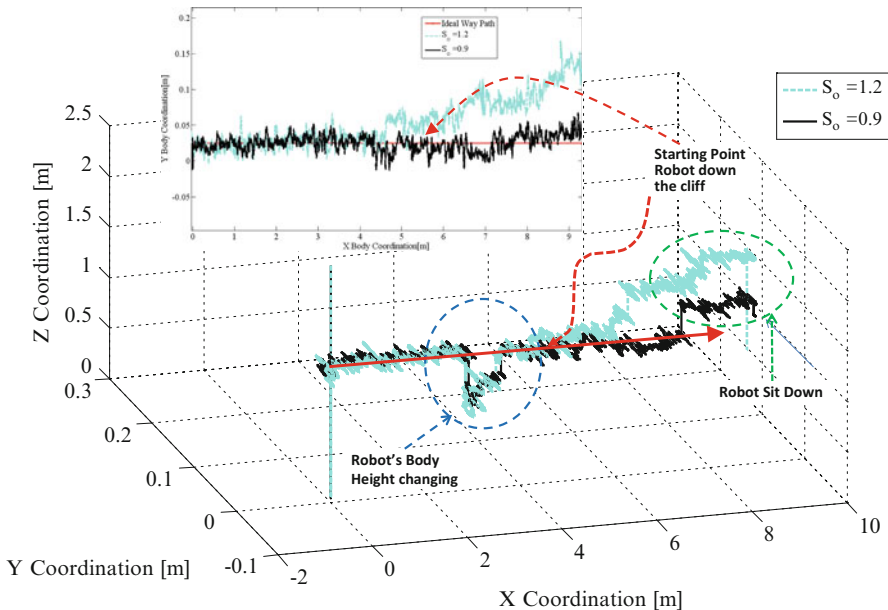


Fig. 7.35 Robot's BMC output performance

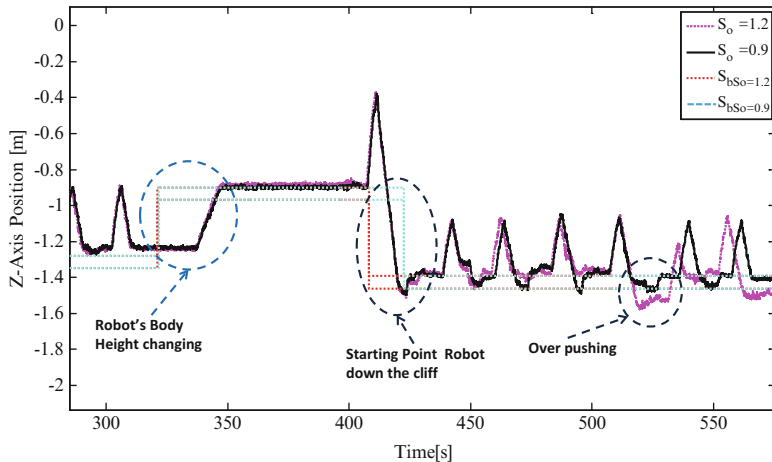


Fig. 7.36 Measured position of foot point on the z -axis (sample data of leg 6)

Fig. 7.37 (vertical bar mark is the value of pitch angle when the robot started down the cliff). However, this defect results are typically out of impedance control scope since a way point control needs another mechanism of control inside the trajectory generation. Due to the overall performances, implementation of FZImp in

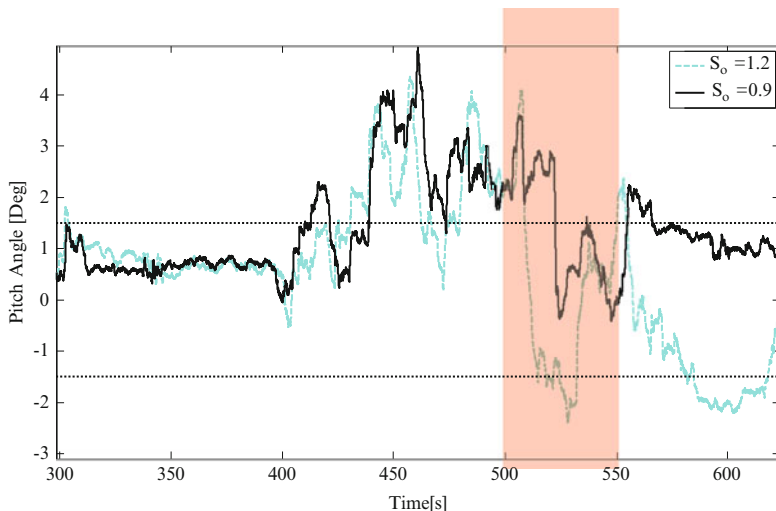


Fig. 7.37 Pitch angle of the robot's body

COMET-IV has solved the instability problem using impedance control for walking on the rough terrain by reducing the shaking problem of the robot's body. Thus attribute to the reliable and safety walking/operation to the robot, as clearly seen from the experimental results.

References

1. Palis F, Rusin V (2004) Adaptive impedance control of legged robot. Paper presented at the proceeding of 11th international conference on power electronics and motion control, Riga
2. Erickson D, Weber M, Sharf I (2003) Contact stiffness and damping estimation for robotic systems. *Int J Robotics Res* 22(1)
3. Lehtinen H (1994) Force based motion control of a walking machine. VTT Publication, Espoo
4. Irawan A, Nonami K (2011) Optimal impedance control based on body inertia for a hydraulically driven hexapod robot walking on uneven and extremely soft terrain. *J Field Robotics* 28 (5):690–713
5. Futagami K, Harada Y, Oku M, Ohroku H, Lin X, Okawa K, Sakai S, Nonami K (2008) Real-time navigation and control of hydraulically actuated hexapod robot COMET-IV. In: Proceeding of the 9th international conference on motion and vibration control 2008 (MOVIC 2008), Munich, 2008
6. Ohroku H, Futagami K, Harada Y, Oku M, Nonami K (2008) Tele-operation and navigation of hexapod robot COMET-IV with real-time gait and trajectory planning. In: 9th international conference on motion and vibration control 2008 (MOVIC 2008), Munich, 2008
7. Oku M, Koseki H, Ohroku H, Harada Y, Futagami K, Tran DC, Li L, Lin X, Sakai S, Nonami K (2008) Rough terrain locomotion control of hydraulically actuated hexapod robot COMET-IV (in Japanese). In: JSME conference on robotics and mechatronics 2008 (ROBOMECH 2008), Nagano, 2008
8. Hespanha JP (2009) Linear Systems Theory, Princeton University Press, Princeton, New Jersey

9. Terashima K, Miyoshi T, Mouri K, Kitagawa H, Minyong P (2009) Hybrid impedance control of massage considering dynamic interaction of human and robot collaboration systems. *J Robotics Mechatronics* 21(1)
10. Jung S, Hsia TC, Bonitz RG (2001) Force tracking impedance control for robot manipulators with an unknown environment: theory, simulation, and experiment. *Int J Robotics Res* 20 (9):765–774
11. Kikuuwe R, Yoshikawa T (2002) Robot perception of environment impedance. In: Proceeding of IEEE international conference of robotics and automation 2002 (ICRA 2002), Kyoto, pp 1661–1666
12. Barai R, Nonami K (2007) Optimal two-degree-of-freedom fuzzy control for locomotion control of a hydraulically actuated hexapod robot. *Info Sci Appl* 117(8):1892–1915
13. Irawan A, Nonami K, Ohroku H, Akutsu Y, Imamura S (2011) Adaptive impedance control with compliant body balance for hydraulically driven hexapod robot. *J Syst Des Dyn* 5 (5):893–908, Special issue of motion and vibration control 2010
14. Takagi T, Sugeno M (1985) Fuzzy identification of systems and its applications to modeling and control. *IEEE Trans Syst Man Cybernetics* 15(1):116–132
15. Cox E, O'Hagan M (1999) The fuzzy systems handbook: a practitioner's guide to building, using, and maintaining fuzzy systems, 2nd edn. Academic, Cambridge
16. Sugeno M, Kang GT (1988) Structure identification of fuzzy model. *Fuzzy Set Syst* 28:15–33
17. Castillo O, Melin P (2008) Type-2 fuzzy logic theory and applications. Springer, Berlin
18. Vasickaninova A, Bakasova M (2010) Locally optimal fuzzy control of a heat exchanger. *WSEAS Trans Syst* 9(9):999–1008
19. Daud MR, Nonami K (2011) LRF assisted force-based walking for hexapod robot COMET-IV. *Int J Automation Robotics Autonomous Syst (ARAS)* 11(1):11–22
20. Daud MR, Nonami K, Irawan A (2011) LRF assisted autonomous walking in rough terrain for hexapod robot COMET-IV. In: Proceeding of the international conference on intelligent unmanned systems 2011 (ICIUS 2011), Chiba, 2011

Chapter 8

Teleoperated Locomotion Control of Hexapod Robot

Abstract Recently the development of the robotics technology is remarkable. Currently most of the large-scale robot designed is focused on various tasks especially for the hazardous operation and disaster situation such as earthquake. Therefore, this chapter has taken a part and designed a hydraulically actuated hexapod robot, namely, as Chiba university operating mine detection electronics tools (COMET) for multitasks on outdoor situation with the unknown environment. For the extreme environment cases, it is difficult to make it fully autonomous. Therefore, teleoperation-based system has been designed on the COMET-IV for extreme environment. The teleoperation assistant system is designed to understand the ambient environment and the movement condition of the robot including the legged robot changes which effect the height of the body and robot's attitude. In this chapter, this operator is applied with omnidirectional vision sensor and 3D robot animation. The online 3D virtual reality technique is proposed to make synchronous control between virtual 3D animation and COMET-IV physical on the real environment. The teleoperation assistant system is verified through the experiment of the obstacle avoidance walking on the outdoor environment. Also, this chapter will describe the proposed method of 3D geometric combination with the designed numerical model-distributed data. On the other hand, this method is applied with the body movement coordination method (BMC) which is designed based on the center of the body of the robot and shoulder of each leg point. The 3D model is designed for hydraulic-based drive hexapod walking robot which is critically to be experimented directly without any strong pre-study. Moreover the force-based controlled walking is the current research for this hydraulic-drive robot current version named as COMET-IV. Therefore, in this chapter, the discussion will be on the 3D geometric modeling with the force-based controlled numerical model that is designed with BMC technique. Simple walking experiment has been done to verify this simulator and the results are nearly same as simulated.

8.1 Movement Control Methods

Recently, the robotics technology has made remarkable development in assisting operation in hazardous area such as disaster-stricken districts, construction, and mountain forest which are mostly the rough terrain. The research group has developed a series of mine detection and clearance robots, like COMET-I, COMET-II, COMET-III [1] and carried out the approaches through application on mine detection assistant problem point of view until now variety of walking algorithms [2–4]. Now, to advance the adaptability on the unknown rough terrain in various hazardous operations, COMET-IV has been developed [5]. For this version, one of the research targets is to make it possible to be controlled on the extreme environment such as disaster situation.

A lot of researches on the mobile robot navigation are reported [6, 7]. But, fully autonomous method is still difficult to be implemented. Therefore, teleoperation-based system with proposed technique is designed for COMET-IV. There are several researches that use the method that selects the fundamental motion prepared beforehand [8] and implement the master-slave technique [9]. Moreover, teleoperation-based control technique for the wheel-type robot has been achieved in real time by generating the environmental map using measured data from the laser distance and simultaneous localization and mapping (SLAM) technique [10]. The difference on COMET-IV compared to the other robot research is this robot is a hexapod-based robot with hydraulic drive. A lot of teleoperation-based control researches reported is for the wheel-type robot [10] and the crawler type [11] with the small-scale body. Only a few researches [12] for the large-scale robot like COMET-IV on the same niche area are reported. In rough terrain environment cases, the legged robot will change the height of the body, attitude, and the leg movement rapidly. Therefore, to make a stable control, the teleoperation assistant system is designed to understand the ambient environment of the robot and the movement condition of the robot. In addition omnidirectional vision sensor and 3D robot animation are combined with this system to achieve the desired objective. There is no report about the teleoperation-based assistant system using omnidirectional vision sensor and 3D robot animation for large-scale walking robot. In this chapter, the proposed technique on the teleoperation assistant system with omnidirectional vision sensor and 3D robot animation design progress will be described.

Commonly the walking or legged robot has various problems that should be hierarchically solved such as navigation, foot placement, gait pattern control, attitude control for balances, and servo system design of each leg [13, 14]. The verification of the walking algorithm by a large-scale robot such as COMET-IV is attended with danger and too risky. Therefore the research and development on COMET-IV simulator has been done to provide indoor validation and planning before doing some experiment to the real COMET-IV system. Previously simulation models are mostly done numerically via MATLAB/SIMULINK system to validate some designed algorithms before being experimented in real COMET-IV system. On the other hand, the latest walking method using force feedback needs to

have better procedure of walking. Thus, its numerical results are not enough to evaluate whether the algorithm can give proper walking on COMET-IV system. In this chapter, 3-dimensional (3D) robot models are expressed in virtual environment, and a remote control of the dual-arm robot by master-slave method in the model base has been described [13]. Moreover, other method proposed by [14, 15] that 3D mapping information is generated visually makes the walking simulation of the humanoid robot in virtual environment (movement in the narrow space with HRP-2 real robot). In addition there is a research case with the generation of the walking pattern of the multi-legged robot that used the genetic algorithm and open dynamics engine (ODE) approaches [16]. The means of achievement is different, but the method is done for the same purpose which is to express the movement of the robot in the virtual environment.

In COMET-IV 3D model research, 3D walking simulator is designed using 3D geometric method [27–29] whereby separately designed with SIMULINK model. It is done in order to make sure that the SIMULINK model is not changed and easy to be used for experiment purpose (real time). Application programmed interface (API) method has been used to combine both MATLAB programmed and C/C++ programmed via Visual C/C++ before it is expressed to the 3D geometric model. This separation method allows algorithms in SIMULINK program which is the main program of actual COMET-IV system that can be updated independently and validated with designed 3D geometric model at any time. In this chapter, the discussions and results will be covered on the interfaces between designed 3D geometric model of COMET-IV and the force-based walking model that have been designed in SIMULINK program.

8.2 COMET-IV System Configuration

Figure 8.1 and Table 8.1 show the specification overview of the hydraulically actuated hexapod robot COMET-IV. This robot is 2.5 m long, 3.3 m wide, 2.8 m high, and approximately 2,000 kg weight. Two gasoline engines drive two hydraulic pumps. The electric power to drive electrical components is supplied from two dry battery installed on this robot.

The coordinate system of a leg is shown in Fig. 8.2. Each link parameter is shown in Table 8.2. Each leg has four degrees of freedom. Shoulder is actuated by hydraulic motor, and thigh, shank, and foot are actuated by hydraulic cylinders. In COMET-IV system, each joint rotation angles (foot, thigh, shank, and shoulder) are acquired by the potentiometer. On the other hand, pressures of cylinder are acquired by the pressure sensor for leg force data acquisition. The attitude sensor attached on the center of the COMET-IV body is used for body posture monitoring (see Fig. 8.3). In addition the stereo vision camera, omnidirectional vision sensor, global positioning system (GPS), and laser range finder (LRF) are installed on the robot for navigation purpose. COMET-IV used GPS for self-location and autonomous navigation. Wireless LAN of the 2.4 GHz belt is used for the video stream



Fig. 8.1 Overview of COMET-IV

Table 8.1 Specifications of COMET-IV

Item	Value
Height (m)	2.8
Width (m)	3.3
Length (m)	2.5
Weight (kg)	2,120
Pump pressure (MPa)	22 × 2
Pump rated flow (L/min)	78 × 2

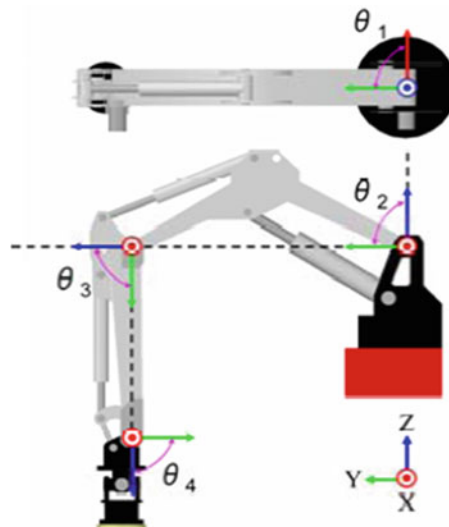
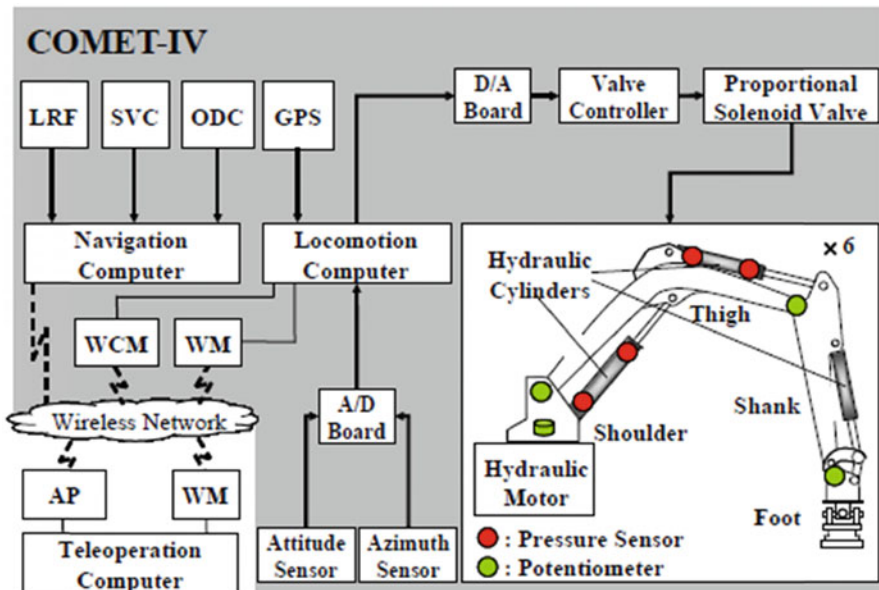


Fig. 8.2 Coordinate system of leg

Table 8.2 Specifications of COMET-IV

Joint	Link	Length (m)	Range (deg)
Shoulder	L1	0.0	$-180^\circ \leq \theta_1 \leq 180^\circ$
Thigh	L2	1.13	$50^\circ \leq \theta_2 \leq 142^\circ$
Shank	L3	0.77	$36.6^\circ \leq \theta_3 \leq 150^\circ$
Foot	L4	0.39	$-47.9^\circ \leq \theta_4 \leq 103^\circ$



LRF : Laser Range Finder, SVC : Stereo Vision Camera, ODC : Omni-Directional Camera
 WCM : Wireless Client Module, WM : Wireless Modem (for sensor data), AP : Access Point

Fig. 8.3 System configuration of COMET-IV

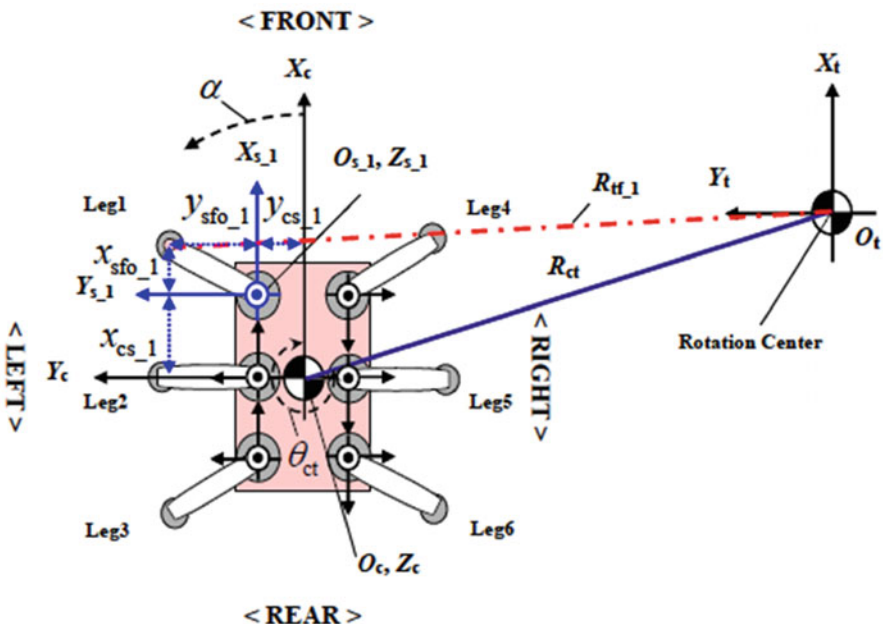
data transceiving between teleoperation computer and locomotion computer. At the same time, it is also used for data acquisition transmission between those units. Analog-to-digital (A/D) converter card and digital-to-analog (D/A) converter card are used for data reading conversion and data control conversion, respectively.

8.3 OmniDirectional Gait Control Procedure

COMET-IV is designed with “the standard circular gait” [17] proposed by Hirose et al. on horizontal foot trajectory and used “low-impact foot trajectory” [18] proposed by Sakakibara et al. on vertical foot trajectory. In this research omnidirectional gait [19] is designed by using both basic algorithms mentioned with center arbitrary setting. Table 8.3 and Fig. 8.4 show the omnidirectional gait parameters.

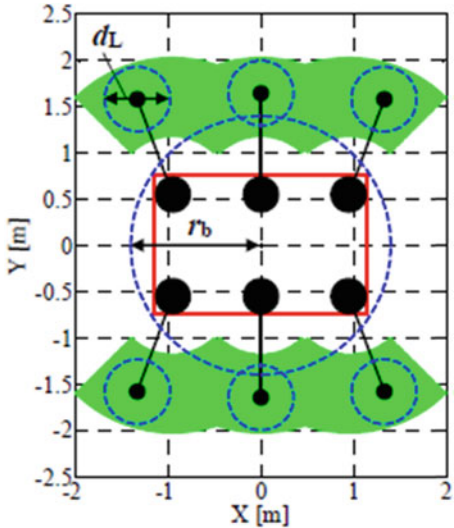
Table 8.3 Parameters of the omnidirectional gait

Symbol	Signification (coordinate system)
O_c	Body coordinate system
O_{s_i}	Shoulder coordinate system
O_t	Rotation center coordinate system
(R_{ct}, θ_{ct})	Position of a rotation center (polar display of O_c)
θ_{tb}	Traverse angle of the body center at one cycle (O_t)
$(R_{tf_i}, \theta_{tf_i}(t))$	Position of each foot (polar display of O_t)
$(X_{tf_i}(t), Y_{tf_i}(t))$	Position of each foot (O_t)
(x_{cs_i}, y_{cs_i})	Position of each shoulder (O_c)
(x_{ts_i}, y_{ts_i})	Position of each shoulder (O_t)
(x_{sfo_i}, y_{sfo_i})	Initial position of each foot (O_{s_i})
(x_{sfc_i}, y_{sfc_i})	Center of each foot trajectory at one cycle (O_{s_i})
$(X_{tf_i}(t), Y_{tf_i}(t))$	Trajectory of each foot (O_{s_i})
T	Cycle time
a	Crab angle

**Fig. 8.4** Definition of coordinate system of the omnidirectional gait

The traverse angle θ_{tb} of the body for one cycle is considered the range of leg motion. The range of motion of 0.65 m in height from ground is shown in Fig. 8.5. The area represented as dashed line is safety movable area for foot on omnidirectional gait (Fig. 8.5). Safety movable area is assumed to be a circle for efficient gait parameter setting. The area to which the body center of the robot moves for one

Fig. 8.5 Horizontal workspace of all legs



cycle becomes a radius $r_b = 2dL$ as shown in a body center circumference in the short dashed line in Fig. 8.5. The traverse angle θ_{tb} of the body center for one cycle is set to follow Eq. (8.1):

$$R_{ct} \sqrt{2(1 - \cos \theta_{tb})} \leq r_b \quad (8.1)$$

The horizontal foot trajectory is derived by setting the rotation center (R_{ct}, θ_{ct}) arbitrarily and setting the traverse angle θ_{tb} that fulfills Eq. (8.1). Arbitrary crab angle walking is achieved by setting the crab angle α using Eq. (8.2) and R_{ct} is set to infinite:

$$\theta_{ct} = \alpha + \frac{\pi}{2} \quad (8.2)$$

8.4 Teleoperation Assistant System

The assist system is designed to present the operator the scene of the environment of COMET-IV. The assist system consists of real-time 360-degree omnidirectional vision sensor with 3-dimensional (3D) animation model. This system is capable of improving the performance of teleoperation and for easy human interfaces. This teleoperation assistant system and remote control is combined for high performance of teleoperation control on COMET-IV. Figure 8.6 shows the graphical user interface of the teleoperation assistant system. The function of each element in teleoperation assistant system is as follows:



Fig. 8.6 View of teleoperation assistant system

Table 8.4 Instruction information commands

Parameter	Signification
Action	Action value
Cycle_time	Cycle time
θ_{ib}	Traverse angle of the body center at one cycle (O_i)
(R_{ct}, θ_{ct})	Position of a rotation center (polar display of O_c)

1. Instruction information
2. Communications log
3. Omnidirectional image and generated image
4. Display of received sensor data
5. Map information
6. 3D animation of robot using sensor data

User datagram protocol (UDP) socket communication is used on data transfer procedure. Table 8.4 shows the instruction information commands. Action is a command for robot movement such as “stand up,” “sit down,” and “walking start and stop.” Gait command is sent from the inclination and the rotation of the joystick. Coordinate of joystick and coordination basic locomotion are shown in

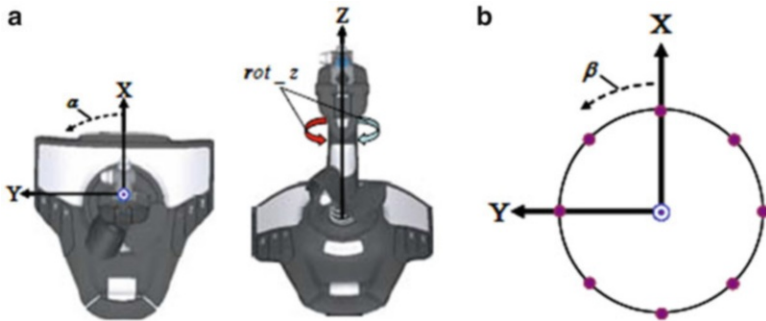


Fig. 8.7 Coordinate system of joystick

Fig. 8.7a, b, respectively. α represented the arbitrary crab angle and β for basic locomotion angle. The eight directions of basic locomotion angle β are selected using the joystick. rot_z is used for traverse angle command for body center in one cycle. The range of traverse angle is set as follows:

$$-10^\circ \leq \theta_{tb} \leq -0.125^\circ \quad (8.3)$$

$$0.125^\circ \leq \theta_{tb} \leq 10^\circ$$

In case of crab gait at arbitrary angle, θ_{tb} is set to the minimal value, and R_{ct} is set to the maximal value. On the other hand, θ_{ct} is derived by using Eq. (8.4):

$$\theta_{ct} = \alpha + \beta + \frac{\pi}{2} \quad (8.4)$$

In case of circular gait, the circular angle of body center is derived from rot_z which is set to θ_{tb} . R_{ct} is derived by using Eq. (8.5). If circle of radius $r_b = 1$, then θ_{ct} is derived by using Eq. (8.6)

$$R_{ct} = \frac{1}{\sqrt{2(1 - \cos \theta_{tb})}} \quad (8.5)$$

$$\theta_{ct} = \alpha + \beta + \gamma \quad (8.6)$$

However, γ is defined as follows:

$$-10^\circ \leq \theta_{tb} \leq -0.125^\circ \quad \gamma = -\frac{\pi}{2}$$

$$0.125^\circ \leq \theta_{tb} \leq 10^\circ \quad \gamma = \frac{\pi}{2}$$

The omnidirectional gait parameter is decided. Operation of the joystick does not change even if basic locomotion angle β is changed.

8.5 Ambient Environmental Image View of Robot

It is general to use camera installed on the rotation stage to obtain ambient environmental images of robot. However, this approach produces a mechanical time delay. Yamazawa et al. proposed a technique to generate arbitrary viewpoint image from omnidirectional image. On the other hand, Geyers et al. proposed a unifying model for geometry projection that induced by catadioptric sensors. In this research perspective, projection image is generated by omnidirectional image with reference to the technique proposed in [20–22]. As shown in Table 8.5, the mirror parameter of omnidirectional vision sensor is used. Detail configuration for this system is shown in Fig. 8.8. Digital video transfer system (DVTS) [23] is used to transmit an input digital video stream between navigation computer and teleoperation computer. With this technique perspective projection image is generated from omnidirectional frame data that is received.

Table 8.5 Parameters of hyperboloidal mirror

a	26.2 (mm)
b	35.4 (mm)
c	44.1 (mm)
Diameter of mirror	55.0 (mm)
Angle of elevation	15.0 (mm)
Angle of depression	50.0 (mm)

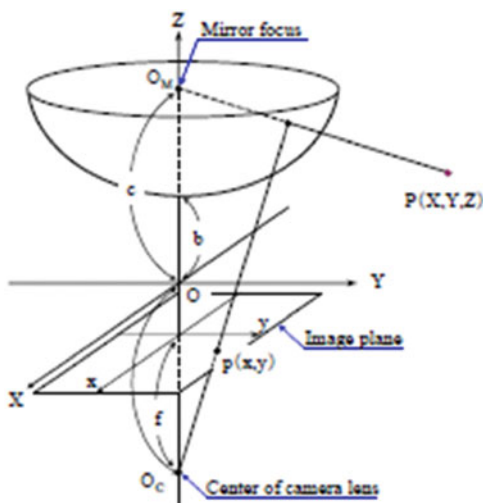


Fig. 8.8 Configuration of omnidirectional vision sensor

Central axis of a mirror that fits an optical axis of a camera is assumed. The direction where the angle of pan and tilt is set to 0° to make X axis and the origin of projection center coordination is $(0, 0)$:

$$\phi = -\text{pan}\left(\frac{\pi}{180}\right) \quad (8.7)$$

$$\theta = -\text{tilt}\left(\frac{\pi}{180}\right)$$

The spherical coordinates are derived by using pan, tilt angle, and focal length which is direction projection plane as against the sphere:

$$\begin{bmatrix} vx_i \\ vy_i \\ vz_i \end{bmatrix} = \begin{bmatrix} \cos \phi \cos \theta & -\sin \phi & \cos \phi \sin \theta \\ \sin \phi \cos \theta & \cos \phi & \sin \phi \sin \theta \\ -\sin \theta & 0 & \cos \theta \end{bmatrix} \begin{bmatrix} f \\ -x_i \\ -y_i \end{bmatrix} \quad (8.8)$$

$$r_i = \sqrt{vx_i^2 + vy_i^2 + vz_i^2} \quad (8.9)$$

$$\phi_{s,i} = \arctan\left(\frac{vy_i}{vx_i}\right) \quad (8.10)$$

$$\theta_{s,i} = \arctan\left(\frac{vz_i}{r_i}\right)$$

The coordinates that derived through Eqs. (8.7)–(8.10) are transformed to rectangular coordinates.

$$\begin{aligned} x_{s,i} &= \cos \phi_{s,i} \sin \theta_{s,i} \\ y_{s,i} &= \sin \phi_{s,i} \sin \theta_{s,i} \\ z_{s,i} &= \cos \theta_{s,i} \end{aligned} \quad (8.11)$$

Mirror parameter a is semimajor axis and mirror parameter b is semiminor axis. Semi-latus rectum is derived in Eq. (8.12):

$$\lambda = \frac{b^2}{a} \quad (8.12)$$

$$\epsilon = \sqrt{1 + \frac{a^2}{b^2}} \quad (8.13)$$

$$l = \frac{2\epsilon}{1 + \epsilon^2} \quad (8.14)$$

$$m = \frac{\mu - \varepsilon(\varepsilon\mu + 2\lambda - 2)}{1 + \varepsilon^2} \quad (8.15)$$

Parameters l and m is used in spherical projection that was derived from Eqs. (8.14) to (8.15). On the other hand, projection coordinates of hyperboloidal is calculated as Eqs. (8.16)–(8.17):

$$s = \frac{m - l}{z - l} \quad (8.16)$$

$$hx_i = sx_{s,i} \quad (8.17)$$

$$hy_i = sy_{s,i}$$

Finally, the pixel coordinate system is determined by using matrix K via Eq. (8.18). Furthermore, projection coordinates are calculated by Eq. (8.18). The values (358.1, 215.1) in the matrix K are XY coordinates of the center point in omnidirectional image:

$$K = \begin{bmatrix} 884.5 & 0 & 358.6 \\ 0 & 788.4 & 215.1 \\ 0 & 0 & 1 \end{bmatrix} \quad (8.18)$$

$$\begin{bmatrix} px_i \\ py_i \\ 1 \end{bmatrix} = K \begin{bmatrix} hx_i \\ hy_i \\ 1 \end{bmatrix} \quad (8.19)$$

Time-consuming factor on the system processing unit still becomes an issue because previous mentioned calculation method does similar process to all image pixels. Consequentially, it is difficult to present the smooth image operator. Therefore, the load of the calculation processing is reduced by using texture mapping. Onoe et al. have been using this method to evaluate the image processing cost, display delay, and warp of the image in order to generate the pseudo-perspective projection image from the omnidirectional image.

As shown in Fig. 8.9a, the lattice points were set to the image. Then the corresponding points in omnidirectional image as against lattice points were derived from Eqs. (8.7) to (8.18). The calculated corresponding points were transformed to texture coordinates as shown in Fig. 8.10. On the other hand, the lattice points were transformed to the coordinate system shown in Fig. 8.9b. The projection image forms omnidirectional image that is generated by parallelizing the lattice points with calculated corresponding points and using a texture mapping. Omnidirectional image and generated projection image are shown in Fig. 8.11. This system projection image is generated with a little warp by doing the calculation that increases the number of lattices.

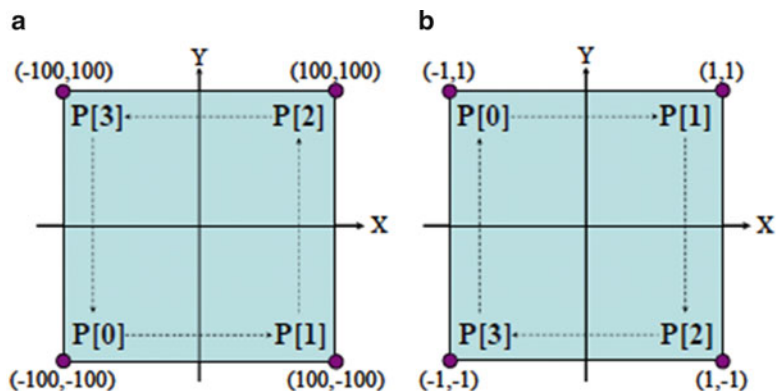


Fig. 8.9 Images of lattice points

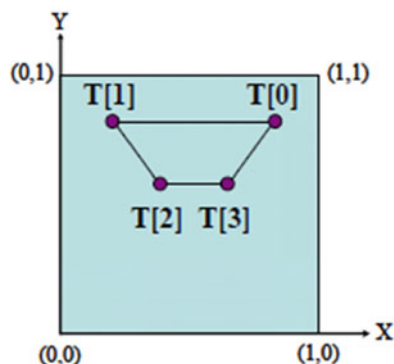


Fig. 8.10 The calculated points on texture coordinate system

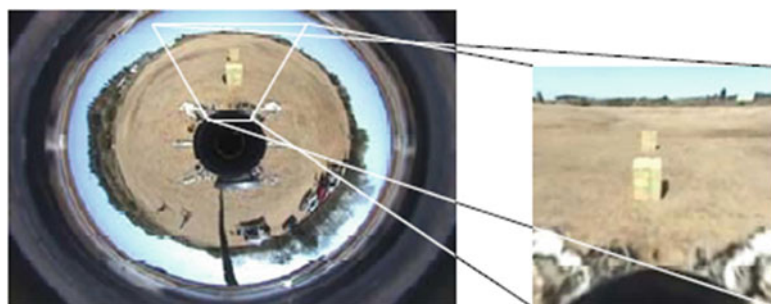


Fig. 8.11 Omnidirectional image and generated image

8.6 Robot Animation Using 3D Geometric Models and Sensor Data

The 3D COMET-IV online model is designed to predict the real-time movement of COMET-IV on the reality environment. Each sensor data is used for the robot 3D animation movement reference which is transmitted from locomotion computer on COMET-IV to teleoperation computer via wireless serial MODEM with data transfer rate 57,600 bps at 10 Hz.

Table 8.6 and Fig. 8.12 show the parameters used for robot 3D animation in virtual environment and coordinate system of 3D robot, respectively. Figure 8.13 shows the coordinate system of GPS. For initialization, received azimuth angle, XY value of GPS, and roll and pitch angle of the body are set up as default values. The robot is rotated using azimuth angle ψ including magnetic variation Δd with y -axis. After initialization, each part is expressed by using the homogeneous transformation matrix from Eqs. (8.20) to (8.25):

1. Each leg (foot–shank–thigh–shoulder)

[Foot]

$$T_1 = \text{Trans}(-P_{\text{foot_}i}) \text{Rot}(\theta_4, Z) \text{Trans}(P_{\text{foot_}i}) \quad (8.20)$$

Table 8.6 Parameters of using in 3D animation

Parameter	Signification
θ_{1_i}	Angle of shoulder (deg)
θ_{2_i}	Angle of thigh (deg)
θ_{3_i}	Angle of shank (deg)
θ_{4_i}	Angle of foot (deg)
λ	Body roll angle (deg)
ρ	Body pitch angle (deg)
ψ	Azimuth angle (deg)
GX	GPS X (m)
GY	GPS Y (m)
Δd	Magnetic variation (deg)
	Parameter used by initialization
ψ_{ini}	$\psi_{\text{ini}} = \psi$
σ_{ini}	$\sigma_{\text{ini}} = \sigma + \Delta d$
GX_{ini}	$GX_{\text{ini}} = GX$
GY_{ini}	$GY_{\text{ini}} = GY$
	Offset parameters
ψ_{offset}	$\psi_{\text{offset}} = \psi - \psi_{\text{ini}}$
GX_{offset}	$GX_{\text{offset}} = GX - GX_{\text{ini}}$
GY_{offset}	$GY_{\text{offset}} = GY - GY_{\text{ini}}$
	Each link position (XYZ) from the origin
$P_{\text{sho_}i}$	Shoulder X act YZ position
$P_{\text{th_}i}$	Thigh XYZ position
$P_{\text{sk_}i}$	Shank XYZ position
$P_{\text{foot_}i}$	Foot XYZ position

Fig. 8.12 Coordinate system of 3D

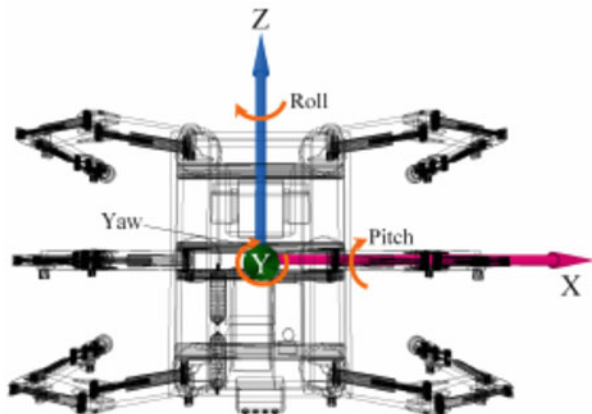
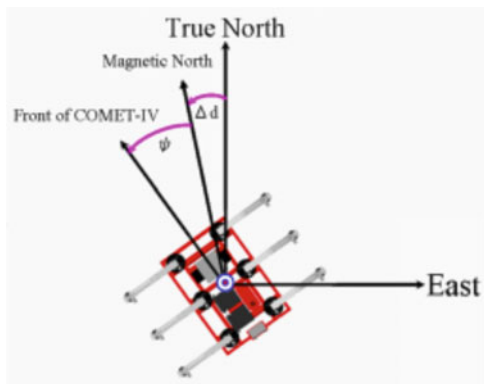


Fig. 8.13 Coordinate system of GPS



[Shank]

$$T_2 = \text{Trans}(-P_{\text{sk_}i}) \text{Rot}(\theta_3, Z) \text{Trans}(P_{\text{sk_}i}) \quad (8.21)$$

[Thigh]

$$T_3 = \text{Trans}(-P_{\text{th_}i}) \text{Rot}(\theta_2, Z) \text{Trans}(P_{\text{th_}i}) \quad (8.22)$$

[Shoulder]

$$T_4 = \text{Trans}(-P_{\text{sho_}i}) \text{Rot}(\theta_1, Z) \text{Trans}(P_{\text{sho_}i}) \quad (8.23)$$

2. Robot body

$$T_5 = \text{Rot}(\lambda, Z)\text{Rot}(\rho, X)\text{Rot}(\phi_{\text{offset}}, Y) \quad (8.24)$$

$$T_6 = \text{Trans}(GY_{\text{offset}}, 0, GX_{\text{offset}}) \quad (8.25)$$

where

$$\text{Trans}(x, y, z) = \begin{bmatrix} 1 & 0 & 0 & 0 \\ 0 & 1 & 0 & 0 \\ 0 & 0 & 1 & 0 \\ x & y & z & 1 \end{bmatrix}$$

$$\text{Rot}(\theta, X) = \begin{bmatrix} 1 & 0 & 0 & 0 \\ 0 & \cos \theta & \sin \theta & 0 \\ 0 & -\sin \theta & \cos \theta & 0 \\ 0 & 0 & 0 & 1 \end{bmatrix}$$

$$\text{Rot}(\theta, Y) = \begin{bmatrix} \cos \theta & 0 & -\sin \theta & 0 \\ 0 & 1 & 0 & 0 \\ \sin \theta & 0 & \cos \theta & 0 \\ 0 & 0 & 0 & 1 \end{bmatrix}$$

$$\text{Rot}(\theta, Z) = \begin{bmatrix} \cos \theta & \sin \theta & 0 & 0 \\ -\sin \theta & \cos \theta & 0 & 0 \\ 0 & 0 & 1 & 0 \\ 0 & 0 & 0 & 1 \end{bmatrix}$$

Equation (8.26) shows all the homogeneous transformation matrix of robot:

$$T_{\text{all}} = T_1 T_2 T_3 T_4 T_5 T_6 \quad (8.26)$$

The movement of the robot can be expressed by doing the homogeneous transformation mentioned above.

8.7 Experiment

Outdoor experiment was done to verify the designed system mentioned in previous sections. The experiment was done by constructing the COMET-IV walking to avoid two obstacles using designed teleoperation assistant system. Tripod gait pattern was set for this experiment with proportional, integral, and derivative (PID) control as position controller. The leg locomotion cycle time is set to 16 s.

Fig. 8.14 Experimental result of obstacle

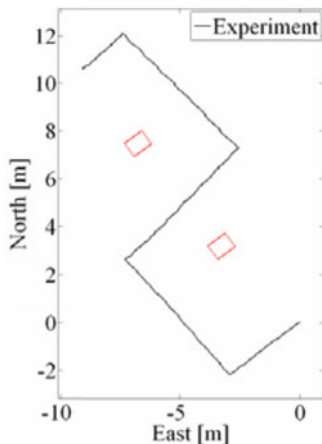
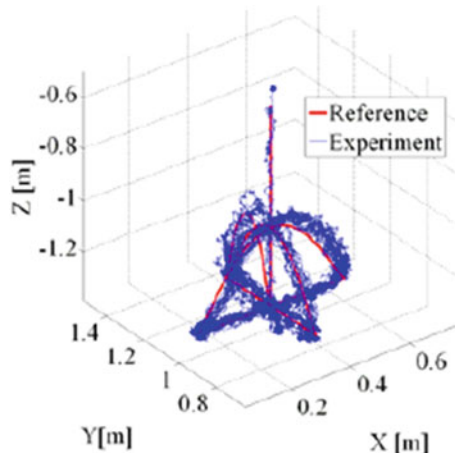


Fig. 8.15 Leg 1 foot trajectory of avoidance walking test



Two obstacles were arranged at position which is operator can not comprehend with sense of the distance. The distance between the obstacle and robot measured beforehand made a virtual obstacle object on the screen and gave an ideal environment. Furthermore, the number of lattices used for omnidirectional image conversion was set as 16×12 . Magnetic variation was $6^{\circ}50'$ in experimental environment. The actual walking trajectory acquired by GPS and the foot trajectory of Leg1 are shown in Figs. 8.14 and 8.15, respectively. The COMET-IV successfully avoided the designed obstacle with the designed teleoperation control (Fig. 8.16). The operator was able to control the robot avoiding two obstacles by operating the robot while confirming the image and the robot 3D animation in real time as shown in Fig. 8.17 and Fig. 8.18.



Fig. 8.16 Photos of the obstacle avoidance walking test



Fig. 8.17 Images of 3D animation

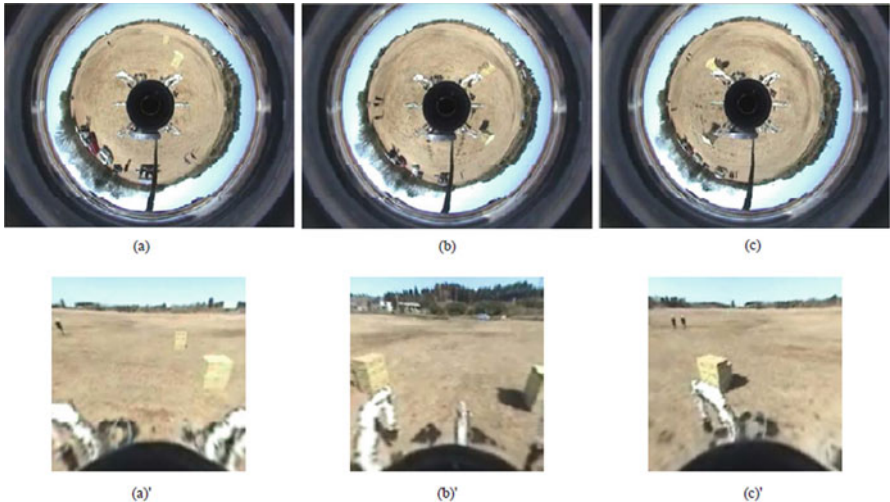


Fig. 8.18 Omnidirectional images and generated projection images

8.8 COMET-IV 3D Simulator Modeling

In COMET-IV simulator design, 3D geometric model and numerical walking generation/control model are prepared separately due to implementation issue. Previously 3D geometric model is successfully implemented in real-time teleoperation control for COMET-IV in outdoor environment walking [17]. As a next step, this 3D model is upgraded for indoor simulation used with SIMULINK

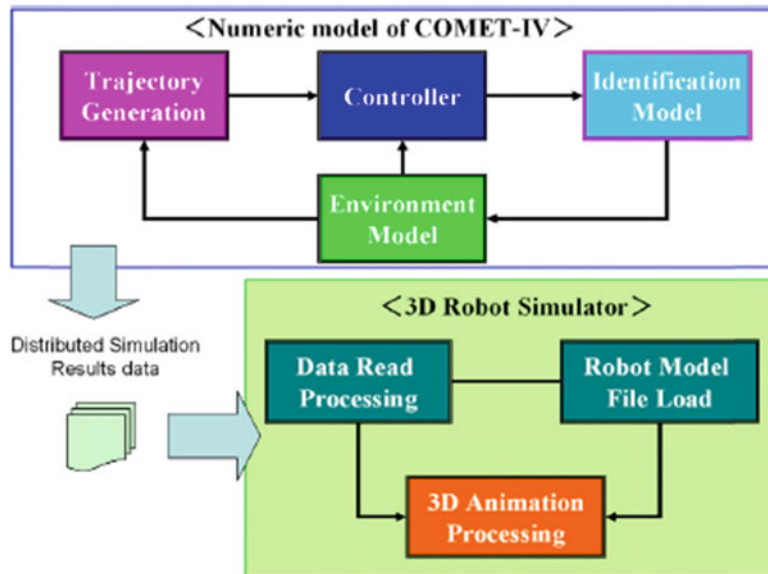


Fig. 8.19 COMET-IV 3D simulator system configuration

program via API method. This upgrading is due to the current issue of COMET-IV research which is focused on force-based controlled walking trajectory. This walking method needs some verification especially on design of the force control. Force control used minimum and maximum pushing during walking ($F \geq 1\text{ kN}$). Therefore, it is too risky and dangerous to directly test this kind of heavy robot with some kind of algorithms such as controller algorithms if the unbalanced or system error occurred during experiment period. The overall model of COMET-IV simulator using 3D geometric is shown as Fig. 8.19. The foot trajectory generation algorithms, the forward and inverse kinematics, control system algorithms, and the identification model of leg are included in numerical model designed in MATLAB / SIMULINK where sampling time is 10 ms. In this section only tripod walking pattern algorithm model is described. This pattern of walking is considered as a stable regular experience. As shown in Fig. 8.19, all executed data from numerical model is downloaded to the 3D geometric model for visualization to motion.

8.8.1 Walking Trajectory Modeling

In force-based walking of view, this trajectory is designed to make sure that the leg trails environment when the body is pushed after a play leg contacted with the ground. In addition, the walk trajectory of the play leg must not follow the targeted

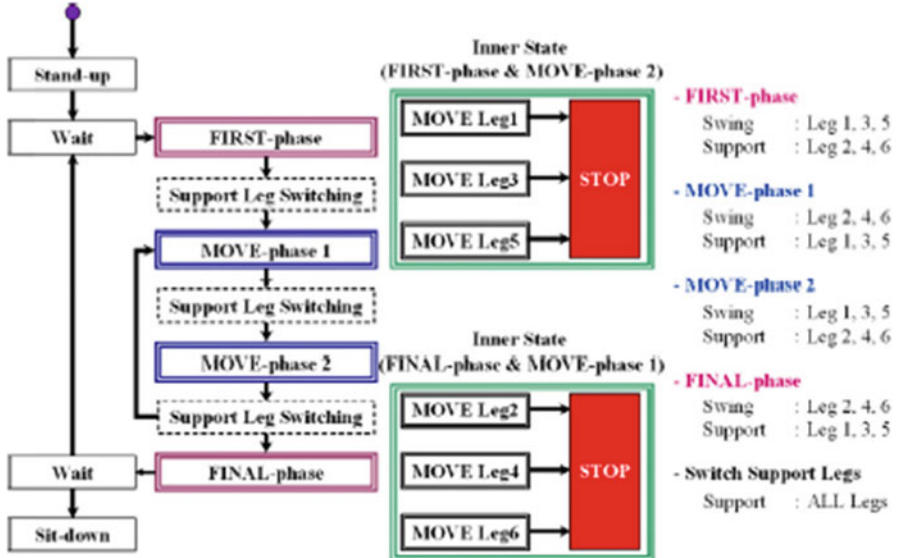


Fig. 8.20 State flow of compliant COMET-IV force-based tripod walking locomotion

value change in the x -axis and y -axis direction after grounding time because a restriction direction of the force control is only on z -axis direction.

The second restriction will be on the environment point of view. It is very important to make sure that foots follow the terrain shape/pattern during walking time. As shown as Fig. 8.20, four phases of walking flows have been designed for compliant tripod walking pattern in this trajectory to perform the restriction mentioned. The trajectory x -, y -, and z -axis is designed and generated based on the shoulder coordinate system. In this design two groups (Leg 1, 3, and 5 and Leg 2, 4, and 6) of leg have been identified which is designed to sequentially change due to the based trajectory as shown in Fig. 8.20. Figure 8.21 shows the plot of COMET-IV walking trajectory from y -axis versus z -axis coordination. Initial foot positions on shoulder coordinate system in each walking phase are shown as follows:

$$\begin{bmatrix} X_{ini_i} \\ Y_{ini_i} \\ Z_{ini_i} \end{bmatrix}_{\text{FIRST-phase}} = \begin{bmatrix} X_{fs_i} \\ Y_{fs_i} \\ Z_{fs_i} \end{bmatrix}_{\text{STAND-UP}}$$

$$\begin{bmatrix} X_{ini_i} \\ Y_{ini_i} \\ Z_{ini_i} \end{bmatrix}_{\text{MOVE-phase1}} = \begin{bmatrix} X_{fs_i} \\ Y_{fs_i} \\ Z_{fs_i} \end{bmatrix}_{\text{FIRST-phase/MOVE-phase2}}$$

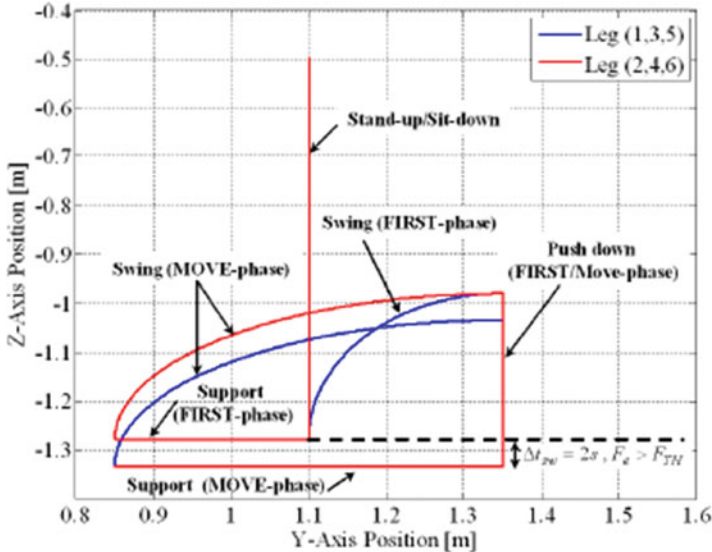


Fig. 8.21 Example of foot trajectory on shoulder coordinate system

$$\begin{bmatrix} X_{\text{ini},i} \\ Y_{\text{ini},i} \\ Z_{\text{ini},i} \end{bmatrix}_{\text{MOVE-phase2}} = \begin{bmatrix} X_{fs,i} \\ Y_{fs,i} \\ Z_{fs,i} \end{bmatrix}_{\text{MOVE-phase1}}$$

$$\begin{bmatrix} X_{\text{ini},i} \\ Y_{\text{ini},i} \\ Z_{\text{ini},i} \end{bmatrix}_{\text{FINAL-phase}} = \begin{bmatrix} X_{fs,i} \\ Y_{fs,i} \\ Z_{fs,i} \end{bmatrix}_{\text{MOVE-phase2}}$$

The foot trajectory equations for Leg 2, 4, and 6 are expressed as Eqs. (8.27)–(8.32) where equations of Leg 1,3, and 5 are omitted due to the mirror form of Leg 2, 4, and 6 equations.

【First phase】

<Time (support phase) for center of gravity (CoG)> $0 \leq t \leq \frac{T_c}{2}$

$$\begin{aligned} X_{fs,i}(t) &= X_{\text{ini},i} + \frac{S}{4} \left(\frac{t}{T_c/2} - \frac{1}{2\pi} \sin 2\pi \frac{t}{T_c/2} \right) \cos \theta_i \\ Y_{fs,i}(t) &= Y_{\text{ini},i} + \frac{S}{4} \left(\frac{t}{T_c/2} - \frac{1}{2\pi} \sin 2\pi \frac{t}{T_c/2} \right) \sin \theta_i \\ Z_{fs,i}(t) &= Z_{\text{ini},i} \end{aligned} \quad (8.27)$$

【Move—phase 1】

<Time during swing> $0 \leq t \leq \frac{T_c}{4}$

$$\begin{aligned} X_{fs_i}(t) &= X_{ini_i} + \frac{S}{2} \left(1 - \cos\left(\frac{1}{T_c/2}t\right) \right) \cos \theta_i \\ Y_{fs_i}(t) &= Y_{ini_i} + \frac{S}{2} \left(1 - \cos\left(\frac{1}{T_c/2}t\right) \right) \sin \theta_i \\ Z_{fs_i}(t) &= Z_{ini_i} + H \sin\left(\frac{\pi}{T_c/2}t\right) \end{aligned} \quad (8.28)$$

<Time during push down to ground> $\frac{T_c}{4} \leq t \leq \frac{T_c}{2} + 2$

$$\begin{aligned} X_{fs_i}(t) &= X_{fs_i} \left(\frac{T_c}{4} - T_s \right) \\ Y_{fs_i}(t) &= Y_{fs_i} \left(\frac{T_c}{4} - T_s \right) \\ Z_{fs_i}(t) &= Z_{fs_i} \left(\frac{T_c}{4} - T_s \right) + H \sin\left(\frac{t - T_c/4}{T_c/4}\right) \end{aligned} \quad (8.29)$$

【Move—phase 2】

<Time (support phase) for CoG> $0 \leq t \leq \frac{T_c}{2} - 1$

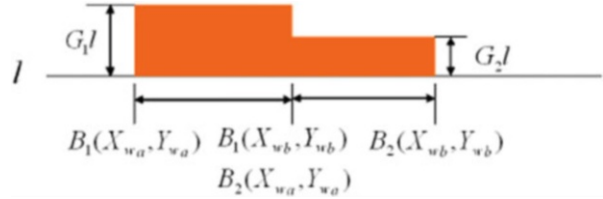
$$\begin{aligned} X_{fs_i}(t) &= X_{ini_i} - S \left(\frac{t}{T_c - 2} \right) \cos \theta_i \\ Y_{fs_i}(t) &= Y_{ini_i} - S \left(\frac{t}{T_c - 2} \right) \sin \theta_i \\ Z_{fs_i}(t) &= Z_{ini_i} \end{aligned} \quad (8.30)$$

【Final phase】

<Time during swing> $0 \leq t \leq \frac{T_c}{4}$

$$\begin{aligned} X_{fs_i}(t) &= X_{ini_i} + \frac{S}{4} \left(1 - \cos\left(\frac{\pi}{T_c/2}t\right) \right) \cos \theta_i \\ Y_{fs_i}(t) &= Y_{ini_i} + \frac{S}{4} \left(1 - \cos\left(\frac{\pi}{T_c/2}t\right) \right) \sin \theta_i \\ Z_{fs_i}(t) &= Z_{ini_i} + H \sin\left(\frac{\pi}{T_c/2}t\right) \end{aligned} \quad (8.31)$$

Fig. 8.22 Illustration of terrain function



<Time during push down to ground> $\frac{T_c}{4} \leq t \leq \frac{T_c}{2} + 2$

$$\begin{aligned} X_{fs-i}(t) &= X_{fs-i} \left(\frac{T_c}{4} - T_s \right) \\ Y_{fs-i}(t) &= Y_{fs-i} \left(\frac{T_c}{4} - T_s \right) \\ Z_{fs-i}(t) &= Z_{fs-i} \left(\frac{T_c}{4} - T_s \right) + H \sin \left(\frac{t - T_c/4}{T_c/4} \right) \end{aligned} \quad (8.32)$$

where T_c is walking cycle time, t is update time, S is distance of movement of CoG at one cycle, H is height of leg rising from initial position, and θ is walking direction angle of robot on the shoulder coordinate reference.

8.8.2 Environment Modeling

On force-based walking, environment model is important in order to estimate the dynamic moment of ground as a feedback force on each foot placement. On the other hand, the level of height environment is also important to validate the walking algorithm to face the uncertainty environment. In this research, body movement coordination (BMC) method has been used to generate the desired ground terrain level as shown in Fig. 8.22 and expressed as Eq. (8.33):

$$L_e(i) = \sum_{\substack{k=x_{wb}y_{wb} \\ k=x_{wa}y_{wa}}}^{k=x_{wb}y_{wb}} G_i l \quad (8.33)$$

where i is leg number and G_i is weight coefficient to the common flat terrain at $l = -1.28$ m from thigh potentiometer point. $B_n(X_{wa}, Y_{wa})$ and $B_n(X_{wb}, Y_{wb})$ are XY values on world coordinate system. n is terrain block number. Proposed BMC is used for the robot position (X_{fs-i} , Y_{fs-i} , Z_{fs-i}) of each leg on the shoulder coordinate system and is derived via reverse kinematics based on each joint angle from the leg identification model. Table 8.7 shows the shoulder XY position of each leg on body

Table 8.7 Shoulder XY position on body coordinate system

Leg no.	X _{sh}	Y _{sh}
1	0.95	0.55
2	0.00	0.55
3	-0.95	0.55
4	0.95	-0.55
5	0.00	-0.55
6	-0.95	-0.55

coordinate system. The foot position (X_{fb_i} , Y_{fb_i} , Z_{fb_i}) on BMC method is derived from Eqs. (8.34) to (8.40):

$$\begin{bmatrix} X_{fs_i} \\ Y_{fb_i} \\ Z_{fb_i} \\ 1 \end{bmatrix} = \begin{bmatrix} 1 & 0 & 0 & X_{sh_i} \\ 0 & 1 & 0 & Y_{sh_i} \\ 0 & 0 & 1 & 0 \\ 0 & 0 & 0 & 1 \end{bmatrix} \begin{bmatrix} \alpha X_{fs_i} \\ \alpha Y_{fs_i} \\ Z_{fs} \\ 1 \end{bmatrix} \quad (8.34)$$

where

$$\alpha = \begin{cases} 1 & i = 1, 2, 3 \\ -1 & i = 4, 5, 6 \end{cases}$$

The foot position (X_{fw_i} , Y_{fw_i} , Z_{fw_i}) on world coordinate system is derived as follows:

$$\begin{bmatrix} X_{fw_i} \\ Y_{fw_i} \\ Z_{fw_i} \\ 1 \end{bmatrix} = \begin{bmatrix} 1 & 0 & 0 & \vec{X} \\ 0 & 1 & 0 & \vec{Y} \\ 0 & 0 & 1 & 0 \\ 0 & 0 & 0 & 1 \end{bmatrix} \begin{bmatrix} -Y_{fb_i} \\ X_{fs_i} \\ Z_{fb_i} \\ 1 \end{bmatrix} \quad (8.35)$$

where X and Y are body center XY position on world coordinate system. The small displacement ΔP_i of each leg is calculated from Eqs. (8.36) to (8.37):

$$\begin{bmatrix} \alpha X_{fs_i} \\ \alpha Y_{fs_i} \end{bmatrix} = \begin{bmatrix} \cos \phi & -\sin \phi \\ \sin \phi & \cos \phi \end{bmatrix} \begin{bmatrix} X_{fs_i} \\ Y_{fs_i} \end{bmatrix} \quad (8.36)$$

$$\Delta P_i = \begin{bmatrix} \Delta X_i \\ \Delta Y_i \end{bmatrix} = \left[\begin{bmatrix} \alpha X_{fs_i} \\ \beta X_{fs_i} \end{bmatrix} \right]_t^{t-1} \quad (8.37)$$

where

$$\alpha = \begin{cases} 1 & i = 1, 2, 3 \\ -1 & i = 4, 5, 6 \end{cases} \quad \beta = \begin{cases} 1 & i = 4, 5, 6 \\ -1 & i = 1, 2, 3 \end{cases}$$

Therefore, the small displacement (ΔX_i , ΔY_i) of the body movement of Leg 1, 3, and 5 and Leg 2, 4, and 6 in support phase is derived as Eqs. (8.38)–(8.39):

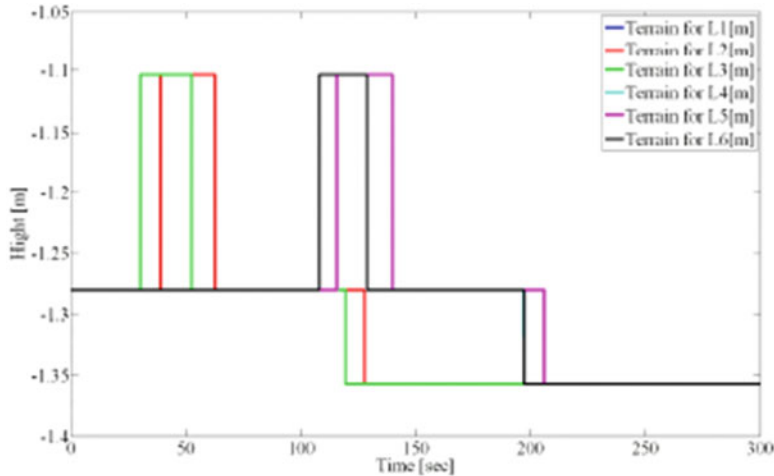


Fig. 8.23 Example of terrain signal generation in SIMULINK numerical model simulation

$$(\Delta \vec{X}_{135}, \Delta \vec{Y}_{135}) = \frac{\Delta P_1 + \Delta P_3 + 2\Delta P_5}{4} \quad (8.38)$$

$$(\Delta \vec{X}_{462}, \Delta \vec{Y}_{462}) = \frac{\Delta P_4 + \Delta P_6 + 2\Delta P_2}{4} \quad (8.39)$$

A body center XY position (X, Y) on world coordinate system can be obtained by integrating the small displacement of body movement. Therefore, terrain signal is generated with the following conditions and used to estimate the foot reaction force:

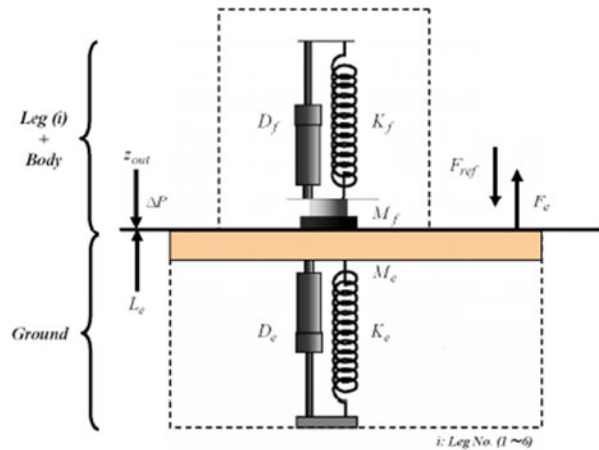
$$P_1 : X_{wa,j} \leq X_{fw,j} \leq X_{wb,j}, P_2 : Y_{wa,j} \leq Y_{fw,j} \leq Y_{wb,j}, P_1 \cap P_2 \Rightarrow L_e(i) \quad (8.40)$$

The example of the terrain signal of each leg for tripod walking pattern from numerical model is shown in Fig. 8.23. The 3D visual view will be described in the next section.

8.8.3 Control System Modeling

In control system module, two levels of controller, outer controller and inner controller, have been set for COMET-IV in order to provide better force and position control on each leg. Previously, many researches have been done on providing better position control which only considered the state error of shoulder, thigh, shank, and foot output signal. In other words the research only focused on inner loop of the system. The focus on control system research progress for

Fig. 8.24 COMET-IV controller hierarchy



COMET-IV is changed after considering the force-based walking. The previous method is only considered on inner loop of the system, not enough to provide better force delivery on each foot of COMET-IV especially on facing the rough terrain environment. Previously [18] start considering the force-based walking control by proposing the hybrid position/force/attitude control. Most of the progressed force-based walking is successfully done on the flat terrain but not very good on facing the rough terrain. The main focus on this part of the research is to provide body balance which is sufficient for each foot placement.

Therefore, the COMET-IV with force-based walking is designed with the particular impedance control. As shown in Fig. 8.24, this impedance control is designed as indirect force control method for each leg of COMET-IV which is considered both position and force control. Inner controller is still needed and playing an important role on giving very small state error shaping on each joint position outputs compared to the trajectory (references). The impedance controller on the other hand is considered as outer controller which will provide the “virtual spring” on each foot placement with some tuning. This outer controller is based on the mass spring equilibrium equation which is expressed as Eq. (8.41):

$$F_{ref} - F_e = E_f = M_f \Delta \ddot{z} + D_f \Delta \dot{z} + K_f \Delta z \quad (8.41)$$

where

$$F_e = D_e \Delta \dot{P} + K_e \Delta P \quad (8.42)$$

Both Eqs. (8.41) and (8.42) are obtained by second-order equation form by environment and movement of each foot as shown in Fig. 8.25. Basically, impedance controller needs to be derived from the kinematics of the system that needs to be applied. For COMET-IV system, z -axis on foot is the part that needs to be applied with impedance controller. As shown in Fig. 8.25, three coefficients, M_f , D_f , and K_f , represented the designed parameters that effect the moment of foot placement. Therefore, the impedance controller output for COMET-IV can be derived

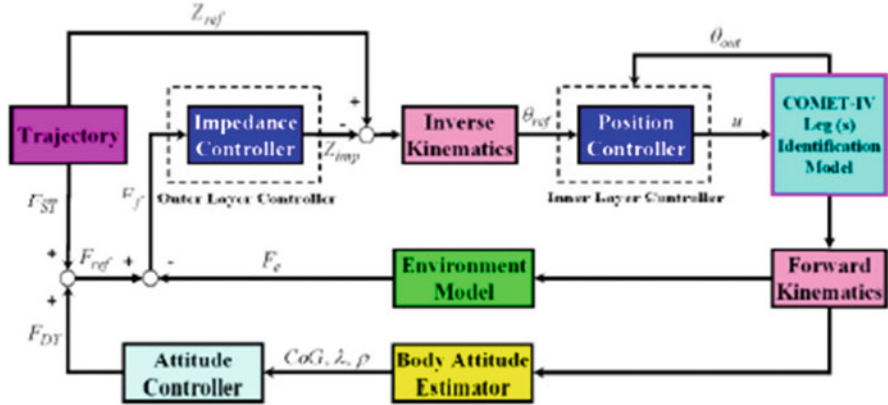


Fig. 8.25 Second-order model between environment and impedance controlled on robot foot

from the current vertical position changes of z -axis for each COMET-IV leg during walking phases:

$$\Delta z = z_{out} - z_{ref}$$

Thus,

$$\Delta \dot{z} = \frac{\Delta z_v - \Delta z_{v-1}}{T_s} \quad (8.43a)$$

$$\Delta \ddot{z} = \frac{\Delta \dot{z}_v - \Delta \dot{z}_{v-1}}{T_s} \quad (8.43b)$$

where

$$\Delta \dot{z}_{v-1} = \frac{\Delta z_{v-1} - \Delta z_{v-2}}{T_s} \quad (8.43c)$$

Then by substituting Eq. (8.43a–8.43c) to Eq. (8.41) and after long mathematical calculations, the impedance vertical position of each COMET-IV leg can be expressed as Eq. (8.44):

$$Z_{imp} = \frac{E_f T_s^2 + M_f (2\Delta z_{v-1} - \Delta z_{v-2}) + D_f \Delta z_{v-1} T_s}{M_f + D_f T_s + K_f T_s^2} \quad (8.44)$$

The damping ratio of the moment equation in Eq. (8.41) can be expressed as Eq. (8.45):

$$\varsigma = \frac{D_f + D_e}{2\sqrt{M_f(K_f + K_e)}} \quad (8.45)$$

External force or force from environment linear elastic model is expressed in Eq. (8.42), where F_e is expressed as another model that counters back to the foot elastic model. The moment force of environment model is dependent on the error changes of the level terrain, $\Delta P = z_{\text{out}} - L_e$ and both natural damping, D_e and natural stiffness, and K_e of environment which is unknown. In this calculation, mass of the ground or terrain and foot system is considered as equal, $M_f = M_e$. In order to achieve critically damped state, $\zeta = 1$, the damping coefficient of the controller can be calculated via Eq. (8.47):

$$D_f = 2\sqrt{M_f(K_f + K_e)} - D_e \quad (8.46)$$

Therefore, any changes of D_e and K_e eventually are proportional to D_f determination. By substituting Eqs. (8.47) to (8.44), the impedance can be controlled by designed parameter. The other part of outer controller is attitude controller. This controller is currently indirectly input to the dynamic force reference, FDY which is sumwith the static force, FST , for each foot force reference [18]. Furthermore, this controller is currently using the linear quadratic regulation (LQR) method to control the CoG of body height state error, roll (λ) state error, and pitch (ρ) state error1.

8.8.4 3D Geometric Modeling

In this part, the 3D geometric model of COMET-IV was designed using 2-dimensional computer-aided drawing (2D-CAD) and actual measurement value with 3D modeling software [19]. In order to achieve the operation by each joint, the 3D model is divided into several parts (robot body and each link) and composed of various layers. In this system, the access to each part of the 3D model data is achieved by using the library (obj2.LIB) [19]. This 3D robot simulator is based on graphic user interface (GUI), and it is a combination of graph function, data display function, and robot walking animation function. The OpenGL is adopted as an API for the 3D graphics processing. The “KISMET 3D Simulation Software [24],” “FlexSim [25],” and “Three Dim Sim mechanics simulator [26]” are known as the commercial and academic 3D simulators. These simulators have achieved the multibody-system dynamics simulation and kinematics simulation with complex mechanisms in the virtual environment and been applied to various fields. On the other hand, the numerical of the robot is separated as another system from developed 3D robot simulator. Therefore, this 3D simulator is a simple structure and it is possible to use it as a means to understand the movement of the robot in the robot teleoperation.

All data which are contained of 3D robot model and simulation results data from numerical simulation model using SIMULINK are read and stored in the virtual environment. Each 3D model part is transformed by using the angle of the corresponded joints. The homogeneous transformation matrix to each part model is expressed from Eqs. (8.47) to (8.55). The transformation is based on coordinate system designed in 3D geometric model as shown in Fig. 8.26 (Table 8.8).

Fig. 8.26 3D geometric model coordinate system

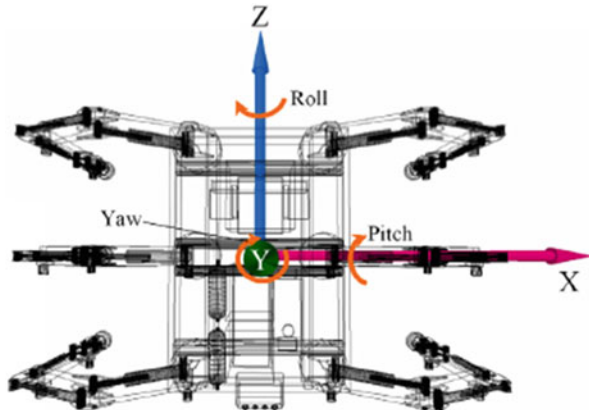


Table 8.8 Parameters used in 3D geometric model

Parameter	Signification
$\theta_{1,i}$	Angle of shoulder (deg)
$\theta_{2,i}$	Angle of thigh (deg)
$\theta_{3,i}$	Angle of shank (deg)
$\theta_{4,i}$	Angle of foot (deg)
λ	Roll angle (deg)
ρ	Pitch angle (deg)
φ	Yaw angle (deg)
X_{cw}	Body center X (m)
Z_{cw}	Body center Z (m)
H_{body}	Body height (m)
P_{sho_i}	Shoulder potentiometer XYZ initial position
P_{th_i}	Thigh potentiometer XYZ initial position
P_{sk_i}	Shank potentiometer XYZ initial position
P_{foot_i}	Foot potentiometer XYZ initial position
$Base_T_Z$	Base ground position
Z_{ft_i}	Foot Z position on shoulder coordinate
T_{offset}	Distance from thigh's potentiometer to body base

1. Link parts (foot–shank–thigh–shoulder)

<Foot part>

$$M_{1,i} = \text{Trans}(-P_{foot_i}) \text{Rot}(\theta_{4,i}) \text{Trans}(P_{foot_i}) \quad (8.47)$$

<Shank part>

$$M_{2,i} = \text{Trans}(-P_{shk_i}) \text{Rot}(\theta_{3,i}) \text{Trans}(P_{shk_i}) \quad (8.48)$$

<Thigh part>

$$M_{3,i} = \text{Trans}(-P_{th_i}) \text{Rot}(\theta_{2,i}) \text{Trans}(P_{th_i}) \quad (8.49)$$

<Shoulder part>

$$M_{4_i} = \text{Trans}(-P_{\text{sho_}i}) \text{Rot}(\theta_{1_i}) \text{Trans}(P_{\text{sho_}i}) \quad (8.50)$$

2. Body part

$$M_5 = \text{Rot}(\lambda, Z) \text{Rot}(\rho, X) \text{Rot}(\varphi, Y) \quad (8.51)$$

$$M_6 = \text{Trans}(X_{cw}, H_{\text{body}}, Z_{cw}) \quad (8.52)$$

where H_{body} is derived as follows:

$$\text{Base_}T_z = \text{Max}(Z_{fs_all}) \quad (8.53)$$

$$H_{\text{body}} = \text{Base_}T_z - T_{\text{offset}} \quad (8.54)$$

where $Z_{fs_all} = (|Z_{fs_1}|, |Z_{fs_2}|, \dots, |Z_{fs_6}|)$

Therefore, all homogeneous transformation matrix of robot is shown as Eq. (8.55):

$$M_{\text{all}} = M_{1_i} M_{2_i} M_{3_i} M_{4_i} M_5 M_6 \quad (8.55)$$

$$\text{Trans}(x, y, z) = \begin{bmatrix} 1 & 0 & 0 & 0 \\ 0 & 1 & 0 & 0 \\ 0 & 0 & 1 & 0 \\ x & y & z & 1 \end{bmatrix}$$

$$\text{Rot}(\theta, X) = \begin{bmatrix} 1 & 0 & 0 & 0 \\ 0 & \cos \theta & \sin \theta & 0 \\ 0 & -\sin \theta & \cos \theta & 0 \\ 0 & 0 & 0 & 1 \end{bmatrix}$$

$$\text{Rot}(\theta, Y) = \begin{bmatrix} \cos \theta & 0 & -\sin \theta & 0 \\ 0 & 1 & 0 & 0 \\ \sin \theta & 0 & \cos \theta & 0 \\ 0 & 0 & 0 & 1 \end{bmatrix}$$

$$\text{Rot}(\theta, Z) = \begin{bmatrix} \cos \theta & \sin \theta & 0 & 0 \\ -\sin \theta & \cos \theta & 0 & 0 \\ 0 & 0 & 1 & 0 \\ 0 & 0 & 0 & 1 \end{bmatrix}$$

Table 8.9 Terrain interface data list

Parameter	Signification
$H_{\text{obj_}n}$	Height of terrain object (m)
$W_{\text{obj_}n}$	Width of terrain object (m)
$L_{\text{obj_}n}$	Length of terrain object (m)
TX_{w_n}	Terrain object X position
TY_{w_n}	Terrain object Y position
TZ_{w_n}	Terrain object Z position

n : terrain block number

The terrain interface data from numerical model via SIMULINK is used to reproduce the terrain environment in 3D geometric model. Vertices and planes of object can be derived by using the parameters ($H_{\text{obj_}n}$, $W_{\text{obj_}n}$, $L_{\text{obj_}n}$) of the terrain block (see Table 8.9). The normal vector that is appropriately set to the plane is derived and the terrain block is generated as quadrangle object in virtual environment. The following transformation is done by using the terrain block location information after the object is generated:

$$M_{\text{terrain_}n} = \text{Trans}(TX_{w_n}, TY_{w_n}, TZ_{w_n}) \quad (8.56)$$

The object generation and the geometric transformation are then repeated according to the number of terrain blocks. Finally the constructed scene is processed by graphics processing and output to the display. The walking motion animation of the COMET-IV in the virtual environment is achieved by the continuous graphics processing that used the transferred data from numerical model. The detail flow of data processing between numerical model and 3D geometric model can be seen in Fig. 8.27, and example of 3D robot simulation running is shown in Fig. 8.28.

8.9 Modeling Verification

In order to verify the designed COMET-IV simulator, a simple experiment has been done to match with the simulation results from numerical model and 3D geometric model visualization. The planning of terrain has been designed using numerical model in SIMULINK and views in 3D geometric model as shown in Fig. 8.29. In this running, walking simulation is done with the PID controller and impedance controller described in Sect. 8.8.3. Two blocks (Step1: 6 cm, Step2: 12 cm) with different height are arranged in the virtual environment as shown in Fig. 8.29. The leg locomotion cycle time was set to $T_c = 16$ s. Distance of movement of CoG at one cycle and height of leg rising from initial position are set to $S = 0.8$ m and $H = 0.3$ m, respectively. Each leg trajectory on world coordinate system (numerical model simulation results) and walking animation images in 3D robot simulator are shown in Figs. 8.32a and 8.30, respectively. It can be confirmed that foot trajectory corresponding to the vertical interval of the step is generated. In addition the change of the CoG, height was able to be expressed in the virtual environment.

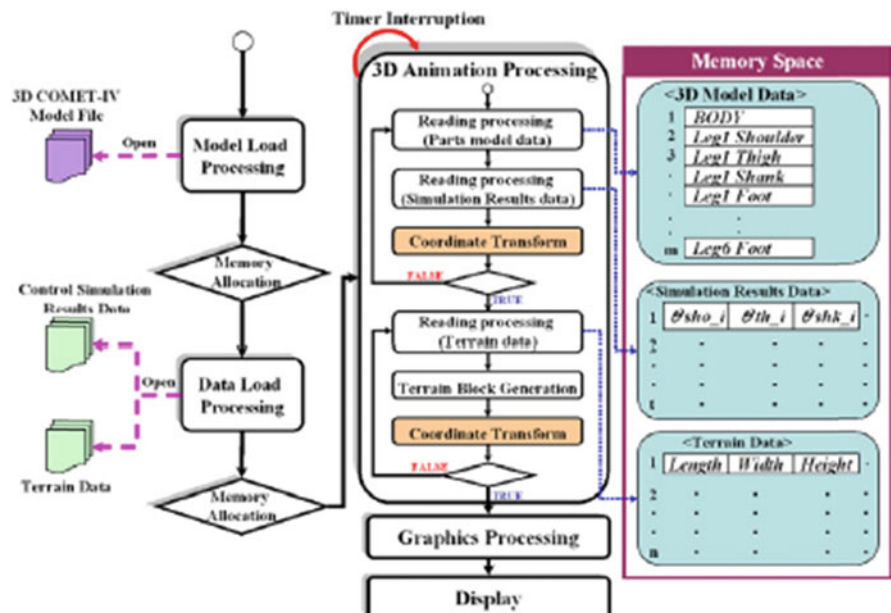


Fig. 8.27 COMET-IV 3D simulator compilation

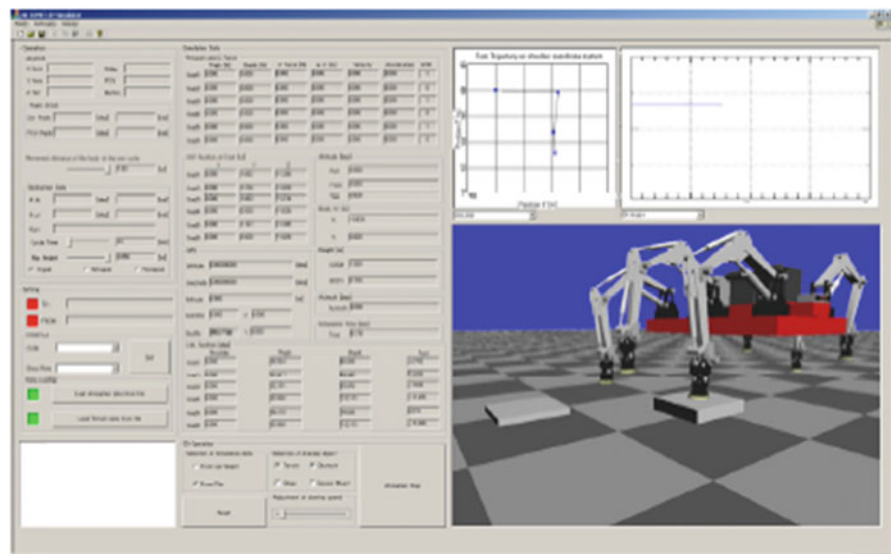


Fig. 8.28 Display image of 3D robot simulation running

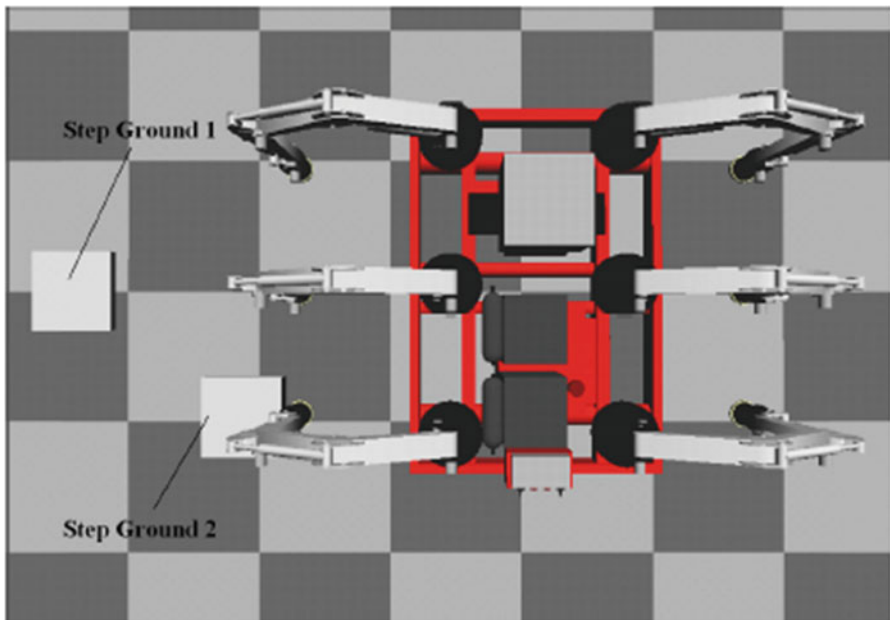


Fig. 8.29 Terrain environment image in simulation

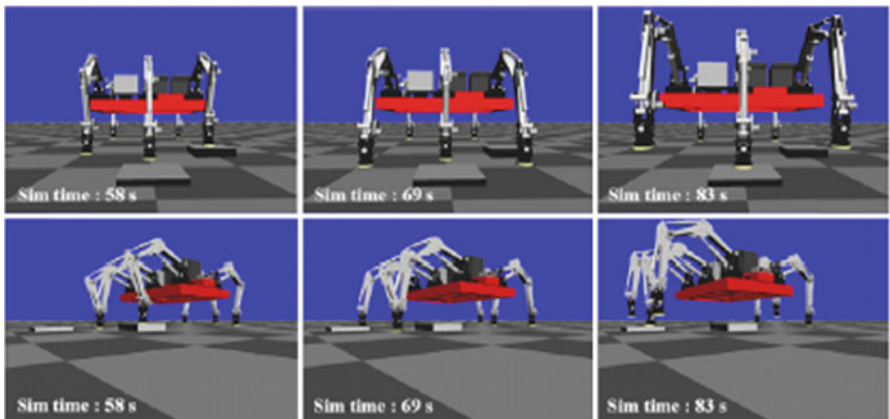


Fig. 8.30 Walking animation images in 3D robot simulation

The same situation is set in the real experiment. As shown in Figs. 8.30 and 8.31, the movement and posture of COMET-IV are nearly same as simulated in 3D geometric model. Furthermore, the similarity of world coordinate system for each foot and body height also can be seen and compared in Fig. 8.32a, b. In this comparison, friction and slipping problem in experiment running was ignored. Moreover, currently a part of the leg of the real robot has bending and distortion.



Fig. 8.31 Overview of step walking experiment

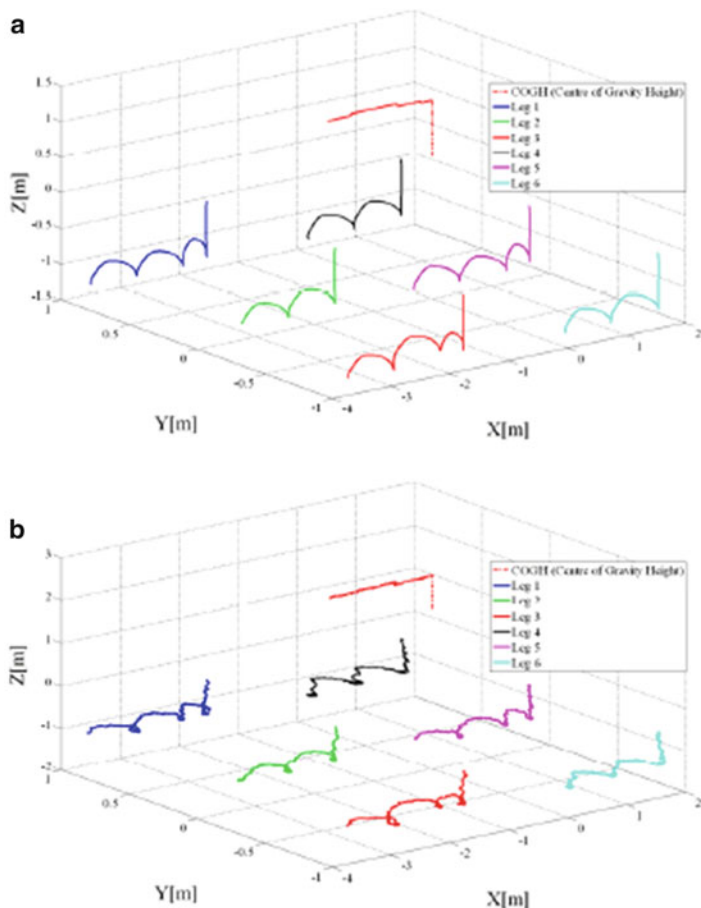


Fig. 8.32 Each leg trajectory on world coordinate system. (a) Stimulation results, (b) Experimental results

Therefore, an actual COMET-IV posture is different from the idealized 3D COMET-IV designed in 3D geometric model. It is necessary to achieve the walking control corresponding to the change of posture and body height.

8.10 Summary

Teleoperation assistant system that utilizes omnidirectional image and robot 3D animation was successfully implemented on COMET-IV system. However, there are two problems still exist. One of them is the communication problems between teleoperation computer and locomotion computer due to high load in the video data transfer. Another problem is that the animated robot body vibrates because sensor information used to express the robot on animation contains the noise. Therefore, the future work will focus on separating the network of the video data transfer and communications. For the second problem, a measure to eliminate the noise of hardware and software will be implemented. Further, the information based on the LRF scan data and the omnidirectional image will be integrated, the accuracy of self-localization of COMET-IV will be increased, and the stability and the smooth walking will be realized using force control.

According to simulation results and verification results from experiment, proposed 3D geometric model with combination of SIMULINK numerical model of COMET-IV system is suitable for indoor design and experiment planning purposes. The most important part in this 3D design is capability of expressing the designed environment and COMET-IV motion due to the designed environment response. In fact proposed BMC method is performed well on providing information on the real-time COMET-IV movement. In addition this method is capable of defining terrain level correctly as real situation. For the future progress, numerical model will be upgraded to be capable of estimating the body attitude via BMC method. This estimation can be used to visualize the body posture in 3D geometric model. On the other hand, identification model for each leg will be improved to perform real motion and precise results on both simulation models. Moreover, the robot walking simulation that uses the real environment positional data acquired from the laser range finder will be improved.

References

1. Nonami K et al (2003) Development and control of mine detection robot COMET-II and COMET-III. JSME Int J Ser C 46(3):881–88.0
2. Fukao Y, Nonami K (2003) Trajectory tracking control and impedance control of mine detection robot. Trans Jpn Soc Mech Eng Ser C 68(678):662–668
3. Ikeda Y, Nonami K (2004) Preview sliding mode walking control for hexapod robot COMETIII. Trans Jpn Soc Mech Eng Ser C 70(700):3484–348.2

4. Sugai H, Nonami K (2006) Reference model following sliding mode for hydraulic mine detection hexapod robot. *Trans Jpn Soc Mech Eng Ser C* 72(721):2828–2837
5. Oku M, Yang H, Paio G, Harada Y, Adachi K, Barai R, Sakai S, Nonami K (2007) Development of hydraulically actuated hexapod robot COMET-IV the 1st report: System design and configuration. In: Proceedings of the 2007 JSME conference on robotics and mechatronics, pp 2A2–G01
6. Parasuraman S, Ganapathy V, Shirinzadeh B (2005) Behavior based mobile robot navigation technique using AI system: experimental investigations. In: ICGST ARAS 05 conference, pp 31–37
7. Thrun S et al (2006) Stanley: the robot that won the DARPA grand challenge. *J Field Robot* 23(8):661–682
8. Matsumoto T, Konno A, Uchiyama M (2003) Teleoperation of the small size humanoid robot HOAP-2. In: The society of instrument and control engineers the 213th research meeting, pp 213–218
9. Tachi S, Komoriya K, Sawada K, Itoko T, Inoue K (2001) Telexistence control cockpit system for HRP. *J Robot Soc Japan* 18(1):16–27
10. Saitoh K, Machida T, Kiyokawa K, Takemura H (2005) A mobile robot control interface using omnidirectional images and 3D geometric models. *Tech Rep IEICE Multimedia Virtual Environ* 105(256):7–12
11. Miyanaka H, Wada N, Kamegawa T, Sato N, Tsukui S, Igarashi H, Matsuno F (2007) Development of an unit type robot KOHGA2 with stuck avoidance ability. In: IEEE international conference on robotics and automation, FrB12.2, pp 3877–3882
12. Hodoshima R, Doi T, Fukuda Y, Hirose S, Okamoto T, Mori J (2005) Development of a quadruped walking robot TITAN XI for steep slopes operation-conceptual design and basic experiment of leg driving mechanism. *J Robot Soc Japan* 23(7):81–91
13. Hayakawa M, Hara K, Sato S et al (2008) Singularity avoidance by inputting angular velocity to a redundant axis during cooperative control of a teleoperated dual-arm robot, 2008. In: IEEE international conference on robotics and automation, pp 2013–2018
14. Kanehiro F, Hirukawa H, Kaneko K, Kajita S, Fujiwara K, Harada K, Yokoi K (2004) Locomotion planning of humanoid robots to pass through narrow spaces. In: Proceedings of 2004 I.E. international conference on robotics and automation, pp 604–608
15. Kanehiro F, Yoshimi T, Kajita S, Morisawa M, Kaneko K, Hirukawa H, Tomita F (2007) Whole body locomotion planning of humanoid robots based on a 3D grid map. *J Robot Soc Japan* 25(4):588–58.7
16. Inagaki S, Suzuki T (2006) Locomotive pattern generation for multi-legged robot with active segmented trunk – learning by GA in multiple friction environments. FAN symposium: intelligent system symposium-fuzzy, vol 16. AI, neural network applications technologies, pp 273–278
17. Ohroku H, Nonami K (2008) Omni-directional vision and 3D animation based teleoperation of hydraulically actuated hexapod robot COMET-IV. *ICGSTARAS J* 8(1)
18. Oku M, Nonami K (2008) Force control of hydraulically actuated hexapod robot. Master thesis, Chiba University
19. LightWave 3D <http://www.newtek.com/>
20. Hirose S, Kikuchi H, Umetani Y (1984) The standard circular gait of the quadruped walking vehicle. *J Robot Soc Japan* 2(6):41–52
21. Sakakibara Y, Kan K, Hosoda Y, Hattori M, Fujie M (1990) Low impact foot trajectory for a quadruped walking machine. *J Robot Soc Japan* 8(6):22–31
22. Yamazawa K, Yagi Y, Yachida M (1996) Visual navigation with omnidirectional image sensor hyper omni vision. *The IEICE J* 78(5):688–707
23. Futagami K, Harada Y, Sakai S, Nonami K (2008) Omni-directional gait of hydraulically actuated hexapod robot COMET-IV. In: The 26th annual conference of the robotics society of Japan, pp ROMBUNNO.1D3-04
24. The KISMET 3D-Simulation Software <http://iregt1.iai.fzk.de/>

25. FlexSim <http://www.flexsim.com/>
26. ThreeDimSim mechanics simulator <http://www.havingasoftware.nl/index.htm>
27. Geyer C, Daniilidis K (2001) Catadioptric projective geometry. *Int J Comput Vis* 45(3):223–243
28. Ogawa A, Kobayashi K, Nakamura O, Murai J (1998) Design and implementation of DV stream over internet. *IEICE Tech Rep Comput Syst* 88(37):77–81
29. Onoe Y, Yamazawa K, Takemura H, Yokoya N (1998) Telepresence by real-time view-dependent image generation from omnidirectional video stream. *Comput Vis Image Und* 71(2):154–165

Chapter 9

Fully Autonomous Locomotion Control of Hexapod Robot with LRF

Abstract This chapter proposes several methods for crossing over an obstacle and descending and ascending a cliff based on LRF 3D point clouds data. The experimental results show that the proposed methods are useful for performing assigned tasks. The reliability and the accuracy of the LRF are basically satisfied to capitalize the capabilities of the legged robot COMET-IV, to increase the autonomy of the robot. Also, in order to increase the robustness of the system, another sensor, such as a stereo-vision camera, can be fused with the LRF. The capability of the stereo-vision camera to recognize colored object can help the system to distinguish between obstacles and not obstacles, such as the grasses.

9.1 Advantages of Hexapod Robot and Typical Quadruped Robot

In general, a walking robot has some advantages over a wheeled or tracked robot for walking through stochastic terrain because it can perform many types of locomotion strategies, not only avoiding obstacles as other types of robots can do. Among the legged robots, the hexapod robot has further advantages over other legged robots because of its static stability during walking, in which its three legs maintain on the ground while walking, and due to that the control complexity is reduced [1]. Figure 9.1 illustrates some of the different locomotion strategies performed by the walking hexapod robot: (a) crossover, (b) ascending, and (c) descending. These strategies would not be feasible for wheeled or tracked robot. The capabilities of the legged robot to perform the locomotion strategies are depending on the leg's joint design structures, materials, and the number of degrees of freedom (DOF) of the robot. Higher DOF gives more capabilities to the robot. In contrast, the control algorithm used becomes more complex.

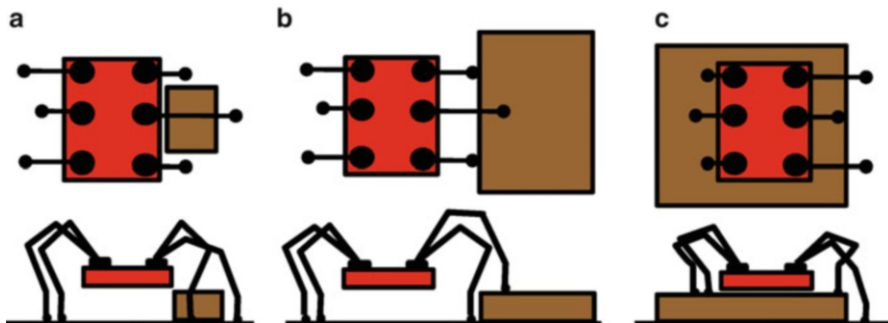


Fig. 9.1 Locomotion strategies performed by a hexapod robot

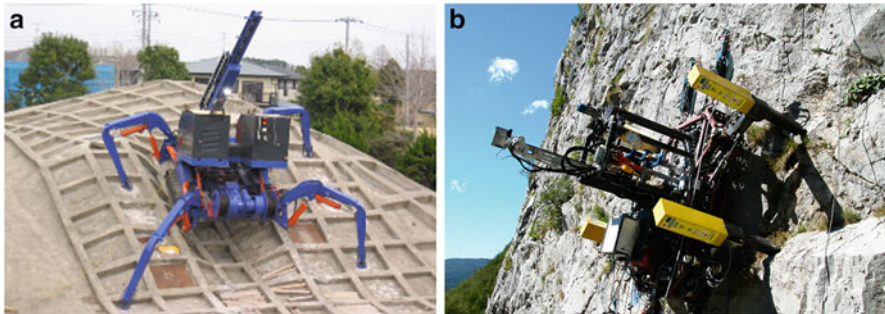


Fig. 9.2 Performing specific tasks: (a) the TITAN-XI and (b) the ROBOCLIMBER

Some examples of legged robots that perform locomotion strategies as shown above are the TITAN-IV [2] and ROBOCLIMBER [3], as shown in Fig. 9.2a, b, respectively. TITAN-XI is a quadruped robot which is developed to carry out autonomous drilling holes of rock bolts or anchor bolts on mountainous area to prevent steep slope failure or landslides. Similarly, the ROBOCLIMBER is also a quadruped robot which is developed for slope consolidation and monitoring, to remotely and automatically perform deep drilling on a mountain. As can be seen from these figures, these strategies can be done because of each of the robot's legs can be moved up-down and forward-backward independently, so that each of the legs can be placed on an appropriate surface in a different surface level.

However, as commonly understood, those strategies only can be performed if the robot or an operator that is controlling the robot from a remote place has information about the environment, which can be acquired using some sensors, either which are being fitted into the robot or somewhere in the environment. Problem in gathering and determining this information is called environment modeling.

9.2 Environment Modeling

An environment modeling or mapping process needs sensory inputs to be tessellated to a kind of representation that can be understood by the robot itself to walk from a start point to a targeted goal, while avoiding obstacles. The environment model also can be used by an operator, who is controlling the robot from a remote place. To be useful, the environment model or a map has to be included with enough geometric information of the pathways and obstacles that exist in the environment. However, all that information can't be gathered by a single sensor since each of the sensors has their disadvantages. Hence, to ensure the disadvantages will not affect the operation of the robot, the combination of sensors is needed, but depending on the objectives of the development of the robot itself, and it is desirable to use cheaper sensors but as a combination they provide enough information with high accuracy.

Many literatures have been found describing the advantages and disadvantages of some sensors that are regularly used in developing a map [4–6]. As can be observed from many literatures, the use of a single sensor will not be enough to really be implemented in real environment because of the disadvantages inherited in each of the sensors. Therefore, sensor integration is a must to ensure the system functions. Based on [7], the advantages and disadvantages of some sensors are tabulated in Table 9.1 below.

The next stage is how to make use the sensory input so that the geometrics of obstacles can be represented and can be used to develop safe walking path for the robot. Many methods are proposed by many researchers in developing the environment map and also safe walking path for a robot. Grid-based method is one of the popular methods because it is easy to be used and maintained. In contrast, the size of the grid cell relatively contributes to higher processing cost and less accuracy. Furthermore, 2-D grid-based mapping is usually used and only implemented for obstacle avoidance. We are, however, implementing 2-D grid-based mapping with additional information that is registered in each grid cell without increasing processing cost and producing higher accuracy for obstacle avoidance, walking over obstacle, and descending and ascending step.

Table 9.1 Sensors and its advantages and disadvantages

Sensor	Advantages	Disadvantages
Camera	Provides bountiful information	Light condition dependent
LRF	High accuracy	Expensive
	Better accuracy	Can't measure object that absorbs its laser beam
Sonar	Large opening angle Cheap in price Small size	Low accuracy

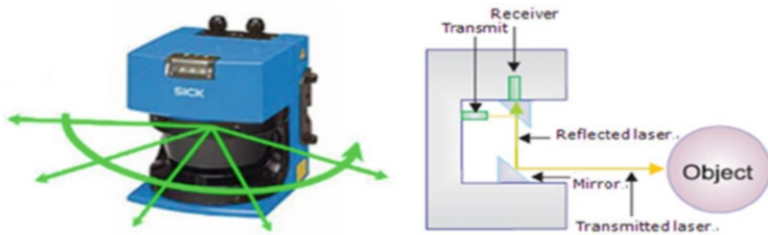


Fig. 9.3 LRF and its operation principle

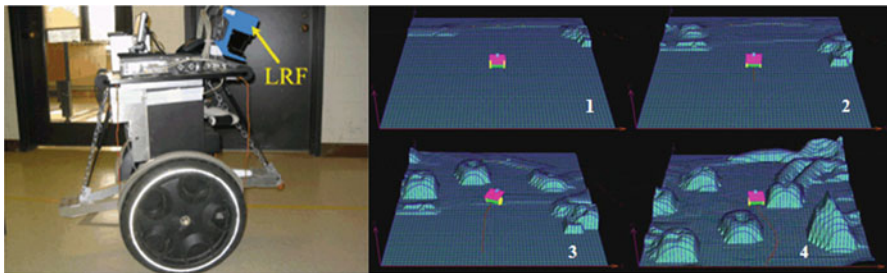


Fig. 9.4 Incrementally built 3D map using moving 2D LRF

9.2.1 Laser Range Finder

Laser Range Finder (LRF) is one of a device that is extensively used in an environment modeling due to its high accuracy. It uses laser beam to determine a distance to an object. The laser beam used in the LRF is not affected by the external light interference, and its accuracy is not depending on the measured distance. Several techniques have been developed to determine the distance, such as time of flight, phase measurement, and triangulation. However, the time of flight is the most common technique that has been used. In this technique, the distance of a point on an object is calculated based on how long the laser takes to bounce back to the sensor as illustrated by Fig. 9.3, and the calculation is made using Eq. (9.1) [7], where c_s is the speed of light (3×10^8 m/s) and Δt is the round trip number.

$$r = \frac{c_s \Delta t}{2} \quad (9.1)$$

In general, an LRF produces 2-D scan data but by manipulation of its mounting method, 3-D point clouds data can be produced. Figure 9.4 shows typical mounting where an LRF is mounted with fixed tilt downward angle and the 3-D environment image incrementally built while the robot moves (http://ualr.edu/cxye/proj01_segway.htm).

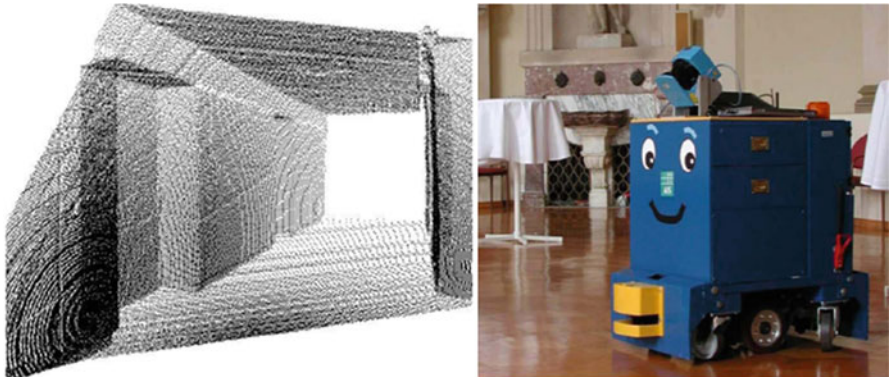


Fig. 9.5 3D mapping using rotating LRF around horizontal axis

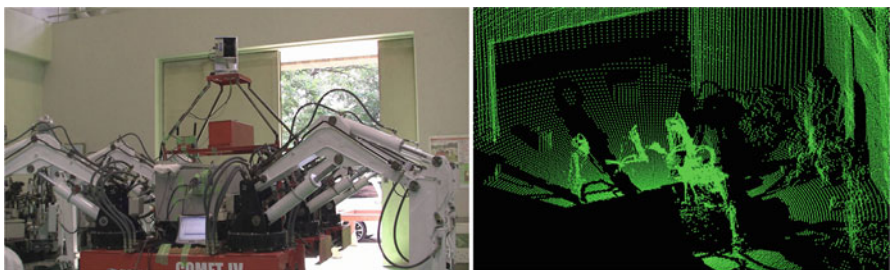


Fig. 9.6 3D mapping using rotating LRF around vertical axis

On the other hand, to make the LRF possible to produce 3-D environment image without need for the robot to move, the LRF can be swung horizontally or by changing the tilt angle continually with appropriate resolution, as illustrated in Fig. 9.5 (<http://www.faculty.jacobs-university.de/anuechter/videos.html>).

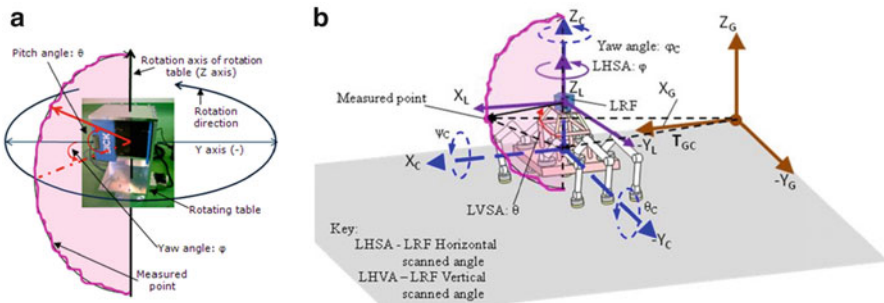
Another technique which is frequently used is by rotating the LRF while it is lying on its side as illustrated in Fig. 9.6, and it is used in this work and the specifications of the LRF are listed in Table 9.2. Since its scanning speed is very fast, a rotating device that is going to be used should be able to rotate fast enough and at the same time very accurately.

9.2.2 Grid-Based Environment Modeling

Grid-based environment modeling is the favorable choice because it is easy to be constructed and maintained (<http://www.faculty.jacobs-university.de/anuechter/videos.html>). In this work, the environment model is developed based on the

Table 9.2 Specifications of LRF (LMS200)

Type	LMS200
Weight	4.5 kg
L × W × H	156 mm × 155 mm × 29 mm
Measurement range	0 ~ 8 m
Field of vision	180°
Distance resolution	9 mm
Angular resolution (scan time)	0.25°; 0.5°; 1° (53.33 ms); (26.66 ms); (13.33 ms)
Measurement accuracy	±15 mm
Data interface (transfer rate)	RS232(9.6/19.2 kbd), RS422(9.6/19.2/38.4/500 kbd)
Operating voltage	24 V DC
Power consumption	Approximately 30 W
International protection	IP65

**Fig. 9.7** Parameters for 3D coordinates and global coordinates transformation

geometrics of obstacles that have been determined based on the point clouds data acquired using an LRF that is laid down on its side and rotated around vertical axis, and they are transformed to 3D coordinate system according to the Eq. (9.2) and the parameters shown in Fig. 9.7a. Then, the global coordinate of the obstacles is determined based on the parameters shown in Fig. 9.7b and according to Eq. (9.2):

$$\left. \begin{aligned} X_c &= R_i \cos \varphi \sin \theta \\ Y_c &= R_i \cos \theta \cos \varphi \\ Z_c &= H + R_i \sin \varphi \end{aligned} \right\} \quad (9.2)$$

where i is the count of the scanned spot; R_i , Euclidean distance of each point on the obstacle measured by the LRF; H , height of the LRF from the center of the COMET-IV body, θ , scanned angle in a vertical direction with 0.5° resolution from bottom to top; and φ , horizontal direction with resolution from right to left:

$$\begin{bmatrix} P_{GD} \\ 1 \end{bmatrix} = R_{GC}(\psi_c)R_{GC}(\theta_c)R_{GC}(\varphi_c)T_{GC} \begin{bmatrix} P_{CD} \\ 1 \end{bmatrix} \quad (9.3)$$

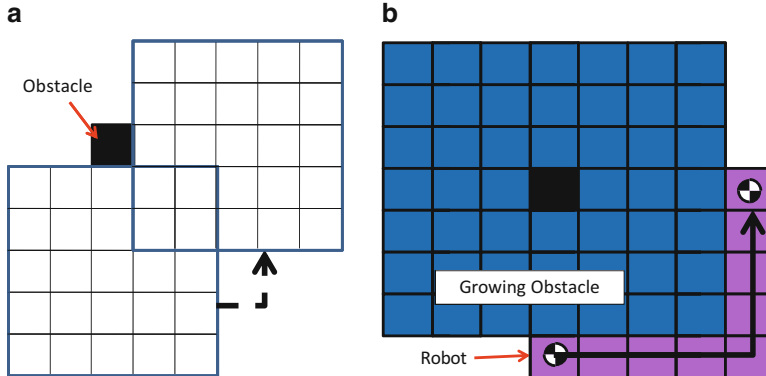


Fig. 9.8 Growing obstacle method: (a) not applied and (b) applied

where $R_{GC}(\psi_C)$, $R_{GC}(\theta_C)$ and $R_{GC}(\varphi_C)$ are the rotational matrices of X , Y and Z axis of COMET-IV body center. T_{GC} is the translational vector that maps the COMET-IV body center coordinate to global coordinates. P_{CD} is the coordinate system of COMET-IV body center.

The data that are transformed using Eq. (9.3) are converted to grid coordinate system by dividing the data with the size of the grid cell, which is $0.2\text{ m} \times 0.2\text{ m}$, and the size is selected based on several experiment results carried out at Nonami's laboratory at Chiba University, Japan. Furthermore, the maximum height of the obstacles presence in of each cell is associated in it and can be retrieved whenever needed.

9.2.3 Path Planning

In order to enable a shortest and safe walking path can be determined with lower computation cost, this work applies Growing obstacle method with some modifications. The size of the robot, and its capability in crossing over and stepping on obstacles which their heights below than 0.75 m are taken into consideration in applying the method. Similarly, for stepping down task, the depth should not be lower than 0.75 m . As can be seen from Fig. 9.8b, by applying growing obstacle method, the robot movement can be considered as a particle movement, instead of considering whole size of the robot as in Fig. 9.8a. Thus, the method provides easiness and faster computation cost.

For generating a shortest and safe pathway, the A* algorithm was applied, but the travel costs for the occupied cells are considered same, except for the cells occupied with obstacles that their height above 0.75 m and the grown obstacles. Then, the proposed system triggers the first path that hits an obstacle as illustrated by Fig. 9.9. Based on the X , Y , and Z coordinate of the cells and the obstacles sizes, including stride length, swing height and body height of the robot are determined.

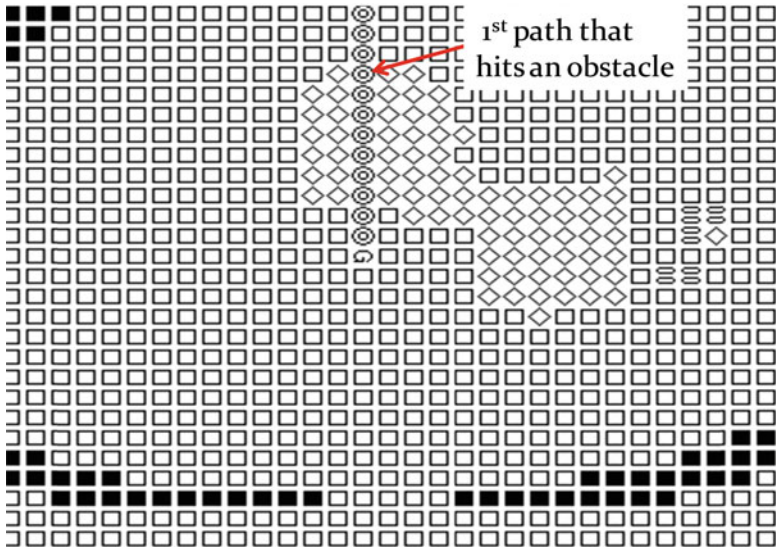


Fig. 9.9 First path hits an obstacle

9.3 Locomotion Strategies in Stochastic Environment

The hexapod robot COMET-IV is developed for hazardous work and capable of walking through stochastic environment, where the surface level of the ground is different at each point. To ensure the robot can walk on this kind of ground surfaces, control strategies of foot are one of the solution, but by applying only foot control strategies, the robot will perform walking like blind men, groping around in the environment, which in turn decreases walking speed and in some conditions of the obstacles would prohibit the robot from moving forward, such as in high step or deep ground surfaces. In order to solve these problems, vision-based locomotion strategies that ally with the foot control strategies are preferred. The authors have proposed an algorithm that enables vision-assisted force-based walking and it is already tested for the hexapod robot COMET-IV and produced very encouraging results [8]. In this book, the algorithm is further improved and it was tested for further challenging tasks such as those mentioned in Sect. 9.1.

9.3.1 Crossing Over and Ascending an Obstacle or a Step

The most crucial part for the robot to cross over an obstacle and ascend a cliff is when the robot swings its leg over the edge of the obstacle/cliff. In order to ensure the leg will not crash with the edge, the position of the leg before it swings over and

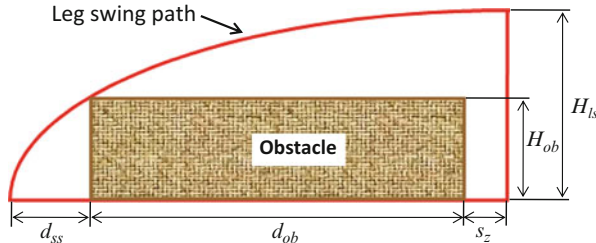


Fig. 9.10 Leg swing trajectory and related parameters

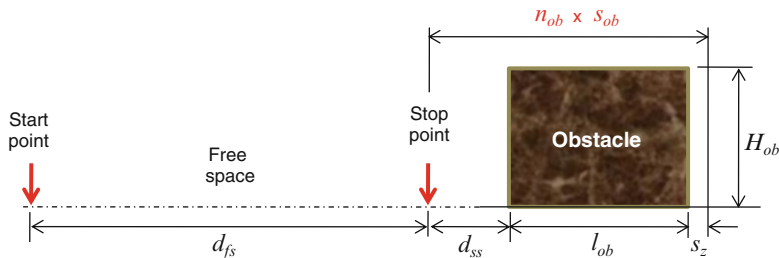


Fig. 9.11 Parameters and conditions for crossing over an obstacle

the swing height have to be determined, using Eq. (9.4), with detailed explanation that can be found in [9]. In addition, depending on the task, leg stride length and the robot's body height also have to be computed according to the size of the obstacle/step. Figure 9.10 illustrates the leg swing trajectory and some parameters used to determine the related measurement as mentioned above, where d_{ob} is the length of the obstacle, S_z is a minimum distance for the robot to place its leg after crossing over the obstacle and H_{ls} is the swing height. The stride length is the total length from the stop point to the position of the leg placed after crossing over the obstacle:

$$Z_{s_i}(t) = Z_{o_i} + H \sin\left(\frac{\pi}{T_c/2} t\right) \quad (9.4)$$

However, the measurements have to be suited to physical limitations of the robot: (1) the body height must be 0.2 m higher than the obstacle and (2) maximum obstacle length should be less than 0.6 m for crossing task.

In the case of the obstacle longer than 0.6 m and its ended edge within 8 m radius, the robot has to step on the obstacle with different stride length, S_{ob} , and the step count, n_{ob} , has to be considered to ensure that both edges of the obstacle are not touched by the robots' legs. Figure 9.11 shows the parameters and the conditions that are needed to be considered.

In order to determine the d_{ss} , referring to Fig. 9.11, some conditions as shown by Eq. (9.5) have to be set and inserted into Eq. (9.4):

$$\left. \begin{array}{l} t = \frac{T_c d_{ss}}{4(d_{ss} + d_{ob})} \\ d_{ob} = l_{ob} + S_z \\ Z_{s_i}(t) = H_{ob} \end{array} \right\} \quad (9.5)$$

In addition, to ensure the rear legs are also safe from hitting the edge of the obstacles, the stride length should be as shown by Eq. (9.6):

$$S_{ob} = \frac{R_l}{n_{ob}} \quad (9.6)$$

where R_l is the distance between the center of rear and front foots, which is 3.6 m.

Referring to Fig. 9.11, in case the length of the obstacle is more than 0.6 m and the ended edge of the obstacle is within 8 m radius, the robot has to step on the obstacle. Thus, the value of t in Eq. (9.5) should be written as below:

$$t = \frac{T_c d_{ss}}{4n_{ob}(d_{ss} + d_{ob})} \quad (9.7)$$

In the case of the ended edge at the outside of 8 m radius, stride length default setting can be used. However, to ensure the rear legs of the robot could step on the obstacle without hitting the frontier edge of the obstacle, the stride length and the step count to be determined should take into account the distance between front legs and rear legs.

9.3.2 Descending a Cliff

Descending task can be performed in two strategies which are descending with outer legs or inner leg as shown by Figs. 9.12 and 9.13, respectively. As can be seen in Fig. 9.12, the stop point is farther from the edge of the step compared to the stop point shown in Fig. 9.13. After the robot stopped at the stop point, the inner leg is moved for a half of the stride length distance and followed by the movement of outer legs, which are moved with a stride length distance. However, in this experiment, the first option is used because of better stability.

On the other hand, Fig. 9.14 shows that the legs of the robots are swung with the same swing height as walking in a free space while descending a cliff, before it is placed down straightly onto the floor. However, for performing this task, unlike ascending a cliff, some different consideration has to be formulated in order for the shank of the robot's leg not to crash with the edge of the cliff and its foot to

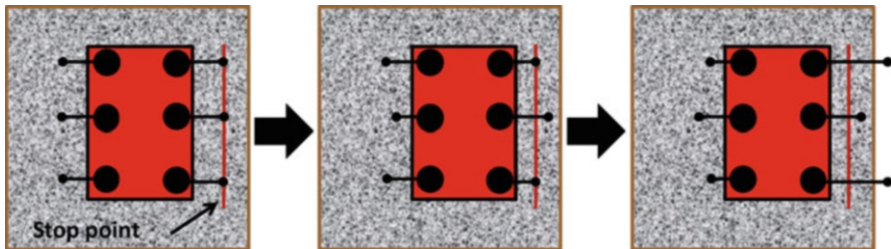


Fig. 9.12 Descending a cliff with outer legs

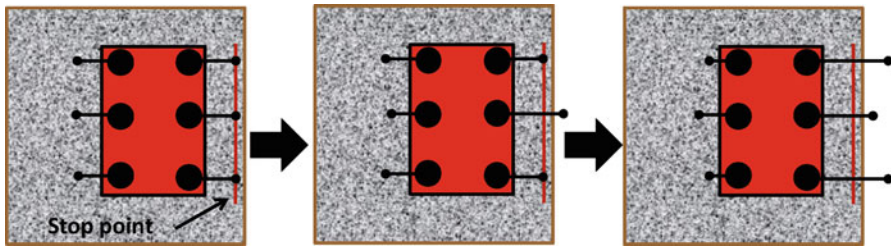


Fig. 9.13 Descending a cliff with inner leg

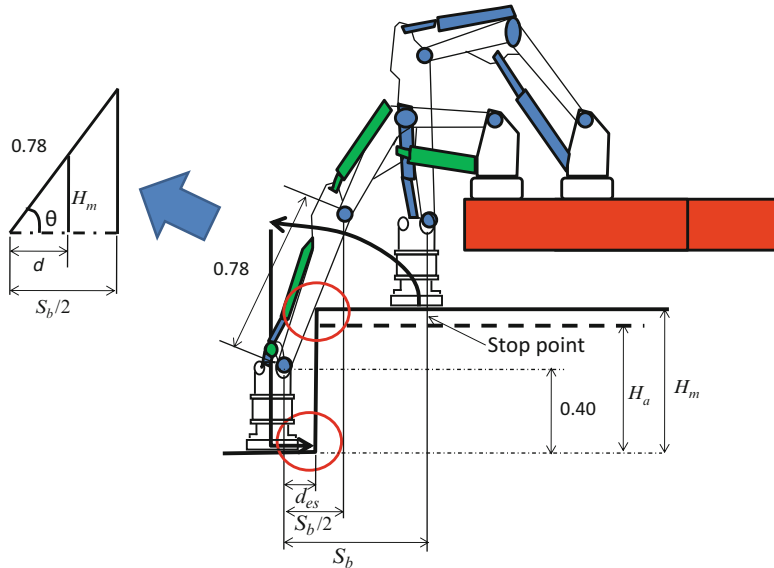


Fig. 9.14 Leg movement during descending a cliff and required parameters

be safe from touching the wall of the step, as shown in below figures. The values of the parameters should fulfill conditions bounded by Eq. (9.8):

$$S_b > d_{es} + d_{fs}$$

$$\theta = \cos^{-1} \left(\frac{S_b}{1.56} \right) \quad (9.8)$$

$$H_a < H_c$$

where H_a is the actual height and H_c is the calculated height, S_b is the stride length, and d_{es} the appropriate distance to ensure the foot touches the cliff after it is little bit pulled in due to control of design property. The value of d_{es} is normally set for 0.07 m. If H_a is smaller than H_c , then the shank will not touch the step.

9.4 Experimental Results

In this section, some experimental results are presented to show the capability of the developed system to determine appropriate parameters for crossing over an obstacle, ascending and descending a cliff, and the reliability and high accuracy of the LRF used in this work. As described above, the system should be able to determine the stride length and step count for walking in the free space and stop point, body height, stride length, swing height, and step count for crossing over or climbing or descending a cliff. The success of the robot to cross over an obstacle and to ascend and descend a cliff without clash with the edge of the step shows that the developed system and the LRF used are capable to determine the above-said parameters correctly and accurately.

9.4.1 Crossing Over an Obstacle: Results and Discussion

As shown by Fig. 9.15, in the first experiment, the size of the obstacle used was $0.30 \text{ m} \times 0.60 \text{ m} \times 0.36 \text{ m}$ which is a stack of several layers of concrete blocks. In addition several layers of papers are located behind the concrete blocks. At front area other concrete blocks covered by rubber mats are located randomly, but their height is less than 0.03 m. The robot was placed at a random position at about 3–4 m from the obstacle, but the value of d_{ss} is set to 0.3 m and the value of S_z is set to 0.2 m.

Figure 9.16 shows the occupancy grid map that has been developed by the system based on the 3-D LRF data and the environment map in Fig. 9.17 is the enlarged view of specific part of the Fig. 9.16. As can be seen from both figures, the system correctly determined the value of d_{fs} which is 3.625 m, and it is within the range of 18th row. For the obstacle length, it is shown that the farthest

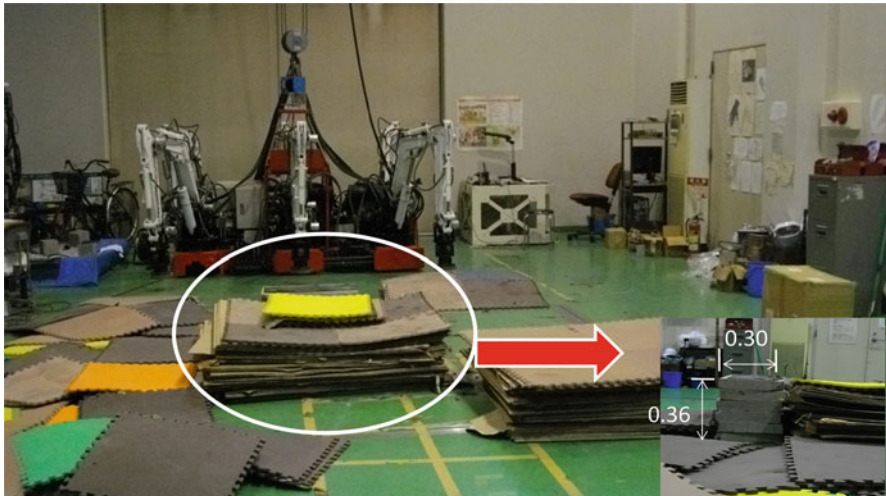


Fig. 9.15 Experiment setup for crossing over task

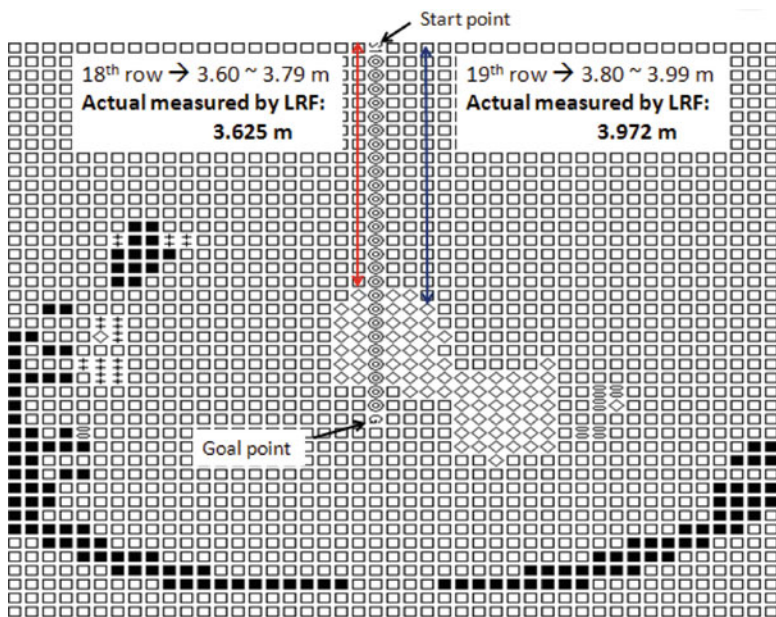


Fig. 9.16 Occupancy grid map of crossing over task

edges of the bricks and the frontier edges of paper layers share the same cells, which is in 19th row, as illustrated by Fig. 9.17. This means the farthest edges of the bricks are unknown. Instead, the frontier edges of the paper layers can be determined. Thus, the distance of the frontier edges of the paper layer should be used, since the

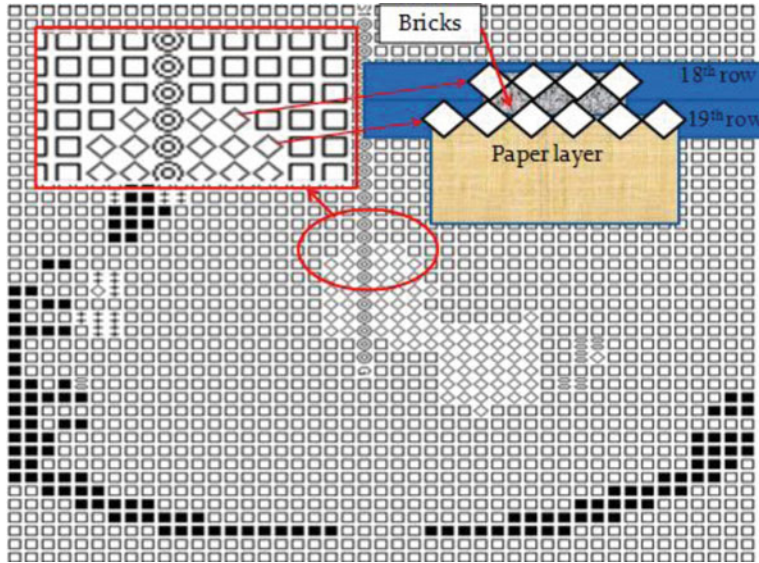


Fig. 9.17 Occupancy grid map with enlarged view

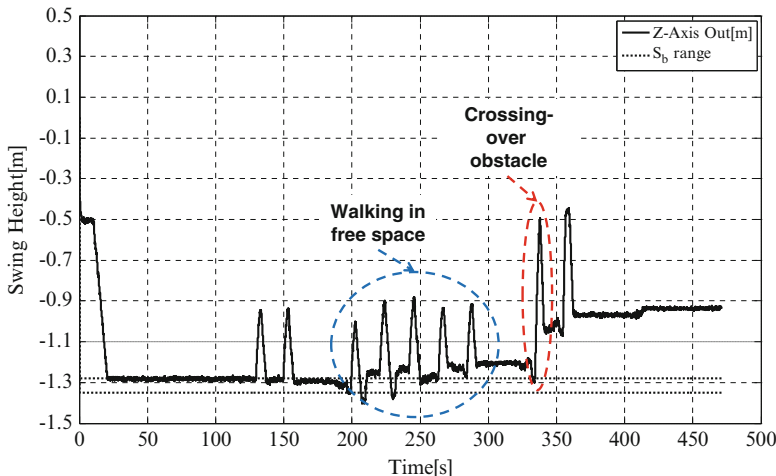


Fig. 9.18 Changes in walking conditions for crossing over task

measurement shows that the probability of existence of empty space between the objects is too small to the leg of the robot to be placed in between them. On the other hand, Fig. 9.18 shows the changes of the leg swing height during walking in the free space and during crossing over the obstacles and Fig. 9.19 shows the snapshot pictures of the experiment that proves the effectiveness of the developed system.



Fig. 9.19 Snapshots of crossing over experiment

9.4.2 Crossing Over an Obstacle Longer than 0.6 m: Results and Discussion

Figure 9.20 shows the steel table ($0.7 \times 9 \times 9$ m) used as an obstacle that requires the robot to climb and cross over it. In this experiment the value of S_z is set to 0.2 m and the maximum swing height is set to 1.2 m; the system determines the stop point based on the height and the length of the obstacle.

Figure 9.21 shows the occupancy grid map and walking path generated by the system. As can be seen all the measurements determined based on the LRF

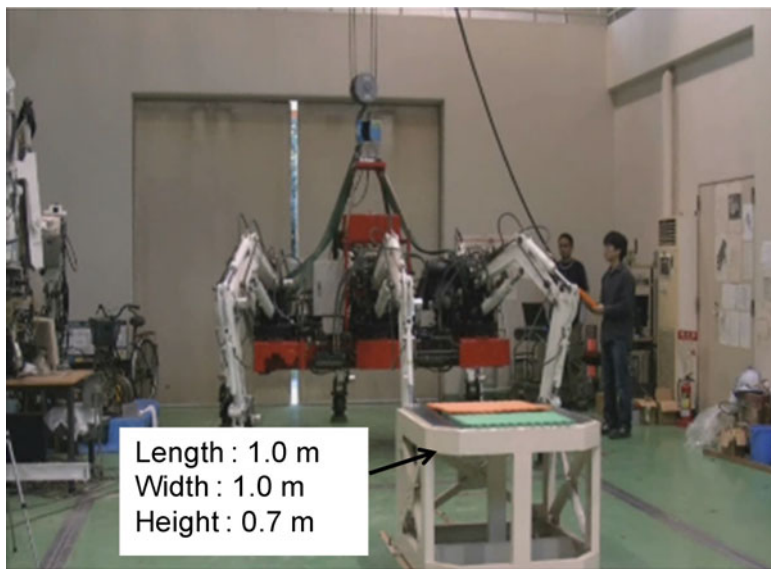


Fig. 9.20 Experiment setup for climbing and crossing over obstacle

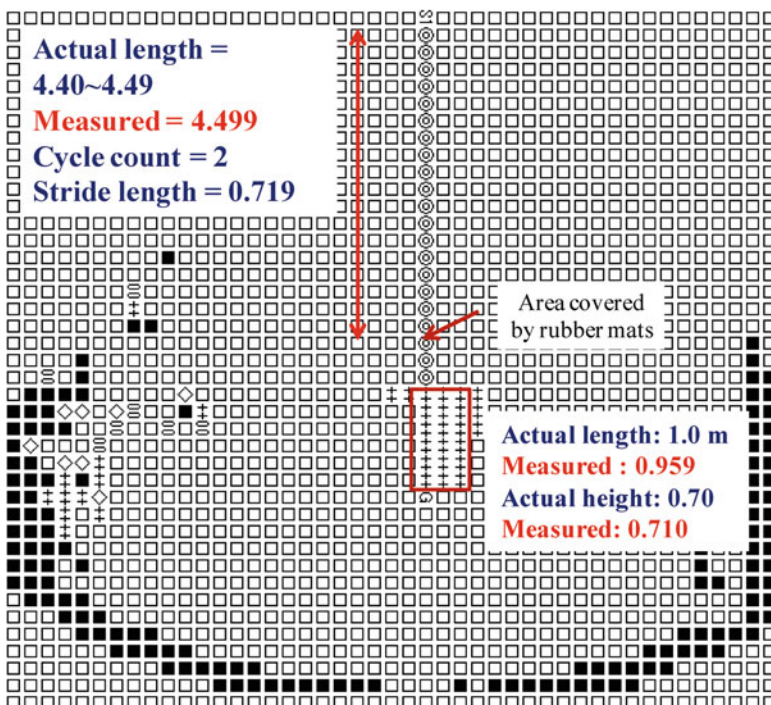


Fig. 9.21 Occupancy grid map of crossing over an obstacle experiment

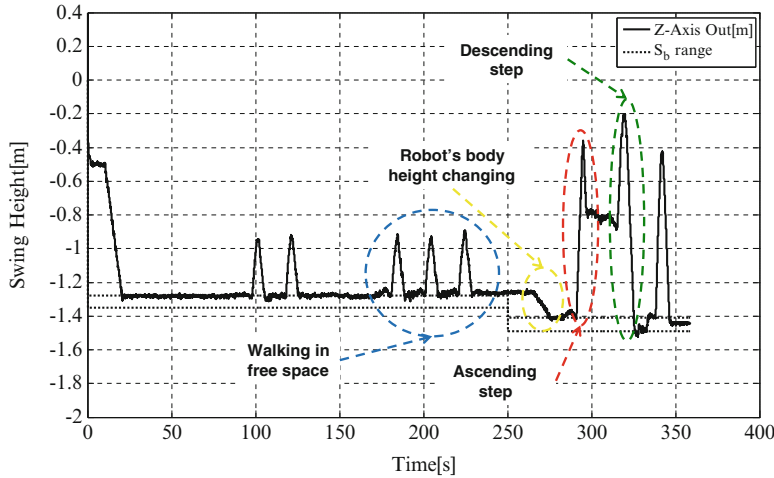


Fig. 9.22 Leg swing height, body height, and stride length of crossing over an obstacle experiment

measurement are closed to actual dimensions. On the other hand, Fig. 9.22 illustrates the data generated by locomotion computer that shows the changes in the stride length, body height, and the swing height while walking from a start point until completed performing the task. The capability of the system to produce high-accuracy results for the robot to perform the task is further justified by the snapshot pictures shown in Fig. 9.23.

9.4.3 Ascending and Descending a Cliff: Results and Discussion

The verification of the effectiveness of the proposed technique is extended to the actual field area and different tasks, in which the robot has to ascend and descend a 0.6-m cliff outside of our laboratory. This is the first time for the robot to ascend and descend the cliff autonomously since it developed. The 0.6-m height step is enough to verify the potential of the high accuracy of the LRF and the effectiveness of the autonomous mapping and path and trajectory planning of the system.

Two trials have been carried out for descending task, where in the first trial, only the stride length has been set to 1.2 m but in the second trial, considering safety factors including stability, the stride length has been set to 0.9 m and the foot placement after the first step has been set at 0.1 m from the edge of the cliff. As can be seen from the below figures, all parameters needed for performing the assigned

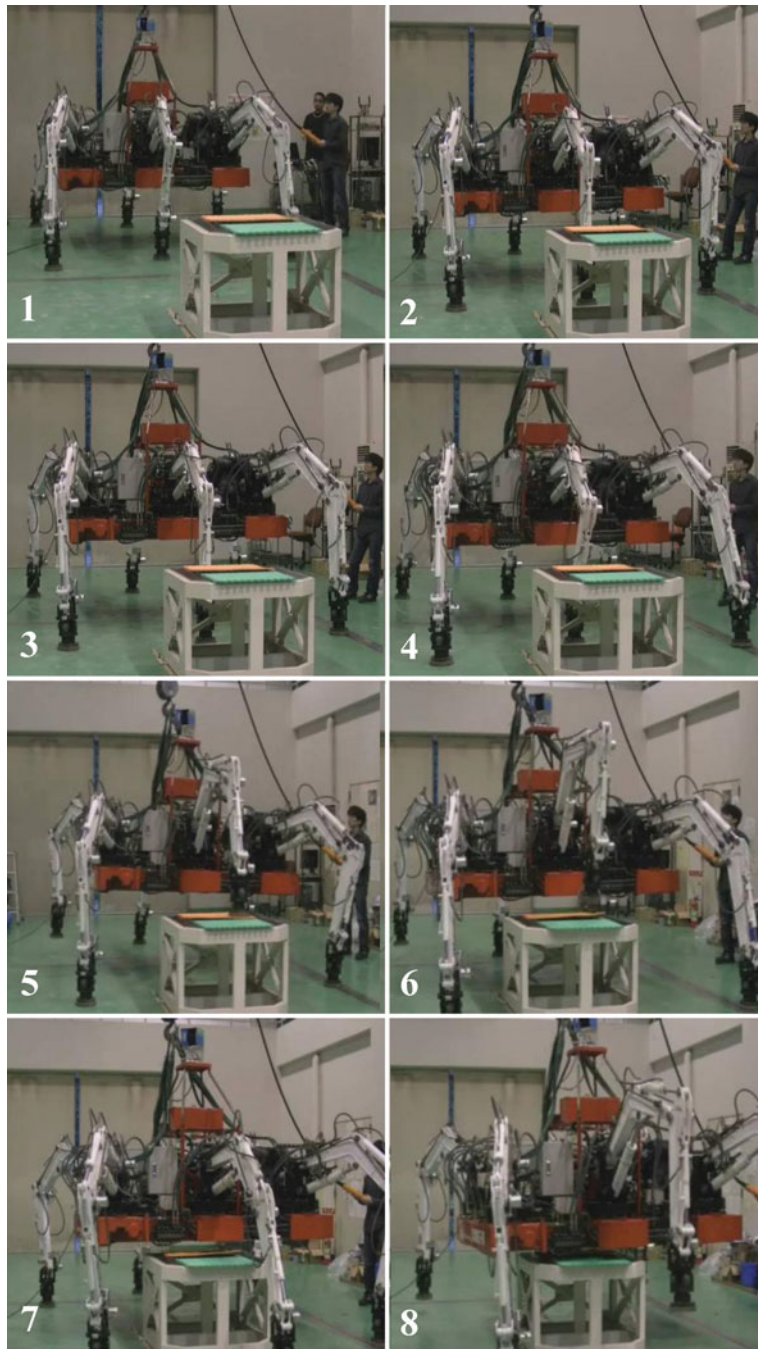


Fig. 9.23 Snapshots of crossing over an obstacle experiment



Fig. 9.24 Snapshots of descending task (stride length = 1.2 m)

tasks have been autonomous and correctly determined by the robot. Therefore the robot has successfully stepped down the cliff. Figures 9.24 and 9.25 show the snapshots of the event that illustrate the steps: (1) stops at a stop point assigned according to the height of the cliff and stride length determined autonomously, (2) lowering its body to an appropriate height, (3) starts walking with first half-cycle (inner leg), (4) front left and right legs step down the cliff, (5) front inner leg steps down the cliff, (6) rear left and right legs reach at almost the same place as front legs stopped, (7) rear inner leg stops almost at the same place the front inner leg stopped before descending the cliff, (8) rear left and right legs step down, and (9) rear inner leg steps down.

The environment maps constructed by the system together with the walking path are shown in Figs. 9.26 and 9.27. As can be seen, the depth of the floor is determined closed to the actual value. On the other hand, Figs. 9.28 and 9.29 show the changes in the stride length, the body height, and the leg swing height during walking in a free space and during descending the cliff.

For ascending task, only one trial can be done and the snapshots of the experiment are shown in Fig. 9.30. However, as can be seen, the front out legs were slipped when the body of the robot is pushed forward and caused the robot to fall down, because the foot is placed too near to the edge of the cliff. In our estimation,

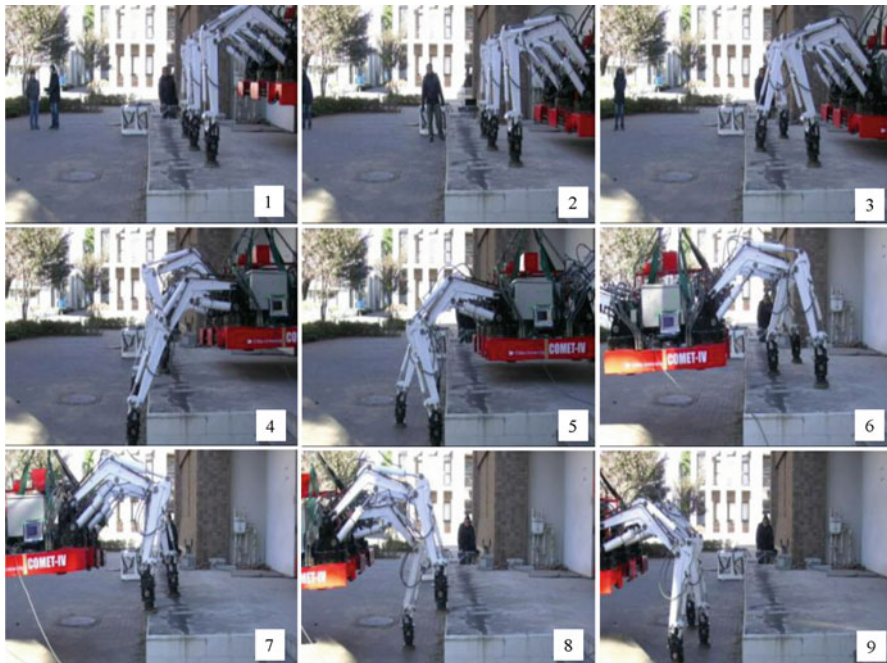


Fig. 9.25 Snapshots of descending task (stride length = 0.9 m)

the foot should be placed at about 0.5 m further ahead, but due to some errors, for instance, the stride length, the actual foot placement was not as our estimation. Another factor of the problem was that the rear leg swing height should be smaller than the front leg and there is a need to consider the height of the cliff to ensure the front and real legs touch ground at the same time. This is to ensure that any time at least three of its legs are on the ground.

The environment map developed by the system is shown in Fig. 9.31 and the graph that illustrates the changes in walking conditions is shown in Fig. 9.32. As can be monitored, the robot's body height was not changed because the default value is big enough for the robot to climb the cliff. However, both figures show that the required parameters are correctly determined by the system.

9.5 Summary

The experiment results of the proposed method for crossing over an obstacle and descending and ascending a cliff based on LRF 3D point clouds data have been presented. The results show that the proposed method has successfully determined

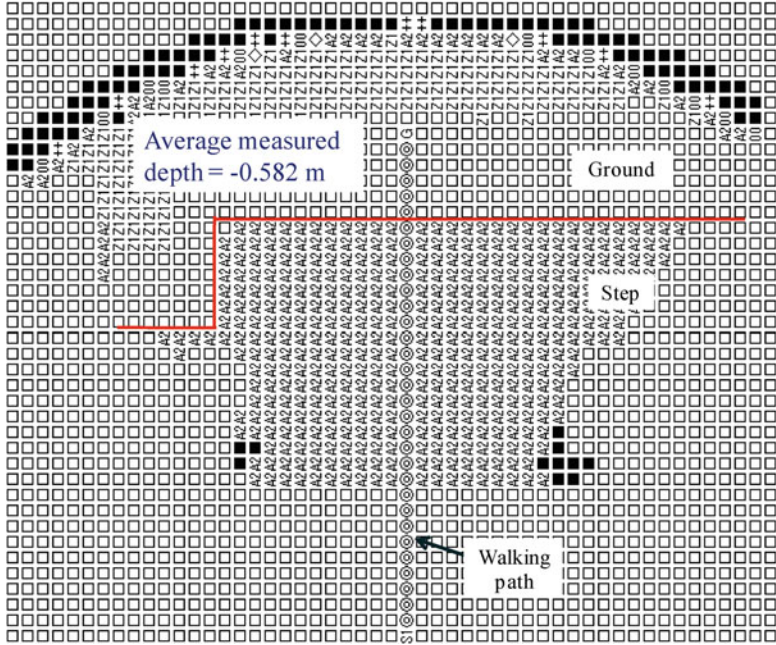


Fig. 9.26 Occupancy grid map of descending task (stride length = 1.2 m)

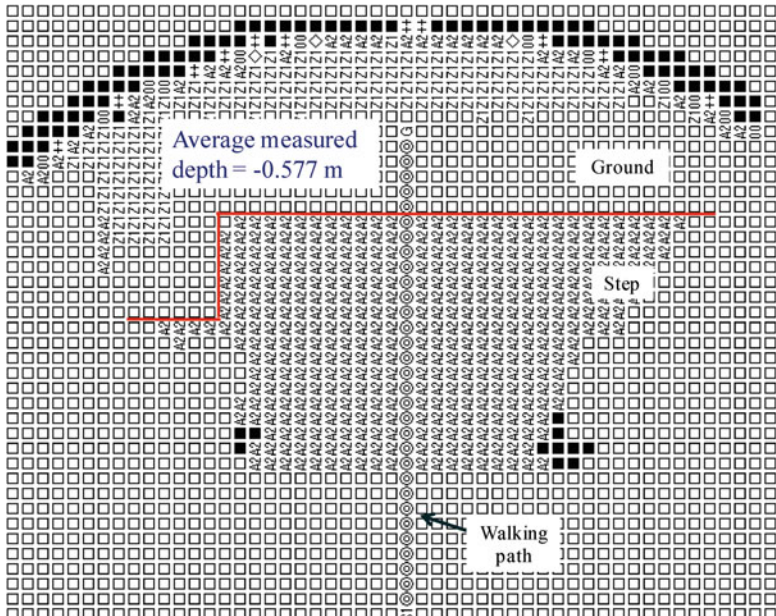


Fig. 9.27 Occupancy grid map of descending task (stride length = 0.9 m)

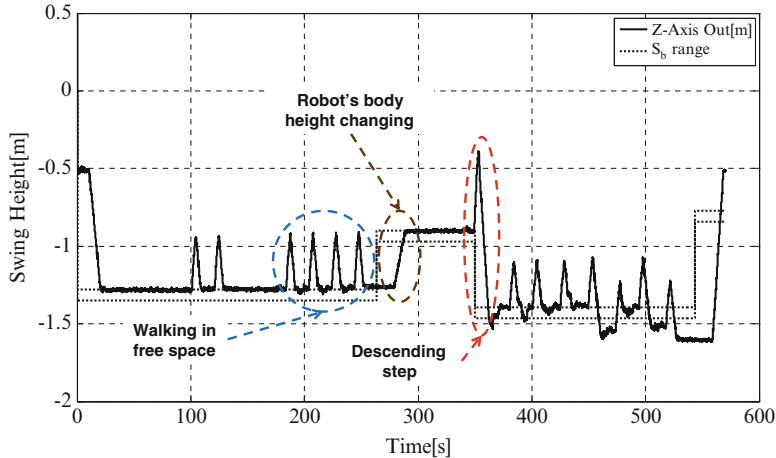


Fig. 9.28 Changes in walking condition for descending task (stride length = 1.2 m)

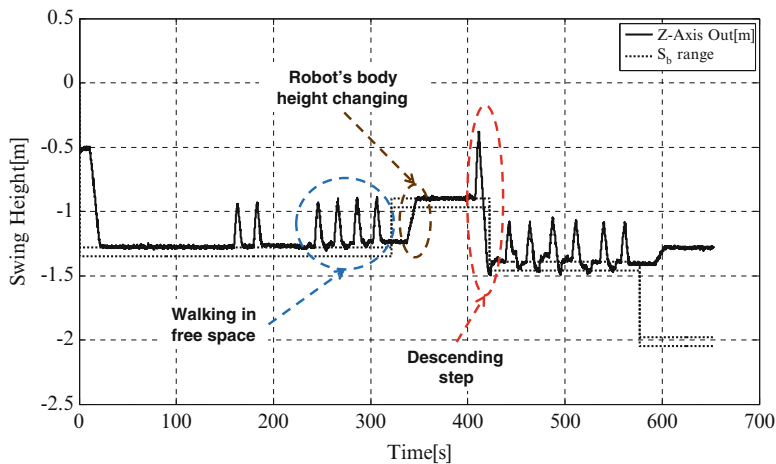


Fig. 9.29 Changes in walking condition for descending task (stride length = 0.9 m)

all required parameters for performing assigned tasks. The successfulness of the system also reflected that the reliability and the accuracy of the LRF are undoubtedly. Therefore, the developed algorithm satisfies the objectives of the research to capitalize the capabilities of the legged robot COMET-IV, to increase the autonomy of the robot, and thus enable the robot to perform complicated tasks.

However, to increase the robustness of the system, another sensor, such as a stereo-vision camera, can be fused with the LRF. The capability of the stereo-vision

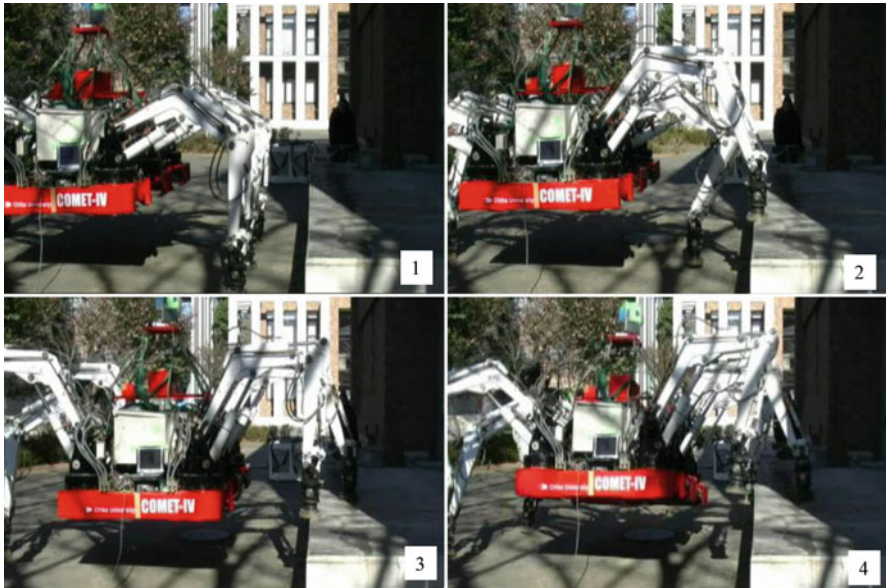


Fig. 9.30 Snapshots of ascending task

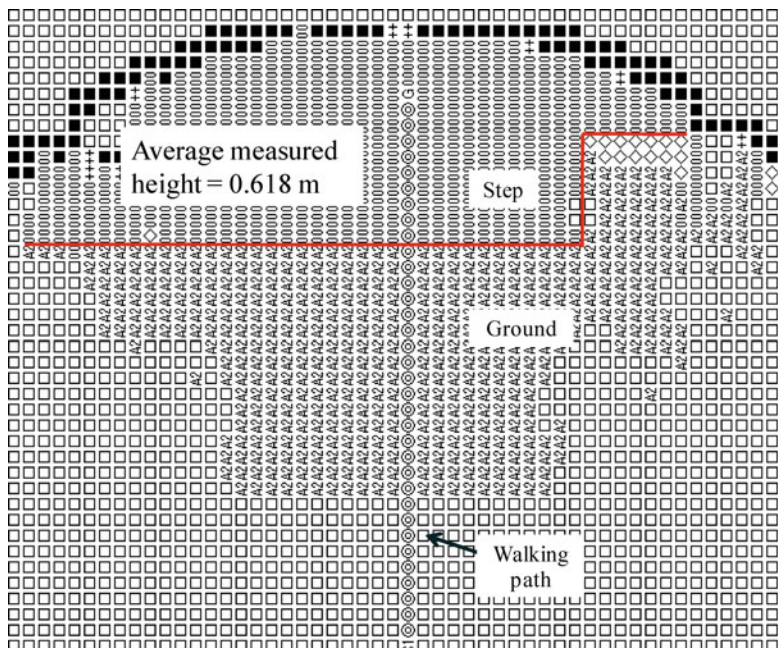


Fig. 9.31 Occupancy grid map of ascending task

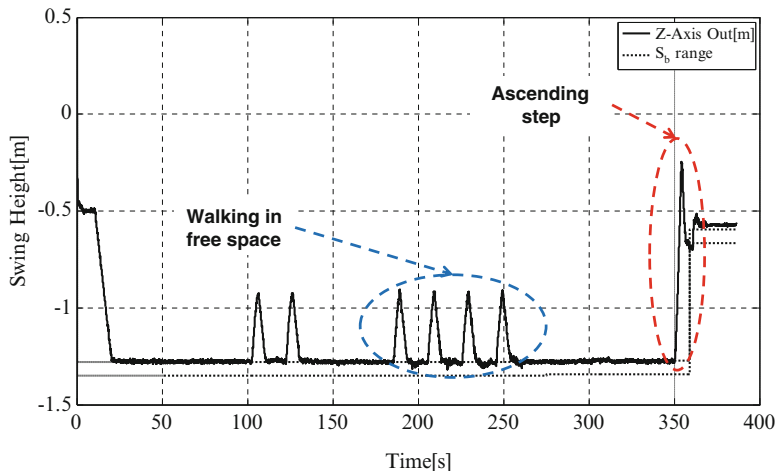


Fig. 9.32 Changes in walking condition for ascending task

camera to recognize colored object can help the system to distinguish between obstacles and not obstacles, such as the grasses, which can be considered as not obstacles, and the black colored object or other objects that absorb the beam of the LRF. Furthermore, by making the camera fully “on” and by applying real-time processing and with appropriate mounting position, it could identify the occluded area that can’t be seen by the LRF.

References

1. Siegwart R, Nourbakhsh IR (2004) Introduction to autonomous mobile robots. MIT, Cambridge
2. Hodoshima R, Doi T, Fukuda Y, Hirose S, Okamoto T, Mori J (2007) Development of TITAN XI: a quadruped walking robot to work on slopes. In: Proceeding of IEEE/RSJ international conference on intelligent robots and systems 2007, Sendai, pp 2A2–G01
3. Molfino R, Armada M, Cepolina F, Zoppi M (2005) ROBOCLIMBER the 3 ton spider. Ind Robot 32(2):163–170
4. Cang Ye (2007) Navigating a mobile robot by a traversability field histogram. IEEE Trans on Syst Man Cybernetics B 37(2):361–372
5. Trabelsi MH (2011) Indoor robot localization based on fusion of visual and ultrasonic sensorial data. ICGST-ARAS J 11(1):1–9
6. Schleicher D, Bergasa LM (2009) Real-time hierarchical outdoor SLAM based on stereovision and GPS fusion. IEEE Trans Intell Transport Syst 9(3):440–452
7. Aboshosha A (2003) An introduction to robot distributed sensors, part I. Faculty of Informatics, University of Tübingen, Germany, Technical report WSI-2003-13
8. Irawan A, Nonami K (2011) Compliant walking control for hydraulic driven hexapod robot on rough terrain. J Robotics Mechatronics 23(1):149–162

9. Cheng C, Cheng Y (2008) Research on map building by mobile robots. In: Proceedings of IEEE international conference on intelligent information application 2008, Ibadan, Nigeria, pp 673–677
10. Razali M, Nonami K (2011) LRF assisted force-based walking for hexapod robot COMET-IV. *Int J Automat Robotics Autonomous Syst* 11(1):11–22

Chapter 10

Challenges and New Frontiers

of Hydraulically Actuated Hexapod Robots

Abstract Hydraulically actuated hexapod robots form a very useful class of walking robots in the context of service robotics, field robotics, search and rescue, and high-risk operations. It can also be utilized as a test bed for designing and validating various gaits and walking behaviors. A lot of potential applications would be possible with the advent of various technologies associated with the design and manufacturing of such robots. A concise description has been presented for the potential application areas of hydraulically actuated hexapod walking robots.

10.1 Introduction

The era of modern robotics began about 50 years back when the company named Unimation, established by D. Engelberger, designed and constructed the first industrial robot and launched it commercially in 1960 [1]. Since then, the research and development on industrial robots gathered new momentum and numerous new and improved industrial robotic manipulators were successfully applied for factory automation in various industries [17]. The technology of industrial manipulator has gone through refinements after mitigating the shortcomings of the earlier designs (like fixed program, simple control system, and weak hardware and software) to meet the performance required due to the increased mechanization and the high rates of technological operations. The technology of industrial manipulator is quite mature now and robotics engineers have successfully prototyped robotic grippers that are similar to the human hand and can perform many tasks in various manners using versatile controls through reprogramming. However, the industrial manipulators did not have any mobility and could be employed to perform a limited range of tasks; therefore, success in the development of industrial manipulator

technology has inspired mankind to develop a variety of robotic devices with mobility, autonomy, and intelligence so that they can interact with the environment and alleviate the necessity of human effort and intervention in day to day activities as well as in various critical situations. This has triggered a widespread research in mobile and walking robot during the first half of the 1990s [1]. In most of the cases, the design of modern walking robots are biologically inspired, employing the observations from the biological world, with an intention to achieve optimal performance like the living creatures and then apply them in all spheres of human activity. This has been possible due to the significant advances in information processing, artificial intelligence, control theory, software, sensors, and machine vision systems.

Various types of walking robots have been designed and developed during the last two decades around the world for different applications or research. However, the number of legs and type of actuation has been a dominant factor in their classification as well as determining their field of applications. This is because of the fact that the number of legs and type of actuation influence the other factors of the design and control. Hydraulically actuated walking robots have attracted the attention of the robotics researchers due to their interesting and useful features [2]. It has been observed that hydraulically actuated hexapod robot possesses some unique features as well as exhibits some extraordinary performances like:

1. High torque (force) to weight ratio of the leg actuators enables it to carry large body weight and payload.
2. The hydraulic actuators are compact and robust. This is advantageous for making the leg mechanism slim and slender. As a result, the legs can be designed such that the joints can rotate over a wide range of angular values.
3. The leg mechanisms are of direct drive type; as a result there is no requirement for transmission systems for transferring force or torque to the leg joints. The energy loss due to friction is also less due to the absence of the transmission systems.
4. The static stability margin of hexapod robot is quite high; therefore, they can be applied for hazardous terrain where locomotion of the robot is itself quite challenging.
5. The hydraulic actuators normally remain at the last position when the power supply to the control valve is failed or withdrawn or the prime mover of the hydraulic pump is accidentally stopped. This actually provides a locking capability of the actuators. As a result the body of the robot, which is quite heavy, is saved from collapse.
6. The hydraulic actuation systems require some accessories like hydraulic tank, hydraulic pump, powerful prime mover for the pump, and pipe lines for hydraulic fluid. These accessories are quite heavy and bulky. Therefore, the robot body is also heavy and bulky in order to accommodate these hydraulic accessories. Thus, the leg mechanism should be made quite strong and big in size so that they are able to lift the body and impart motion on it. This is actually advantageous

for crossing big obstacles in rough terrain during field applications. The kinematic design of the leg and body of a hydraulically actuated walking robot should be performed to maintain appropriate proportions between the leg and body.

These advantageous features of hydraulically actuated hexapod robots have rendered them as a suitable candidate for deployment in field applications. Few hydraulically actuated hexapod robots have been developed around the world for their actual deployment and research for field applications. The lessons learned from them will help for further improvements and consequently they will find many more application areas. We will give a brief account of the applications of hydraulically actuated hexapod robots in various fields in the next sections.

10.2 Mine Detection and Removal

According to United Nation's estimates, more than hundred million land mines lie buried under the ground around the whole world, causing about 10,000 deaths and twice of this are injured annually due to the explosion of land mines [2]. People around the world are working on the various techniques for removal of buried land mines for more than last 70 years [3]. The most common de-mining technique used today is the manual method [12]. This technique is very primitive, high-risk, and human labor intensive. It is also very dangerous, because a wrong step can maim or kill the operating personnel. This manual method makes complete de-mining of the world virtually impossible, and due to its slow speed of operation, another few centuries may be necessary to completely remove the buried land mines from the earth.

Therefore, we need some fast, safe, and robust technique for de-mining operation and walking robots can be thought of as an effective and efficient means for that [3]. Hydraulically actuated hexapod walking robot can be applied for the detection and removal of land mines with safety and security of the operating personnel. As the hydraulically actuated hexapod robot is mechanically robust, has high level of static stability margin, and suitable for operation in rough terrain, their deployment for the de-mining task is advantageous from the point of view of its safe locomotion capability in the mine field and the capability to carry large payload of the tools required for de-mining mission. Authors' group at the Robotics and Control Laboratory, Chiba University, Japan, has developed and successfully tested hydraulically actuated hexapod robots COMET-III and COMET-IV for achieving robot-assisted de-mining. Their predecessors COMET-I and COMET-II were also designed and developed for robot-assisted de-mining. However, their actuation systems were electric motor drives.

The hydraulically actuated hexapod robot can be operated either autonomously or by teleoperation. In either case, the operator need not worry about his safety. As a result, much time is saved during the search and removal of the buried land mines, which ultimately makes the robot-assisted de-mining faster than manual one.

10.3 Rescue and Disaster Management Applications

Hydraulically actuated hexapod robot can also be applied in rescue and disaster management operation. Rescue operation becomes a big challenge for the government and the municipality after any natural disaster, like earthquake, typhoon, cyclone, tornado, tsunami, flood, and landslide. Normally, the rescue operation suffers from the inaccessibility of the affected site due to road blockage, broken road, big landslide under the road, or complete disappearance of the road. Wheeled vehicle cannot reach to the affected site for sending food and other assistance to the trapped and affected people and evacuating the ailing and injured persons. Autonomous walking robots can search the trapped persons in the devastated areas without human intervention [4]. Hydraulically actuated hexapod walking robot can be sent to the affected site very easily. As it can walk on rough terrain with large obstacle, it can take detour from the spot of damaged road and can arrive at the affected site by crossing rocks, rubbles, bush, forest, or even mountain. A brief account of the development of various types of walking robots for rescue and disaster management can be found in [5, 6].

In other disastrous situations like train or road accidents, collapse of multistoried building, fire, explosion, or poisonous chemical gas leakage, hydraulically actuated hexapod robot can be utilized for the search and rescue of the trapped and affected human without risking the life of the rescue team personnel. In these situations the hydraulically actuated hexapod robot will be able to reach the affected site and search for the trapped human, either autonomously or by teleoperation, and then can safely bring them outside by carrying them on the robot body.

10.4 High-Risk Operations

Maintenance and monitoring inside a nuclear power plant is subjected to exposure to high-level nuclear radiation and consequently is a high-risk task for human. Therefore, deployment of walking robots in nuclear power plants for maintenance and monitoring is quite useful and beneficial for the safe operation of nuclear power plant [7]. Hydraulically actuated hexapod robot can find a good application in such high-risk operations. As they have a higher payload capacity compared to electrically actuated walking robots, they can be gainfully utilized for nuclear waste disposal and removal of the radioactive rubbles around the damaged nuclear power plant in addition to the maintenance and monitoring of the nuclear power plant. It can perform this job autonomously or by teleoperation. Its robust structure and large obstacle-crossing capability also help it to work in such adverse and high-risk situation. Hydraulically actuated hexapod robot-assisted monitoring, damage repair, and removal of nuclear waste can result into a very safe and useful way of managing such a high-risk and crisis-prone situation.

Another high-risk area of application of hydraulically actuated hexapod robot is exploration inside the volcanic craters. It is almost impossible for human to explore the active volcanic craters to collect samples of rocks, gases, and other substances and deployment of walking robot in such a situation has been proved to be quite fruitful [8]. Due to the same reason as stated above, hydraulically hexapod robot can also be deployed in such situations.

10.5 Construction Application

Hydraulically actuated hexapod robot can also be applied in construction industry. Most of the time, the construction project is started in remote and distant place, like construction of dam, bridge, road, and tunnel. In such situations it is difficult to employ construction workers because of their unwillingness to work in those remote and hostile project sites, high wages, or life risk of the workers. Hydraulically actuated hexapod robot can be applied in these situations and they can be either autonomously operated for performing some repetitive job or can be teleoperated from the construction office located far away from the construction site.

As the legs are hydraulically powered, the legs can be fitted with construction tools and it can work very well for removing and filling of earth, digging holes, making tunnels, etc. Thus the hydraulically actuated hexapod robot can also play the roles of heavy construction machinery.

10.6 Cargo Application

Hydraulically actuated hexapod robots can also be applied for cargo applications. The commercial shipment of goods is becoming costly for the involvement of human labor and in many countries human labor is becoming expensive because of falling population. Therefore, hydraulically actuated hexapod robot can offer an economically viable solution for cargo industry. It can perform the loading and unloading of heavy goods quite fast and can easily be programmed for such repetitive operation. It can be teleoperated for more complex operation.

10.7 Underwater Operation

Hydraulically actuated hexapod robot can also be applied for underwater operation with proper design. The mechanical design of the robot may need minor modification as the water pressure and buoyancy will affect the motion of the robot. Underwater operation like seafloor exploration, underwater construction, and undersea cable laying require skilled workers and special techniques so that their

life remains safe and secure. Hydraulically actuated hexapod robot can be applied to perform these jobs without worrying about the safety and security of the life of the operating personnel.

10.8 Forest-Cutting Machine

Forest cutting and handling of the timber requires a large manual operation because the dense forests are not accessible by wheeled vehicle. Forest is a good example of rough terrain and mobilization of heavy machinery for cutting and transportation of the timber inside the deep forest is impossible. Therefore, hydraulically actuated hexapod robot can find good application in such forest cutting and removal operation. The robot can enter into the forest by walking over the rough terrain of the forest, and after cutting the tree with the cutting tools, it can also transport it from deep inside of the forest up to the road outside the forest.

10.9 A Test Bed for Study and Research of Biological Walking

Modern robotics research aims to design and implement biologically inspired walking robots. Although biological inspiration does not mean exactly mimicking the walking creatures of the biological world, the principles underlying in the evolution of their morphological structure and control of the body joints to manifest different gaits during locomotion have been studied for the last few decades and this knowledge base has been applied for the design and control of the present-day biologically inspired walking robots. However, legged robots differ significantly from their biological counterparts [9] and a good test bed is needed to validate the ideas and knowledge gathered from the observations of the biological world [10]. Hydraulically actuated hexapod robot is a good test bed for validation of various concepts regarding the gaits and locomotion behaviors of the biological creatures like insects and crab.

10.10 Other Possible Applications of Hydraulically Actuated Hexapod Robot

There may be numerous other possible applications of hydraulically actuated hexapod robot in the future. They may be applied for lunar [11] or mars exploration and assisting human for setting up colony there. In heavy industry like steel and coal, hydraulically actuated hexapod robot may find good applications for

improving the productivity. Hydraulically actuated hexapod robot may also find application in agriculture where the cost of cultivation is high. These are the only few application areas where the hydraulically actuated hexapod robot can be applied with the present state of the art. With the progress and development of more and more sophisticated and cheaper technology, hydraulically actuated hexapod robot may find even more application areas [13–16].

References

1. Petrina AM (2010) Advances in robotics (review). *Automatic Doc Math Linguist* 45(2):43–57
2. Semini C (2010) HyQ – design and development of a hydraulically actuated quadruped robot. Ph.D Thesis, University of Genoa, Italy, and Italian Institute of Technology (IIT)
3. Nonami K, Shimoi N, Huang QJ, Komizo D, Uchida H (2000) Development of teleoperated six-legged walking robot for mine detection and mapping of mine field. In: Proceedings of the IEEE/RSJ international conference on intelligent robots and systems, Takamatsu, pp 775–779
4. Thomas T (2010) Development of an autonomous hexapod robot for search and rescue. <http://teyvoniathomas.com/index.php/projects/24-search-and-rescue.html>
5. Billah MM, Ahmed M, Farhana S (2008) Walking hexapod robot in disaster recovery: developing algorithm for terrain negotiation and navigation. *World Acad Sci Eng Technol* 42:328–333
6. Ahmed M, Khan MR, Billah MM, Farhana S (2010) Walking hexapod robot in disaster recovery: developing algorithm for terrain negotiation and navigation. In: Lazinica A (ed) New advanced technologies. InTech, Rijeka, Croatia, 341–350
7. Moore T (1985) Robots for nuclear power plants. *IAEA Bull Autumn* 1985:31–38
8. Wettergreen D, Pangels H, Bares J (1995) Behavior-based gait execution for the Dante II walking robot. In: Proceedings IEEE international conference on intelligent robots and systems, Pittsburg, vol 3, pp 274–279
9. Belter D, Skrzypczyn'ski P (2010) A biologically inspired approach to feasible gait learning for a hexapod robot. *Int J Appl Math Comput Sci* 20(1):69–84
10. Beer R, Quinn RD, Ciel HJ, Ritzmann RE (1997) Biologically inspired approaches in robotics: what we can learn from insects. *Commun ACM* 40(3):30–38
11. Hauser K, Bretl T, Latombe J C, Wilcox B (2006) Motion planning for a six-legged lunar robot. In: Proceedings of the 7th International workshop on the algorithmic foundations of robotics (WAFR), New York City, pp 16–18
12. Schreiner K (2002) Landmine detection research pushes forward, despite challenges. *IEEE Intell Syst* 17(2):4–7
13. Schmucker U, Schneider A, Ihme T (1996) Six-legged robot for service operations. In: Proceedings of the 1st Euromicro workshop on advanced mobile robots (EUROBOT '96), Kaiserslautern, 9–10 October, pp 135–142
14. Laboratoire de robotique de l'Universite Laval (2011) HEXAPODE (WALKING ROBOT). <http://robot.gmc.ulaval.ca/en/research/theme401.html>
15. G'orner M, Wimb'ock T, Baumann A, Fuchs M, Bahls T, Grebenstein M, Borst C, Butterfass J, Hirzinger G (2008) The DLR-crawler: a test bed for actively compliant hexapod walking based on the fingers of DLR-Hand II. In: Proceedings of the IEEE/RSJ international conference on intelligent robots and systems, France, pp 1525–1531
16. Tesar D (1997) Where is the field of robotics going? www.robots.utexas.edu/rwg/docs/pubs/publications/whereisfieldofroboticsgoing.pdf
17. Saha SK (2008) Introduction to Robotics. Tata McGraw-Hill, New Delhi, India

Index

- A**
- A* algorithm, 243
 - Aarc motion, 180
 - Action period, 162
 - Active suspension, 141
 - Actuators, 4, 6
 - Actuator saturation, 122, 134
 - Adaptability, 41, 43–45
 - Adaptation block, 131
 - Adaptation law, 130, 131, 133–135
 - Adaptive law, 180
 - Adaptive suspension vehicle (ASV), 33
 - AIBO, 36
 - Algebraic Riccati's, 171, 188
 - Ambient environment, 199, 200
 - Ambient environmental image view, 208–211
 - Angle command input, 95
 - Angular position, 105, 111, 113
 - Angular space, 106
 - Angular velocity, 105, 111
 - Anomalous attitude, 63
 - Antecedent, 187
 - Application programmed interface (API)
 - method, 201
 - ARL-II, 35
 - Arm, 45, 49, 53, 55, 59, 61, 66, 68, 69, 71, 75
 - Armored knight, 23
 - Artificial legged locomotion, 21–26
 - Artificial walking systems, 5
 - Ascending an obstacle, 244–246
 - ASIMO, 34
 - Asimov, Isaac, 26
 - Attitude control, 179–185
 - Attitude control for balances, 200
 - Attitude counter, 150, 151
- B**
- Attitude sensor, 201
 - Autonomous operation, 4, 17, 265–267
 - Azimuth angle, 212
- C**
- Backward-forward walking, 114
 - Basis function, 129, 132
 - BigDog, 36
 - Big Muskie*, 30
 - Biological inspiration, 6
 - Biological systems, 5, 6
 - Biped robot(s), 7, 9, 10
 - Body coordination system (BCS), 94
 - Body height, 243, 245, 248, 253, 255, 256
 - Body movement coordination (BMC)
 - method, 199, 221
 - Body's moment of inertia, 169–179
 - Boolean expression, 149
 - Boom mechanism, 45, 53, 55, 57, 59, 61, 66, 68–71, 74
 - Bucket, 45, 53, 56, 66

- Cliff, 174, 190, 192–195
 Clockwise (CW), 96
 Closed-loop identification, 115, 116
 CoB rotational based, 94, 95
 CoG. *See* Center of gravity (CoG)
 CoM. *See* Center of mass (CoM)
 COMET-I, 37
 COMET-II, 37
 COMET-III, 37, 113–117
 COMET-IV, 37
 Compensator gain, 173
 Compliant control, 145–152, 165
 Compliant switching mechanism, 149, 162, 163, 165
 Compliant tripod walking pattern, 218
 Computation time, 109
 Computed torque control, 107
 Computing element, 4
 Computing system, 4
 Construction, 200
 Construction industry, 267
 Continuous switching function, 134
 Control, 2–8, 10, 14, 16–17
 Control algorithms, 4, 17
 Control law, 4, 8
 Controller hierarchy, 224
 Control system, 41, 46, 48, 50, 51
 Coordinate system of a leg, 201
 Coriolis vector, 111
 Cost function, 171, 180, 183
 Counterbalance, 142
 Counter-clockwise (CCW), 96
 Coupling, 107, 109, 112
 Crawler type, 42, 200
 Criterion, 179, 180, 183
 Cross over an obstacle, 244, 248, 256
 Ctesibius (c. 270 BC), 21
 Cycle time, 15
 Cylindrical-coordinate type, 45
- 3-D environment image, 240, 241
 Descending a cliff, 246–248, 253–256
 Design, 42–53, 55, 71, 75, 78
 Designed numerical model-distributed data, 199
 3D geometric combination, 199
 3D geometric model, 201, 212–214, 216, 217, 226, 227, 229, 231, 233
 3D geometric model coordinate system, 227
 3D geometric modeling, 199, 226–229
 3D graphics processing, 226
 2-D grid-based mapping, 239
 Digital video transfer system (DVTS), 208
 3-dimensional (3D) robot models, 201
 Direct adaptive fuzzy controller, 130
 Direct drive, 264
 Direct kinematics, 90
 Disaster-stricken districts, 200
 Discontinuous nonlinearities, 110
 Distance of foot placement, 102
 Distributed control system, 48
 Disturbance observer (DO), 118, 122
 3D mapping, 201
 3D modeling software, 226
 Downward angle, 240
 Drive system, 41, 42, 44, 45
 3D robot animation, 199, 200
 3D robot simulator, 226, 229
 Dry friction, 110
 3D simulator compilation, 230
 3D simulators, 226
 3D simulator system configuration, 217
 Durability, 41
 Duty factor, 15
 Dynamically coupled, 107
 Dynamically stable locomotion, 6, 7
 Dynamic force reference, 226
 Dynamic H_0 (DH_0), 151
- D**
- Damping, 159–161
 Dangerous operations, 41–43, 46, 49, 50
 Dangerous works, 3
 DANTE, 34, 35
 da Vinci, Leonardo, 22
 Dead zone, 110, 126, 130, 134–136, 169
 Dead zone compensation, 130
 Defuzzification, 187
 Defuzzifier, 131
 De-mining operation, 265
 Denavit-Hartenburg (D-H) notation, 105
- E**
- Easy human interfaces, 205
 Eight-legged locomotion, 7, 8, 10, 13, 14
 Elastic model, 159, 161
 Electrohydraulic valve controllers, 110
 End-effector(s), 14, 41, 45, 78
 Energy efficiency, 5
 Environment trailed trajectory (ETT), 98
 Euclidian norm, 62
 Euler angles, 170
 Exploration, 92

External force, 98
Extra force, 98, 102
Extra time, 90
Extreme environment, 199, 200
Extremely soft terrain, 169, 179

F

Factory automation, 5
Feedback gain, 117, 119, 134
Field application(s), 3, 14
Field robotics, 8, 10, 14–17, 263
Final phase, 101
First phase, 100
Fixed trajectory, 141, 145
Flat terrain, 142, 145, 146
FlexSim, 226
Foot, 87, 95, 98, 100, 102, 103
Foothold position(s), 7, 14, 16, 105, 106
Foot placement, 200, 221, 224
Foot trajectory, 106, 128, 130, 138
Foot trajectory generation algorithm, 217
Foot turning radius, 95
Force acting, 87, 98
Force-based controlled numerical model, 199
Force-based controlled walking, 199, 217
Force-based motion, 94
Force control, 41, 51
Force equilibrium matrix, 90
Force feedback, 169, 174, 185
Force manipulability ellipsoid, 64
Force redundancies, 141, 143, 145, 158, 161
Force threshold method, 97
Form and disposition of legs, 45–46
Forward and inverse kinematics, 217
Forward kinematics, 55–56
Fully autonomous method, 199, 200
Fully autonomous walking navigation system, 81
Fundamental motion prepared beforehand, 200
Fundamental test, 91
Fuzzifier, 131, 187
Fuzzy associative memory (FAM) table, 136
Fuzzy inference engine, 131
Fuzzy logic control, 185–196
Fuzzy regressor, 129
Fuzzy rule base, 131, 136
Fuzzy sets, 131, 132, 136, 137

G

Gait(s), 41, 43–45, 76
Gait pattern control, 200
General electric quadruped, 27, 28
Genetic algorithm, 201
Genghis, 34
Geometric information, 239
Geometrics of obstacles, 239, 242
Global positioning system (GPS), 92, 201
Graphic user interface (GUI), 226
Gravity force vector, 111
Grid-based environment modeling, 241–243
Grid cell, 239, 243
Grid coordinate system, 243
Growing obstacle method, 243
Grown obstacles, 243

H

Hanging, 141, 143
Hazardous operation, 199
Hazardous terrain, 14
Height of leg rising, 102
Hero (c. 85 AD), 21
Heuristic method, 148
Hexapod(s), 3, 7, 8, 10, 14–17
Hexapod robot, 237–238, 244
Hierarchical control, 107
High-risk operations, 263, 266–267
High-risk task, 266
High-speed switching, 117
Historical account, 3
Historical evolution, 20
Homer (VIII c. BC), 21
Homogeneous transformation matrix, 212, 214, 226, 228
Horizontally incline, 141
Horizontal workspace, 95, 96
Humanitarian de-mining robot, 113
Humanoid robot, 7
Humanoid robotics program (HRP), 36
Hybrid position/force/attitude control, 224
Hydraulically actuated hexapod robot(s), 199, 201, 263, 265, 267
Hydraulically actuated hexapod walking robot, 112, 113
Hydraulic cylinder pressure, 97, 98
Hydraulic cylinders, 110, 113, 201
Hydraulic fluid, 110, 111
Hydraulic motor(s), 110, 113, 201
Hydraulic power, 113
Hydraulic pumps, 201
Hyperboloidal mirror, 208

I

- IF-THEN rules, 128, 131, 133
 Impedance control, 41, 78–80, 169–185,
 188–190, 192, 195, 196, 224
 Impedance equilibrium, 159, 161
 Impedance model, 159–161
 Impedance output, 173, 174, 185, 186, 189, 190
 Impulse signal, 183
 Inclining downward, 148
 Inclining upward, 148
 Inclinometer, 169
 Independent joint control, 109, 112–113, 130
 Indeterminate problem, 64, 65
 Indirect adaptive fuzzy controller, 130
 Indirect force control method, 224
 Indoor simulation, 216
 Industrial robots/manipulators, 4
 Inertia matrix, 111
 Inner leg, 246, 247, 255
 Inner loop, 118
 Insect behavior, 5
 Insect-type, 45
 Intelligence, 4, 5, 17
 Inverse kinematics, 55–56, 87, 125
 Irregular terrain, 2
 Iterative Jacobian-analysis, 41

J

- Jacobian, 56, 57, 65, 71
 Joint angle, 145
 Joint angle trajectory, 106
 Joint space trajectory, 115

K

- Khalif of Baghdad (786–833), 22
 Kinematic analysis, 55–64
 Kinematic design, 265
 Kinematics, 85–89, 93, 94, 96
 KISMET 3D simulation software, 226

L

- Large opening angle, 239
 Large-scale robot, 199, 200
 Laser beam, 239, 240
 Laser range finder (LRF), 201, 240–241
 Lattice points, 210, 211
 Leg coordination control, 3
 Legged locomotion, 2, 5, 12, 14
 Legged robot(s), 2, 3, 5, 7, 8, 10, 13, 14,
 89, 92, 93, 237, 238, 258

Legged type, 42

- Leg mechanism, 264
 Leg phase, 15
 Leg slipped, 142
 Leg stride length, 245
 Leg stroke, 15, 16
 Leg swing trajectory, 245
 Light condition dependent, 239
 Linear interpolation method, 90
 Linear parameterizing model, 129
 Linear quadratic regulation (LQR), 226
 Linear quadratic regulator (LQR), 169
 Linear vertical static force, 90
 Link parameter, 201
 Load-sensing system, 48
 Load-sensitive valve, 48
 Local area network, 114
 Locomotion control, 93
 Locomotion strategies, 237, 238, 244–248
 Logical bit, 98
 Logical body attitude (LBA), 148
 Logical terrain level detection (LTLD), 148
 Low-impact foot trajectory, 203
 LRF. *See* Laser range finder (LRF)
 Lyapunov synthesis, 130

M

- Magnitude vectors, 180
 Mammal-type, 45
 Maneuverability, 5
 Manipulability, 53, 61–64, 71, 76
 Manipulability ellipsoid, 61–64, 69, 76
 Mass spring equilibrium equation, 224
 Master-slave technique, 200
 Matching condition, 119
 Maximum thrust, 65
The mechanical horse, 24, 25
 Mechanical vibration, 110
 Mechanism(s), 4, 7, 17, 41–43, 45, 46, 51,
 53, 55, 58, 61, 64–71, 74–78
 Mechanism design, 69, 74
 MECHANT, 34
 Mechatronics, 38
 Mechatronic structure, 3
 Membership function, 135, 187, 188
 Mine detection and clearance robots, 200
 Mirror parameter, 208, 209
 Mobile robot navigation, 200
 Mobile robots, 2
 Model reduction, 112
 Model reference sliding mode control
 (MRSMC), 113, 118

Model uncertainty, 107, 108, 112, 113
 Monopod hopping robot, 7
 Morphological structure, 268
 Motion, 87, 89, 90, 94, 95, 99, 100, 102
 Mountain forest, 200
 Move phase, 101
 MRSMC. *See* Model reference sliding mode control (MRSMC)
 Multibody-system dynamics simulation and kinematics simulation, 226
 Multi-DOF, 93, 94
 Multifunctional, 4, 5
 Multi-input single-output (MISO), 187
 Multi-legged locomotion, 20, 93, 94
 Multivariable control, 107, 111
 Multivariable MIMO plant, 108
Mu Niu Lu Ma, 22

N

Natural terrain, 2, 14
 Navigation, 91–93
 Navigation computer, 208
 Necessary flow rate, 70–71
 Necessary workspace, 69–70, 76
 Newton’s law, 160
 Nonlinearities, 105, 107, 110–112
 Nonlinear MIMO system, 106
 Nonlinear robust control techniques, 105
 Non-uniform gravitational, 89
 Number of legs, 44
 Numerical walking generation/control, 216

O

Obstacle avoidance walking, 199, 216, 239
 Obstacles, 3, 16
 Occupancy grid map, 248
 Occupied cells, 243
 ODEX-I, 33
 Omni-directional, 93, 94, 96
 frame data, 208
 gait, 203, 204, 208
 gait control procedure, 203–205
 image, 206, 208, 210, 211, 215, 216, 233
 vision sensor, 199, 200, 205, 208
 One-step-ahead control, 134
 Online 3D virtual reality technique, 199
 Open dynamics engine (ODE) approaches, 201
 Operating speed, 5
 Optimization, 169–196
 Optimization-based design, 41
 OSU hexapod, 31, 33

Outdoor auxiliary robot, 42
 Outdoor environment walking, 199, 216
 Outer controller and inner controller, 223
 Outer legs, 246, 247
 Output membership functions, 135
 Outstanding ability, 41
 Overturn, 142, 148

P

Padé approximation, 115
 Parallel manipulators, 107
 Parameter variation, 110, 117, 126, 130, 133, 135
 Parameter vector of the controller, 133
 Patching, 100
 Path of the robot, 106
 Path planning, 16, 17, 91–93, 243–244
 Payloads, 14
 Pedestrian lane change, 93
 Pentapod, 14
 Perspective projection image, 208
 Phase measurement, 240
 Philo of Byzantium (c. 200 BC), 21
 Phony Pony, 27–30
 Physical solution, 181
 PID control, 122, 136
 Pixel coordinate system, 210
 Point clouds data, 240, 242, 256
 Polar-coordinate type, 45
 Polyarticular type, 45
 Polynomial input, 187
 Position-based force control, 141–156
 Position based locomotion control, 105, 106, 110
 Position control, 105, 106, 118
 Posture angle, 141, 148, 149, 154, 164, 166
 Power source, 42, 44, 46
 Preparation period, 146
 Pressure sensor, 201
 Preview feedforward control, 122
 Preview sliding mode control, 122, 125
 Preview steps, 123, 125
 Product inference, 132
 Programmable logic valve controller (PLVC), 142
 Projection coordinates, 210
 Projection coordinates of hyperboloidal, 210
 Proportional electromagnetic control valve, 110, 130
 Propulsion(s), 1, 4, 5, 14
 Protraction, 7, 15
 Pseudoperspective projection image, 210

- Pull-back action, 145, 147, 148, 152–154
 Pump flow rate, 74
 Pump overall efficiency, 74
 Push-pull motion, 156, 158, 165
 PV-II, 31, 32
- Q**
 Quadruped robot(s), 7, 237–238
- R**
 Radiation-type, 45
 Real time, 8, 105, 107, 108, 118, 122, 135–136
 Real-time teleoperation control, 216
 Rectangular-coordinate type, 45
 Regular gait, 106
 Remote control, 201, 205
 Remote-operations control system, 50
 Renaissance, 20, 22, 23
 Reprogrammable, 4
 Reprogrammable multi-functional, 4
 Required maximum force, 74, 75
 Rescue and disaster management
 operation, 266
 Reset action, 142, 143, 150
 Retraction, 7, 15
 Robota, 26
 Robot-assisted de-mining, 265
 Robotic Institute of America (RIA), 4
 Robots, definition of, 4
 Robust adaptive fuzzy control, 105, 113,
 130, 135–136
 Robust control techniques, 107, 108, 111–138
 Rotating LRF, 241
 Rotational angle, 95
 Rough terrain locomotion, 2, 3, 5, 10, 14,
 106, 200, 224
 Rule base, 187
- S**
 Safe walking path, 239, 243
 Scanned angle, 242
 Scanning speed, 241
 SCOUT-II, 36
 SCS. *See* Shoulder-based coordination
 system (SCS)
 Search and rescue, 263, 266
 Second-order system, 115
 Self-localization, 233
 Self-tuning stiffness, 179–185
 Semi-latus rectum, 209
 Semimajor axis, 209
 Sensing period, 146
 Sensor integration, 239
 Sensors, 2, 4, 6, 14
 Service robotics, 263
 Servo control law, 112
 Servo system design of each leg, 200
 Shaking, 169, 185, 189, 196
 Shank, 87, 88, 98
 SH4 computer-2, 114
 Shoulder, 45, 51, 53, 57, 85, 89, 94
 Shoulder-based coordination system
 (SCS), 86, 94
 Shoulder coordinate system, 218, 219
 SILO4, 36
 Simulator, 199–201, 216–229
 Simultaneous localization and mapping
 (SLAM), 200
 Single-leg impedance control, 159–161, 164
 Singleton fuzzifier, 132
 SISO plant, 109, 112
 Six-legged, 6, 7, 10, 14
 Sliding mode control, 113, 117–122, 124
 Small-scale body, 200
 Spherical coordinates, 209
 Spherical projection, 210
 Stability criteria, 143
 Stability margin(s), 8, 10, 14–16
 Stable locomotion, 109
 Stable range, 148, 154, 157, 164
 Stable rotational range, 179
 Stable walk, 100
 Stance phase, 7
 Standard circular gait, 203
 State flow, 218
 State-space model, 171
 State-space technique, 107
 Statically stable locomotion, 3, 7, 112, 113,
 142, 159, 162
 Statically stable walking machine, 112
 Static force, 173
 Static move-based walking, 100
 Static stability, 106, 237
 Step count, 245, 246, 248
 Stereo vision camera, 201
 Stiffness, 161, 179
 Stochastic terrain, 237
 Stride, 3, 7
 Stride length, 15, 243, 245, 246, 248, 253,
 255–258
 Supervisory controller, 108
 Support pattern(s), 7, 15
 Support phase, 90, 99–101

- Support polygons, 7
Support/stance phase, 15
Swing(s), 4, 6, 7, 14, 17
height, 243, 245, 246, 248, 250, 251,
253, 255, 256
motion, 105
phase, 100, 101
Switching function, 181
Switching hyperplane, 117, 124
- T**
TCP/IP network, 114
Teleoperated locomotion control, 199–233
Teleoperation, 114, 265, 266
assistant system, 200, 205–208, 214, 233
computer, 203, 208, 212, 233
Terrain adaptive foot trajectory, 97–103
Terrain condition, 106, 107
Terrain levels, 102
Tetrapod gait, 114, 115, 136
Texture coordinates, 210
Texture mapping, 210
Thigh, 87, 88, 98
Thigh, shank, and foot, 201
Three Dim Sim mechanics simulator, 226
Three laws of robotics, 26
Tilt angle, 241
Time delay, 107, 110, 115, 122, 130, 134, 138
Time of flight, 240
TITAN-III, 32
TITAN-XI, 32
Torque correction, 169
Torque gain, 88, 89
Torque (force) to weight ratio, 264
Touching force, 98
Tracked robot, 237
Tracking performance, 107, 111, 113,
120–122, 126, 127, 134, 136–138
Trajectory planning, 253
Transfer/swing phase, 15
Travel costs, 243
Traverse angle, 95
Triangulation, 240
Tripod gait, 7, 8, 70, 71, 76, 89, 91, 96, 98, 102
Tripod walking pattern, 217, 223
Truth table, 149
- U**
Unbiased type of membership function, 135
Uncertainties, 110–112, 117, 130
Underwater operation, 267–268
- Uneven terrain, 41
United Nation, 265
Unnecessary area, 147, 153
User datagram protocol (UDP), 206
- V**
Variable-displacement hydraulic pump,
46, 48, 50
Various hazardous operations, 200
Vector of force, 98
Vertical foot trajectory, 203
Vertical force, 98, 99
Vibration, 141, 160
Virtual environment, 201, 212, 226, 229
Virtual force, 169–179
Virtual position, 172, 173
Virtual spring, 224
Viscosity coefficient, 159–160
Viscous friction, 110
Vision-based locomotion strategies, 244
Visualization, 217
- W**
WABIAN, 35, 36
Walk down/descend, 193
Walking algorithm, 200, 221
Walking behaviors, 263
Walking control, 107, 117, 118, 122, 136
Walking cycle time, 102
Walking gaits, 3
Walking harvester, 36
Walking machine(s), 2–4, 6–8, 10, 14, 15
Walking robots, 237
classification of, 6–8
definition, 4
historical perspective of, 21–37
Walking speed, 41, 43, 45, 55, 64, 70–71,
76, 78
Wave gait(s), 3, 14, 106
Wheeled robot, 92
Wheeled-type mechanism, 42
Wheeled vehicles, 1–3, 5, 20
Wheel-type robot, 200
Workspace, 2, 4
World coordinate system, 221–223, 229,
231, 232
- Z**
Zero moment point (ZMP), 89
Zig-zag/flanking movement, 93, 95